POINT PROCESS ANALYSIS TECHNIQUES:

THEORY AND APPLICATIONS TO COMPLEX NEUROPHYSIOLOGICAL SYSTEMS

A thesis
submitted to the Faculty of Engineering
of the University of Glasgow
for the degree of

Doctor of Philosophy

by

Joe Wing-Nin LAU

July 1991

ProQuest LLC.
789 East Eisenhower Parkway
P.O. Box 1346
Ann Arbor, MI 48106 – 1346

This thesis is dedicated to
my parents

Table of Contents

Acknowledgements

I am indebted to my supervisor Professor D.J. Murray-Smith firstly for introducing me to the interesting area studied in this thesis and secondly for his patient guidance, encouragement and many useful suggestions throughout this project.

I would like to express my deepest gratitude to Dr. Jay R. Rosenberg of the Department of Physiology, not only for the many intriguing discussions we had on the subject, but also for his continual support and efforts in helping me complete this thesis.

Many thanks are due to Professor J. Lamb for the provision of research and computing facilities, and also for his invaluable assistance in helping me to acquire the necessary financial support during the period of my research. I am also grateful to the Croucher Foundation for financially supporting me. In particular, I would like to thank Dr. Payne and Lord Todd for granting me this scholarship.

Thanks are also due to Dr. D.M. Halliday who offered a considerable amount of help at the beginning stage of my research; and Dr. B.A. Conway, who kindly provided the physiological data.

Throughout this research, many people have contributed through the many discussions we had. Their interests in this project are greatly appreciated. In particular, Dr. N. Daves and Dr. L. Harrison deserve a mention. I would also like take this opportunity to thank Dr. U.M. Shahani for her moral support.

Finally, I wish to express my heartfelt thanks to my family whose continual understanding, encouragement and support have carried me through the years of my study.

Notations

Operators		Symbols	
^	denotes "estimate of".	M,N	Point processes M and N.
E{.}	denotes "expected value of".	X	Ordinary time series X.
Var{.}	denotes "variance of".	$Po(\mu)$	Poisson variate with mean μ.
Cov{.}	denotes "covariance of".	$N(\mu,\sigma^2)$	Normal variate with mean μ and variance σ^2.
Pr{.}	denotes "probability of".	χ^2_n	Chi-square variate with degree of freedom n.
Corr{.,.}	denotes "correlation of".	$F_{m,n}$	F variate with degrees of freedom m and n.

Functions

M(t)	Counting measure that counts the number of events in the interval (0,t].
dM(t)	Differential increment of point process M.
P_M	Mean intensity of point process M.
$P_{MM}(u)$	Product density function of point process M at lag u.
$P_{MN}(u)$	Cross-product density function between point processes M and N at lag u.
$m_{MM}(u)$	Auto-intensity function of point process M at lag u.
$m_{MN}(u)$	Cross-intensity function between point processes M and N at lag u.
$q_{MM}(u)$	Auto-cumulant density function of point process M at lag u.
$q_{MN}(u)$	Cross-cumulant density function between point processes M and N at lag u.
$f_{MM}(\lambda)$	Auto-spectrum of point process M at angular frequency λ.
$f_{MN}(\lambda)$	Cross-spectrum between point processes M and N at angular frequency λ.
$\|R_{MN}(\lambda)\|^2$	Ordinary coherence function between point processes M and N at angular frequency λ.
$f_{11.2}(\lambda)$	Partial auto-spectrum of order-1 of point process 1 after removing the effects of point process 2.
$f_{12.3}(\lambda)$	Partial cross-spectrum of order-1 between point processes 1 and 2 after removing the effects of point process 3.
$\|R_{12.3}(\lambda)\|^2$	Partial coherence function of order-1 between point processes 1 and 2 after removing the effects of point process 3.
$f_{11.23}(\lambda)$	Partial auto-spectrum of order-2 of point process 1 after removing the effects of point processes 2 and 3.
$f_{12.34}(\lambda)$	Partial cross-spectrum of order-2 between point processes 1 and 2 after removing the effects of point processes 3 and 4.
$\|R_{12.34}(\lambda)\|^2$	Partial coherence of order-2 between point processes 1 and 2 after removing the effects of point processes 3 and 4.
$q_{123}(u,v)$	Third-order cumulant density function between the point processes 1, 2 and 3 at lags u and v.

Summary

The main objective of this thesis is the development of analytical techniques and computational procedures for the analysis of complex neuronal networks. The techniques are applied to data obtained from elements of neurophysiological systems and simulated models to illustrate different aspects of these analysis tools.

The nerve signals that occur within neuromuscular control systems are widely accepted to be stochastic in nature and are characterised by the times of occurrence of events, typically 1 msec. in duration of fixed amplitude, within the process. This provides the basis for considering these processes as stochastic point processes. The analytical approach adopted is similar to that used in ordinary time series and requires an inter-disciplinary approach involving linear and non-linear system analysis, estimation theory, probability theory and statistical inference. In this thesis a considerable amount of work is devoted to the discussion of these various areas related to the point process analysis techniques. In addition, neurophysiological concepts are discussed to provide a basis for the application of these techniques. These techniques are applied to the analysis of real data obtained from physiological experiments and simulated data generated by model neuronal networks of different complexities. Finally, some possibilities for future work opened up by the present investigation are considered.

An introduction together with some historical notes are given in Chapter 1. The objectives of this thesis are set down and some general ideas of a point process and neurophysiology are introduced. The historical notes at the end of Chapter 1 are intended to give a picture of the trend of developments concerning point processes.

Chapter 2 presents a simplified account of the relevant neurophysiological background. Some features of the neuromuscular system which lead to the use of point process analysis techniques are discussed. This is followed by a brief description of the organisation of neuromuscular system and some of its elements. The idea that the generation of an action potential occurs when the membrane potential at the trigger zone of a neurone exceeds the threshold forms the basis for the neurone model used in this thesis. The multiple input and output nature of neuromuscular systems in addition to the short duration of an action potential justify the realisation of a spike train as stochastic point process. Chapter 2 is concluded by considering some findings from the application of point process analysis techniques to data recorded from

neuromuscular elements. The details of the techniques are then explained in Chapter 3-5.

Chapter 3 gives a development of the theory of linear point process system analysis. The formal definitions of the assumptions involved, namely stationarity, mixing, and orderliness are explained. These assumptions are important in simplifying the theories involved and are seen to be valid in our applications. Theories for univariate, bivariate and multi-variate point processes are considered. The asymptotic value of the auto- spectrum of a point process is shown to be a non-zero constant, which marks the distinction from the auto-spectrum of an ordinary time series. Various quantities in both time and frequency domains are introduced and, among them, the coherence function and its partial and multiple forms are explained in particular details. The application of coherence is emphasised in Chapter 6.

Since the processes involved are stochastic in nature, appropriate estimation procedures for the time and frequency domain quantities should be used. Chapter 4 is devoted to explaining the estimation procedure used and the statistical properties of these estimates. Also the Poisson point process - which possesses similar properties to Gaussian white noise in the case of ordinary time series - is introduced. The importance of the Poisson point process lies on the fact that it may be used as a 'reference process' to indicate departure of independence within a point process. At the end of Chapter 4, the confidence intervals of the time and frequency domain estimates under the hypothesis of independence are developed. The confidence interval approach forms the basis of inferring whether there is any significant association between processes or within a process.

Chapter 5 describes briefly the implementation of the neurophysiological and simulation experiments. The digital algorithm for generating the exponential and Gaussian variables to provide the required stimuli in the experiment are explained. The neurone model, which is the building block of more complicated neuronal networks, is also described.

Chapter 6 presents results and discussion. First some simulated spike trains of different structures are analysed using histogram, auto-intensity and auto-spectrum. The histogram is found to be least sensitive in revealing significant information concerning the processes. Then the time and frequency domain analysis techniques discussed in Chapter 3-4 are applied to the input and output spike trains of a

model neurone. The cases where an input spike has an excitatory effect on the output, and that when an input spike has an inhibitory effect on the output are looked at. Some general findings from the analysis are pointed out, and in particular the distinctions of these two situations lie in the shape of the cross-intensity estimates and the phase spectra. The analysis of the bivariate point process is followed by the study of a neuronal network model in which a pair of neurones are influenced by a common input. The shape of the ordinary coherence estimate is seen to be related to the frequency content of the common input and some analytical studies of this observation are also presented. In addition, the use of partial coherence of order-1 is demonstrated and is seen to be able to remove the contribution of the common input mathematically. The analysis is then extended to a neuronal network model in which a pair of neurones are influenced by two common inputs. Cases where both inputs are point processes, and where one input is a continuous signal are considered. The analysis techniques in the frequency domain are seen to work well in either case, and the usefulness of partial coherence of order-1 and 2 is demonstrated. Some addition notes of the interpretation of partial coherence are also given and expanded in Appendix 2 and 4. Next, it is attempted to investigate the non-linear interactions between the discharge of a single Ia afferent and the response of a single motor unit based on a model neurone incorporating after-hyperpolarisation. The third-order cumulant density function is seen to be more sensitive than the cross-intensity and the time course of the after-hyperpolarisation is related to the trough that appears in the cumulant. This result leads to the possibility of deducing the time course of the after-hyperpolarisation obviating the use of invasive methods like intracellular recording.

Chapter 7 indicates some possible areas in the future work, namely: (1) further investigations of higher order parameters, (2) maximum likelihood approach to estimate model parameters and (3) Lanczos analysis of electric current flow in excitable cells. These are outlined in Chapter 7 as a conclusion of the present work.

Chapter 1

Introduction and Historical Notes

Chapter 1 Introduction and Historical Notes

The work of this thesis is primarily concerned with developing analytical techniques and computational procedures for the analysis of complex neuronal networks. The use of models of neuronal networks plays a key role in this project. In the study of real neuronal networks several kinds of signals may occur. In this thesis, we will be primarily concerned with signals that can be modelled as stochastic point processes, although the interaction between point processes and the type of continuous signals that occur in the analysis of dynamic systems will also be considered.

Stochastic point processes belong to a class of stochastic processes which concern the occurrence of events in time or space. Examples of stochastic point processes are vast: queues, neuronal electrical activities, heartbeats, population growth, accident or failure processes, radioactivity and many others. In contrast to the ordinary time series, where a process is represented by the magnitude of the process as a function of time, a point process may be completely characterised by the times of occurrence of the point events. Since in everyday life, data arises as both ordinary time series and point processes, the study of point processes may be considered in parallel with the study of ordinary time series. (See Brillinger 1978a for a comparative analysis of ordinary time series and point processes)

The techniques for the analysis of point processes are, in

many cases, similar to those used for ordinary time series (see for examples Barlett 1963a and Beutler and Leneman 1968). The methods of analysis are statistical in nature and may be divided into time and frequency domain; the time domain parameters usually have their frequency domain equivalence and vice versa. There are, however, situations in which unique techniques are applicable only to one type of domain but not to the other. In addition, a situation may arise where the processes involve a mixture of ordinary time series and point processes. In this case, hybrid parameters in both time and frequency domains are to be defined and the analysis techniques needed to be modified. The study of these forms part of the main theme of this thesis.

Neurophysiology is an area where the signals of interest are a rich combination of ordinary time series (such as excitatory post-synaptic potentials and length changes) and point processes (such as action potentials). The short duration of an action potential compared with the intervals between successive pulses provides the basis for considering the spike train as a realisation of a point process. Under the same experimental conditions, the pattern of firing of the action potentials would vary with the statistical (or average) properties unchanged. Hence the neurophysiological system may be consider as stochastic in nature. In addition, the system may be considered as stationary (short term) and this allows considerable simplification in the analysis techniques. These considerations suggest that the use of point process analysis techniques are appropriate in neurophysiology. A more detailed description of

these terms is given in Chapter 2.

In the experimental study of a biological system such as the neurophysiological system, it may be difficult sometimes to interpret the results due to the inherent complexity of the system. Several hypotheses may seem to be possible or no immediate interpretation can be made to explain a certain observation in the results. In these cases simulation can provide an invaluable guide to the interpretation through the investigation of a model with known structure and properties. Such an approach can facilitate the interpretation of results obtained from the unknown system. In this thesis, simulation studies are based on a model neurone and interconnected groups of model neurones. The properties of this type of model neurone have been investigated previously and were shown to be satisfactory in representing the properties of the real system (Halliday 1986). This model then forms the basic building unit of a network of the desired structure.

The main objectives of this thesis is to (1) investigate the analysis techniques and computational procedures for point processes and (2) to apply these techniques to the analysis of complex neuronal networks along with simulation studies. Original contributions have been made to (a) identify different patterns of spike trains with the aid of simulation, (b) to demonstrate, by simulation and analytically, how the coherence between the outputs of a single input, two-output neuronal model may reflect statistical properties associated with the common input and (c) to

investigate, based on simulation studies, the hypothesis that the time course of post-spike depression can be deduced from the third-order cumulant density function and (d) to demonstrate different aspects of point process analysis techniques through simulation studies and to show how the analysis techniques can extract useful information concerning the functional and structural aspects of the neurophysiological system.

A wide variety of examples of point processes are discussed in Lewis (1972a) and Snyder (1975). An extensive discussion with examples comparing ordinary time series and point process can be found in Brillinger (1978a). The fundamental theory and applications of ordinary time series can be found in monographs by Bloomfield (1976), Box and Jenkins (1970), Brillinger (1975d), Jenkins and Watts (1968) and Koopmans (1974). In the case of point processes the relevant theory can be found in Brillinger (1975a), Cox and Isham (1980), Cox and Lewis (1966), Daley and Vere-Jones (1988) and Lewis (1972).

1.1 A Historical Note on Point Process

While the frequency domain analysis of a signal may be said to have commenced in 1664 when Isaac Newton decomposed a light signal into separate components by passing the light through a glass prism, the earliest study of point processes began when J. Graunt (1620-1674) constructed life tables as an application of mathematics to the study of population. The table corresponds to the superposition of many independent point processes, each containing a single point at the time of death of an individual. For an early history describing this study see Westergaard (1968).

The Poisson point process was introduced over a long period of time. It has a Poisson counting distribution (hence its name) and is credited to de Moivre in 1718 and Poisson in 1837. Clausius (1858) in his studies on the kinetic theory of gas showed that the exponential distribution of intervals in a point process was related to the free path length of a gas molecule. In 1868, Boltzmann further derived the expression $\exp(-\mu t)$ for the probability of no randomly placed points in an interval of length t. Bateman (1910) showed that the numbers of particles from radioactive emissions in fixed time intervals satisfied a simple set of differential equations, and that the solutions to these equations were Poisson probabilities. Erlang, in his pioneering work, made extensive use of Poisson process in the studies of congestion problems in traffic systems and telephone systems. For a historical review, see Jensen (1948) and Haight (1967).

Another class of point processes with a long history of study is that of renewal processes. They are defined as stationary point processes where the interval between two successive events is independently distributed. The appropriate application of these processes results in a considerable amount of simplification since the probability density function of the intervals is sufficient to describe the process completely. The renewal process generalises the Poisson process in the sense that the interval density is not limited to exponential form. There has been extensive studies of general renewal theory with emphasis on the analytical problems involved (Smith, 1958, Feller, 1971). For a more applied accounts, see Cox (1962).

Recently, increasing attention has been drawn to the application of point process analysis techniques to neurophysiological problems. Point process analysis techniques have been found to be useful in assessing associations between neuronal signals and in the estimation of biologically meaningful parameters. Examples include Amjad (1989), Brillinger (1986, 1988a,b) and Halliday (1986) .

Chapter 2

Neurophysiological Background

Chapter 2 Neurophysiological Background

Neurophysiology is a branch of science concerned with how the elements of the nervous system function and work together. The aim of this chapter is to present a simplified account of some aspects of neurophysiology which are relevant to the discussions in the following chapters. A recurrent area of neurophysiology considered throughout this thesis is the neuromuscular system. The neuromuscular system may be defined loosely as all those parts of the nervous and muscular systems concerned with the initiation and control of movement and the maintenance of posture. Obviously the inherent nature and the kinds of data arising from the neuromuscular system determine the particular type of analysis techniques used. In this chapter, some features of the neuromuscular system which lead to the use of point process analysis techniques are discussed. This is followed by a simplified description of the organisation of the neuromuscular system and some of its elements. Finally, some findings related to the application of point process analysis techniques are discussed to illustrate the usefulness of the techniques.

2.1 Some Characteristics of Neuromuscular Systems related to the Point Process Analysis Techniques

Many biological systems have the important feature that under normal conditions they are acted upon by several inputs simultaneously, which in turn give rise to several outputs. The muscle spindle, an important element of the neuromuscular control

system which is thought to be responsible for the control of movement and maintenance of posture, is inherently multiple input and output. The muscle spindle, under normal conditions, is acted upon by continuous changes in the length of the parent muscle which it is attached to. In addition to this continuous length change, the output activity from the spindle is further modified by several other input processes in the form of nerve impulses. Figure 2.1.1 is an example illustrating how the output point process activity of a muscle spindle is affected by the various kinds of input conditions. A nerve impulse is a localised voltage change of approximately 100 mV in amplitude and 1 msec. in duration which occurs across the membrane surrounding the nerve cell body and axon. Nerve impulses are often referred to as 'action potentials' or, because of their relatively short duration, as 'spikes'. The short duration of action potentials, compared with the time intervals between successive pulses (see Figure 2.1.1), provides the basis for considering the spike trains as realisations of stochastic point processes and thus allowing point process analysis techniques to be applied. In the analysis of a muscle spindle, the neurophysiologist may want to characterise the input-output relationship of the muscle spindle based on the recordings of the input and output processes. In another example, the processes involved may not be directly related by a input-output relationship, but simply simultaneous recordings of some combination of spike trains and continuous signals obtained from cell bodies, axons, electroencephalograms (EEGs) etc. In this case, one might want to determine if these processes are related, and how the relation between any two may be

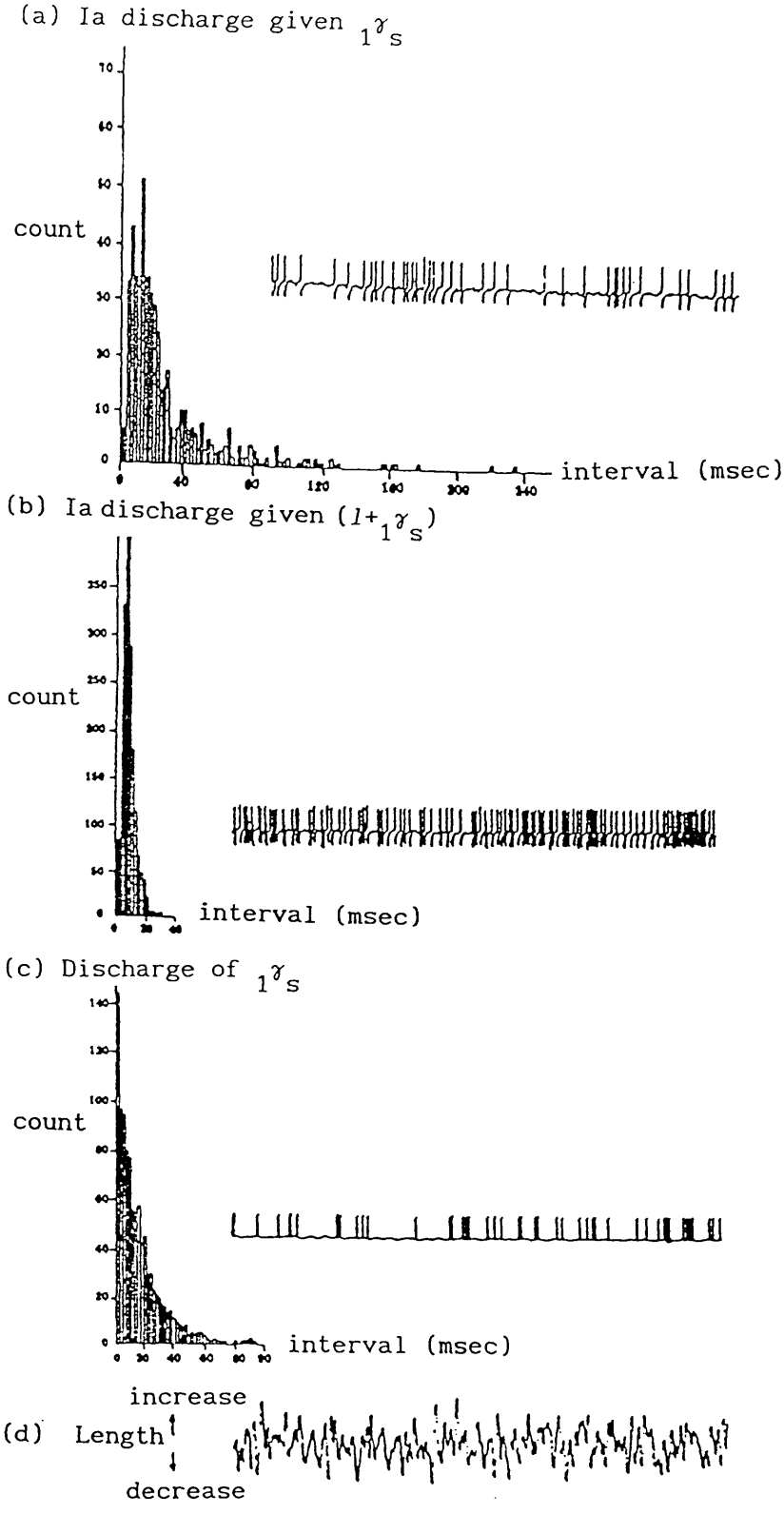

of a muscle spindle

Figure 2.1.1 Interval histogram of the Ia discharge subject to different input conditions. (a) Ia discharge in the presence of a static gamma input $_1\gamma_s$. (b) Ia discharge in the presence of $_1\gamma_s$ when a length change is also imposed on the parent muscle. (c) Static gamma input $_1\gamma_s$. (d) A section of the length changes in (b). The insert in each figure gives a sequence of the spikes of the corresponding discharge.

influenced by the other processes.

It has been found that some neuromuscular elements have non-linear features so that the application of linearised mathematical descriptions may not be adequate. For example there is evidence which shows that muscle spindles have significant amplitude-dependent and velocity dependent non-linearities (Chen and Poppele, 1978; Hasan and Houk, 1972; Hulliger et al, 1977a, b; Houk et al, 1981 and Matthews and Stein, 1969). In addition, the input, output relationships of an alpha-motoneurone has been found to be non-linear due to the presence of significant post-spike depression duration (Conway et al., 1989; Lau et al., 1989a).

The features of the neuromuscular system discussed above indicate that the analysis tools required by neurophysiologists should be flexible enough to tackle non-linear systems which involve multiple processes consisting a combination of point processes and continuous signals.

2.2 The Peripheral Nervous System

The neuromuscular control system consists of all parts of nervous and muscular systems concerned with the initiation and control of movement and the maintenance of posture. The system has been divided into peripheral and central parts on anatomical and functional grounds. At the level of the spinal cord, the peripheral nervous system is arranged in a sequence of repeating units. The components of the peripheral neuromuscular system at one segmental level of the spinal cord are illustrated in Figure 2.2.1.

There are several classes of nerve cells which lie within the spinal cord. One of these involves alpha-motoneurones which have long processes, called axons, innervating the load-bearing or extrafusal muscle fibres responsible for generation of forces or changes of length. The cell bodies of the alpha-motoneurones have diameters ranging from 25 to 100 μm and the axons are from 8 to 20 μm in diameter. The axons conduct nerve impulses, which travel at velocities in the range 50-120 m/sec., from the cell bodies to the extrafusal muscle fibres. The mean frequencies of action potentials generated by the nerve cell may vary from one pulse every few seconds to several hundred pulses per second. The fine branches of the alpha-motoneurone axon end on specialised areas of the extrafusal muscle called the 'motor endplate'. When a nerve impulse reaches the junction between the axon and the muscle fibre, a sequence of electro-chemical events occur which leads to the contraction of the load-bearing muscle fibres. The force of

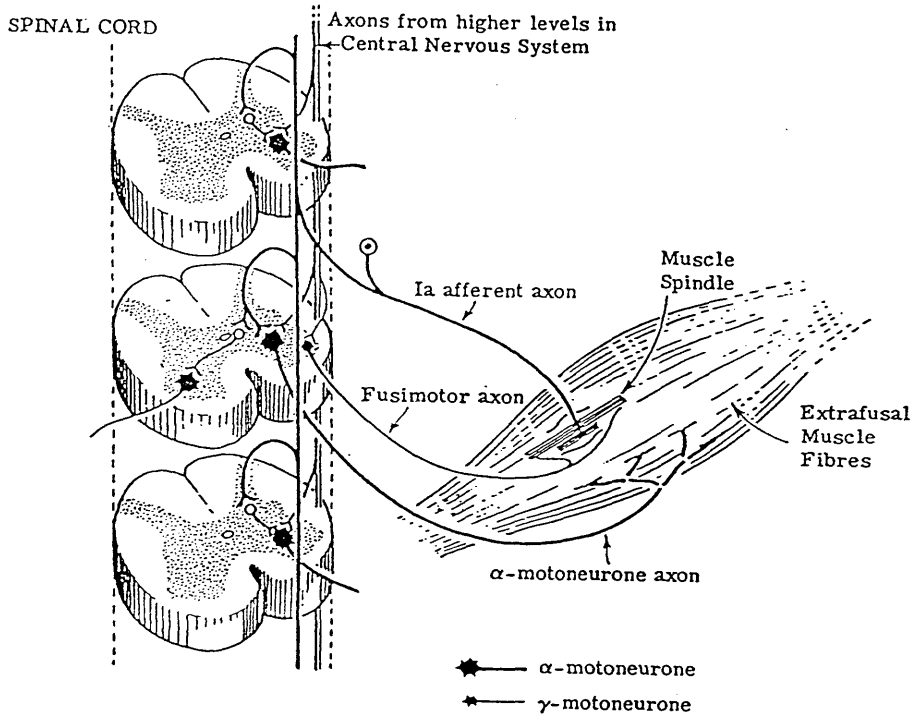

Figure 2.2.1 Diagrammatic representation illustrating some of the pathways connecting a muscle spindle and its parent muscle to the spinal cord. Some of the interactions between, and distribution of, the neuronal circuits within the spinal cord are also shown (see Rosenberg, et al., 1982). Note that a branch of the Ia afferent axon is feedback to the α-motoneurone that innervates the extrafusal muscle fibres.

the contraction of the entire muscle may be graded by increasing the number of active alpha-motoneurones associated with a muscle and by altering the frequency of the nerve impulses reaching the muscle over the axons of the alpha-motoneurones.

Once the axon of an alpha-motoneurone reaches a muscle, it divides into a number of fine branches. Each terminal branch innervates a single extrafusal fibre, and all of the extrafusal fibres innervated by one alpha-motoneurone lie within the same muscle. The alpha-motoneurone together with all the extrafusal fibres that it innervates is called a 'motor unit'. The number of motor units within a muscle and the size of a motor unit, which depends on the number of extrafusal fibres innervated by a particular alpha-motoneurone, are closely related to the function of that muscle. Motor units may be related to the incremental units of force that a muscle can develop. Muscles concerned with the control of delicate movements have small motor units and can generate the small increments of force required for these movements, whereas muscles with large motor units produce large increments of force and may function simply to maintain a fixed attitude or posture.

Buried within the extrafusal muscle fibres are a number of physiological transducers, or 'receptors', that respond to imposed length changes or force acting on the parent muscle. These receptors are known as muscle spindles. They transmit pulse coded information as sequences of spikes via the sensory nerves to the groups of nerve cells lying within the spinal cord. The junctions

at which the sensory axons make contact with these cells are called 'synapses'. Each sensory nerve divides into a number of branches after entering the spinal cord and may make synaptic contact with a large number of nerve cells over several segmental layers in the spinal cord. Conversely, each nerve cell in the spinal cord may receive information from a large number of receptors associated with different muscles. The train of action potentials travelling along the axon releases a sequence of electro-chemical events at the synapses between the sensory axon and the nerve cell within the spinal cord which then modify the on-going activities of the nerve cell.

In addition, nerve cells within the same segmental layer may interact with each other and interactions between different segmental layers may also exist. The segmental and intersegmental circuits in the spinal cord are further acted upon by axons arising from nerve cells at higher levels of the central nervous system. It is possible for a single alpha-motoneurone to be affected by up to 10000 different inputs. An introduction to the organisation of the spinal cord can be found in Shepherd (1974), and a detailed review of this along with the properties of the spinal cord and its interconnections is given in Burke and Rudomin (1977).

2.3 The Neurone

Although there are many kinds of neurones with significant structural and functional differences, four basic components can be identified in a neurone (see Figure 2.3.1). (1) The axon is the element that links the neurone to a neighbouring neurone or peripheral systems. (2) The synapses are the junctions between the incoming axon and the soma (or cell body) where electro-chemical reactions take place. The effectiveness of an input depends on its position of innervation. (3) The soma or cell body along with the dendrites are the processing elements of the cell. (4) The dendrites are hair-like processes emanating from the soma. Note that synapses can also occur at dendrites. These four components are discussed in more details in the following sections.

2.3.1 The Axon

The axon is surrounded by a cylindrical semi-permeable membrane and contains axoplasm, and is in turn surrounded by extra-cellular fluid. The internal and external fluids of the axon are composed mainly of ionised potassium chloride and sodium chloride; with the concentration of potassium ions inside the axon much higher than that outside. This leads to a concentration gradient across the membrane which causes a movement of the excess potassium ions to the outside. This diffusion of ions disturbs the charge balance and results in an electric field which opposes the 'chemical field'. Equilibrium is attained when the two forces are equal, resulting in a potential difference across the

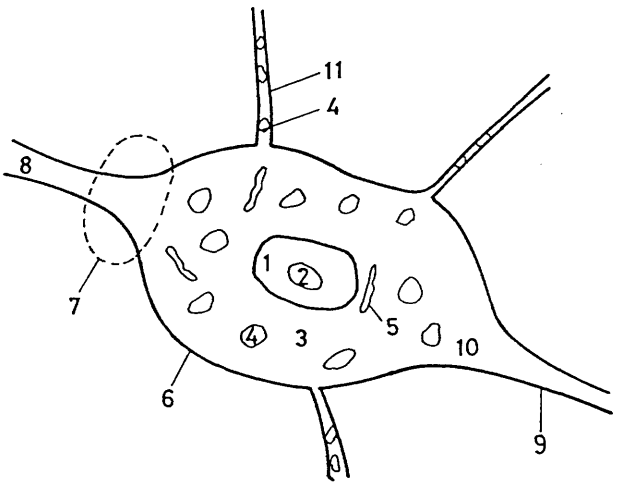

1. Nucleus
2. Nucleolus
3. Soma
4. Nissl body
5. Ribosome
6. Cell membrane
7. Synaptic region
8. Incoming axon
9. Outgoing axon
10. Axon Hillock
11. Dendrite

Figure 2.3.1 Diagrammatic representation of a typical nerve cell illustrating the basic components.

membrane, the inside being more negative. This negative potential compared to the surrounding fluid is called the resting potential, and in the squid giant axon, Loligo, is about -70 mV.

Equilibrium is disturbed by either changing the extracellular ionic concentration or externally applying an electrical potential gradient across the membrane. If this change is such that it causes the inside of the axon to be more negative, it is called hyperpolarisation; otherwise it is called depolarisation. If the depolarisation is so large that the membrane potential exceeds a certain value, known as the threshold, the potential across the stimulated part shoots up and then returns to the resting level (see Figure 2.3.2). This leads to an action potential. The change in membrane potential excites the adjacent parts of the membrane and the phenomenon propagates along the axon by contiguous stimulation, the direction of propagation is usually away from the neurone cell body. The waveform has a characteristic shape and is known as action potential. When an action potential has been generated, the region of stimulation cannot be excited for a short time thereafter. This property is called refractoriness. Immediately following an action potential, the region cannot for some time generate another, with any strength of stimulus. This is the absolute refractory period and lasts for about 1 msec. After this, there is a period of about 3 msec. when excitation is possible, but only with a very powerful stimulus. This is the relative refractory period.

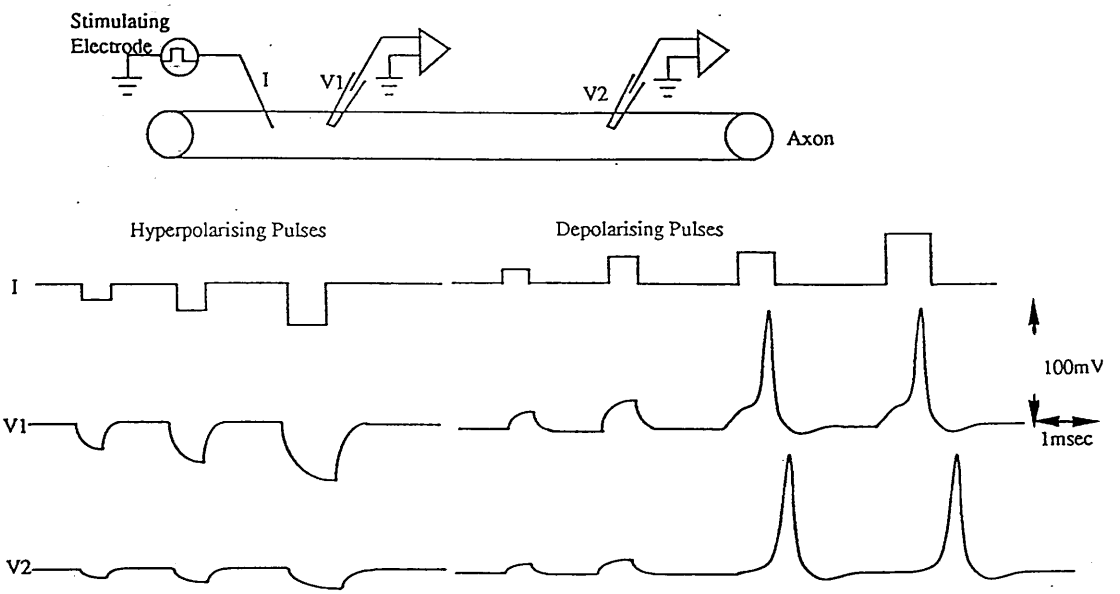

Figure 2.3.2 Voltage recorded intracellularly in an axon in response to current pulses. All potentials are measured relative to the extracellular fluid as earth and in the absence of a current pulse the inside has a potential of -70 mV relative to the extracellular fluid. Pulses which make the potential across the membrane more negative are termed hyperpolarising pulses and those which make it more positive are termed depolarising pulses. Once the depolarising pulse's magnitude exceed that of the threshold the voltage across the membrane shoots up and this is termed an action potential, nerve impulse or spike.

2.3.2 The Synapse

Interactions between neurones take place at the synapse where the activity of one neurone is transferred to another by the axon. The terminal end of an axon broadens into a bulge called the bouton and lies adjacent to the cell membrane or a dendrite of the soma (see Figure 2.3.3). Generally the bouton does not make physical contact with the membrane and there is a cleft that separates the two. Small packets called vesicles are found in the bouton which contain a chemical known as the transmitter; the type of transmitter depends on the kind of junction. When an action potential arrives at the bouton, a transmitter is released from the vesicles and the transmitter molecules modify the permeability of the membrane to different ions. If the resulting change in the potential in the soma or dendrite is positive, it is called an excitatory post-synaptic potential (EPSP); otherwise it is called an inhibitory post-synaptic potential (IPSP). In the absence of an input spike, the membrane potential tends to decay to the resting level which is below the threshold.

2.3.3 The Soma

When post-synaptic potentials are induced at several points along the soma due to successive arrivals of action potentials, the resulting membrane potential may be the linear sum of the individual potentials. This phenomenon is known as spatial or temporal summation. As in the axon, recovery effects keep taking place in the absence of inputs, ie. the membrane is 'leaky'. When

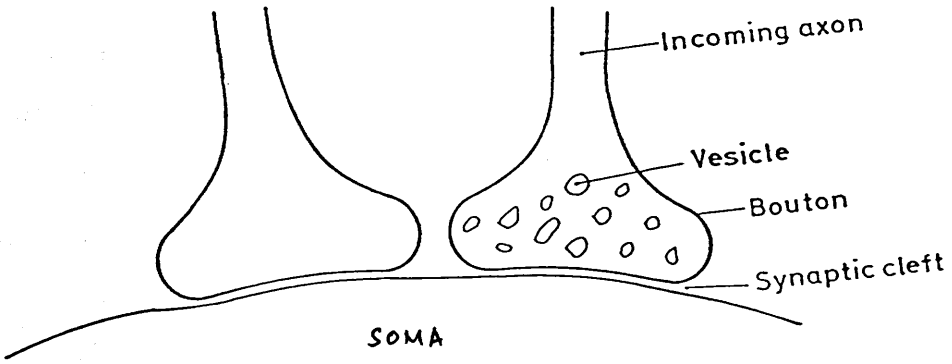

Figure 2.3.3 Schematic representation of two synapses at the junctions of two axons and a nerve cell. The boutons at the terminal end of the axons do not make physical contact with the membrane. The small packets, vesicles, found in the bouton contain a chemical known as the transmitter which varies with the kind of junction. This transmitter acts as a mediator in the transfer of activity from the axon to the soma.

the integrative effect exceeds the threshold the neurone 'fires', sending an action potential along its axon. The origin of the axon at the soma, known as the hillock (see Figure 2.3.1), has a lower threshold than the other parts of the membrane and is thus the impulse generating region of a neurone. Like the axon, the soma also has the properties of decreased excitability following the generation of an action potential. In the case of an alpha-motoneurone, this property is known as the after-hyperpolarisation and its period is correlated with the upper and lower frequency limits of the firing of the motoneurone and the type of muscle innervated. Hence after-hyperpolarisation may be thought to play an important role in the control of repetitive firing and in characterising the function of the alpha-motoneurone.

2.3.4 The Dendrites

These hair-like processes protruding from the soma may be numerous and thus present an increased area of contact to incoming axons, each of which may branch out to form many synapses. The role of dendrites in the firing of the cell is still unclear. Action potentials can also arise in dendrites but the behaviour of dendrites is highly non-linear and is not understood clearly but are thought to possess computational properties.

2.4 Some Examples of the Application of Point Process Analysis Techniques

This section illustrates the usefulness of the point process analysis technique through the application to some elements of the neuromuscular system. A tenuissimus muscle spindle and a single Ia-afferent and motor unit from soleus and lateral gastrocnemius muscle are considered. The theories and background to the techniques used are explained in the later chapters.

2.4.1 Application to an Isolated Muscle Spindle

The following examples are based on experiments involving cat tenuissimus muscle spindles where the primary (Ia) and secondary (II) endings were isolated in dorsal root filaments. Figure 2.4.1 illustrates the application of both cross-intensity (Figure 2.4.1a, b) and coherence (Figure 2.4.1c, d) to the same data set to provide a comparison of the effects that each of two static fusimotor axons has alone on the response of the same Ia sensory ending during concurrent and independent stimulation of both fusimotor axons with the parent muscle held at a fixed length. In this example the two cross-intensities differ both in shape and in the magnitude of the peak. The coherence confirms this difference in the strength of association, but also allows a further characterisation of the differences between the effects of the two fusimotor axons on the same Ia ending. The coherences (Figure 2.4.1c, d) suggest that $_2\gamma_s$ has a stronger effect on the Ia ending than $_1\gamma_s$ at each frequency over a broad range of

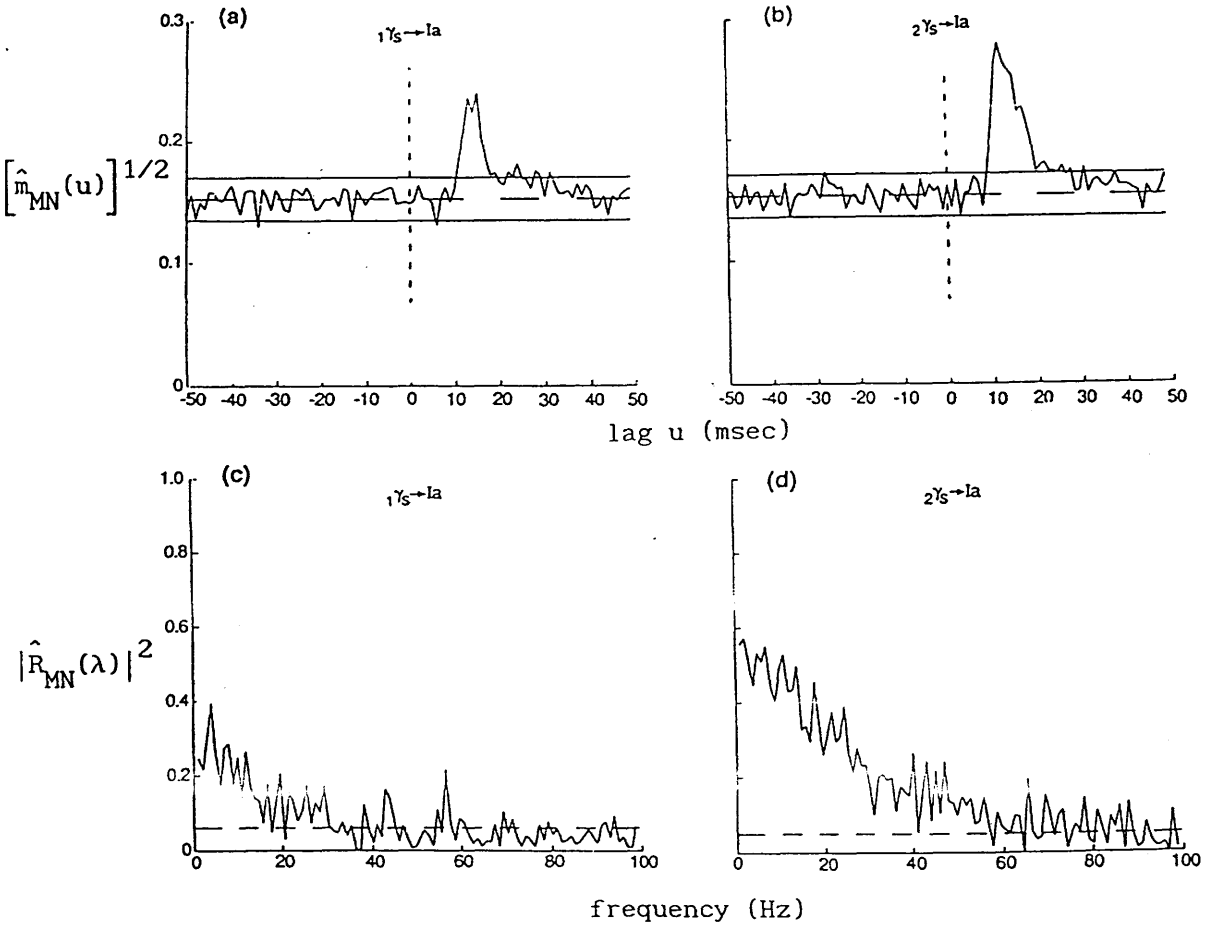

Figure 2.4.1 Comparison of (a,b) the square-root of the estimated cross-intensity functions with (c,d) the estimated coherences of the response of a muscle spindle Ia sensory ending to concurrent and independent stimulation of two static fusimotor axons denoted as $_1\gamma_S$ and $_2\gamma_S$. The fusimotor axons were stimulated for periods of 60 seconds with sequences of pulses having an exponential distribution of intervals. In (a,b) the horizontal dashed line is the asymptotic value of the square-root of the estimated cross-intensity function equal to the square-root of the mean rate of the Ia discharge. The horizontal solid lines represent an approximate 95% confidence interval for the value of the cross-intensity function for any specific value of the lag u under the assumption that the two processes are independent. In (c,d) the horizontal dashed line represents the upper level of the approximate 95% confidence interval for the coherence under the hypothesis that the two processes are independent. (Rosenberg et al. 1989)

frequencies. A quantitative measure of this difference, represented by the difference between the inverse hyperbolic tangent of the respective coherency, is shown in Figure 2.4.2. The difference plot suggests that the two coherences exhibit a small but significant difference over the range from 0 to about 20 Hz. Over this range of frequencies, $_2\gamma_s$ is more strongly coupled to the Ia ending than $_1\gamma_s$. Above 20 Hz, the difference between the two coherences is not significant.

The second example illustrates the application of partial coherence. The data is taken from the responses of a primary (Ia) and secondary (II) ending from the same muscle spindle during stimulation of a static fusimotor axon innervating the muscle spindle (Gladden et al., unpublished observations). In the absence of fusimotor stimulation, the discharge of the Ia and II endings are uncorrelated, whereas in the presence of fusimotor stimulation they are strongly correlated as illustrated in Figure 2.4.3c. The partial coherence between the responses of the Ia and II endings taking into account the presence of the fusimotor input shows that the coupling between these responses is due entirely to the presence of fusimotor stimulation (Figure 2.4.3d).

2.4.2 Application to Ia Afferent/Motor Unit Interactions

Analysis on data obtained from recordings of single motor unit electromyogram (EMG) and identified single Ia afferents from the same muscle were performed (Conway, Halliday and Rosenberg, 1991, to be published). Second-order interactions were examined

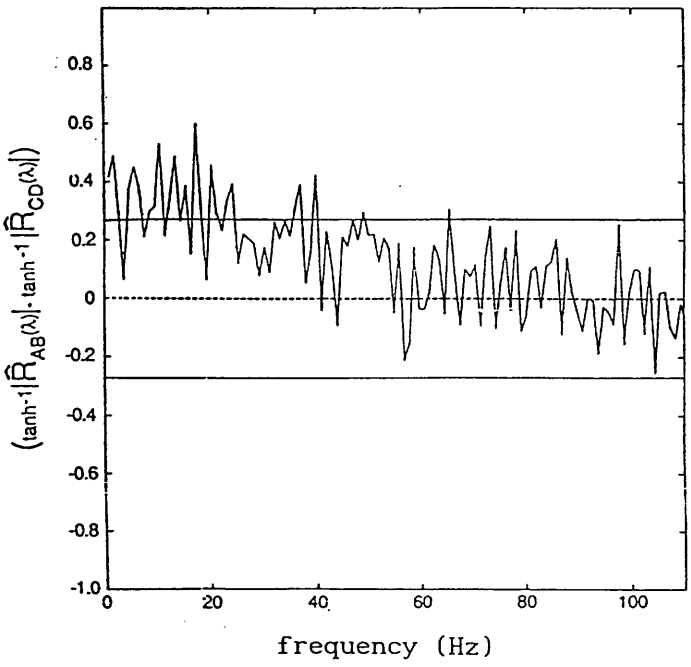

Figure 2.4.2 Graph of the difference of the $\tanh^{-1}$ of the moduli of the coherencies corresponding to the estimated coherences shown in Figure 2.4.1c, d along with the approximate 95% confidence interval - solid horizontal lines - for the hypothesis that the two moduli are equal at any given frequency λ. Points lying outside this interval indicate frequencies where the difference between the strength of association of the pair of processes may plausibly be non-zero. (Rosenberg et al 1989)

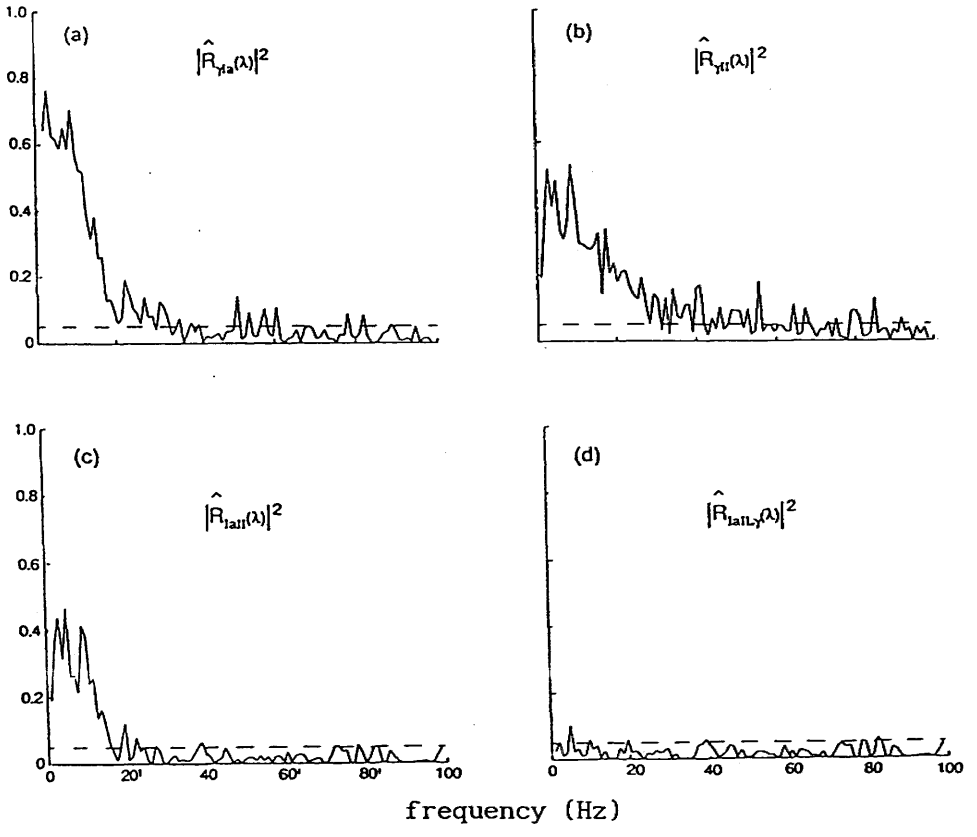

Figure 2.4.3 (a)-(c) The estimated pairwise coherences between a fusimotor input and the responses of Ia and II sensory endings from the same muscle spindle. (d) The estimated partial coherence between the responses of the Ia and II endings taking into account the presence of the static fusimotor input. The static fusimotor axon was stimulated for 60 seconds with a sequence of pulse having an exponential distribution of intervals. The horizontal dashed line in each panel represents the upper level of an approximate 95% confidence interval for the coherences under the assumption that the two processes are independent. (Rosenberg et al 1989)

and four types of interactions were identified based on second-order cross-intensity.

Two different interactions between a Ia afferent and a motor unit may be detected during simultaneous recordings from in-continuity Ia-afferents and single motor-units. One is the presence of a central interaction between the afferent and the motoneurone, and the other is the peripheral interaction between the motor unit and the muscle spindle. In a recording from the Ia afferent/motor unit pair, both or neither of these interactions may be present. Hence a total of four modes of interactions between the motor unit and the Ia-afferents is possible. The four patterns, as revealed by the second-order intensities, are depicted in Figure 2.4.4. Type I (Figure 2.4.4a) refers to Ia afferent/motor unit pairs where no second-order interactions were present. Type II (Figure 2.4.4b) is characterised by a strong motor unit to Ia afferent interaction as indicated by the significant depression in the estimated cross-intensity for negative values of lag u. This depression is attributed to an unloading of the muscle spindle by the twitch initiated by the motor unit EMG spike. In Type III (Figure 2.4.4c), both Ia afferent to motor unit and motor unit to Ia afferent interactions were present. The sharp peak to the right of the origin in the estimated cross-intensity illustrated in Figure 2.4.4c occurs at a lag u corresponding to the latency (uncorrected for conduction delays) in a monosynaptic pathway between the Ia afferent and the motor unit, whereas, the trough occurring for negative values of lag u (as in Figure 2.4.4b) corresponds to the unloading of the

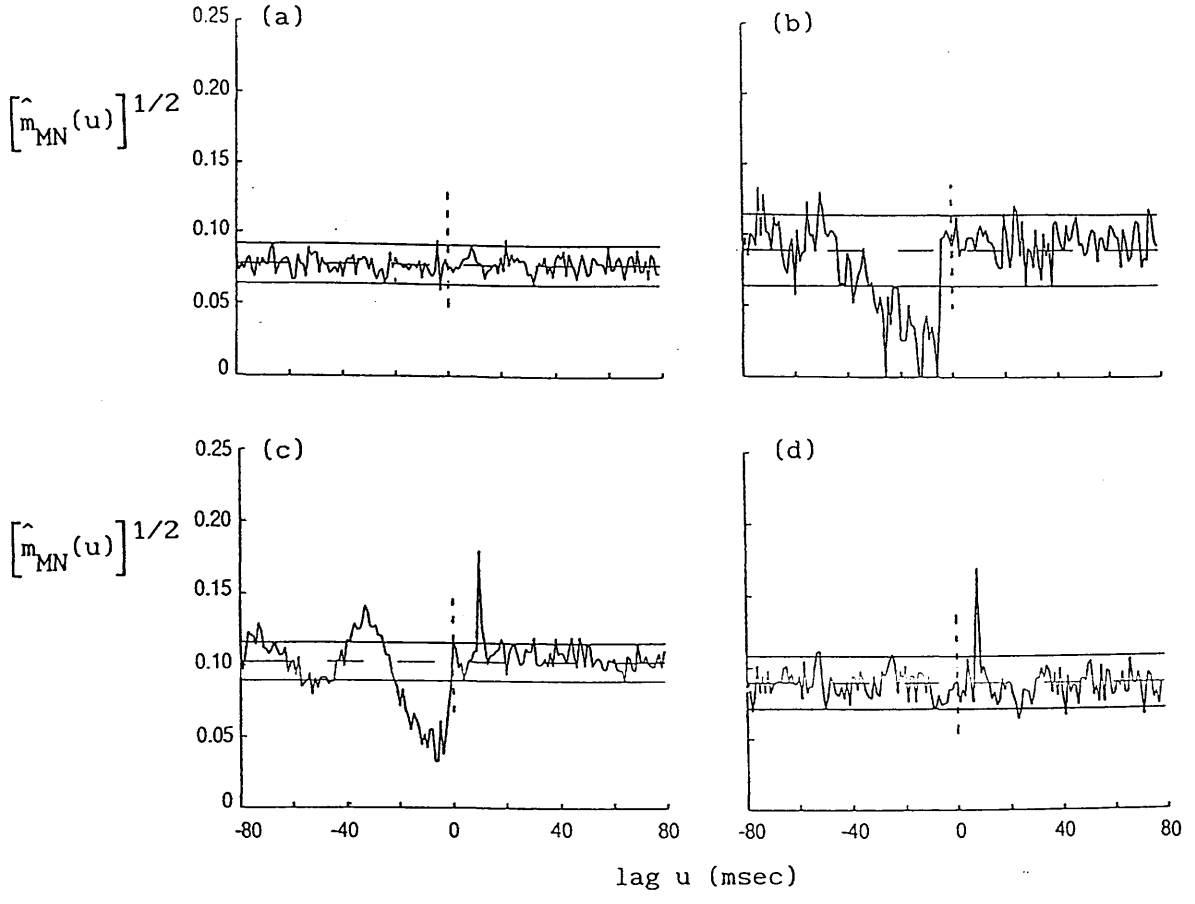

Figure 2.4.4 Square root of the estimated cross-intensity function computed between the spontaneous discharge of a single Ia afferent recorded in-continuity with the spinal cord, and the discharge of a single motor unit from the same muscle as the afferent. Four types of interactions are characterised by the second-order cross-intensity estimates (a) Type I: no significant interaction between afferent and motor unit, (b) Type II: peripheral interaction between motor unit and muscle spindle, (c) Type III: both a central Ia afferent motoneurone interaction and a peripheral motor unit muscle spindle interaction are present, and (d) Type IV: only a central Ia afferent/motor unit interaction is present. The solid horizontal lines in each panel represent approximate 95% confidence intervals under the hypothesis that the two processes are independent. The horizontal dashed line is the asymptotic value of the estimated cross-intensity function, and is equal to the square root of the mean rate of the motor unit discharge.

muscle spindle by the motor unit twitch. Type IV (Figure 2.4.4c) were defined as second-order interactions where Ia afferent/motor unit pairs displayed only a central interaction which was consistent with a monosynaptic pathway.

Chapter 3

A Summary of the Theories of Linear Analysis for Point Processes

Chapter 3 A Summary of the Theories of Linear Analysis for Point Processes

3.1 Introduction

Just as there are several different ways of characterising an ordinary time series - Brillinger (1978a) gives six - there are various approaches to the theory of point processes and to characterising these processes. The choice of definition or representation depends on the particular need of a given problem. While in ordinary time series a signal may be defined by the magnitude of the signal as a function of time, a point process M may be defined (1) in terms of the generalised function $X_M(.)$, ie.

$$X_M(t) = \sum_{k=1}^{m} \delta(t-t_k) \qquad (3.1.1)$$

where $\delta(.)$ is the Dirac delta function and t_k $(k=1,2,..,m)$ are the times of occurrence of the M events. The Dirac delta function $\delta(u)$ may be considered as a rectangular pulse with a width of du $(du \rightarrow 0)$ and an area of one unit situated at u=0. (2) Alternatively, a point process may be defined by a counting measure denoted as

$$M(t) = \#\{t_k : 0 < t_k \leq t\} \qquad (3.1.2)$$

where $t>0$ and $\#\{A\}$ indicates the number of elements in the set A. (3) By differentiating expression (3.1.2), differential increments of process M is obtained as

$$dM(t) = M(t+dt)-M(t) \qquad (3.1.3)$$

which gives the number of events in a small interval (t,t+dt]. It can be seen that $X_M(t)$ and dM(t) are related by

$$dM(t) = X_M(t)dt \qquad (3.1.4)$$

The idea of the three definitions is depicted in Figure (3.1.1).

The last definition (3.1.3) has two advantages: (1) it is convenient in defining a number of point process quantities, and (2) because a discretised realisation of a point process is readily obtained by setting dt as the sampling interval. On the other hand, the first definition (3.1.1) is useful in developing hybrid parameters in the situation where there are ordinary time series as well as point processes. In all three cases, a point process is defined by the sequence of the times of occurrence t_k (k=1,2,..,m). Assuming that the point process is stochastic in nature and that it is digitised every small time interval dt, a stochastic point process may then be defined as a random, non-negative, integer-valued measure (Brillinger 1975). In our application, this measure corresponds to the time of occurrence of an action potential sampled at a frequency of 1 kHz. The details of the experimental and computational aspects may be found in Chapter 5.

Generally, M(t) may be used to denote a r vector-valued point process, ie.

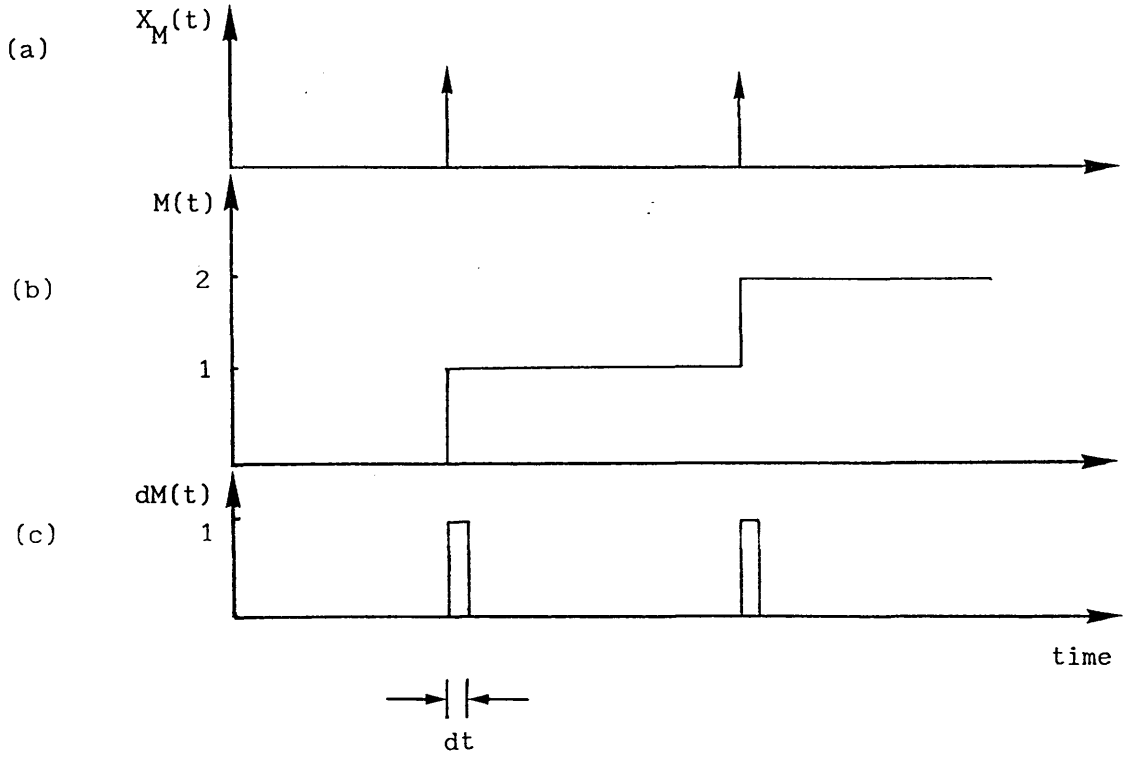

Figure 3.1.1. Diagram to illustrate the definition of a point process based on (a) the analogy with the ordinary time series as a sequence of Dirac delta functions (b) the counting variate M(t) which represents the number of events in the time interval (0,t] and (c) the differential increments dM(t) which takes a value of 1 or 0 depending on whether an event has occurred between the time interval (t,t+dt].

$$M(t) = \{M_1(t), M_2(t), .., M_r(t)\} \qquad (3.1.5)$$

In this thesis, the particular class of point processes considered are assumed to obey the assumptions of stationary, mixing and orderliness. These assumptions are discussed in sections (3.1.1-3).

3.1.1 Stationarity

The quantitative idea of stationarity for a point process is basically the same as for stochastic processes in general, ie. the statistical properties of the process are unaffected by a translation of the time axis. Formally speaking, a point process is completely stationary (or strictly stationary) if all the joint probability distributions are time invariant. However, the full power of complete stationarity is seldom required and other forms of stationarity have been defined. A point process is simply stationary if the probability distribution of the number of events in the interval $(t,t+h]$ is the same as that of $(t+u,t+u+h]$, where $t,h,u>0$. A point process is weakly stationary, or second-order stationary, if in addition to being simply stationary, the second-order joint probability distribution between the number of events in the intervals $(t,t+h]$ and $(t+u,t+u+h]$ is the same as that of between $(t+v,t+v+h]$ and $(t+u+v,t+u+v+h]$ where $t,u,v,h>0$. Put another way, the second-order joint probability depends only on the interval between the two events. In this thesis, second-order stationarity is assumed for the processes being analysed.

Stationarity has important implications in the analysis of stochastic processes. Besides the immediate implication of an arbitrary time origin, the assumption of stationarity provides a basis for the Fourier or harmonic analysis of point processes. The argument can be found in Brillinger (1975d) p. 7.

3.1.2 Mixing

A second assumption concerning the class of point processes of interest is that they have a short span of dependence. If a point process is defined using expression (3.1.3), the differential increments dM(t) and dM(t+u) become statistically independent as u becomes large. This is known as the mixing condition.

Formally, the mixing condition may be divided into two categories. Given the r-vector valued stationary point process $M=[M_1,M_2,..M_r]$ with all of whose cumulant density functions exist (cumulant density function is discussed in the later sections, it is adequate here to note that it is analogous to covariance functions in ordinary time series), then the strong mixing condition is defined as (See Brillinger, 1975d)

$$\int_{-\infty}^{\infty}\cdots\int_{-\infty}^{\infty}\{1+|u_j|^{l}\}\,|q_{a_1..a_k}(u_1,..,u_{k-1})|<\infty \qquad (3.1.6a)$$

for $l\geq 0$, j=1,..,k-1 and any k tuple $a_1,\ldots,a_k$ when k=2,3,... In expression (3.1.6a), $q_{a_1..a_k}(.)$ is the cumulant density function of order-k. A less stringent condition occurs when $l=0$, ie.

$$\int_{-\infty}^{\infty}\cdots\int_{-\infty}^{\infty} |q_{a_1..a_k}(u_1,..,u_{k-1})| < \infty \qquad (3.1.6b)$$

The condition implied by expression (3.1.6b) means that the processes involved are more associated with each other compared with the condition implied by expression (3.1.6a). In fact, condition (3.1.6a) implies condition (3.1.6b). However the converse is not true.

3.1.3 Orderliness

An orderly point process is one with isolated events. Mathematically,

$$Pr\{M(t+h)-M(t)>1\} = o\{h\} \qquad (3.1.7)$$

where Pr{A} denotes the probability for A to happen and o{h} is a standard mathematical symbol defined such that $o\{h\}/h \to 0$ when $h \to 0$. This assumption is satisfied in the case of action potentials since a neurone has the physical/chemical determined property that once it has generated an action potential it can not produce a second one until a small but finite period of time, called the absolute refractory period, has elapsed. The period may be in the order of a few milliseconds and limits the rate at which a neurone may generate action potentials.

Under this assumption, the differential increment of the process has the properties,

$$dM(t) = \begin{cases} 1 & \text{if an event occurred in } (t, t+h] \\ 0 & \text{otherwise} \end{cases} \qquad (3.1.8)$$

where $h \longrightarrow 0$.

3.2 Univariate Point Process Parameters

3.2.1 Time Domain Analysis

For a point process M satisfying the assumptions outlined in sections (3.1.1-3), the product density of order-1, P_M, may be defined as

$$P_M dt = E\{dM(t)\} \qquad (3.2.1)$$

where "E" denotes "expected value of" and $dt \rightarrow 0$. P_M is also known as the mean intensity. Under assumption (3.1.3), P_M may be interpreted as

$$P_M dt = Pr\{dM(t)=1\} \qquad (3.2.2)$$

This quantity is a principal descriptor of a point process since it is effectively the mean rate of the process M. Note that it is independent of time t due to the assumption of simple stationarity.

The second-order product density at lag u, $P_{MM}(u)$, may be defined as

$$P_{MM}(u)dudt = E\{dM(t)dM(t+u)\} \qquad (3.2.3)$$

where $du,dt \rightarrow 0$. $P_{MM}(u)$ may be interpreted as

$$P_{MM}(u)dudt = Pr\{dM(t)=1 \text{ and } dM(t+u)=1\} \qquad (3.2.4)$$

and gives a measure of the probability that two events are separated by a time interval u. Expression (3.2.3) and (3.2.4) are based on the assumption of second-order stationarity and orderliness. Note that at u=0, expression (3.2.3) becomes

$$P_{MM}(u)dudt\Big|_{u=0} = E\{[dM(t)]^2\} \qquad (3.2.5)$$

Now, dM(t)=1 if an event has occurred in (t,t+h] and dM(t)=0 otherwise. In any case, $dM(t)=[dM(t)]^2$. Hence

$$P_{MM}(u)dudt\Big|_{u=0} = E\{dM(t)\} = P_M dt$$

which gives

$$P_{MM}(u)\Big|_{u=0} = P_M/du \longrightarrow P_M\delta(u) \qquad (3.2.6)$$

where $\delta(.)$ is the Dirac delta function.

Under the mixing condition, ie. dM(t) and dM(t+u) become dependent of each other as u becomes large, it follows that

$$\lim_{u\to\infty} P_{MM}(u) = P_M^2 \qquad (3.2.7)$$

Another important function which describes the second-order properties of a stationary point process is the auto-intensity function $m_{MM}(u)$. It is defined as

$$m_{MM}(u)du = E\{dM(t+u) \mid dM(t)=1\} \qquad (3.2.8)$$

where du$\rightarrow$0 and "|" denotes "given". Using similar arguments as for $P_{MM}(u)$, $m_{MM}(u)$ may be interpreted as

$$m_{MM}(u)du = Pr\{dM(t+u)=1 \mid dM(t)=1\} \qquad (3.2.9)$$

This provides a measure of the probability for an M event to occur given that another M event has occurred u time units earlier. From the definition of conditional probability, it follows that expression (3.2.9) may be written as

$$m_{MM}(u) = P_{MM}(u)/P_M \qquad (3.2.10)$$

In addition, as u becomes large, we have

$$\lim_{u\rightarrow\infty} m_{MM}(u) = P_M \qquad (3.2.11)$$

Expression (3.2.11) suggests that for large values of u, the function $m_{MM}(u)$ would fluctuate around the mean rate of the process M until it eventually settles to the value P_M.

The second-order cumulant density function at lag u, $q_{MM}(u)$, is defined as

$$q_{MM}(u)\ dudt = cov\{dM(t),dM(t+u)\} \qquad (3.2.12)$$

where cov{a,b} denotes the covariance of a and b. It can be seen

that the cumulant density function is analogous to the covariance function in the case of ordinary time series. In terms of product density functions, $q_{MM}(u)$ can be expressed as

$$q_{MM}(u) = P_{MM}(u) - P_M^2 \qquad (3.2.13)$$

This result follows immediately from expressions (3.2.1), (3.2.3) and (3.2.12).

When lag $u \to 0$, it follows from expressions (3.2.6) and (3.2.13) that

$$\lim_{u \to 0} q_{MM}(u) = P_M \delta(u) \qquad (3.2.14)$$

The singularity of $q_{MM}(u)$ at $u \to 0$ plays an important role in the auto-spectrum of a point process. As will be shown later, this causes the spectrum of a point process to tend to a non-zero asymptotic value as the frequency becomes large, which marks a major distinction between the spectrum of an point process and that of an ordinary time series.

From expression (3.2.7) and (3.2.13), it can be seen under the mixing condition that

$$\lim_{u \to \infty} q_{MM}(u) = 0 \qquad (3.2.15)$$

This suggests that the second-order cumulant density function may be considered as a measure of association between pairs of spikes.

In practice, a value of 0 indicates independence, a positive value indicates an excitatory effect due to the earlier spike whereas a negative value indicates an inhibitory effect due to the earlier spike.

A final point to note is that all the three density functions $P_{MM}(u)$, $m_{MM}(u)$ and $q_{MM}(u)$ are even functions in u, ie. they are all symmetrical about the y-axis. In the next section (3.2.2), it will be seen that the power spectrum of a process M may be defined as the Fourier transform of the cumulant density function. From the properties of Fourier-Stieltjes transform of an even function, it can be deduced that the power spectrum of a point process is an even and real function.

3.2.2 Frequency Domain Analysis

A fundamental parameter of a stationary point process is the power spectrum. It can be defined in two ways : (1) The Fourier transform of the cumulant density function (Barlett, 1963a, Brillinger ,1974a, b) or (2) It may also be defined in terms of the periodogram of the process (Brillinger, 1972, 1974a, b). The former definition is analogous to the Wiener-Khintchine theorem in the case of ordinary time series. Both definitions are asymptotically equivalent (see for example Otnes and Enochson, 1978 p 317).

Suppose M is a stationary point process satisfying the conditions of orderliness and mixing. Under the mixing condition (3.1.6b),

$$\int_{-\infty}^{\infty} |q_{MM}(u)|\, du < \infty \qquad (3.2.16)$$

(Brillinger, 1975d). This implies the existence of the auto-spectrum of the process M, $f_{MM}(u)$, which is defined as the Fourier transform of $q_{MM}(u)$, ie.

$$f_{MM}(\lambda) = (1/2\pi) \int_{-\infty}^{\infty} \exp(-i\lambda u) q_{MM}(u) du \qquad (3.2.17)$$

One important way in which the auto-spectrum of a point process differs from that of an ordinary time series follows from the Riemann-Lebesque lemma (Katznelson, 1968; Papoulis, 1962) which states that for an function g(x) which does not consist of singular points and vanishes for large x, then

$$\lim_{|\lambda| \to \infty} \int_{-\infty}^{\infty} \exp(-i\lambda u) g(u) du = 0 \qquad (3.2.18)$$

Hence from expressions (3.2.14) and (3.2.17), since the cumulant density function $q_{MM}(u)$ consist of a Dirac delta function at $u \to 0$, it follows that

$$\lim_{|\lambda| \to \infty} f_{MM}(\lambda) = P_M/2\pi \qquad (3.2.19)$$

In the case of ordinary time series, the spectrum of any realistic signals would go to zero for large λ. However, the auto-spectrum is similar to that of an ordinary time series in that it is a

symmetrical and non-negative function of λ as can be seen in expression (3.2.17).

The inverse relationship to the definition (3.2.17) may be provided by

$$q_{MM}(u) = \int_{-\infty}^{\infty} \exp(+i\lambda u) f_{MM}(\lambda) d\lambda \qquad (3.2.20)$$

The second definition of the auto-spectrum of a point process involves the periodogram $I_{MM}^{(T)}(\lambda)$ which is defined as the modulus squared of the finite Fourier-Stieltjes transform of the process, ie.

$$I_{MM}^{(T)}(\lambda) = (1/2\pi T) d_M^{(T)}(\lambda) \overline{d_M^{(T)}(\lambda)}$$

where

$$d_M^{(T)}(\lambda) = \int_0^T \exp(-i\lambda t) dM(t) \qquad (3.2.21)$$

In expression (3.2.21), T is the record length and the overbar "——" denotes a complex conjugate quantity. Now the power spectrum can be defined as:-

$$f_{MM}(\lambda) = \lim_{T\to\infty} E\{I_{MM}^{(T)}(\lambda)\} \qquad (3.2.22)$$

In words, the power spectrum may be defined as the expected value of the periodogram as $T\to\infty$. This suggests that the power spectrum may be estimated from the periodogram. In fact, in terms of computational efficiency, the second definition is preferred in the estimation of power spectrum. The details of the estimation

procedures can be found in Chapter 4.

3.3 Bivariate Point Process Parameters

3.3.1 Time Domain Analysis

Time domain quantities for bivariate point process are useful in assessing timing relations between the two processes. Suppose M and N are two point processes that satisfy assumptions (3.1.1-3). The second-order cross-product density function $P_{MN}(u)$ between M and N is defined as

$$P_{MN}(u)dudt = E\{dM(t)dN(t+u)\} \qquad (3.3.1)$$

where $du, dt \rightarrow 0$. $P_{MN}(u)$ may be interpreted as

$$P_{MN}(u)dudt = Pr\{dM(t)=1 \text{ and } dN(t+u)=1\} \qquad (3.3.2)$$

and provides a measure of the probability for an N event to occur u time units after an M event. Note that $P_{MN}(u)$ is not an even function. In fact,

$$P_{MN}(-u) = E\{dM(t)dN(t-u)\}$$

Let $\tau=t-u$,

$$P_{MN}(-u) = E\{dM(\tau+u)dN(\tau)\} = P_{NM}(u) \qquad (3.3.3)$$

Another distinction from the second-order product density function $P_{MN}(u)$ is that at lag u=0,

$$P_{MN}(u)dudt\Big|_{u=0} = E\{dM(t)dN(t)\} \qquad (3.3.4)$$

ie., it does not involve the Dirac delta function. If the two processes are independent of each other,

$$P_{MN}(u)dudt = E\{dM(t)dN(t+u)\}$$
$$= P_M P_N dudt$$

which gives

$$P_{MN}(u) = P_M P_N \qquad \text{for all } u \qquad (3.3.5)$$

where P_M and P_N are the mean intensities of M and N respectively. Similarly, under the mixing condition, the same result is obtained, ie.

$$\lim_{u \to \infty} P_{MN}(u) = P_M P_N \qquad (3.3.6)$$

The cross-intensity function $m_{MN}(u)$ is defined as

$$m_{MN}(u)du = E\{dN(t+u) \mid dM(t)=1\} \qquad (3.3.7)$$

It can be interpreted as

$$m_{MN}(u)du = Pr\{dN(t+u)=1 \mid dM(t)=1\} \qquad (3.3.8)$$

and provides a measure of the conditional probability of an N event to occur given an M event has occurred u time units earlier. It can also be expressed as

$$m_{MN}(u) = P_{MN}(u)/P_M \qquad (3.3.9)$$

Hence, $m_{MN}(u)$ should be expected to possess the same properties as $P_{MN}(u)$ as discussed earlier. Applying the mixing condition, it follows that

$$\lim_{u\to\infty} m_{MN}(u) = P_N \tag{3.3.10}$$

which implies that for u large, the occurrence of an M event does not alter the probability of an N event to occur.

The cross-cumulant density function for the bivariate process, $q_{MN}(u)$, is defined as

$$q_{MN}(u) = \text{cov}\{dM(t), dN(t+u)\} \tag{3.3.11}$$

In terms of the cross-product density function, $q_{MN}(u)$ may be expressed as

$$q_{MN}(u) = P_{MN}(u) - P_M P_N \tag{3.3.12}$$

As will be seen in the next section, the cross-spectrum is defined as the Fourier transform of $q_{MN}(u)$. Since $P_{MN}(u)$ does not involve the Dirac delta function, the same is true for $q_{MN}(u)$. This implies the cross-spectrum would behave in the same way as that in the case of ordinary time series, ie. it has an asymptotic value of 0 as the frequency becomes large. In addition, $q_{MN}(u)$ is not even in general, which implies that the cross-spectrum is complex in general.

Finally from expression (3.3.6) and (3.3.12), the mixing condition implies,

$$\lim_{u \to \infty} q_{MN}(u) = 0 \qquad (3.3.13)$$

3.3.2 Frequency Domain Analysis

The fundamental frequency domain quantity in bivariate point process analysis is the cross-spectrum. As the auto-spectrum is the Fourier transform of the auto-cumulant density function, the cross-spectrum is the Fourier transform of the cross-cumulant density function. Provided the condition

$$\int_{-\infty}^{\infty} |q_{MN}(u)| du < \infty \qquad (3.3.14)$$

is satisfied, the cross-spectrum $f_{MN}(\lambda)$ for the point processes M and N may be defined as

$$f_{MN}(\lambda) = (1/2\pi) \int_{-\infty}^{\infty} \exp(-i\lambda u) q_{MN}(u) du \qquad (3.3.15)$$

where $q_{MN}(u)$ is the cross-cumulant density function between the processes M and N. In fact, condition (3.3.14) is automatically satisfied due to the mixing assumption. Alternatively, in terms of the finite Fourier transforms of processes M and N, the cross-spectrum may be defined as

$$f_{MN}(\lambda) = \lim_{T\to\infty} (1/2\pi T)E\{\overline{d_M^{(T)}(\lambda)}d_N^{(T)}(\lambda)\} \qquad (3.3.16)$$

Both definitions can be shown to be asymptotically equivalent as in the case of the auto-spectrum.

Due to the mixing condition and the fact that it does not have any singularities, the cross-cumulant density function satisfies the conditions of the Riemann-Lebesque Lemma, hence

$$\lim_{|\lambda|\to\infty} f_{MN}(\lambda) = 0 \qquad (3.3.17)$$

Hence the cross-spectrum for point processes behaves in the same way as that in the case of ordinary time series.

Since in general, $q_{MN}(u)$ may not be an even function in u, the cross-spectrum is usually a complex quantity. It may be represented by the magnitude squared, and the phase, ie. if

$$f_{MN}(\lambda) = C_{MN}(\lambda)+iQ_{MN}(\lambda)$$

then

$$|f_{MN}(\lambda)|^2 = C_{MN}(\lambda)^2+ Q_{MN}(\lambda)^2 \qquad (3.3.18a)$$

and

$$\theta_{MN}(\lambda) = \arctan\left[Q_{MN}(\lambda)/C_{MN}(\lambda)\right] \qquad (3.3.18b)$$

The phase $\theta_{MN}(\lambda)$ may be interpreted as the phase difference between the harmonics of the processes M and N at frequency λ. Note that it is an odd function in λ which implies

$$\lim_{\lambda \to 0} \theta_{MN}(\lambda) = 0 \qquad (3.3.19)$$

In the analysis of neuronal networks, the cross-spectrum is rarely an end result by itself. Rather, it is usually an intermediate step in obtaining the closely related transfer function and coherence function. These important functions are discussed in the next section.

3.3.3 Identification of a Single-Input, Single-Output Point Process System

The consideration of point process systems is basically similar to that of ordinary time series. A point process system consists of the input point processes, the output point processes and the operator "S" which transforms the input processes over into the output processes. As in the case of ordinary time series, a linear time-invariant point process system refers to a system such that the statistical properties between the input and output point processes can be related by linear combinations with constant weights. In addition, a point process system is said to have a refractory period if there exists a time interval immediately following an output event during which time there can be no further output. Refractoriness in neuronal discharges, and dead time in a Geiger counter are examples.

To identify a point process system is to determine the characteristics of the system, ie., the operator "S", from observing the input and output processes. In the case of a

stochastic system, it is not possible to identify the system completely. The most that can be done is to determine the average quantities or parameters that characterise the statistical or average properties of "S".

In this section, the case of a single-input, single-output linear point process system is considered. The assumptions (3.3.1-3) again apply to the bivariate point process involved.

Suppose M and N are the input and output point processes of a linear time-invariant system as illustrated in Figure (3.3.1)

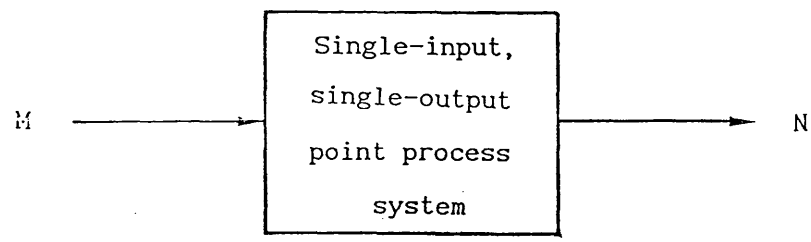

Figure 3.3.1. Single-input, single-output linear point process model with input point process M and output point process M.

An important element characterising the system is provided by

$$\eta_N(t)dt = \Pr\{dN(t)=1 \mid M\} = E\{dN(t) \mid M\} \quad (3.3.20)$$

where $\eta_N(t)$ may be considered as the probability intensity of an N event occurring at time t given the input events in M. Obviously,

for a physical system, only input events prior to time t can affect the occurrence of the output event at time t. The developments below discuss plausible forms for $\eta_N(t)$. First, assume the output emit points at a rate s_0 when there is no input, ie M(.)≡0. So,

$$\eta_N(t) = s_0 \tag{3.3.21}$$

Next, suppose M corresponds to a single event at time v_1. Then we might alter (3.3.21) to

$$\eta_N(t) = s_0+s_1(t-v_1) \tag{3.3.22}$$

Here $s_1(t)$ represents the effect, on the output intensity, of an input event at time 0. Finally, suppose M corresponds to a series of events at times v_k (k=1,2,..,m). Expression (3.3.22) may be generalised to

$$\begin{aligned}\eta_N(t) &= s_0+s_1(t-v_1)+s_1(t-v_2)+ \ .. \ +s_1(t-v_m) \\ &= s_0+ \int s_1(t-v)dM(v)\end{aligned} \tag{3.3.23}$$

This is the linear model we base our discussion on in this chapter. It also resembles strikingly the linear model used in ordinary time series except that it has the further interpretation in terms of probability.

To solve for s_0 in expression (3.3.23), we take the expected value with respect to time. It follows that

$$s_0 = P_N - P_M \int s_1(v)dv \qquad (3.3.24)$$

To solve for $s_1(.)$, one substitutes expression (3.3.24) into expression (3.3.23) which gives,

$$\eta_N(t)-P_N = \int s_1(v)[dM(t-v)-P_M dv] \qquad (3.3.25)$$

For a pair of times t and t+u, the product $[\eta_N(t)-P_N][\eta_N(t+u)-P_N]$ is seen to be given by

$$\iint s_1(v)s_1(w)[dM(t-v)-P_M dv][dM(t+u-w)-P_M dw] \qquad (3.3.26)$$

Taking the expected value of expression (3.3.26) followed by additional manipulations gives

$$q_{NN}(u) = \iint s_1(w)s_1(v)q_{MM}(u+v-w)dvdw \qquad (3.3.27)$$

The cross-cumulant density function $q_{MN}(u)$ may be derived in a similar manner by finding the product $[\eta_M(t)-P_M][\eta_N(t+u)-P_N]$ followed by taking the expected value, which yields,

$$q_{MN}(u) = \int s_1(v)q_{MM}(u-v)dv \qquad (3.3.28)$$

The transformation of equations (3.3.27) and (3.3.28) to a complex valued frequency domain form by taking Fourier transforms yields the important power spectra and cross-spectra

relations

$$f_{NN}(\lambda) = |S_1(\lambda)|^2 f_{MM}(\lambda) \qquad (3.3.29a)$$

and

$$f_{MN}(\lambda) = S_1(\lambda)\, f_{MM}(\lambda) \qquad (3.3.29b)$$

where $S_1(\lambda)$ and $s_1(u)$ are related by

$$S_1(\lambda) = \int_{-\infty}^{\infty} \exp(-i\lambda u) s_1(u) du \qquad (3.3.30)$$

$S_1(\lambda)$ is known as the transfer function whereas $s_1(u)$ is known as the first-order kernel. A few points should be noted here. (1) Expressions (3.3.27-29) are directly analogous to the corresponding relationships in the case of ordinary time series (see for example Bendat and Piersol, 1971). (2) Expression (3.3.29b) shows that the transfer function may be estimated from the cross-spectrum and auto-spectrum. (3) From expressions (3.3.29), it can seen that

$$\frac{|f_{MN}(\lambda)|^2}{f_{MM}(\lambda) f_{NN}(\lambda)} = 1 \qquad (3.3.31)$$

This result is obtained under the assumption that the system is linear time invariant with single-input, single-output and no extraneous noise is present. The quantity $|f_{MN}(\lambda)|^2 / f_{MM}(\lambda) f_{NN}(\lambda)$ is also known as the ordinary coherence function and is denoted by $|R_{MN}(\lambda)|^2$. The possible interpretations of this function are discussed in the next section.

3.3.4 The Ordinary Coherence Function

The ordinary coherence function $|R_{MN}(\lambda)|^2$ between two point processes M and N is defined as

$$|R_{MN}(\lambda)|^2 = \frac{|f_{MN}(\lambda)|^2}{f_{MM}(\lambda)f_{NN}(\lambda)} \qquad (3.3.32)$$

The ordinary coherence can be interpreted as (1) The degree of linear predictability of the process N by the process M (2) The limiting correlation-squared between the finite Fourier-Stieltjes transforms of M and N. These interpretations are derived as follows.

The first interpretation arises from the mean square error of expression (3.3.23). To find the mean square error of the linear point process model, expression (3.3.25) suggests the intensity of the error process to be defined as

$$\eta_\varepsilon(t) = [\eta_N(t)-P_N]-\int s_1(v)[dM(t-v)-P_M dv] \qquad (3.3.33)$$

where $\eta_\varepsilon(t)$ may be considered as the error intensity of N after a linear least square prediction from the contribution of M is removed. Clearly from expression (3.3.33), $E\{\eta_\varepsilon(t)\}=0$. The cumulant density function $q_{\varepsilon\varepsilon}(u)$ is determined by

$$q_{\varepsilon\varepsilon}(u) = E\{\eta_\varepsilon(t)\eta_\varepsilon(t+u)\} \qquad (3.3.34)$$

From expressions (3.3.33) and (3.3.34),

$$q_{\varepsilon\varepsilon}(u) = q_{NN}(u) - \int s_1(v) q_{MN}(u-v)dv \qquad (3.3.35)$$

The Fourier-Stieltjes transform of expression (3.3.35) yields

$$\begin{aligned} f_{\varepsilon\varepsilon}(\lambda) &= f_{NN}(\lambda) - S_1(\lambda) f_{MN}(\lambda) \\ &= f_{NN}(\lambda) - f_{MN}(\lambda) f_{NM}(\lambda) / f_{MM}(\lambda) \\ &= f_{NN}(\lambda)\left[1 - |R_{MN}(\lambda)|^2\right] \end{aligned} \qquad (3.3.36)$$

where $f_{\varepsilon\varepsilon}(\lambda)$ is the auto-spectrum of the error process. It may be considered as the residue spectrum of N after the linear least square prediction from M is removed. From expression (3.3.36), it can be seen that when $|R_{MN}(\lambda)|^2=1$, the error spectrum becomes zero, indicating perfect prediction from M. On the other hand, when $|R_{MN}(\lambda)|^2=0$, the error spectrum becomes equal to the auto-spectrum of N, indicating whatever predicted are errors. This discussion concludes that in the case where the input point process is M whereas the output point process is N, the ordinary coherence function $|R_{MN}(\lambda)|^2$ may be used as a measure of the linear predictability of N from M.

The second interpretation can be illustrated by considering the limiting correlation squared between the finite Fourier-Stieltjes transforms of M and N that is defined as

$$\lim_{T\to\infty} \frac{|\mathrm{cov}\{d_M^{(T)}(\lambda), d_N^{(T)}(\lambda)\}|^2}{[\mathrm{var}\{d_M^{(T)}(\lambda)\}\mathrm{var}\{d_N^{(T)}(\lambda)\}} \qquad (3.3.37)$$

Now from expression (3.3.16), the numerator of expression (3.3.37) is seen to be $|2\pi T f_{MN}(\lambda)|^2$ whereas from expressions (3.2.21) and

(3.2.22), the denominator of expression (3.3.37) is equal to $(2\pi T)^2 f_{MM}(\lambda) f_{NN}(\lambda)$. Hence the ordinary coherence function $|R_{MN}(\lambda)|^2$ may be defined as the limiting linear correlation squared between the frequency components at frequency λ of M and N. Another important implication of expression (3.3.37) is that it is in such a form that the Schwarz inequality in the theory of vector space geometry may be applied (Koopmans, 1974). The Schwarz inequality states that

$$|\langle x,y \rangle| \leq \|x\| \, \|y\| \tag{3.3.38}$$

where $|\langle x,y \rangle|$ is the inner product of x and y, and $\|x\| = |\langle x,x \rangle|$ with similar definition for $\|y\|$. Since the covariance and variance operators may be considered as inner product operators, it follows that

$$0 \leq |R_{MN}(\lambda)|^2 \leq 1 \tag{3.3.39}$$

The upper and lower bounds of this quantity enable assessments of perfect association and independence respectively making it a more useful quantity than the cumulant density functions which have no upper bound. (See the discussion in Rosenberg et al, 1989).

3.4 Multi-Variate Point Process Parameters

The frequency domain description of the single-input, single-output relations described in the previous section is obviously much simpler than the time domain description. This leads to the extension of the techniques to describe situations where the system concerned involves multiple inputs and multiple outputs.

Among the key concepts is the idea of residual or partial random variables. It may be considered as the value of the random variable after taking into account of the linear effects of other known process(es). The best way to introduce the idea is probably to consider a two-input, single-output linear point process model.

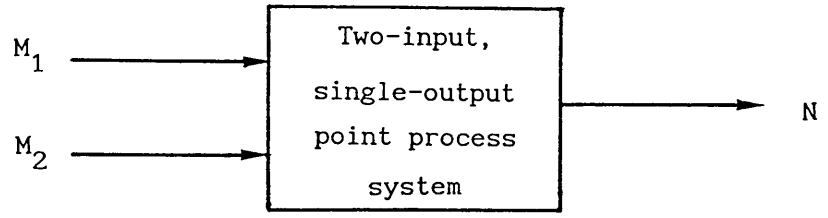

Figure 3.4.1. Two-input, single-output linear point process model with input point processes M_1 and M_2, and output point process N.

3.4.1 Partial Quantities of Order-1

Consider the linear model illustrated in Figure (3.4.1). Suppose the two input point processes M_1 and M_2 are correlated and

let processes N and M_1 be the linear least-square prediction based on process M_2 and are described by the expressions

$$\eta_N(t) = s_N + \int s_{2N}(v)dM_2(t-v) \qquad (3.4.1a)$$

$$\eta_1(t) = s_1 + \int s_{21}(v)dM_2(t-v) \qquad (3.4.1b)$$

where $\eta_N(t)$ may be interpreted as

$$\eta_N(t)dt = Pr\{dN(t)=1 \mid M_2\} = E\{dN(t) \mid M_2\}$$

and $\eta_N(t)$ may be considered as the probability intensity of an N event occurring at time t given the input events in M_2. The interpretation for $\eta_1(t)$ is similar. The function $s_{2N}(t)$ represents the effect, on the output intensity of N, of an M_2 event at time 0 with similar meaning for $s_{21}(t)$. Taking the expected values with respect to time in expression (3.4.1), it follows that

$$\eta_N(t)-P_N = \int s_{2N}(v)[dM_2(t-v)-P_2dv] \qquad (3.4.2a)$$

$$\eta_1(t)-P_1 = \int s_{21}(v)[dM_2(t-v)-P_2dv] \qquad (3.4.2b)$$

If the objective of the analysis is to find the relations between M_1 and N after taking account of the linear contribution from M_2, we start by defining the residue or partial intensities of and N and M_1 given by

$$\eta_{\varepsilon N}(t) = (\eta_N(t)-P_N)-\int s_{2N}(v)[dM_2(t-v)-P_2dv] \qquad (3.4.3a)$$

$$\eta_{\varepsilon 1}(t) = (\eta_1(t)-P_1)-\int s_{21}(v)[dM_2(t-v)-P_2 dv] \qquad (3.4.3b)$$

where $\eta_{\varepsilon N}(t)$ may be interpreted as the residue intensity of N after subtracting the linear least-squares prediction from M_2, with similar interpretation for $\eta_{\varepsilon 1}(t)$. The treatment is similar to section (3.3.4) except that the quantities related to the error process are now interpreted as the residual quantities of the process. Now, we may define the residue spectrum of N after removing the contributions from M_2 as the partial auto-spectrum $f_{NN.2}(\lambda)$, and the residue spectrum of M_1 after removing the contributions from M_2 as $f_{11.2}(\lambda)$ using the results obtained in expression (3.3.36), ie.

$$f_{NN.2}(\lambda) = f_{NN}(\lambda)[1-|R_{2N}(\lambda)|^2] \qquad (3.4.4a)$$

$$f_{11.2}(\lambda) = f_{11}(\lambda)[1-|R_{21}(\lambda)|^2] \qquad (3.4.4b)$$

where

$$|R_{2N}(\lambda)|^2 = |f_{2N}(\lambda)|^2 / f_{22}(\lambda)f_{NN}(\lambda)$$

$$|R_{21}(\lambda)|^2 = |f_{21}(\lambda)|^2 / f_{22}(\lambda)f_{11}(\lambda)$$

For the derivation of the partial cross-spectrum between M_1 and N, $f_{1N.2}(\lambda)$, we start with expression (3.4.3) and obtain the residue cross-cumulant density function between N and M_1, $q_{1N.2}(u)$, which is given by

$$q_{1N.2}(u) = E\{\eta_{\varepsilon 1}(t)\eta_{\varepsilon N}(t+u)\}$$

$$= q_{1N}(t) - \int s_{2N}(v)q_{12}(u-v)dv \qquad (3.4.5)$$

Taking the Fourier transform of expression (3.4.5)

yields

$$f_{1N.2}(\lambda) = f_{1N}(\lambda) - S_{2N}(\lambda)f_{12}(\lambda)$$
$$= f_{1N}(\lambda) - f_{2N}(\lambda)f_{12}(\lambda)/f_{22}(\lambda) \qquad (3.4.6)$$

Both partial auto-spectrum and partial cross-spectrum can be interpreted as the resulting quantities after the portion linearly correlated with a third process is removed.

More generally, for an r vector-valued stationary point process $\mathbf{M}(t)=\{M_1(t),M_2(t),..,M_r(t)\}$, the partial cross-spectrum of order-1 between processes M_a, M_b after removing the linear contributions from M_c is given by

$$f_{ab.c}(\lambda) = f_{ab}(\lambda)-f_{ac}(\lambda)f_{cb}(\lambda)/f_{cc}(\lambda) \qquad (3.4.7)$$

for $a,b,c=1,2,..r$ and $a\neq b\neq c$. In the case $a=b$ but $a\neq c$, the quantity $f_{aa.c}(\lambda)$ is known as partial auto-spectrum of process M_a after removing the linear contributions from M_c.

The partial cross-spectrum $f_{ab.c}(\lambda)$ may also be interpreted as the covariance between the limiting finite Fourier transforms of M_a and M_b after the linear effects of the process M_c have been removed. It may be stated as,

$$f_{ab.c}(\lambda) = \lim_{T\to\infty} \left(\frac{1}{2\pi T}\right) \operatorname{cov}\{d_a^{(T)}(\lambda)-d_c^{(T)}(\lambda)\frac{f_{ca}(\lambda)}{f_{cc}(\lambda)}, d_b^{(T)}(\lambda)-d_c^{(T)}(\lambda)\frac{f_{cb}(\lambda)}{f_{cc}(\lambda)}\} \qquad (3.4.8)$$

Hence when there is no direct connections between processes M_a and M_b, the value of $f_{ab.c}(\lambda)$ would be zero. However, the value of this quantity is not bounded above to enable us to assess the strength of direct connection between the processes. This disadvantage leads to the normalisation of partial cross-spectrum. The resulting quantity is known as the partial coherence of order-1 and is given by

$$|R_{ab.c}(\lambda)|^2 = \frac{|f_{ab.c}(\lambda)|^2}{f_{aa.c}(\lambda)\, f_{bb.c}(\lambda)} \qquad (3.4.9)$$

Similar interpretations exist for $|R_{ab.c}(\lambda)|^2$ as in the case of ordinary coherence (see section 3.3.4). $|R_{ab.c}(\lambda)|^2$ may be interpreted as the degree of linear predictability of the process M_b by M_a after the linear contribution from M_c is removed, or it may also be interpreted as the limiting correlation-squared between finite Fourier transforms of M_a and M_b, with the linear contributions from M_c removed. Again the second interpretation allows the Schwarz inequality to be applied and gives the result

$$0 \leq |R_{ab.c}(\lambda)|^2 \leq 1 \qquad (3.4.10)$$

Finally the relations between the partial coherence of order-1 and the ordinary coherence may be expressed as

$$|R_{ab.c}(\lambda)|^2 = \frac{|R_{ab}(\lambda) - R_{ac}(\lambda)R_{cb}(\lambda)|^2}{[1-|R_{ac}(\lambda)|^2][1-|R_{cb}(\lambda)|^2]} \qquad (3.4.11)$$

In practice, situations can arise in which the value of the

partial coherence $|R_{ab.c}(\lambda)|^2$ may be higher or lower than that of the ordinary coherence $|R_{ab}(\lambda)|^2$. Generally, in the case when the process M_c is correlated to either M_a or M_b but not both, then $|R_{ab.c}(\lambda)|^2 \geq |R_{ab}(\lambda)|^2$. On the other hand, when the process M_c is correlated with both M_a and M_b, for example when M_c is the common input to both M_a and M_b, then $|R_{ab.c}(\lambda)|^2 \leq |R_{ab}(\lambda)|^2$. It is obvious that if M_c is not correlated to M_a or M_b, then $|R_{ab.c}(\lambda)|^2 = |R_{ab}(\lambda)|^2$.

3.4.2 Identification of a Two-Input, Single-Output Linear Point Process Model

The analysis that follows is a direct extension of the discussions outlined in section (3.3.3). Consider the point process model illustrated in Figure (3.4.2).

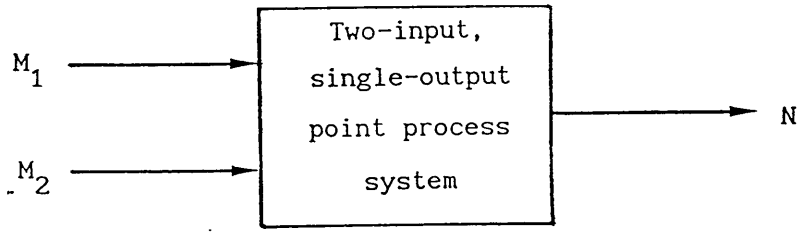

Figure 3.4.2. Two-input, single-output linear point process model with input point processes M_1 and M_2, and output point process N.

Suppose that both inputs M_1 and M_2 act additively on the output process N. Extending the model in expression (3.3.23), the linear least-squares prediction of N from M_1 and M_2 is given by

$$\eta_N(t) = s_0 + \int s_1(v)dM_1(t-v) + \int s_2(v)dM_2(t-v) \qquad (3.4.12)$$

where $\eta_N(t)$ may be interpreted as

$$\eta_N(t)dt = Pr\{dN(t)=1 \mid M_1 \text{ and } M_2\} = E\{dN(t) \mid M_1 \text{ and } M_2\}$$

and $\eta_N(t)$ may be considered as the probability intensity of an N event occurring at time t given the input events in M_1 and M_2. The function $s_1(t)$ represents the effects, on the output intensity of N, of inputting a single M_1 point at time 0 with $M_2 \equiv 0$ whereas the function $s_2(t)$ represents the effects, on the output intensity of N, of inputting a single M_2 point at time 0 with $M_1 \equiv 0$. The constant s_0 may be considered as the mean rate of N when both M_1 and M_2 are inactive.

Taking the expected value of expression (3.4.12), it follows that

$$\eta_N(t) - P_N = \int s_1(v)[dM_1(t-v) - P_1 dv] + \int s_2(v)[dM_2(t-v) - P_2 dv] \qquad (3.4.13)$$

To find the auto-cumulant density and auto-spectrum, we multiply expression (3.4.13) by $[\eta_N(t+u)-P_N]$ followed by taking the expected values, ie.

$$q_{NN}(u) = \iint s_1(v)s_1(w)q_{11}(u+v-w)dvdw + \iint s_2(v)s_2(w)q_{22}(u+v-w)dvdw$$
$$+ \iint s_1(v)s_2(w)q_{12}(u+v-w)dvdw + \iint s_1(w)s_2(v)q_{21}(u+v-w)dvdw$$

(3.4.14)

By taking the Fourier transform of expression (3.4.14), the expression is simplified to

$$f_{NN}(\lambda) = S_1(\lambda)\ f_{N1}(\lambda) + S_2(\lambda)\ f_{N2}(\lambda) \tag{3.4.15}$$

where $S_1(\lambda)$ and $S_2(\lambda)$ are the Fourier transforms of $s_1(v)$ and $s_2(v)$ respectively. Note that $f_{NN}(\lambda)$ given by expression (3.4.15) is a real quantity.

Similarly, the cross-cumulant densities can be obtained as,

$$q_{1N}(u) = \int s_1(v)q_{11}(u-v)dv + \int s_2(v)q_{12}(u-v)dv \tag{3.4.16a}$$

$$q_{2N}(u) = \int s_1(v)q_{21}(u-v)dv + \int s_2(v)q_{22}(u-v)dv \tag{3.4.16b}$$

which after taking the Fourier transform yields

$$\begin{aligned} f_{1N}(\lambda) &= S_1(\lambda)f_{11}(\lambda) + S_2(\lambda)f_{12}(\lambda) \\ f_{2N}(\lambda) &= S_1(\lambda)f_{21}(\lambda) + S_2(\lambda)f_{22}(\lambda) \end{aligned} \tag{3.4.17}$$

Now expression (3.4.17) can be viewed as a system of simultaneous equations with two unknowns $S_1(\lambda)$ and $S_2(\lambda)$. The solutions for $S_1(\lambda)$ and $S_2(\lambda)$ are given by

$$S_1(\lambda) = \frac{f_{22}(\lambda)f_{1N}(\lambda) - f_{12}(\lambda)f_{2N}(\lambda)}{f_{11}(\lambda)f_{22}(\lambda) - f_{12}(\lambda)f_{21}(\lambda)}$$

$$= \frac{f_{1N.2}(\lambda)}{f_{11.2}(\lambda)} \qquad (3.4.18a)$$

$$S_2(\lambda) = \frac{f_{11}(\lambda)f_{2N}(\lambda)-f_{21}(\lambda)f_{1N}(\lambda)}{f_{11}(\lambda)f_{22}(\lambda)-f_{21}(\lambda)f_{12}(\lambda)}$$

$$= \frac{f_{2N.1}(\lambda)}{f_{22.1}(\lambda)} \qquad (3.4.18b)$$

3.4.3 Multiple Coherence Function of Order-2

The multiple coherence function is an direct extension of the ordinary coherence function introduced in section (3.3.4). It arises from the mean square error consideration of a linear model with multiple inputs. In the case of a two-input, single-output model, we define the error intensity $\eta_\varepsilon(t)$ as

$$\eta_\varepsilon(t) = [\eta_N(t)-P_N]-\int s_1(v)[dM_1(t-v)-P_1dv]$$
$$-\int s_2(v)[dM_2(t-v)-P_2dv] \qquad (3.4.19)$$

Clearly $E\{\eta_\varepsilon(t)\}=0$. The cumulant density function for the error process is given by $E\{\eta_\varepsilon(t)\eta_\varepsilon(t+u)\}$ which after substituting (3.4.19) and simplifying gives

$$q_{\varepsilon\varepsilon}(u) = q_{NN}(u)-\int s_1(v)q_{N1}(u-v)-\int s_2(v)q_{N2}(u-v)dv$$
$$-\int s_1(v)q_{1N}(u+v)dv-\int s_2(v)q_{2N}(u+v)dv+\iint s_1(v)s_1(w)q_{11}(u+v-w)dvdw$$
$$+\iint s_2(v)s_2(w)q_{22}(u+v-w)dvdw+\iint s_1(v)s_2(w)q_{12}(u+v-w)dvdw$$
$$+\iint s_2(v)s_1(w)q_{21}(u+v-w)dvdw \qquad (3.4.20)$$

Using expression (3.4.16), expression (3.4.20) simplifies to

$$q_{\varepsilon\varepsilon}(u) = q_{NN}(u) - \int s_1(v) q_{N1}(u-v)dv - \int s_2(v) q_{N2}(u-v)dv \quad (3.4.21)$$

The Fourier transform of expression (3.4.21) gives the error spectrum, ie.

$$f_{\varepsilon\varepsilon}(\lambda) = f_{NN}(\lambda) - S_1(\lambda) f_{N1}(\lambda) - S_2(\lambda) f_{N2}(\lambda) \quad (3.4.22)$$

Equation (3.4.22) may be expressed as

$$f_{\varepsilon\varepsilon}(\lambda) = f_{NN}(\lambda)\left[1 - |R_{N.12}(\lambda)|^2\right] \quad (3.4.23)$$

where
$$|R_{N.12}(\lambda)|^2 = \frac{S_1(\lambda) f_{N1}(\lambda)}{f_{NN}(\lambda)} + \frac{S_2(\lambda) f_{N2}(\lambda)}{f_{NN}(\lambda)}$$
$$= 1 - f_{\varepsilon\varepsilon}(\lambda)/f_{NN}(\lambda)$$

The quantity $|R_{N.12}(\lambda)|^2$ is called the multiple coherence function of order-2 between the output process N and the input processes M_1 and M_2. Since $0 \leq f_{\varepsilon\varepsilon}(\lambda) \leq f_{NN}(\lambda)$, it can be seen from expression (3.4.23) that

$$0 \leq |R_{N.12}(\lambda)|^2 \leq 1 \quad (3.4.24)$$

The multiple coherence function may be interpreted as the degree of linear predictability of N from M_1 and M_2. In fact, the multiple coherence function may be considered to include both the ordinary and partial coherence functions defined earlier. In particular, for the 2-input, single-output case, a partial coherence function may be considered as the multiple coherence

function applied to the respective residual processes whereas the ordinary coherence function is equivalent to the multiple coherence function of order-1.

Using expressions (3.4.18) and (3.4.23), the multiple coherence function of order-2 may be expressed as (3.4.11)

$$|R_{N.12}(\lambda)|^2 = |R_{N1}(\lambda)|^2 + |R_{N2.1}(\lambda)|^2\left[1-|R_{N1}(\lambda)|^2\right]$$
$$= |R_{N2}(\lambda)|^2 + |R_{N1.2}(\lambda)|^2\left[1-|R_{N2}(\lambda)|^2\right] \quad (3.4.25)$$

which shows that the multiple coherence function $|R_{N.12}(\lambda)|^2$ accounted by the inputs M_1 and M_2 may be decomposed into the respective ordinary and partial coherence functions.

3.4.4 Matrix Formulation for the Multiple-Input, Multiple-Output Linear Model

The results obtained in the previous sections may be seen to be more apparent when expressed in matrix notation. In this section, the general case of a m-input, n-output linear model is considered. The results are expressed in matrix notation and it will be clear that the kind of analysis involved is similar to multiple regression analysis in the theory of statistics.

Consider a point process system with m-input and n-output, as illustrated in Figure 3.4.3.

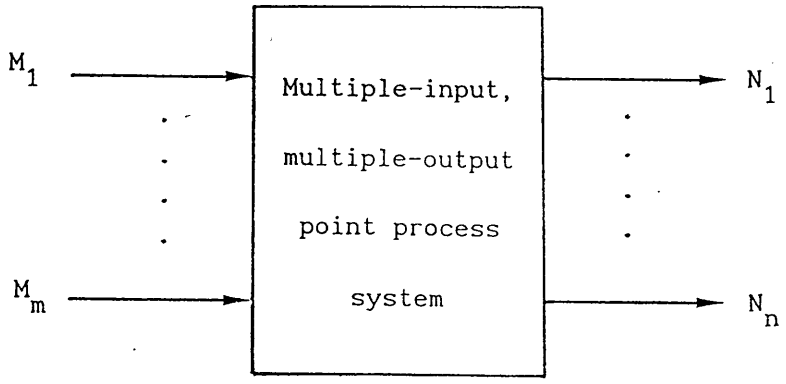

Figure 3.4.3 Multiple-input, multiple-output linear point process model with input point processes $\mathbf{M}=[M_1,..,M_m]$ and output point processes $\mathbf{N}=[N_1,..,N_n]$.

First, the quantities involved are defined in matrix form as:-

The matrices of auto-spectrum for **M** and **N** are defined as

$$\mathbf{F_{MM}}(\lambda) = \begin{bmatrix} f_{M_1M_1}(\lambda) & .. & f_{M_1M_m}(\lambda) \\ \vdots & & \vdots \\ f_{M_mM_1}(\lambda) & .. & f_{M_mM_m}(\lambda) \end{bmatrix} \qquad (3.4.26a)$$

and

$$\mathbf{F_{NN}}(\lambda) = \begin{bmatrix} f_{N_1N_1}(\lambda) & .. & f_{N_1N_n}(\lambda) \\ \vdots & & \vdots \\ f_{N_nN_1}(\lambda) & .. & f_{N_nN_n}(\lambda) \end{bmatrix} \qquad (3.4.26b)$$

The matrices of cross-spectrum are defined as

$$\mathbf{F_{MN}}(\lambda) = \begin{bmatrix} f_{M_1N_1}(\lambda) & .. & f_{M_1N_n}(\lambda) \\ \vdots & & \vdots \\ f_{M_mN_1}(\lambda) & .. & f_{M_mN_n}(\lambda) \end{bmatrix} \qquad (3.4.27a)$$

and

$$F_{NM}(\lambda) = \begin{bmatrix} f_{N_1M_1}(\lambda) .. f_{N_1M_m}(\lambda) \\ \vdots \\ f_{N_nM_1}(\lambda) .. f_{N_nM_m}(\lambda) \end{bmatrix} \qquad (3.4.27b)$$

The matrix of transfer function is defined as

$$S_{MN}(\lambda) = \begin{bmatrix} S_{M_1N_1}(\lambda) .. S_{M_1N_n}(\lambda) \\ \vdots \\ S_{M_mN_1}(\lambda) .. S_{M_mN_n}(\lambda) \end{bmatrix} \qquad (3.4.28)$$

The matrix of partial output spectrum is defined as

$$F_{NN.M}(\lambda) = \begin{bmatrix} f_{N_1N_1.M}(\lambda) .. f_{N_1N_n.M}(\lambda) \\ \vdots \\ f_{N_nN_1.M}(\lambda) .. f_{N_nN_n.M}(\lambda) \end{bmatrix} \qquad (3.4.29)$$

where a typical entry $f_{N_aN_b.M}(\lambda)$ represents the partial spectrum between N_a and N_b after removing the linear effects of the processes $M_1,..,M_m$.

Now the matrix formulation of the solution of the linear model is given by

$$F_{MN}(\lambda) = F_{MM}(\lambda)S_{MN}(\lambda) \qquad (3.4.30)$$

which gives

$$S_{MN}(\lambda) = F_{MM}(\lambda)^{-1}F_{MN}(\lambda) \qquad (3.4.31)$$

where A^{-1} denotes the inverse of matrix **A**. Let M_a* denotes the set of all components of **M** omitting M_a, then the typical entry $S_{M_aN_b}(\lambda)$ is generally given by

$$S_{M_a N_b}(\lambda) = \frac{f_{M_a N_b . M_a *}(\lambda)}{f_{M_a M_a . M_a *}(\lambda)\, f_{N_b N_b . M_a *}(\lambda)} \qquad (3.4.32)$$

for a=1,2,..,m, b=1,2,..,n.

The matrix of the partial spectrum is given by

$$F_{NN.M}(\lambda) = F_{NN}(\lambda) - F_{NM}(\lambda) F_{MM}^{-1}(\lambda) F_{MN}(\lambda) \qquad (3.4.33)$$

Now the partial coherence of order-m between the output processes N_a and N_b after removing the effects of the m-input processes $M_1, M_2, .., M_m$, $|R_{N_a N_b . M}(\lambda)|^2$, may be expressed by the corresponding elements of the matrix $F_{NN.M}(\lambda)$, ie.

$$|R_{N_a N_b . M}(\lambda)|^2 = \frac{|f_{N_a N_b . M}(\lambda)|^2}{f_{N_a N_a . M}(\lambda)\, f_{N_b N_b . M}(\lambda)} \qquad (3.4.34)$$

Finally, the multiple coherence of order-m between a typical output N_a and the inputs $M_1, M_2, .., M_m$ may be expressed as

$$|R_{N_a . M}(\lambda)|^2 = 1 - \frac{f_{N_a N_a . M}(\lambda)}{f_{N_a N_a}(\lambda)} \qquad (3.4.35)$$

Chapter 4

Estimation Procedures and Statistical Inferences

Chapter 4 Estimation Procedures and Statistical Inferences

4.1 Introduction

In Chapter 3, various parameters in both time and frequency domains are introduced and defined in a theoretical manner. In practice, these theoretical parameters that represent the "true" characteristics of the processes and systems involved are usually unknown and need to be estimated from the observed processes and any known information concerning the system. The aim of this chapter is to present the estimation procedures for those parameters that have particular relevance to the analysis of neurophysiological systems.

In the context of the work described in this thesis, the observed signals are characterised by the sampled times of occurrence of the events within the spike trains. Hence, for a sample of an univariate point process M of duration T, the observations occur at times $t_1, t_2, .., t_T$ where $t_j = j\Delta t$, Δt is the sampling interval. We write the j-th observation as

$$dM(t_j) = \begin{cases} 1 & \text{if an event occurred in } (t_j, t_j+\Delta t] \\ 0 & \text{otherwise} \end{cases} \qquad (4.1.1)$$

and Δt=1 msec., ie. a sampling rate of 1 kHz is used in the work involved in this thesis. The details of the experimentation can be found in Chapter 5.

Throughout this chapter, the assumptions stated in sections (3.1.1-3) apply to the underlying processes, namely stationarity,

mixing and orderliness. In addition, the property of ergodicity is assumed to justify the validity of estimating the parameters from one realisation. Also, the sampling rate of 1 kHz ensures that the Nyquist criterion is fulfilled since the refractory time of neurophysiological system is greater that 1 ms in general (see Chapter 2).

It is important to stress that the estimates obtained, no matter what procedures are used, can never represent the true values of the quantities. This is due to the fact that the neurophysiological systems concerned are essentially stochastic in nature and the best that one can obtain are the average values of the parameters. In addition, there are other factors that affect the estimates such as finite record length, which leads to the fact that the estimates are discrete in nature, whereas the true quantities are continuous. It can be shown that the estimates are only representatives of the values over a bin width around the neighbourhood of the true quantities (see, for example, Brillinger 1974a and Rigas 1983 for a discussion of the validity of the stationarity and ergodicity assumptions, the choice of resolution, etc). Hence the estimates obtained are susceptible to errors or uncertainties. This chapter includes consideration of procedures to reduce the uncertainties involved. Also, in order to construct the confidence intervals for these estimates, a knowledge of the distribution properties of these quantities is called for. It will be seen that for most cases, the large sample properties of the estimates may be applied to simplify the construction of confidence interval.

A class of point process known as a Poisson point process is described and its similarity to Gaussian white noise in the case of ordinary time series is emphasised. A Poisson point process may be considered as a point process in which the individual events are independent of each other. In the univariate case, the Poisson point process is used as a "reference process" to reveal the departures of a spike train from complete randomness. Such departures can reveal significant effects concerning the process. Extending the idea of independence to bivariate and multi-variate cases, tests of independence are established and form a set of useful tools in measuring associations between the processes concerned.

The treatment used in this chapter is closely related to the theory of statistical inference which is concerned primarily with the problem of drawing inferences about the values of unknown parameters on the basis of observational data. A detailed account of the theory of statistical inference may be found in Kendall and Stuart (1961). An applied contemporary account of the estimation of ordinary time series quantities may be found in Shumway (1988) whereas in the case of point processes, a preliminary account may be found in Cox and Lewis (1966, 1972) and the extension of this in Brillinger (1975a).

4.2 Estimation of Time Domain Parameters

In this section, the estimation procedures for the first and second-order time domain parameters are considered. At appropriate points, the asymptotic distribution and the variance of the estimates are given based on the mixing condition stated in section (3.1.2).

4.2.1 Mean Intensity

Suppose for a point process M, M(T) represents the number of events in the interval (0,T] and the process is sampled every Δt seconds such that Δt is sufficiently small to ensure that not more than one event can take place in this interval. A possible estimate for P_M may be arrived at by considering the definition (3.2.2), ie.

$$\begin{aligned}\hat{P}_M\Delta t &= \text{Prob}\{\text{M event in an interval } (t,t+\Delta t]\} \\ &\approx \frac{\text{Number of times the event actually occurs}}{\text{Total number of elements in the sample space}} \\ &= \frac{M(T)}{T/\Delta t}\end{aligned}$$

Hence a natural estimate for P_M may be written as

$$\hat{P}_M = \frac{M(T)}{T} \qquad (4.2.1)$$

ie. The mean intensity P_M simply represents the mean rate of the process. Alternatively, a formal way of expressing (4.2.1) is to

write

$$\hat{P}_M = (1/T)\int_0^T dM(t) \qquad (4.2.2)$$

Obviously, one would be interested to know if $\hat{P}_M$ is an unbiased estimate of P_M. It is straight- forward to see that

$$E\{\hat{P}_M\} = (1/T)\int_0^T E\{dM(t)\} = (1/T)\int_0^T P_M dt = P_M \qquad (4.2.3)$$

Expression (4.2.3) uses the definition of $\hat{P}_M$ stated in expression (3.2.1). Hence $\hat{P}_M$ is an unbiased estimate of P_M. To investigate the efficiency of the estimate $\hat{P}_M$, one can evaluate $Var\{\hat{P}_M\}=E\{(\hat{P}_M-P_M)^2\}$. Using expression (4.2.2) one has

$$\begin{aligned} Var\{\hat{P}_M\} &= E\left\{(1/T^2)\int_0^T\int_0^T dM(t)dM(s) - P_M^2\right\} \\ &= (1/T^2)\int_0^T\int_0^T E\{dM(t)dM(s)\} - P_M^2 \\ &= (1/T^2)\int_0^T\int_0^T P_{MM}(t-s)dtds - (1/T^2)\int_0^T\int_0^T P_M^2 dtds \\ &= (1/T^2)\int_0^T\int_0^T q_{MM}(t-s)dtds \qquad (4.2.4) \end{aligned}$$

In expression (4.2.4), $P_{MM}(t-s)$ and $q_{MM}(t-s)$ are the second-order product density function and cumulant density function at lag (t-s) respectively. The result has made use of definitions (3.2.3) and (3.2.13).

By introducing a change of variable u=t-s, the integration on the square on the t-s plane is transformed to a triangle on the t-u plane. This operation simplifies expression (4.2.4) to

$$\mathrm{Var}\{\hat{P}_M\} = (1/T^2)\int_{-T}^{T} (T-|u|)q_{MM}(u)du \qquad (4.2.5)$$

Now applying the mixing assumption in expression (3.1.6a), it can be seen that for T large with respect to the span of effects of $q_{MM}(u)$,

$$\mathrm{Var}\{\hat{P}_M\} = (1/T)\int_{-T}^{T} q_{MM}(u)du \qquad (4.2.6)$$

A further simplification can be made by applying the mixing assumption in expression (3.1.6b). Hence for T large

$$\mathrm{Var}\{\hat{P}_M\} \simeq 0 \qquad (4.2.7)$$

One may conclude that $\hat{P}_M$ is a consistent estimate of P_M. As we will see later in this chapter the estimation of other higher order quantities involves $\hat{P}_M$ and the result in expression (4.2.7) is assumed in order to simplify calculations.

4.2.2 Second-Order Parameters

While the first-order counting variate M(T) is used to

estimate the mean intensity, the second-order counting variate $J_{MM}^{(T)}(u_k)$ may be employed to estimate the second-order time domain parameters. It is defined as

$$J_{MM}^{(T)}(u_k) = \#\{(t,s) : u_k - b/2 < t^{(M)} - s^{(M)} \leq u_k + b/2\} \qquad (4.2.7)$$

for some small bin width b>0. Here $u_k = kb$ and $t^{(M)}, s^{(M)}$ denote the times of occurrence of a pair of M events. The symbol #{A} denotes the number of elements in set A. Essentially, the variate $J_{MM}^{(T)}(u_k)$ counts the number of M events falling inside a bin of width b whose mid-point is u_k time units along from another M event in a record of length T. The situation is depicted in Figure (4.2.1). The expected value of this histogram type estimate for b small can be shown to be

$$E\{J_{MM}^{(T)}(u_k)\} = bTP_{MM}(u_k) \qquad (4.2.8)$$

The proof can be found in the original paper by Cox (1965) or in Brillinger (1975a). The result has assumed that $P_{MM}(u)$ remains sufficiently constant in the interval $(u_k - b/2, u_k + b/2]$.

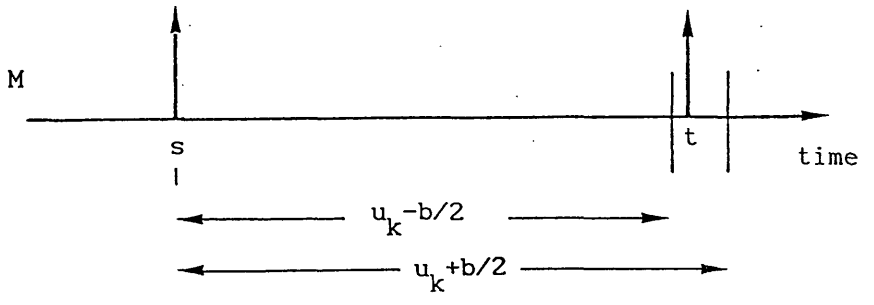

Figure 4.2.1. Schematic diagram that explains the second-order counting variate $J_{MM}^{(T)}(u_k)$. The M spike at time t falls into a bin of width b whose centre is u_k time units away from another M spike at time s.

Now from expression (4.2.8), a unbiased estimate for $P_{MM}(u_k)$ may be obtained as

$$\hat{P}_{MM}(u_k) = (1/bT)J_{MM}^{(T)}(u_k) \qquad (4.2.9)$$

The second-order counting variate $J_{MM}^{(T)}(u_k)$ is important not only in estimating the second-order time domain parameters but also in that the concept can be extended to estimate higher order time domain parameters. These are discussed in Chapter 6.

At the moment, it is worthwhile to examine the properties of $J_{MM}^{(T)}(u_k)$ in detail. The properties to be discussed are asymptotic in nature in the sense that they are strictly true only when the record length T tends to infinity. First of all, note that expression (4.2.8) is strictly true only when $|u_k| \ll T$, otherwise the end effects would introduce bias. However, this presents no problem in our applications since a pair of spikes are rarely associated when they are more than 1 second apart while the record length is usually 60 seconds. Secondly, it can be shown that the variates $J_{MM}^{(T)}(u_1),..,J_{MM}^{(T)}(u_k),..$ are asymptotically independent Poisson variates (Brillinger, 1975a). This result is not unexpected since we are counting "rare" events. If the record length T is large so that the mean value of $J_{MM}^{(T)}(u_k)$ is large, it may be approximated by the normal distribution, with mean and variance both equal to $bTP_{MM}(u_k)$. This allows the approximate confidence interval to be constructed. Finally, the normal approximation may be improved by applying the square root transformation. In this case, the approximate distribution for

$[J_{MM}^{(T)}(u_k)]^{1/2}$ would be

$$[J_{MM}^{(T)}(u_k)]^{1/2} = N\left[[bTP_{MM}(u_k)]^{1/2}, 1/4\right] \qquad (4.2.10)$$

where $N[\mu,\sigma^2]$ denotes a normal variate with mean μ and variance σ^2 (Kendall and Stuart, 1966). Figure (4.2.2) illustrates the transformation process. It should be noted that the square root transformation is applicable only when $[bTP_{MM}(u_k)]^{1/2} \gg 1/2$, ie. the mean of the normal variate is significantly larger than the standard deviation of the normal variate (Poisson variate is positive). This in turn implies that whenever the square root transformation is applicable, the transformation would improve the efficiency of the estimate. For situations where the count rate is really low such that the normal approximation is not justified, Brillinger (1975a) suggests using the transformation $[2+4J_{MM}^{(T)}(u_k)]^{1/2}$.

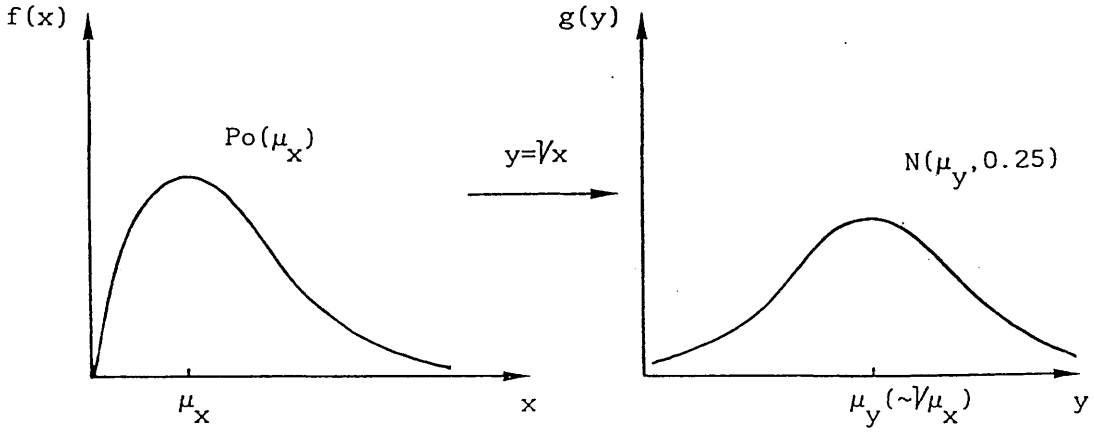

Figure 4.2.2. The transformation of a Poisson variate to an approximate normal variate. (a) The probability density function f(x) of a Poisson variate x. (b) The probability density function g(y) of the transformed variate y which has an approximate normal distribution.

Now, based on the expression (4.2.10), $[P_{MM}(u_k)]^{1/2}$ may be estimated by

$$[\hat{P}_{MM}(u_k)]^{1/2} = \left[(1/bT)J_{MM}^{(T)}(u_k)\right]^{1/2} \qquad (4.2.11)$$

and it has an asymptotic distribution of

$$[\hat{P}_{MM}(u_k)]^{1/2} = N\left[[P_{MM}(u_k)]^{1/2}, 1/4bT\right] \qquad (4.2.12)$$

Likewise, to estimate $[m_{MM}(u_k)]^{1/2}$,

$$[\hat{m}_{MM}(u_k)]^{1/2} = \left[[1/bM(T)]J_{MM}^{(T)}(u_k)\right]^{1/2} \qquad (4.2.13)$$

where M(T) is the number of M events in the interval (0,T]. The approximate asymptotic distribution for $[\hat{m}_{MM}(u_k)]^{1/2}$ is given by

$$[\hat{m}_{MM}(u_k)]^{1/2} = N\left[[m_{MM}(u_k)]^{1/2}, 1/4bM(T)\right] \qquad (4.2.14)$$

In a similar manner, the second-order cross-product density and intensity functions for point processes M and N may be estimated from the counting variate $J_{MN}^{(T)}(u_k)$ defined as

$$J_{MN}^{(T)}(u_k) = \#\{(t,s) \text{ such that } u-b/2 \le t^{(N)} - s^{(M)} < u+b/2\} \qquad (4.2.15)$$

where $t^{(N)}, s^{(M)}$ denote spike-times of N and M respectively. The rest of the symbols are defined as in expression (4.2.7). This variate counts the number of pairs of events such that an N event falls inside a bin of width b whose mid-point is u time units

along from an M event. See Figure (4.2.3).

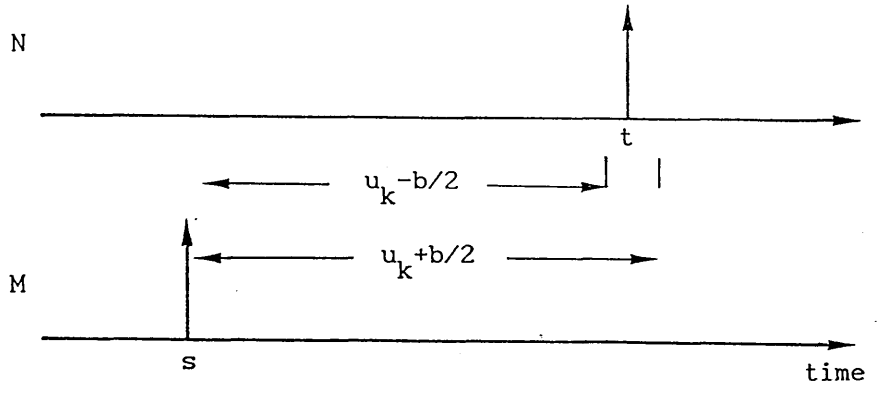

Figure 4.2.3. Schematic diagram that explains the second-order counting variate $J_{MN}^{(T)}(u_k)$. The N spike falls into a bin of width b whose centre is u_k time units away from an M spike.

From $J_{MN}^{(T)}(u_k)$, $P_{MN}(u_k)$ may be estimated as

$$\hat{P}_{MN}(u_k) = (1/bT)J_{MN}^{(T)}(u_k) \qquad (4.2.16)$$

After applying the square root transformation $[P_{MN}(u_k)]^{1/2}$ has an asymptotic distribution of

$$[\hat{P}_{MN}(u_k)]^{1/2} = N\left[[P_{MN}(u_k)]^{1/2}, 1/4bT\right] \qquad (4.2.17)$$

Similarly, the estimate for $[m_{MN}(u_k)]^{1/2}$ is given by

$$[\hat{m}_{MN}(u_k)]^{1/2} = \left[[1/bM(T)]J_{MN}^{(T)}(u_k)\right]^{1/2} \qquad (4.2.18)$$

and the approximate asymptotic distribution is

$$[\hat{m}_{MN}(u_k)]^{1/2} = N\left[[m_{MN}(u_k)]^{1/2}, 1/4bM(T)\right] \qquad (4.2.19)$$

Expressions (4.2.11-14) and (4.2.16-19) summarise the results for the distribution of the estimates for the second-order time domain estimates. They belong to the class of natural estimate and the advantage is that the estimation procedure is simple and fast to implement on digital computers. This is because in the point process case, we only need to compute all possible values of (t-s) in order to determine the value of the counting variate at all u_k's. The speed of computation only depends on the number of events in each record of M and N. The details of the algorithm for evaluating the counting variate can be found in Chapter 5.

A final point to note is the effect of the choice of bin width b. Obviously, a choice of b greater than the sampling interval essentially smooths out the estimate. The consequence of smoothing is well known in digital signal processing - it reduces the variance of the estimate (ie. improves efficiency) but also reduces the resolution. In addition, too large a bin width would introduce bias since the assumptions underlying expression (4.2.8) are no longer true. This point may also be seen by thinking of the Fourier transform pair relationship between the time parameter and the frequency domain parameter. A low resolution in the time domain parameter is effectively equivalent to a slow sampling rate so that aliasing may incur in the frequency domain parameter. Based on this argument, a rough guide for the maximum bin width b may be obtained as $b \approx 1/P$ where P is the span of frequency range of the effects lying outside the confidence interval.

4.3 Estimation of Frequency Domain Parameters

In this section, the estimation procedures for the frequency domain parameters are considered. Again, the importance of a knowledge of the asymptotic distributions and the variance of these estimates is emphasised.

4.3.1 Auto-Spectrum and Cross-Spectrum

The estimates for auto-spectra and cross-spectra are of fundamental importance in the estimation of frequency domain parameters due to the fact that it is from these quantities that other estimates are constructed. As mentioned in section (3.2.2) the auto-spectrum may be defined in two ways: (1) The Fourier transform of the cumulant density function, and (2) the asymptotic expected value of the periodogram. Hence two different approaches exist for estimating the auto-spectrum. However, Jones (1965), Bingham et al (1967) and others pointed out that the fast Fourier transform (FFT) algorithms enable the periodogram to be computed more efficiently and most computing procedures take this route. In addition, due to the fact that the general FFT algorithm is intended for a complex data array and the data array is real-valued in nature, further improvements on the speed of calculation can be achieved. (The details of the specialised FFT algorithm for real data values can be found in Chapter 5) Throughout this thesis, the estimates for auto-spectrum and cross-spectrum are based upon the periodogram.

- Stieltjes

From expression (3.2.21), the finite Fourier transform of a point process M in discrete form may be written as

$$d_M^{(T)}(\lambda_k) = \int_0^T \exp(-i\lambda_k t)[dM(t)-P_M dt] \qquad (4.3.1)$$

where $\lambda_k=2\pi k/T$ is the angular frequency in radians per second. The frequency of the k-th ordinate in cycles per second is given by k/T. The zero mean process $[dM(t)-P_M dt]$ is used in place of dM(t) for clarity in the following derivation. In practice, using either $[dM(t)-P_M dt]$ or dM(t) makes no difference except for the component at $\lambda_k=0$ which is of no interest.

Now the periodogram is written as

$$I_{MM}^{(T)}(\lambda_k) = (1/2\pi T)\overline{d_M^{(T)}(\lambda_k)}d_M^{(T)}(\lambda_k) \qquad (4.3.2)$$

To show that the auto-spectrum can be estimated by the periodogram, one may proceed as follows. From expression (4.3.1-2), the expected value of the periodogram may be seen to be

$$E\{I_{MM}^{(T)}(\lambda_k)\} = (1/2\pi T)\int_0^T\int_0^T \exp[-i\lambda_k(t-s)]E\{[dM(t)-P_M dt][dM(s)-P_M ds]\} \qquad (4.3.3)$$

Now, using the definition of the second-order cumulant density function given by expression (3.2.12), it follows that

$$E\{I_{MM}^{(T)}(\lambda_k)\} = (1/2\pi T)\int_0^T\int_0^T \exp[-i\lambda_k(t-s)]q_{MM}(t-s)dtds \qquad (4.3.4)$$

where $q_{MM}(t-s)$ is the second-order cumulant density function at lag (t-s). In expression (4.3.4), the integrand is a function of (t-s) only, hence a change of variable u=t-s gives

$$E\{I_{MM}^{(T)}(\lambda_k)\} = (1/2\pi T)\int_{-T}^{T}(T-|u|)\exp[-i\lambda_k u]q_{MM}(u)du \qquad (4.3.5)$$

Applying the mixing condition (3.1.6a), the asymptotic value of expression (4.3.5) becomes

$$\lim_{T\to\infty} E\{I_{MM}^{(T)}(\lambda_k)\} = (1/2\pi)\int_{-\infty}^{\infty}\exp[-i\lambda_k u]q_{MM}(u)du$$

$$= f_{MM}(\lambda_k) \qquad (4.3.6)$$

The result in expression (4.3.6) has made use of the definition of the auto-spectrum in expression (3.2.17). Hence it can be concluded that the expected asymptotic value of the periodogram $I_{MM}^{(T)}(\lambda_k)$ is an unbiased estimate of the auto-spectrum $f_{MM}(\lambda_k)$.

Concerning the variance of this estimate, one might proceed as follows. It should be noted that $d_M^{(T)}(\lambda_k)$ may be decomposed into the cosine and sine transforms as

$$d_M^{(T)}(\lambda_k) = d_{MC}^{(T)}(\lambda_k) - id_{MS}^{(T)}(\lambda_k) \qquad (4.3.7)$$

where

$$d_{MC}^{(T)}(\lambda_k) = \int_0^T \cos(\lambda_k t)[dM(t)-P_M dt]$$

and

$$d_{MS}^{(T)}(\lambda_k) = \int_0^T \sin(\lambda_k t)[dM(t)-P_M dt]$$

Now, consider the case where dM(t) is Gaussian, then the linear combination of dM(t) would also be Gaussian. Hence the cosine and sine transforms of dM(t) is normally distributed if dM(t) is Gaussian. However, dM(t) is obviously binomial (dM(t) can only be either 0 or 1). Hence more stringent conditions are required to establish that $d_{MC}^{(T)}(\lambda_k)$ and $d_{MS}^{(T)}(\lambda_k)$ are asymptotically normal. One approach used in Brillinger (1975d) is to assure that M(t) is a weakly dependent process such that the mixing condition of the form

$$\vartheta = \int_{-\infty}^{\infty} |u|\,|q_{MM}(u)|\,du < \infty \qquad (4.3.8)$$

holds. Then it would be sufficient to establish that $d_{MC}^{(T)}(\lambda_k)$ and $d_{MS}^{(T)}(\lambda_k)$ are asymptotically independent normal variates with zero mean. Condition (4.3.8), as seen from expression (3.1.6a), is justified.

Now gathering the information concerning the asymptotic properties of $I_{MM}^{(T)}(\lambda_k)$, one may say that it is related to the sum of the squares of two independent zero mean normal variates and it has a asymptotic mean of $f_{MM}(\lambda_k)$. Hence it can be related to a Chi-square variate with 2 degrees of freedom given by

$$2I_{MM}^{(T)}(\lambda_k)/f_{MM}(\lambda_k) = \chi_2^2 \qquad (4.3.10)$$

(Brillinger 1974a). Since the mean and variance of a χ_n^2 variate are n and 2n respectively, one can see from expression (4.3.10) that for T large

$$E\{I_{MM}^{(T)}(\lambda_k)\} = f_{MM}(\lambda_k) \qquad (4.3.11a)$$

and

$$Var\{I_{MM}^{(T)}(\lambda_k)\} = [f_{MM}(\lambda_k)]^2 \qquad (4.3.11b)$$

Expressions (4.3.11) conclude our discussion of the asymptotic properties of $I_{MM}^{(T)}(\lambda_k)$. Note that the variance does not vanish for large T. Hence $I_{MM}^{(T)}(\lambda_k)$ alone should not be used as an estimate for $f_{MM}(\lambda_k)$. The suitable smoothing procedures required to improve the estimate will be discussed shortly.

One might argue that the use of a longer record (ie. more sampling points) should give more information in estimating the periodogram. However, the fact is that the extra information does not contribute to the reduction of variance. Instead, the effect of more sampling points is to produce estimates at a greater number of discrete frequencies. If a longer run of data is sampled using the same sampling rate, the Nyquist critical frequency $1/2\Delta t$ remains unchanged but a finer frequency spacing is obtained. On the other hand, if the same length of data is sampled with a finer sampling interval, the frequency spacing remains unchanged but the Nyquist frequency range is now extended to a higher frequency. In neither case does the extra information contributes to the reduction of variance.

The periodogram can be smoothed using a number of techniques. Basically, these techniques may be divided into two approaches. The first is to compute a periodogram estimate with finer discrete frequency spacing than is really needed, and then to sum the periodogram estimates at K consecutive discrete frequencies to get one "smoother" estimate at the mid frequency of those K. The second technique is to partition the original sampled data into K segments. Each segment is separately FFT'd to produce a periodogram estimate. Finally the K periodograms are averaged at each frequency. Both approaches can be shown to be very nearly identical mathematically although they are different in implementation (See Press, W.H, et al, 1986, Chapter 12). Since the periodogram estimates averaged may be assumed to be asymptotically independent, the variances of the final estimates obtained from both techniques are both reduced by a factor of K. However, for various reasons, the second technique has been employed throughout the work reported in this thesis. First, the second technique is computationally more efficient than the first one by a modest factor, since it is logarithmically more efficient to take short FFT's than one long one. Also, the amount of computer memory storage required for the second technique for each FFT is less than that of the first technique. This implies the second technique is a sensible choice for processing long runs of data, so as to reduce the variance of the final estimate.

Mathematically, the adopted smoothing technique may be described as follows. For the sake of clarity, the results given

below are asymptotic in nature (ie. $T \rightarrow \infty$). Suppose for a point process M the record length is L and it is divided into K disjoint sections so that

$$L = KT \tag{4.3.12}$$

where T is the length of the individual sections. If the periodogram of the j-th disjoint section is written as $I_{MM}^{(Tj)}(\lambda_k)$, an estimate of the auto-spectrum may be constructed as

$$\hat{f}_{MM}(\lambda_k) = (1/K) \sum_{j=1}^{K} I_{MM}^{(Tj)}(\lambda_k) \tag{4.3.13}$$

Using the results in expression (4.3.10) and (4.3.11), the estimate $\hat{f}_{MM}(\lambda_k)$ may be seen to relate to the Chi-square distribution with 2K degrees of freedom, ie.

$$2K\ \hat{f}_{MM}(\lambda_k)/f_{MM}(\lambda_k) = \chi^2_{2K} \tag{4.3.14}$$

The mean and variance of the estimate $\hat{f}_{MM}(\lambda_k)$ follows as

$$E\{\hat{f}_{MM}(\lambda_k)\} = f_{MM}(\lambda_k) \tag{4.3.15a}$$

and

$$Var\{\hat{f}_{MM}(\lambda_k)\} = (1/K)[f_{MM}(\lambda_k)]^2 \tag{4.3.15b}$$

For K large, the large sample property implies that the estimate $\hat{f}_{MM}(\lambda_k)$ may be considered to be normally distributed given by

$$\hat{f}_{MM}(\lambda_k) \approx N\left[f_{MM}(\lambda_k), (1/K)[f_{MM}(\lambda_k)]^2\right] \tag{4.3.16}$$

Now, from expressions (4.3.15-16), the variance of the estimate is a function of frequency. From the result of Rao (1984, p385), the logarithmic transformation has the effect of stabilising the variance, so that when K is large,

$$\log_e[\hat{f}_{MM}(\lambda_k)] \approx N\left[\log_e[f_{MM}(\lambda_k)], 1/K\right] \qquad (4.3.17)$$

Hence, the distribution characteristics of $\log_e[\hat{f}_{MM}(\lambda_k)]$ is simpler than that of $\hat{f}_{MM}(\lambda_k)$. One may use logarithms to the base 10 if the magnitude of the spectrum is interpreted in terms of decibels (dB). In this case, expression (4.3.17) may be written as

$$\log_{10}[\hat{f}_{MM}(\lambda_k)] \approx N\left[\log_{10}[f_{MM}(\lambda_k)], (0.434)^2/K\right] \qquad (4.3.18)$$

Expression (4.3.18) concludes the distribution properties for the estimate of the auto-spectrum.

In a similar fashion, the cross-spectrum between the processes M and N is estimated from the cross-periodogram which is defined as

$$I_{MN}^{(T)}(\lambda_k) = (1/2\pi T)d_M^{(T)}(\lambda_k)\overline{d_N^{(T)}(\lambda_k)} \qquad (4.3.19)$$

Writing $I_{MN}^{(Tj)}(\lambda_k)$ as the cross-periodogram of the j-th segment, the estimate for $f_{MN}(\lambda_k)$ may be written as

$$\hat{f}_{MN}(\lambda_k) = (1/K) \sum_{j=1}^{K} I_{MN}^{(Tj)}(\lambda_k) \qquad (4.3.20)$$

At this point, it may be appropriate to consider the effects of the choice of the disjoint segment T. First of all, it is obvious that T should be a integral power of 2 for the application of FFT (the radix-2 algorithm is used, see Chapter 5 for details of the algorithm). Since the discrete finite Fourier transform is estimated as angular frequencies at $\lambda_k=2\pi k/T$, the resolution of the estimate obtained would be $2\pi/T$ rad/sec. Suppose a record of length L is available and that L=KT. If a long disjoint segment T is used, a fine resolution would be obtained. On the other hand if a short disjoint segment is used, a broader resolution would be obtained. However, the FFT works exponentially faster for short records, so that the price for a finer resolution would be a longer computational time. In addition, the idea of resolution bandwidth is that the estimate obtained at a particular angular frequency λ_k is a representative of the true continuous spectrum within the bandwidth $\lambda_k-\pi/T\leq\lambda<\lambda_k+\pi/T$. Expression (4.3.6) in fact assumes that the true spectrum is sufficiently constant within this bandwidth. Hence, too short a disjoint segment would induce bias to the estimate since it will tend to smooth out valid peaks. On the other hand, in the case of too long a disjoint segment is used, the confidence interval (or variance) may be too wide for isolating and comparing significant peaks. Hence, there are conflicts between computational efficiency and stability on one hand, and resolution and unbiasness on the other. A possible solution may be to check the span of dependence as seen in the

cumulant density estimate. Since the cumulant density function and the spectrum form a Fourier-Stieltjes transform pair, it can be deduced that a rough guide to the maximum frequency bandwidth would be 1/R where R is the span of dependence in the cumulant estimate. In this thesis, all frequency domain analyses are based on a choice of T=1024 msec.

4.3.2 Ordinary Coherence Function

The estimate for the ordinary coherence function between the processes M and N follows naturally from the definition given by expression (3.3.32). It is given by

$$|\hat{R}_{MN}(\lambda_k)|^2 = \frac{|\hat{f}_{MN}(\lambda_k)|^2}{\hat{f}_{MM}(\lambda_k)\hat{f}_{NN}(\lambda_k)} \qquad (4.3.22)$$

where $\hat{f}_{MN}(\lambda_k)$ is the cross-spectrum estimate given by expression (4.3.20); $\hat{f}_{MM}(\lambda_k)$ and $\hat{f}_{NN}(\lambda_k)$ are the auto-spectrum estimates of M and N respectively given in expression (4.3.13). The problem now is to define the statistical accuracy of the estimate $|\hat{R}_{MN}(\lambda_k)|^2$.

In Amjad (1989), it is shown that $|\hat{R}_{MN}(\lambda_k)|^2$ is an asymptotically unbiased estimate of the coherence function. Also, the estimate is asymptotically normal with variance given by

$$\mathrm{Var}\{|\hat{R}_{MN}(\lambda_k)|^2\} = (4/n)|R_{MN}(\lambda_k)|^2\left[1-|R_{MN}(\lambda_k)|^2\right] \qquad (4.3.23)$$

where n is the degree of freedom of the estimate $|\hat{R}_{MN}(\lambda_k)|^2$. The

disadvantage of this approach is that the variance actually depends on the true value of the parameter which is unknown. In addition, there is no obvious stabilising transformation to transform this variance to a constant. Another approach makes use of the similarity of the estimate $|\hat{R}_{MN}(\lambda_k)|$ (ie. square root of the coherence function; known as coherency in some literatures eg. Bloomfield,1976; Jenkins and Watts, 1968) to the correlation coefficient in linear correlation analysis (see for example Brownlee, 1965). A transformation, which was first suggested by Fisher, may be used to normalise the correlation coefficient estimate, ie.

$$w_{MN}(\lambda_k) = (1/2)\ \log_e\left[\frac{1+|\hat{R}_{MN}(\lambda_k)|}{1-|\hat{R}_{MN}(\lambda_k)|}\right]$$
$$= \tanh^{-1}\ |\hat{R}_{MN}(\lambda_k)| \qquad (4.3.24)$$

It has been shown, using empirical studies, that for estimates of coherence functions in the range $0.35 \leq |\hat{R}_{MN}(\lambda_k)|^2 \leq 0.95$ with degree of freedom $n \geq 20$, $w_{MN}(\lambda_k)$ has an approximate normal distribution with mean and variance of

$$E\{w_{MN}(\lambda_k)\} = (n-2)^{-1} + \tanh^{-1}|R_{MN}(\lambda_k)| \qquad (4.3.25a)$$
$$Var\{w_{MN}(\lambda_k)\} = (n-2)^{-1} \qquad (4.3.25b)$$

where n is the degree of freedom used to estimate $|\hat{R}_{MN}(\lambda_k)|^2$ (Koopmans, 1974). In the case where disjoint sections are used to estimate the spectral estimates $\hat{f}_{MM}(\lambda_k)$, $\hat{f}_{MN}(\lambda_k)$ and $\hat{f}_{NN}(\lambda_k)$, n=2K where K is the number of disjoint sections averaged.

Sometimes it is desirable to test the hypothesis that independent bivariate point processes have the same coherence structure, ie. to test whether the coherence between the processes a and b is equal to the coherence between the processes c and d at all frequencies. A statistical test for such a hypothesis may be based on the transformed variates $w_{ab}(\lambda_k) = \tanh^{-1}|\hat{R}_{ab}(\lambda_k)|$ and $\hat{w}_{cd}(\lambda_k) = \tanh^{-1}|\hat{R}_{cd}(\lambda_k)|$. The null hypothesis may be stated as

$$|R_{ab}(\lambda_k)|^2 = |R_{cd}(\lambda_k)|^2 \qquad (4.3.26)$$

In terms of the transformed variates $w_{ab}(\lambda_k)$ and $w_{cd}(\lambda_k)$, the null hypothesis may be restated as

$$w_{ab}(\lambda_k) = w_{cd}(\lambda_k) \qquad (4.3.27)$$

Under this null hypothesis, the results of expressions (4.3.25a,b) may be utilised to obtain the distribution of the difference of the transformed variates as (assuming the experiments are independent of each other)

$$\hat{w}_{ab}(\lambda_k) - \hat{w}_{cd}(\lambda_k) = N[0,1/(K-1)] \qquad (4.3.28)$$

for K (the number of disjoint sections average) large. Hence it may be concluded that one should reject the null hypothesis when

$$|\hat{w}_{ab}(\lambda_k) - \hat{w}_{cd}(\lambda_k)| > 1.96/\sqrt{(K-1)} \qquad (4.3.29)$$

where a 95% confidence limit is used.

4.3.3 Multiple Coherence Function and Partial Coherence Function

An estimate of the multiple coherence function $|R_{N_a.\mathbf{M}}(\lambda_k)|^2$ between an point process N_a and the vector valued point process $\mathbf{M}=[M_1,M_2,..,M_r]$ may be obtained following expression (3.4.35) as

$$|\hat{R}_{N_a.\mathbf{M}}(\lambda_k)|^2 = 1 - \frac{\hat{f}_{N_aN_a.\mathbf{M}}(\lambda_k)}{\hat{f}_{N_aN_a}(\lambda_k)} \qquad (4.3.30)$$

where

$$\hat{f}_{N_aN_a.\mathbf{M}}(\lambda_k) = \hat{f}_{N_aN_a}(\lambda_k) - \hat{f}_{N_a\mathbf{M}}(\lambda_k)\hat{f}^{-1}_{\mathbf{MM}}(\lambda_k)\hat{f}_{\mathbf{M}N_a}(\lambda_k)$$

and

$$\hat{f}_{N_a\mathbf{M}}(\lambda_k) = [\hat{f}_{N_aM_k}(\lambda_k)] \qquad k=1,2,..,r$$

$$\hat{f}_{\mathbf{MM}}(\lambda_k) = [\hat{f}_{M_jM_k}(\lambda_k)] \qquad j,k=1,2,..r$$

$$\hat{f}_{\mathbf{M}N_a}(\lambda_k) = \hat{f}_{N_a\mathbf{M}}(\lambda_k)^T \qquad k=1,2,..,r$$

In expression (4.3.30), A^T denotes the transpose of the matrix A. The individual elements $\hat{f}_{N_aM_k}(\lambda_k)$ and $\hat{f}_{M_kM_k}(\lambda_k)$ may be estimated using the procedures discussed in section (4.3.1)

Similarly, the estimate for the partial coherence function $|R_{N_aN_b.\mathbf{M}}(\lambda_k)|^2$ between the point processes N_a and N_b after removing the linear effects of $\mathbf{M}$ is given by

$$|\hat{R}_{N_a N_b . \mathbf{M}}(\lambda_k)|^2 = \frac{|\hat{f}_{N_a N_b . \mathbf{M}}(\lambda_k)|^2}{\hat{f}_{N_a N_a . \mathbf{M}}(\lambda_k)\hat{f}_{N_b N_b . \mathbf{M}}(\lambda_k)} \qquad (4.3.31)$$

where

$$\hat{f}_{N_a N_b . \mathbf{M}}(\lambda_k) = \hat{f}_{N_a N_b}(\lambda_k) - \hat{f}_{N_a \mathbf{M}}(\lambda_k)\hat{f}^{-1}_{\mathbf{M}\mathbf{M}}(\lambda_k)\hat{f}_{\mathbf{M}N_b}(\lambda_k)$$

with similar definitions for $\hat{f}_{N_a N_a . \mathbf{M}}(\lambda_k)$ and $\hat{f}_{N_b N_b . \mathbf{M}}(\lambda_k)$. The rest of the parameters are explained in expression (4.3.30).

The same transformation used in the case of ordinary coherence estimation may be employed to transform the multiple coherence function and the partial coherence function to asymptotic normal variates (Otnes and Enochson, 1978). The expressions for mean and variance of the estimates may be obtained by replacing expression (4.3.25) with the approximate degree of freedom. In the case of multiple coherence function, if $w_{N_a . \mathbf{M}}(\lambda_k)$ $= \tanh^{-1}|\hat{R}_{N_a . \mathbf{M}}(\lambda_k)|$,

$$E\{w_{N_a . \mathbf{M}}(\lambda_k)\} = r/2(K-r) + \tanh^{-1}|R_{N_a \mathbf{M}}(\lambda_k)|$$
$$Var\{w_{N_a . \mathbf{M}}(\lambda_k)\} = 1/2(K-r) \qquad (4.3.32)$$

where r is the number of processes in **M**. In the case of partial coherence, one must reduce the number of degrees of freedom by the number of conditional variables whose effects have been removed. For the estimate $|\hat{R}_{N_a N_b . \mathbf{M}}(\lambda_k)|^2$, the effects of r inputs are subtracted out, hence

$$E\{w_{N_a N_b . M}(\lambda_k)\} = 1/2(K-r-1) + \tanh^{-1}|R_{N_a M}(\lambda_k)|$$

$$\mathrm{Var}\{w_{N_a N_b . M}(\lambda_k)\} = 1/2(K-r-1) \qquad (4.3.33)$$

In practice, the results in expression (4.3.33) are useful in testing equality of two partial coherences after the effects of other inputs are removed. Similar expression for the 95% confidence interval can be derived by substituting $\sqrt{K}$ by $\sqrt{(K-r)}$ in expression (4.3.29).

4.4 Test for Independence

This section discusses the various results obtained in the case where the point processes of interest are independent. The confidence intervals for the estimates discussed in the previous sections are constructed to provide a statistical test for the hypothesis that the processes are independent.

A Poisson point process belongs to a class of point processes which may be considered to be completely random. It will be shown that the Poisson point process possesses similar properties as the Gaussian signal does in the case of ordinary time series. The importance of Poisson point process is emphasised through its use as a "reference signal" to represent complete independence between the events within the process.

This section begins with a brief description of the Poisson point process followed by the key results obtained under the hypothesis that the process is Poisson. Finally, the distribution of bivariate and multi-variate parameters are presented based on the hypothesis that the processes are independent. Throughout the section, the results obtained in sections (4.2-3) are referred to and some results discussed in this section are considered as special cases of those presented in sections (4.2-3).

4.4.1 Definition and Properties of a Poisson Point Process

A Poisson point process may be considered as point events

occurring singly in time and completely at random. It may serve as a mathematical model for a wide range of empirical phenomena, including the arrival of calls at a telephone exchange, the emission of particles from a radioactive source, and the occurrence of serious coal-mining accidents. A variety of examples may be found in Haight (1967).

It is important to realise that a Poisson point process is a consequence of the assumptions that are stated below. This means that whenever these assumptions are valid, the Poisson point process may be used as an appropriate model. The four assumptions may be stated as (Meyer, 1980)

1. The number of events during non-overlapping time intervals are independent random variables.
2. The number of events during any interval depends only on the length of that interval.
3. For a sufficiently small time interval the probability of obtaining exactly one event during that interval is directly proportional to the length of that interval.
4. The probability of obtaining two or more events during a sufficiently small interval is negligible, ie. a Poisson point process is orderly (see section 3.1.3).

Assumptions 1 and 2 essentially relate to stationarity and the fact that a Poisson point process is a renewal process. Assumption 3 and 4 may be expressed formally as (Cox and Isham, 1980)

$$\Pr\{M(t,t+\Delta t)=0\} = 1-P_M\Delta t+o(\Delta t) \qquad (4.4.1a)$$

$$\Pr\{M(t,t+\Delta t)=1\} = P_M\Delta t+o(\Delta t) \qquad (4.4.1b)$$

and

$$\Pr\{M(t,t+\Delta t)>1\} = o(\Delta t) \qquad (4.4.1c)$$

where $M(t,t+\Delta t)$ represents the number of M events in the interval $(t,t+\Delta t]$, and P_M is the mean intensity of the process M. The standard function $o(\Delta t)$ (known as little o of Δt) has the property that $o(\Delta t)/\Delta t \rightarrow 0$ for $\Delta t \rightarrow 0^+$.

Based on these assumptions, two important and fundamental properties of a Poisson point process may be deduced: one is concerned with the distribution of the inter-event time interval and the other the distribution of the number of events within a time interval of duration T. Suppose x is a continuous random variable representing the inter-event time interval and y a discrete random variable representing the number of events within a time interval T. It can be shown (see for example Meyer, 1980) that the respective probability density functions of x and y, f(x) and g(y), are given by

$$f(x) = P_M\exp(-P_Mx) \qquad (4.4.2a)$$

and

$$g(y) = (P_MT)^y\exp(-P_MT)/y! \qquad (4.4.2b)$$

Expression (4.4.2a) is important since the simulation of a Poisson point process relies on the generation of the required inter-event time intervals. The details of the computational algorithm may be found in Chapter 5. Expression (4.4.2b) is recognised as a

Poisson distribution with mean $P_M T$; hence the name of the process.

4.4.2 Results obtained from a Poisson Point Process

An immediate implication of the assumptions stated in the previous section is that the cumulant density function of any order for a Poisson point process M is zero, ie.

$$q_{a_1..a_k}(u_1,..,u_{k-1}) = 0 \qquad (4.4.3)$$

for $u_1,..,u_{k-1} \neq 0$ and k=2,3,... In the second-order case, one can deduce that for a Poisson point process, the second-order product density function has the property

$$P_{MM}(u) = P_M^2 \qquad u \neq 0 \qquad (4.4.4)$$

From expressions (4.2.9) and (4.4.4) and the fact that $J_{MM}^{(T)}(u_k)$ is approximately normal for T large, the estimate $\hat{P}_{MM}(u)$ would be bounded by the 95% confidence interval

$$\hat{P}_M^2 - 1.96\hat{P}_M/(bT)^{1/2} \leq \hat{P}_{MM}(u) \leq \hat{P}_M^2 + 1.96\hat{P}_M/(bT)^{1/2} \qquad (4.4.5)$$

Similarly, the estimate for the auto-intensity function would be bounded by the 95% confidence interval

$$\hat{P}_M - 1.96/(bT)^{1/2} \leq \hat{m}_{MM}(u) \leq \hat{P}_M + 1.96/(bT)^{1/2} \qquad (4.4.6)$$

After applying the square root transformation, expression

(4.4.5-6) become

$$\hat{P}_M - 1/(bT)^{1/2} \leq [\hat{P}_{MM}(u)]^{1/2} \leq \hat{P}_M - 1/(bT)^{1/2} \qquad (4.4.7a)$$

and

$$\hat{P}_M^{1/2} - 1/[bM(T)]^{1/2} \leq [\hat{m}_{MM}(u)]^{1/2} \leq \hat{P}_M^{1/2} + 1/[bM(T)]^{1/2} \qquad (4.4.7b)$$

Expression (4.4.7) represents the region of fluctuation of a Poisson point process. If a point process of the same mean rate has density and intensity estimates outside these regions, it may be concluded that the process possesses significant effects at those estimates.

Concerning the auto-spectrum of a Poisson point process, one should note that a special case of expression (4.4.3) at k=2 may be written as

$$q_{MM}(u) = \begin{cases} P_M \delta(u) u=0 \\ 0 \qquad \text{otherwise} \end{cases} \qquad (4.4.8)$$

The auto-spectrum is the Fourier transform of the auto-cumulant density, hence

$$f_{MM}(\lambda) = P_M/2\pi \qquad (4.4.9)$$

ie. The auto-spectrum of a Poisson point process is constant at $P_M/2\pi$ for all frequencies. This suggests that the Poisson point process may be considered analogous to Gaussian signal in the case of ordinary time series.

An interesting point to note is that the result obtained in expression (4.4.9) is the same as that of the asymptotic value of the auto-spectrum of any point processes. This implies that for λ large, the spectrum of a point process which observes the Riemann-Lebesque Lemma (see the discussion in section 3.2.2) would behave like a Poisson point process and hence would be bounded by the confidence interval stated in expression (4.4.10).

From expression (4.3.18) and (4.4.9), the 95% confidence interval of the auto-spectrum of a Poisson point process follows as

$$\log_{10}\left[\frac{\hat{P}_M}{2\pi}\right] - 0.85\sqrt{2/K} \leq \hat{f}_{MM}(\lambda_k) \leq \log_{10}\left[\frac{\hat{P}_M}{2\pi}\right] + 0.85\sqrt{2/K} \qquad (4.4.10)$$

Expression (4.4.10) is very useful in comparing the frequency content of a point process with a Poisson point process of the same mean rate. Any value outwith the limits implies departure from complete randomness and hence may be considered as a significant periodic component.

4.4.3 Results for Bivariate and Multi-Variate Point Process Under the Hypothesis of Independence

The treatment for the second-order time domain parameters in the bivariate case is essentially similar to the univariate cases. When two point processes M and N are independent, the cross-cumulant density function is zero and hence,

$$P_{MN}(u) = P_M P_N \qquad (4.4.11)$$

The confidence intervals for $\hat{P}_{MN}(u_k)$, $\hat{m}_{MN}(u_k)$, $[\hat{P}_{MN}(u_k)]^{1/2}$ and $[\hat{m}_{MN}(u_k)]^{1/2}$ can then be stated as

$$\hat{P}_M\hat{P}_N - 1.96\left[\frac{\hat{P}_M\hat{P}_N}{bT}\right]^{1/2} \le \hat{P}_{MN}(u_k) \le \hat{P}_M\hat{P}_N + 1.96\left[\frac{\hat{P}_M\hat{P}_N}{bT}\right]^{1/2} \qquad (4.4.12a)$$

$$\hat{P}_N - 1.96\left[\frac{\hat{P}_N}{bM(T)}\right]^{1/2} \le \hat{m}_{MN}(u_k) \le \hat{P}_N + 1.96\left[\frac{\hat{P}_N}{bM(T)}\right]^{1/2} \qquad (4.4.12b)$$

$$\left[\hat{P}_M\hat{P}_N\right]^{1/2} - (1/bT)^{1/2} \le \left[\hat{P}_{MN}(u_k)\right]^{1/2} \le \left[\hat{P}_M\hat{P}_N\right]^{1/2} + (1/bT)^{1/2} \qquad (4.4.12c)$$

$$\hat{P}_N^{1/2} - \left[\frac{1}{bM(T)}\right]^{1/2} \le \left[m_{MN}(u_k)\right]^{1/2} \le \hat{P}_N^{1/2} + \left[\frac{1}{bM(T)}\right]^{1/2} \qquad (4.4.12d)$$

Expressions (4.4.12a-d) may be used to detect any significant effects indicated by values lying outside these limits.

In the frequency domain, the cross-spectrum between independent point processes of order-2 and above are zero, ie.

$$f_{a_1..a_k}(\lambda_1,..,\lambda_{k-1}) = 0 \qquad k \ge 2 \qquad (4.4.13)$$

This result may be seen from the fact that the cross-cumulant density functions do not involve any Dirac delta function as auto-cumulant density functions do. The construction of the 95% confidence interval for a zero cross-spectrum does not seem to be very meaningful. Instead, a test of zero normalised cross-spectrum, ie. the coherence function, is more desirable.

First of all, it should be noted that the method based on the Fisher's transformation is not suitable due to the fact that zero is outwith the range for which the assumption is valid (see section 4.3.2). Hence other approaches are called for. Two approaches are available. The first one makes use of the quantity

$$F_{2,2(K-1)} = \frac{|\hat{R}_{MN}(\lambda_k)|^2}{1-|\hat{R}_{MN}(\lambda_k)|^2}\left[\frac{2(K-1)}{2}\right] \qquad (4.4.14)$$

This is an F-distributed variate with 2 and 2(K-1) degrees of freedom under the assumption that processes M and N are independent (Mood et al, 1963). However, this method requires looking up the table of F-distribution and so from a computational point of view, another approach is preferred. The result used was first derived by Abramowitz and Stegun (1964) and is an extension to the work of Goodman (1963). The 95% confidence interval of $|\hat{R}_{MN}(\lambda_k)|^2$ under the assumption that $|R_{MN}(\lambda_k)|^2=0$ can be shown to be given by

$$\Pr\{|\hat{R}_{MN}(\lambda_k)|^2 \le \beta\} = 0.95 \qquad (4.4.15)$$

where $\beta = 1-0.05^{1/(K-1)}$

Hence if M and N are independent, about 95% of the values of $|\hat{R}_{MN}(\lambda_k)|^2$ should lie within the region between zero and β. Any values outwith this interval indicate that the two processes are dependent at those frequencies. Note that in the extreme case when K=1 (ie. without averaging), then β=1 and it is impossible to tell whether the two processes are independent or not.

In the case of partial coherence of order r between N_1 and N_2 after removing the effects of $M=\{M_1,M_2,..,M_r\}$, the 95% confidence interval under the hypothesis $|R_{N_1N_2.M}(\lambda_k)|^2=0$ is given by

$$\Pr\{|\hat{R}_{N_1N_2.M}(\lambda_k)|^2 \leq \beta\} = 0.95 \qquad (4.4.16)$$

where $\beta = 1-0.05^{1/(K-r-1)}$

If the values of $|\hat{R}_{N_1N_2.M}(\lambda_k)|^2=0$ are outwith this level β, it can be concluded that the processes N_1 and N_2 are dependent even after removing the effects of **M**.

Chapter 5

Experimental and Computational Considerations

Chapter 5 Experimental and Computational Considerations

5.1 Introduction

The complexity of experiments on the neuromuscular system - particularly those experiments where several input channels are active simultaneously while recording from a number of output channels - requires that the experimenter be able to generate multiple test signals, collect multivariate response data, analyse these interactions at the time of the experiment, and adjust the experimental procedures in the light of the analysis. This chapter describes some aspects of the design of the experiments for the analysis of the behaviour of neuromuscular and associated model systems. In Chapter 2, the elements of neuromuscular system involved have been described. The purpose of this chapter is (1) to describe the model used in the simulation experiment (2) to describe the computational procedures used to generate the stimuli to both the real and model systems (3) to describe very briefly the experimental systems employed in the generation and collection of data obtained in both the real and simulation experiments and (4) to set out some techniques that were used to improve the computational efficiency of some of the algorithms used to analyse the collected data.

5.2 The Model

The model has several components and may be adapted to represent properties of the muscle spindle or a single neurone, each with several inputs or outputs. It is based on a pulse frequency modulator first suggested by Meyer (1961) and Pavlidis and Jury (1965). Later a more general formulation of a "leaky integrator" is adopted which explains the experimental observation in that there exists a marked phase-locking between each cycle of a stimulus and the impulse generation. The model in this thesis is implemented on an EAI 2000 analog computer. The different components of the model are described as follows.

Figure (5.2.1) shows the diagram of the encoder portion of the model. The symbols used are standard in analog computing and are explained in Appendix A1. The encoder consists of a first-order filter followed by a threshold detector. When a continuous signal is applied to the encoder input, the integrator output ramps upwards. The rate of increase of the filter output depends on the amplitude of the input. When the filter output exceeds V_T, the preset threshold value, a spike is generated and the integrator output is reset to zero for the duration of the pulse. This duration, which is set to 1 millisecond, matches the typical pulse width of an action potential and is controlled by a timing circuit consisting of an integrator and a comparator. The first order filter making up the initial stage of the encoder plays an important role, allowing pulse frequency modulators to observe the input signal for a finite period of time before a pulse can be

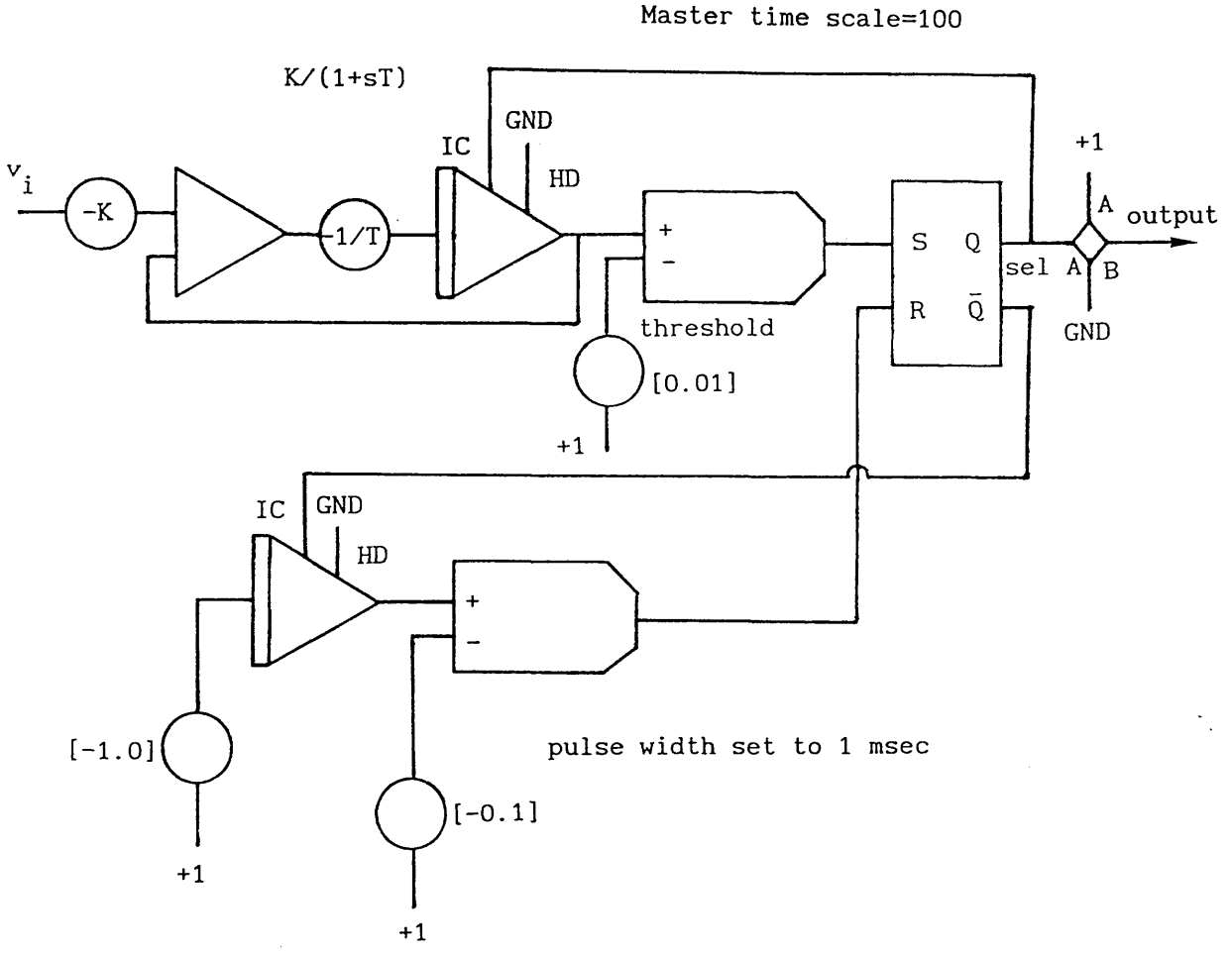

Figure 5.2.1. Patch diagram showing the analogue simulation of a pulse encoder on the EAI 2000 analogue computer. The explanation of the symbols used can be found in Appendix 1.

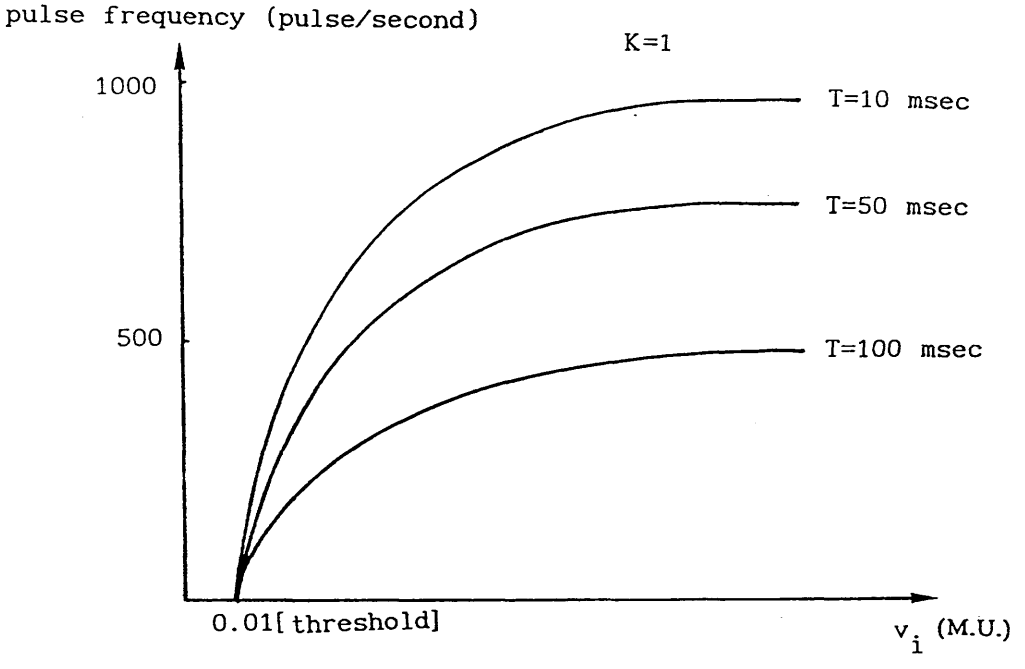

Figure 5.2.2. Diagram showing the output characteristics of the pulse encoder illustrated in Figure 5.2.1 for different values of encoder time constant T.

emitted. The use of a first order filter has been found to give better agreement between simulated and physiological results in previous simulation studies (Angers and Delilse, 1971; Downie and Murray-Smith, 1981 and Halliday, 1986). Figure (5.2.2) shows the output characteristics of the encoder. From Figure (5.2.2), it can be seen that the time constant of the filter determines the maximum pulse frequency that can be emitted by the encoder. Also, from the simulation studies by Halliday (1986), the time constant of the filter plays an important part in determining the coherence between the input and output spike trains of the model.

Figure (5.2.3) shows the model employed to simulate the contractile and mechanical properties of the intrafusal fibres of a muscle spindle. The transfer function of the model has the form $G/(1+s\tau)$ where G is the mid-band gain and τ is the time constant. It has been shown that the phenomenon of "driving" observed in the muscle spindle can be simulated using this model in conjunction with the encoder in Figure (5.2.1) (see Halliday 1986).

The model shown in Figure (5.2.4) represents the element used to generate the excitatory post-synaptic potential (EPSP, see Chapter 2). The transfer function of the model has the form $G/(1+s\tau)^2$ and the impulse response is given by $t(G/\tau)^2\exp(-t/\tau)$. The choice of a double-pole second order filter is based on the time course of the EPSP. Various sizes and durations of EPSP may be modelled by adjusting the values of the gain G and time constant τ. The output from this second-order filter is used as the input to the encoder, together they represent a model neurone.

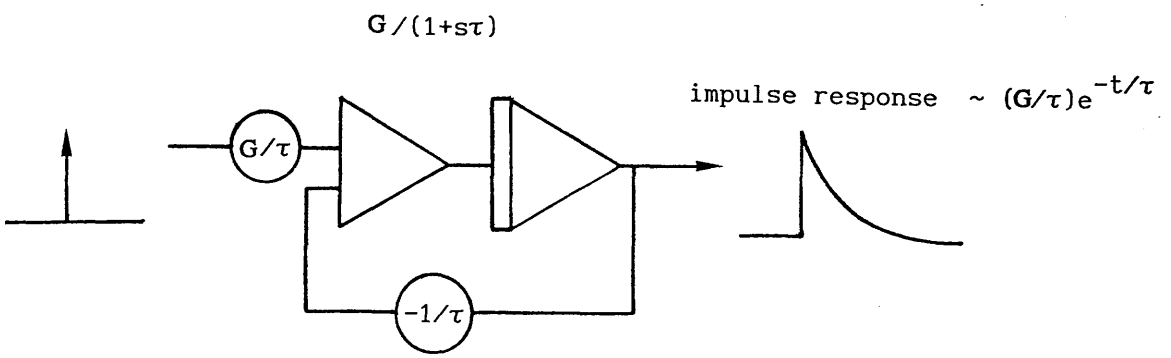

Figure 5.2.3. Patch diagram of the analogue simulation of a first-order filter used to simulate the contractile and mechanical properties of the intrafusal fibres of a muscle spindle. The transfer function has the form $G/(1+s\tau)$ where G is the gain and τ is the time constant. The response of the filter under a Dirac delta impulse input is also illustrated.

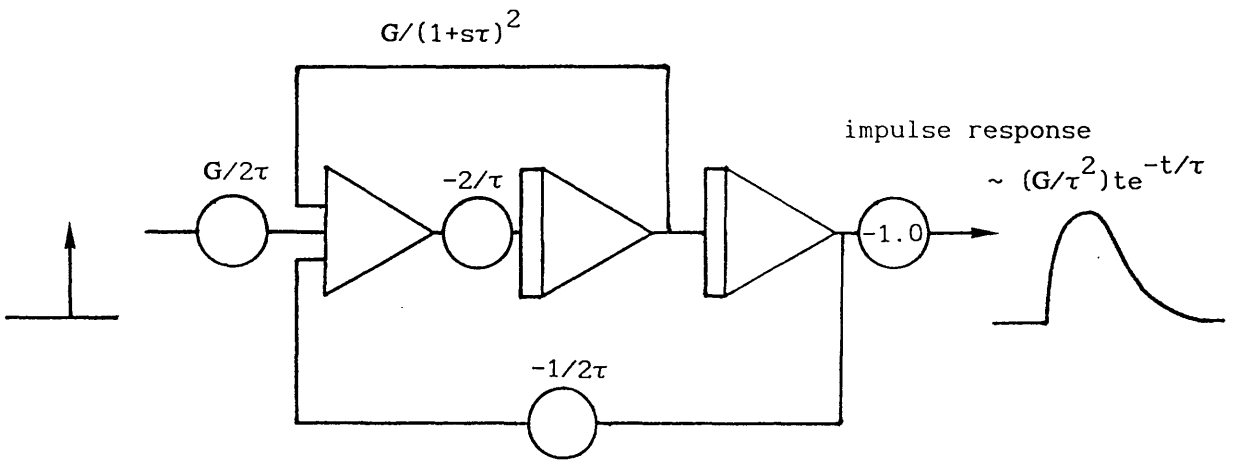

Figure 5.2.4. Patch diagram of the analogue simulation of a second-order filter used to generate the excitatory post-synaptic potential (EPSP). The transfer function is chosen as $G/(1+s\tau)^2$ such that impulse response has the shape similar to an EPSP.

The three kinds of elements described above may be configured in different ways forming neuronal networks of different degrees of complexity. The analysis of such networks are investigated in Chapter 6.

5.3 Generation of Stimuli

5.3.1 An Algorithm to Generate Poisson Processes

Generation of Poisson processes may be achieved by several methods. A traditional method records the signal produced by a Geiger counter with a radioactive source placed near the detector. The mean rate of the process can be adjusted by altering the position of the radioactive source. In general this procedure is poor, due to the lack of precise control over the mean rate of the process. In this thesis Poisson processes were produced based on computational methods. From expression (4.4.2a), it is seen that the inter-spike intervals of a Poisson process are independently exponentially distributed. Based on this property, a Poisson process may be simulated. The exponential deviate is generated through the transformation of uniform deviates (Press et al, 1986). This has the advantage that the mean rate of the Poisson point process can be obtained to a high degree of accuracy, and that the time required to generate the sequence is much less than that of the duration of the process.

The basic principle used to generate the uniform deviates is based on the conventional linear congruential generator, which generates a sequence of integers I_1, I_2, I_3,..., each between 0 and m-1 (a large number) by the recurrence relation

$$I_{j+1} = aI_j + c \bmod mj > 0 \qquad (5.3.1)$$

where a, c and m are positive integers. After an initial value I_1

is chosen and positive integers a, c and m are specified, I_2 is computed from $aI_1+c \bmod m$. Similarly, I_3 can then be computed from $aI_2+c \bmod m$. The recurrence will eventually repeat itself. To increase the period of the sequence, the shuffle algorithm suggested by Bays and Durham and described in Knuth (1981) is employed to improve the linear congruential method. The algorithm is illustrated in Figure (5.3.1). The uniform deviates obtained from the shuffle algorithm are normalised (ie. divide by m) to give a probability density function

$$f(x) = \begin{cases} 1 & 0 \le x < 1 \\ 0 & \text{otherwise} \end{cases} \qquad (5.3.2)$$

For an exponential deviate y, the probability density function is given by

$$g(y) = \begin{cases} \beta\exp(-\beta y) & y>0 \\ 0 & \text{otherwise} \end{cases} \qquad (5.3.3)$$

where β can be interpreted as the reciprocal of the mean of y. Suppose y=T(x) is required to transform the uniform deviates x to exponential deviates y, our task is then to find T(x).

Since

$$|f(x)dx| = |g(y)dy| \qquad (5.3.4)$$

and the fact that both f(x) and g(y) are non-negative, one may deduce from expressions (5.3.2-4) that

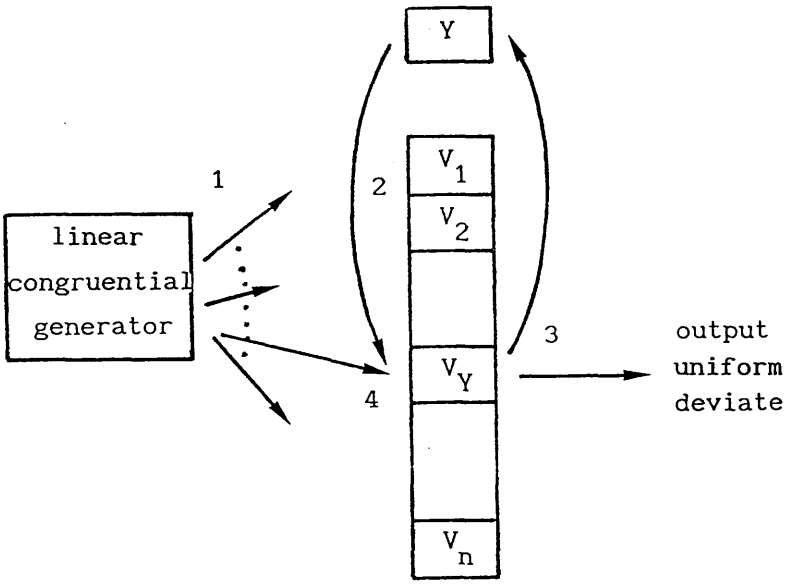

Step 1: fill Y and array V

2: point to the element V_Y

3: output V_Y as the uniform deviate and set Y as V_Y

4: fill V_Y from the linear congruential generator

5: repeat from step 2

Figure 5.3.1. Schematic diagram illustrating the shuffle algorithm suggested by Bays and Durham to randomise the sequence of uniform variates generated by the conventional linear congruential method.

$$|dx/dy| = \beta\exp(-\beta y)$$

which gives

$$y = -1/\beta \log_e(x) = T(x) \qquad (5.3.5)$$

Hence by substituting the required value for β, a sequence of exponential deviates of specified mean can be obtained. The transformation process is summarised in Figure (5.3.2). Now a Poisson process of required mean rate may be generated by employing the exponential deviates as the inter-spike intervals.

5.3.2 An Algorithm to Generate Point Processes with Gaussian Distributed Inter-Spike Intervals

The generation of a point process with Gaussian distributed inter-spike intervals depends upon the generation of a series of Gaussian deviates. In this thesis, the generation of Gaussian deviates is based on the Box-Muller method. Consider the transformation between two uniform deviates on (0,1), x_1, x_2 and two quantities y_1, y_2, a two-dimensional extension of expression (5.3.4) may be written as,

$$g(y_1,y_2) = f(x_1,x_2)\left|\frac{\partial(x_1,x_2)}{\partial(y_1,y_2)}\right| \qquad (5.3.6)$$

where $|\partial(.)/\partial(.)|$ is the Jacobian determinant of the x's with respect to the y's. Now if x_1 and x_2 are two uniform deviates in the range (0,1) and we want y_1 and y_2 to be two independent normal deviates having distribution $[1/\sqrt{(2\pi)}]\exp(-y^2/2)$, ie. N(0,1), one

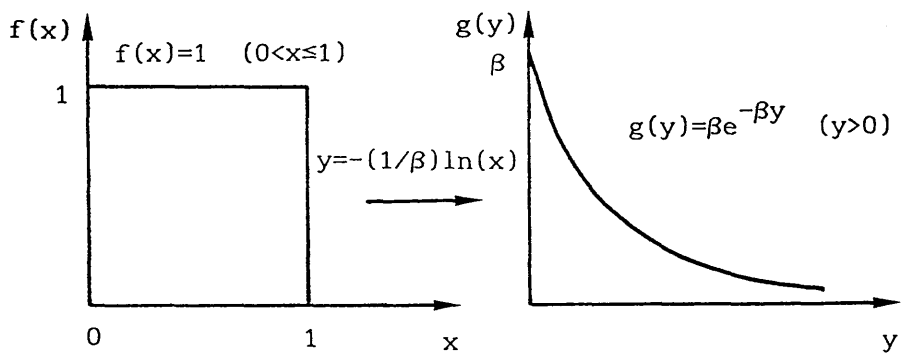

f(x) : probability density function of x

g(y) : probability density function of y

Figure 5.3.2. Transformation of an uniform deviate x to an exponential deviate $y=-(1/\beta)\ln(x)$ where β is the reciprocal of the mean of y.

requires

$$\left|\frac{\partial(x_1,x_2)}{\partial(y_1,y_2)}\right| = \left[\sqrt{1/2\pi}\,\exp(-y_1^2/2)\right]\left[\sqrt{1/2\pi}\,\exp(-y_2^2/2)\right] \quad (5.3.7)$$

It may be shown that a possible solution of equation (5.3.7) is given by

$$y_1 = [-2\,\ln(x_1)]^{1/2}\cos(2\pi x_2) \quad (5.3.8a)$$

and

$$y_2 = [-2\,\ln(x_1)]^{1/2}\sin(2\pi x_2) \quad (5.3.8b)$$

Hence, the required transformation is obtained. One further way to simplify the computation of expression (5.3.8) is to choose the random point v_1, v_2 inside the unit circle around the origin instead of the uniform deviates x_1, x_2 in the unit square. Then $R \equiv v_1^2+v_2^2$ is a uniform deviate which can be used for x_1, while the angle can be taken as $2\pi x_2$. Now, the sine and cosine terms in expression (5.3.8) can be written as $v_1/\sqrt{R}$ and $v_2/\sqrt{R}$, avoiding the trigonometric function calls in a program and hence improve the speed of computation. Once the standardised normal deviates are available, the required normal deviates $N(\mu,\sigma^2)$ may be obtained by a simple transformation $\sigma N(0,1)+\mu$.

5.4 A Brief Description of the Experimental Systems

The experimental systems include the development of both hardware and software for signal generation and data collection. Two such systems were built, one for the use on neuromuscular experiments in the Department of Physiology and the other for the simulation experiments performed in the Department of Electronics and Electrical Engineering.

The signal generation/data collection system developed for experiments involving neuromuscular elements incorporates the Cambridge Electronics Design (C.E.D) 1401 intelligent peripheral that generates and receives analog, digital and timing signals using its own processor, clocks and memory under the control of a host computer. A two megabytes mass RAM has been installed in the C.E.D. device to improve its ability for mass data storage. At present, the host computer is a Tandon microcomputer (IBM AT compatible).

The program DIGAD, which combines the power of the Tandon microcomputer and the C.E.D. unit, provides for concurrent generation of point process stimuli and collection of point processes and continuous signals. In some applications, a noise generator was used to generate the stimuli, and a record of the noise signals and the resulting point process signal was digitised via the CED interface. (See Figure 5.4.1) The data, which is stored in ASCII format, is then readily examined and analysed.

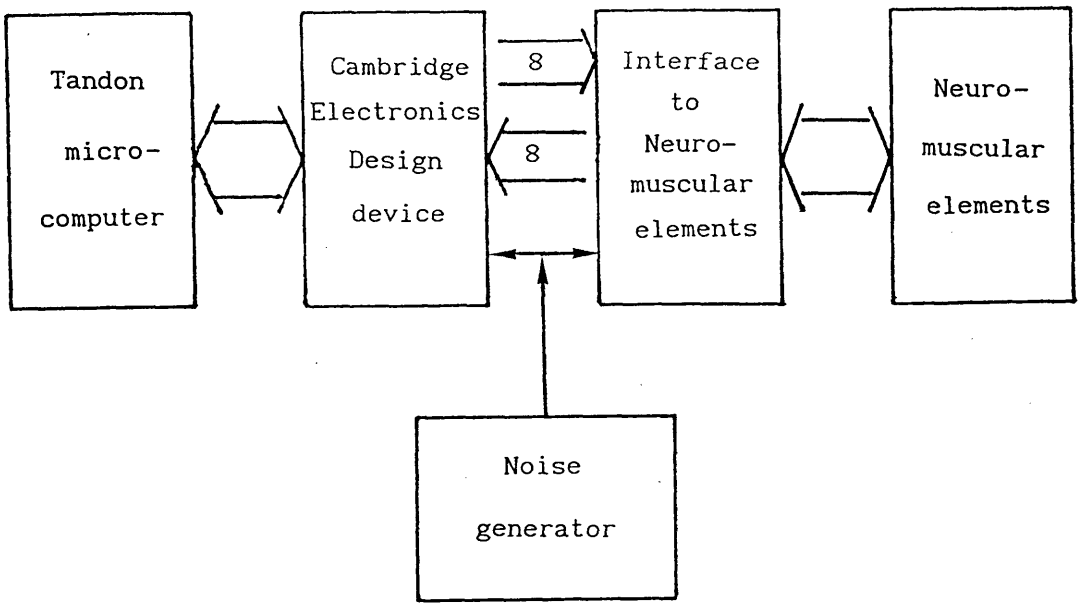

Figure 5.4.1. Schematic diagram illustrating the experimental setup involved in the generation of stimuli and collection of spike trains during an neuro-physiological experiment.

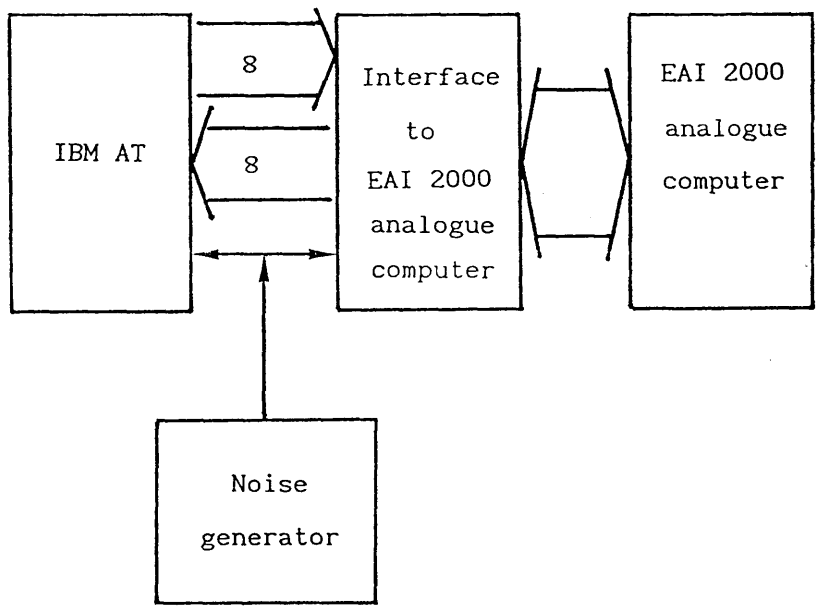

Figure 5.4.2. Schematic diagram illustrating the experimental setup involved in the generation of stimuli and collection of model response data during an simulation experiment.

The main features of DIGAD are:

a. Collection of eight channels of point process data with accuracy within one millisecond.

b. Collection of an analog signal at a sampling rate of 1 kHz. The resolution of the analog to digital (A/D) conversion is $10/2^{12}$=2.44 mV.

c. Generation of Poisson and Gaussian point processes through eight independent channels. Generation of spike trains of other structures is also possible provided the required data file is available.

d. The maximum duration of signal collection/generation (ie. the memory available to capture the data) is approximately 255 seconds with a, b and c above all operating simultaneously.

e. An user-friendly environment is used to simplify the operation of DIGAD so that the user can concentrate on the experiment instead of the operation of DIGAD.

The experimental system used for the simulation experiments essentially does the same job as the Tandon microcomputer and the C.E.D. device in the case of the neurophysiological experiments. It consists of three parts: (1) An IBM AT (2) An EAI 2000 analog computer and (3) An interface between the EAI 2000 and the IBM AT. The block diagram is shown in Figure (5.4.2). However, the amount of RAM inside the IBM AT is 512 kilobytes which limits the maximum duration of a simulation experiment to 60 seconds.

5.5 Two efficient Algorithms

5.5.1 An Algorithm for Computing $J_{MN}^{(T)}(u_j)$

Let N and M be two spike trains realised in (0,T]. Suppose r_j, j=1,2,...,N(T), and s_k, k=1,2,..,M(T) are the observed spike times of processes N and M respectively. The algorithm for the fast computation of the variate $J_{MN}^{(T)}(u_j)$ (see Section 4.2.2 for definition of $J_{MN}^{(T)}(u_j)$) with bin width b is explained as follows:-

1. Store the ordered times r_j and s_k in two separate arrays.
2. Initialise an integer array JT(LAGMIN:LAGMAX) (note: FORTRAN format used) where LAGMIN is the minimum lag value and LAGMAX is the maximum lag value, eg. JT(-100:100).
3. Initialise two pointers a and b to 1: a for process N and b for process M.
4. For the b^{th} spike of process N, increment a by 1 until u_j= integer part of $(r_a-s_b)/b$ lies inside the interval (LAGMIN,LAGMAX). Retain the pointer a.
5. Set $JT(u_j) = JT(u_j)+1$. Repeat steps (4) and (5) until u_j>LAGMAX.
6. Increment b by 1 and go back to step (4) until b>M(T).

The algorithm described above may be extended to compute counting variates of order-3 or above. To compute the third-order counting variate, for example, set u_j and compute $J_{123}^{(T)}(u_j,v_k)$ for different values of v_k using the above algorithm. Then set u_j to another value and repeat the procedure.

5.5.2 Fast Fourier Transform of a Single Real Function

The fast Fourier transform (FFT) of a single real function is of fundamental importance since it forms the basis in estimating the frequency domain parameters discussed in section (4.3). Suppose a conventional radix-2 FFT subroutine FOUR1 is available for calculating the fast Fourier transform for a single complex function. To avoid redundancy for computing a single real function, the following method is employed.

Suppose the real function is represented by f_j, $j=0,..,N-1$, where N is a integer power of 2. First the data set is spilt into two halves: the even-numbered f_j as one data set, and the odd-numbered f_j as the other. Then we form a complex function

$$h_j = f_{2j} + if_{2j+1} \qquad j=0,..,N/2-1 \qquad (5.5.1)$$

where i is the complex number = $\sqrt{(-1)}$. We submit this to FOUR1 and it will return a complex array $H_n=F_n^e+iF_n^o$, $n=0,..,N/2-1$ with

$$F_n^e = \sum_{k=0}^{N/2-1} f_{2k} \exp[-2\pi ikn/(N/2)]$$

$$F_n^o = \sum_{k=0}^{N/2-1} f_{2k+1} \exp[-2\pi ikn/(N/2)] \qquad (5.5.2)$$

Now if F_n is the FFT of the original data f_j, it can be shown that

$$F_n = F_n^e + F_n^o \exp(-2\pi i n/N) \quad n=0,..,N/2-1 \qquad (5.5.3)$$

Hence expressed directly in terms of the transform H_n

$$F_n = (1/2)(H_n+\overline{H_{N/2-n}}) - (1/2)(H_n-\overline{H_{N/2-n}})\exp(-2\pi i n/N) \qquad (5.5.4)$$

where n=0,..,N/2-1. In addition, the following points should be noted. Since $\overline{F_{N-n}} = F_n$, there is no point in saving the entire spectrum. The positive frequency half is sufficient and can be stored in the same array as the original data. The final point to note is that in order to actually get the entire F_n in the original array space, it is convenient to return $F_{N/2}$ as the imaginary part of F_0 since the values F_0 and $F_{N/2}$ are real and independent.

Chapter 6

Results and Discussion

Chapter 6 Results and Discussion

In this chapter, the techniques discussed in the previous chapters are applied to various data sets obtained during neuromuscular experiments and simulation studies. The procedures to reduce bias and uncertainties concerning the quantities described in Chapter 4 have been taken into account and the objective of this chapter is to concentrate on the interpretation of the results obtained.

The chapter begins with the studies on some examples univariate point processes generated by a neurone model described in Chapter 5. These point processes are characteristic of some physiological systems in the sense that they are generated under the assumptions which are relevant to the experimental data obtained. Both time and frequency domain descriptions are discussed. The objective is to provide some simple intuitive examples of univariate point processes which may help to facilitate understanding and identifying different patterns of spike trains. Some preliminary works in this aspect have been done by ten Hoopen (1974) and the work discussed in this thesis may be considered as an extension to it.

Following the consideration of univariate point processes attention is directed to bivariate point processes and multi-variate point processes. In the bivariate case, simulation studies are used to demonstrate the analysis of a single-input, single-output neurone model under the influence of a noise signal.

The effects of different sizes of excitatory post-synaptic potentials (EPSP's) and inhibitory post-synaptic potentials are considered. The findings of such analysis form an important basis in the later discussions. Single-input, single-output model studies similar to this but applied to the modelling of muscle spindle can be founded in Halliday (1986).

The shape and position of the primary peak in the cross-correlation histogram computed from the discharges of a pair of neurones has been used as the basis for inferring the presence of shared or common inputs to these neurones (eg. Datta and Stephens, 1990; Ellaway and Murthy, 1981a; Kirkwood, Sears, Tuck and Westgaard, 1982; Michalski, Gerstein, Czarkowska and Tarnecki, 1983). The original work of Perkel, Gerstein and Moore (1967a,b) and Moore, Segundo, Perkel and Levitan (1970), based largely on computer simulations of neuronal interactions, described the features that shared inputs to pairs of neurones may produce in the cross-correlation histogram estimated from the discharges of these neurones. Other workers have investigated the interactions between neurones within neuromuscular systems of different kinds. The primary intention of these investigations was to detect the presence of common or correlated inputs to pairs of neurones. The recent work of Cope, Fetz and Matsumura (1987) extended these studies by suggesting how the EPSP amplitude and time course would contribute to the size and shape of the primary peak in the cross-correlation histogram. It was first found out, based on a single-input, two-output neurone model, that the coherence function may reveal the frequency content of the common input

(Rosenberg, et al. 1991; to be published). Ferrell, Rosenberg, Baxendale, Halliday and Wood (1990) used the coherence and partial coherence functions to demonstrate that coupling between pairs of gastrocnemius motor units occurred at the frequency of the mechanical activation of small groups of joint afferent neurones, and that the joint afferent induced coupling acted independently of other sources of coupling.

Following the study on a single neurone, a neuronal network model in which a pair of neurones is influenced by a common input is studied both analytically and based on simulation. The focus of the analysis is placed on the inferred properties of the common input based on the observed discharges of the two neurones. The analysis is then extended to the situation where a pair of neurones receives inputs from two common inputs; one of the common inputs may be a continuous signal. Based on simulation studies, the techniques of partial coherence of order-1 and order-2 are applied to the extended model. The significance of the results with relevance to physiological systems is discussed. This concludes the results obtained which are related to the linear point process theory.

Finally, the extension of the linear system analysis in which the input point process exerts a non-linear influence on the output process is considered. The analysis is based on a neurone model which incorporates the features of after-hyperpolarisation, or post-spike depression (see Chapter 2). The analysis leads to the possibility of inferring the time course of the

after-hyperpolarisation based on the third-order cumulant density estimate derived from the input and output spike trains.

6.1 Examples of Univariate Point Processes

6.1.1 Poisson Point Processes

The theoretical basis of the definition and properties of a Poisson point process has been discussed in Chapter 4. In this section, two examples of Poisson point processes are considered. They are generated using the algorithms described in Chapter 5. Three techniques, namely interval histogram, auto-intensity and auto-spectrum, are applied to the examples to illustrate some aspects of a Poisson point process. The interval histogram is commonly used by neurophysiologists and is essentially an inter-spike interval histogram. For a renewal process (ie. a process in which the inter-event intervals are independently distributed, see Chapter 1), the interval histogram alone is adequate to define a point process (Cox and Miller, 1965). The Poisson point is a class of renewal point processes, with exponential interval histogram. For a renewal point process M with interval probability density function h(x), the auto-spectrum of the process can be expressed as

$$f_{MM}(\lambda) = \frac{P_M}{2\pi}\left[\frac{h^*(\lambda)}{1-h^*(\lambda)} + \frac{h^*(-\lambda)}{1-h^*(\lambda)} + 1\right] \qquad (6.1.1)$$

where $h^*(\lambda)$ is the Laplace Transform of h(x) (Cox and Miller, 1965). Hence for a renewal point process, any one of the three quantities is adequate to define the properties of the process. The interval histogram has the advantage that it is straight-forward to interpret and compute. However, it may

non-renewal processes and to
present difficulties in being extended to describe properties of multiple point processes or to the situation where one or more of the components are continuous. In the later sections, emphasis will be placed on the point process analysis techniques discussed in the earlier chapters.

Figure (6.1.1) illustrates the estimates for the interval histogram, the auto-intensity and the auto-spectrum of a simulated Poisson point process of mean rate 25.4 spikes/sec. and duration 60 seconds. The interval histogram in Figure (6.1.1a) follows an exponential distribution as expected from expression (4.4.2a). The bin width used in the interval histogram is 4 msec. Note that the shorter the interval, the higher the number of occurrences. This may be explained by the fact that for a completely random process, the longer the time interval, the greater the chance for an event to have occurred. Note also that from the interval histogram, there is no accurate way of deducing other information concerning the process such as the mean rate. On the other hand, the mean rate of the process is readily obtained from the auto-intensity in Figure (6.1.1b). The auto-intensity fluctuates about the value $0.16=\sqrt{(0.0254)}=\sqrt{(\hat{P}_M)}$ and stays within the 95% confidence interval given by expression (4.4.7b). It indicates that the probability for an spike to occur given another spike has occurred earlier is constant, ie. the two spikes are independent. The auto-spectrum is shown in Figure (6.1.1c). Again it has no structure and fluctuates about the value $-2.4=\log_{10}(\hat{P}_M/2\pi)$. All values stay within the 95% confidence interval given by expression (4.4.10) indicating that the simulated point process is

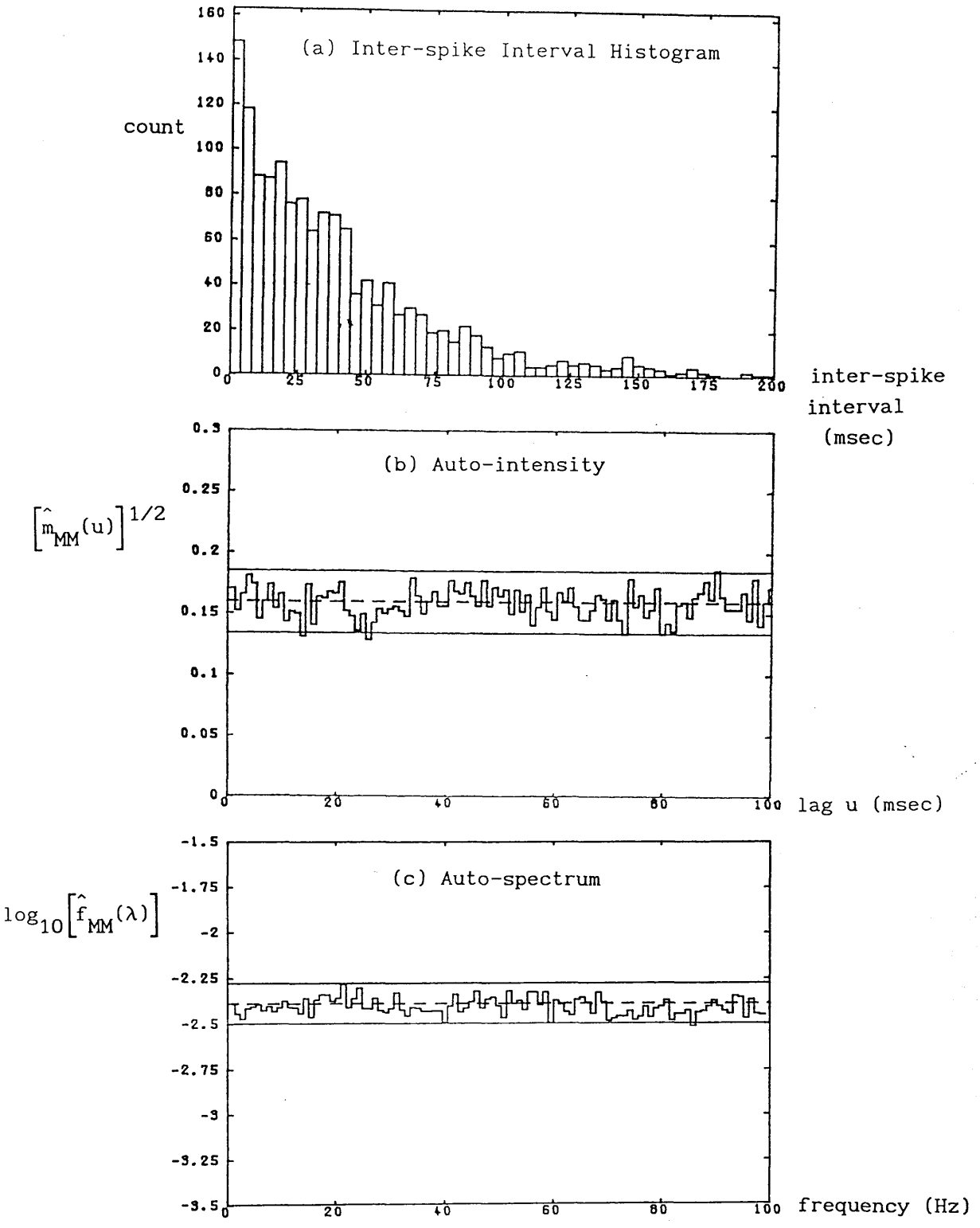

Figure 6.1.1. Estimates of (a) Inter-spike interval histogram, (b) square root of the auto-intensity and (c) logarithm to the base 10 of the auto-spectrum of a simulated Poisson point process with a mean interval of approximate 40 msec. The solid lines in (b) and (c) represent the bounds for the 95% confidence intervals for the Poisson process. The dashed line in (b) is the value of the auto-intensity for lag u large; whereas in (c) it is the value of auto-spectrum for λ large.

essentially Poisson in nature. It is important to note that the auto-spectrum of a Poisson point process resembles the auto-power spectrum of a Gaussian white noise in the case of ordinary time series.

The second example is illustrated in Figure (6.1.2). In this case, the mean rate of the simulated Poisson point process is 50 spikes/sec. The interval histogram in Figure (6.1.2a) again follows an exponential distribution and indicates that most of the intervals occur below 100 msec. One implication is that for a high mean rate, the simulation of a Poisson point process using a large minimum time interval (such as 1 msec.) may not be adequate. In Figure (6.1.2b), the peak at u=1 msec. probably reflects this. For the rest of u, the auto-intensity behaves as a Poisson point process. The auto-spectrum illustrated in Figure (6.1.2c) is typical of a Poisson point process.

6.1.2 Point Processes with Gaussian Interval Histograms

It is quite common to encounter spike trains experimentally that exhibit a Gaussian interval histogram (Sampath and Srinivasan, 1977). This implies that the spike train is basically periodic in nature but with additional noise components. If τ_k, k=1,..,M(T), are the inter-spike intervals of such a point process, the intervals τ_k follow a normal distribution with mean μ and variance σ^2. Figures (6.1.3-5) show the effects of increasing the variance σ^2 of a simulated point process with Gaussian interval histogram; all of which have the same mean interval μ=33

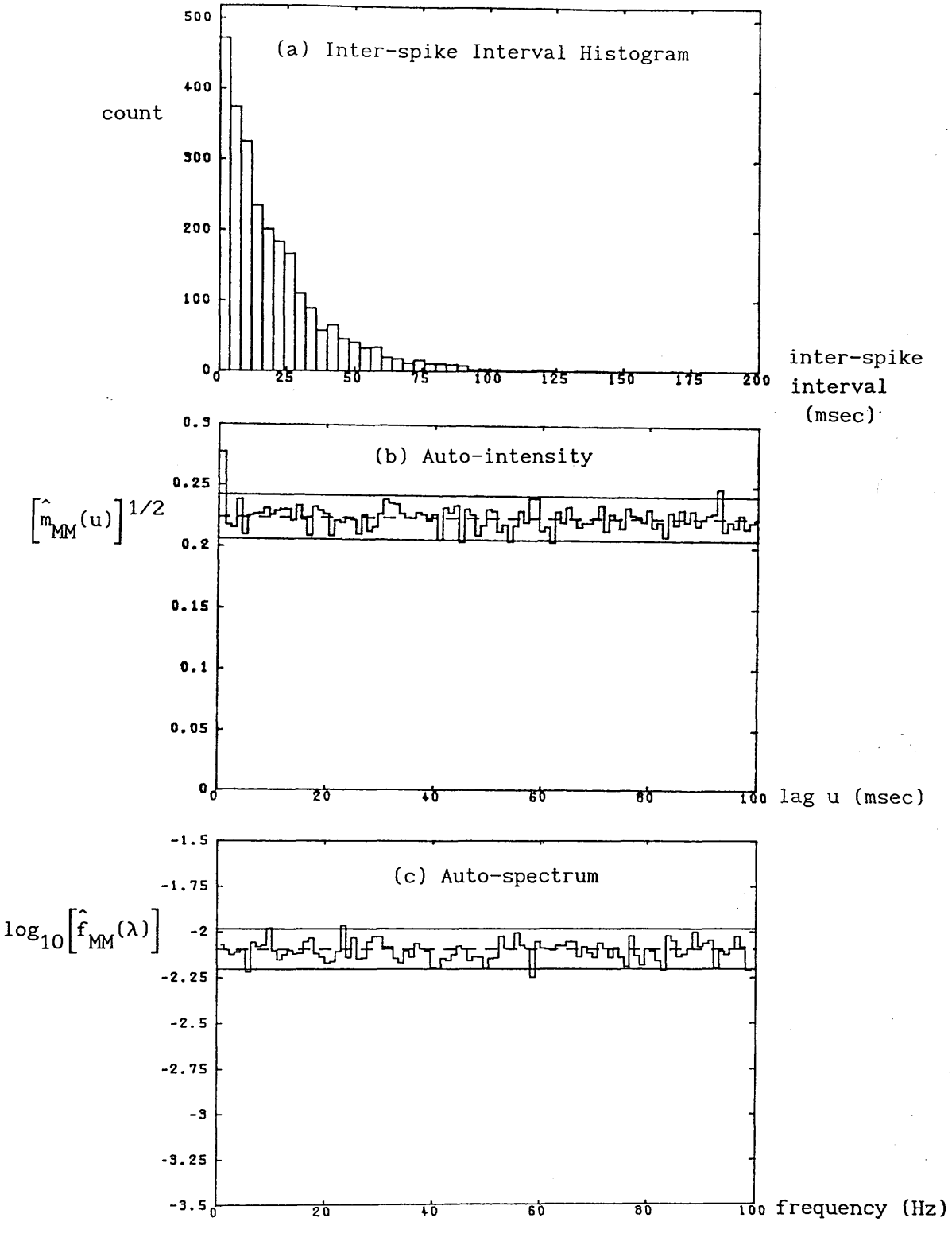

Figure 6.1.2. Estimates of (a) Inter-spike interval histogram, (b) square root of the auto-intensity and (c) logarithm to the base 10 of the auto-spectrum of a simulated Poisson point process with a mean interval of approximate 20 msec. The solid lines in (b) and (c) represent the bounds for the 95% confidence intervals for the Poisson process. The dashed line in (b) is the value of the auto-intensity for lag u large; whereas in (c) it is the value of auto-spectrum for λ large.

msec. The details of the generation of Gaussian deviates is given in Chapter 5. From Figure (6.1.3), all the interval histograms have the same peak at 33 msec. As σ^2 increases, the spread of the histograms increase accordingly. The auto-intensities are shown in Figure (6.1.4). All the three auto-intensities fluctuate about the same mean value with the same confidence interval. However, the periodicity, as is clear from Figure (6.1.4a), gradually disappears as the variance increases as is illustrated in Figure (6.1.4c). The first peak and the distance between successive peaks in Figures (6.1.4a-b) all suggest that the mean intervals of the process is 33 msec. However, in Figure (6.1.4c), the variance is so large that no peak or periodicity lies outside the confidence interval. It is also clear that the auto-intensity in Figure (6.1.4c) settles much earlier within the confidence interval than that in Figure (6.1.4b) which in turn settles much earlier than that in Figure (6.1.4a). This implies that the span of dependence of two spike decreases as the variance increases. Figure (6.1.5) shows the auto-spectra of the three point processes. The frequencies after which the processes behave as Poisson point processes are about 70Hz, 50 Hz and 30 Hz respectively, indicating a decreasing span of dependence in the frequency domain as the variance increases. In Figure (6.1.5a), the peaks occur at multiples of the fundamental frequency (30 Hz) until it settles down to the Poisson confidence interval, indicating strong periodicity. In Figure (6.1.5b), only one peak is clear and in Figure (6.1.5c), no peak is shown at all.

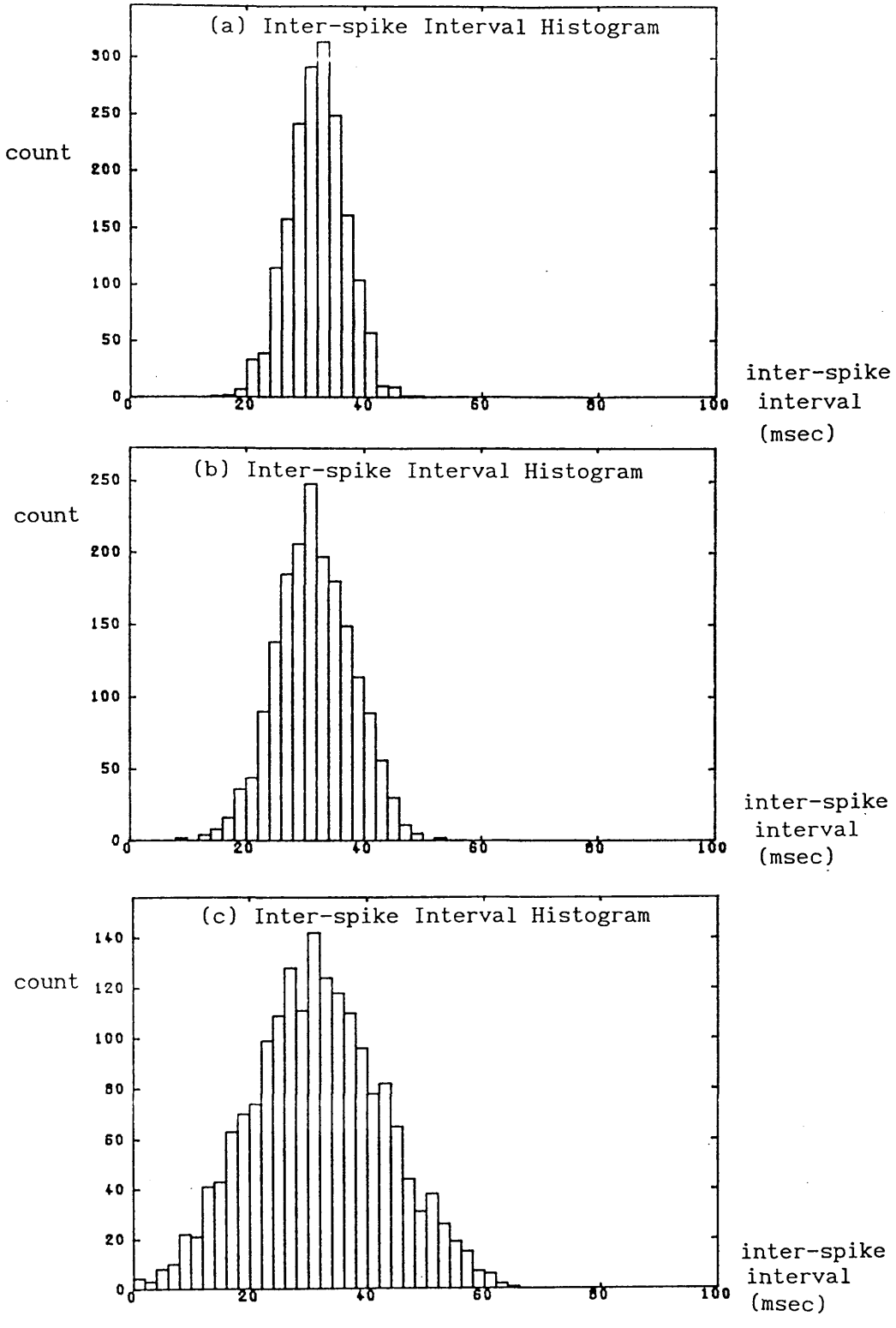

Figure 6.1.3. Estimates of the inter-spike histograms of three different computer generated point processes with normally distributed inter-spike intervals. The mean intervals for the three processes are approximately the same (33 msec.). The standard deviations of the intervals change from (a) 5 msec. (top row), to (b) 7 msec. (second row), to (c) 11 msec. (bottom row).

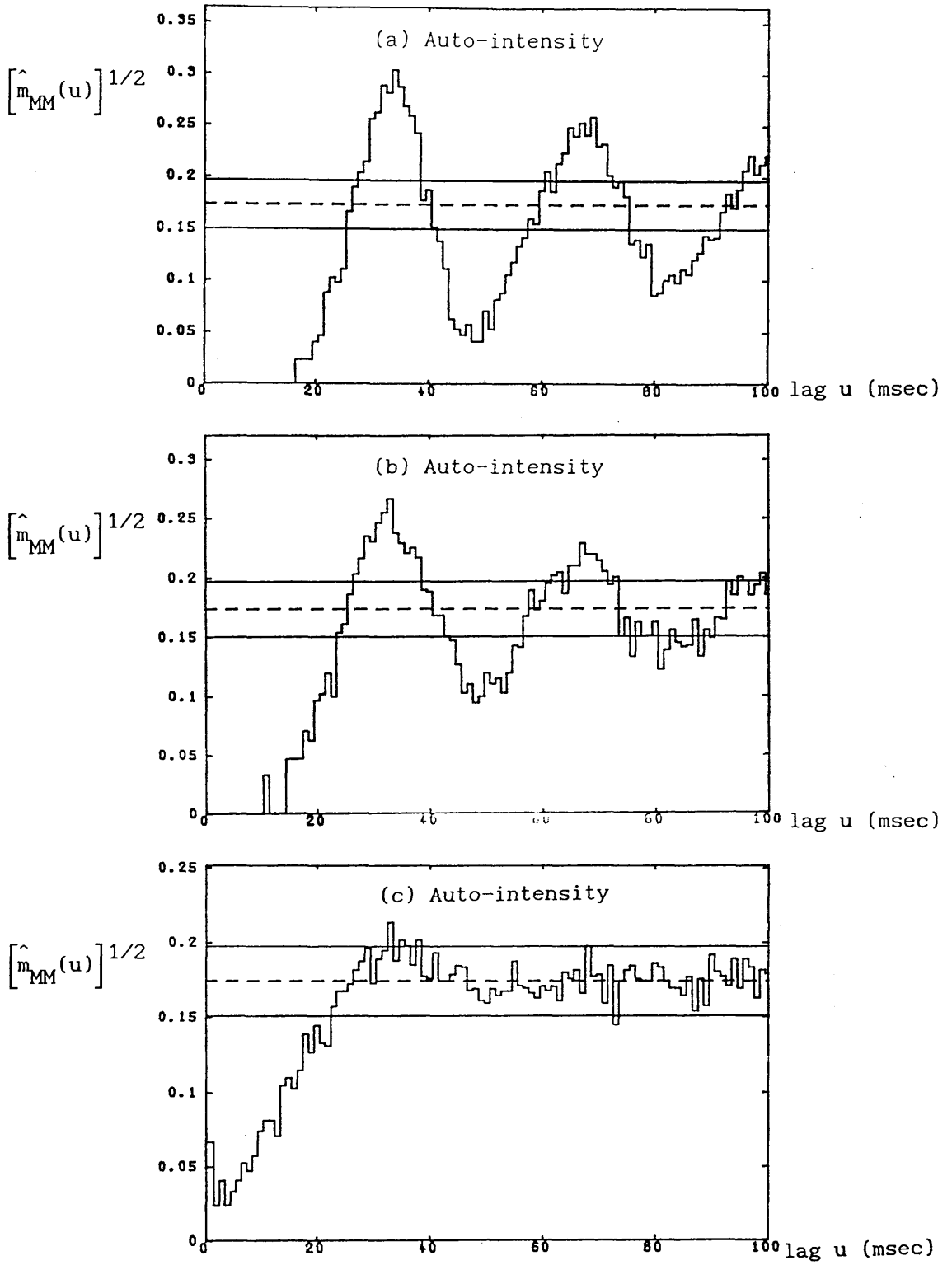

Figure 6.1.4. Estimates of the square root of the auto-intensity functions of the three processes corresponding to Figure 6.1.3. The solid lines represent the 95% confidence interval for the auto-intensity of a Poisson point process with the same mean rate and the dashed lines indicate the square root of the mean rate in spike/msec.

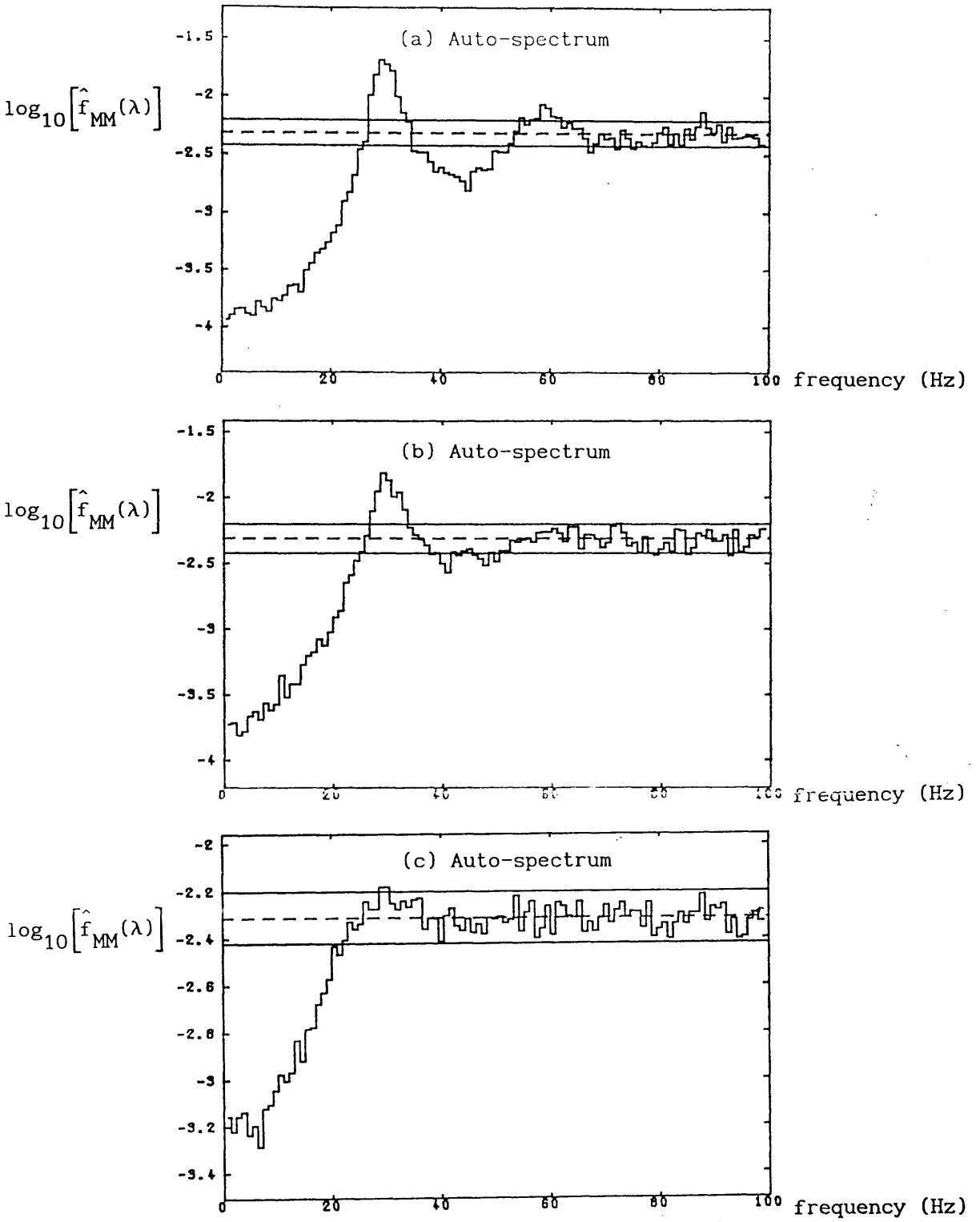

Figure 6.1.5. Estimates of the auto-spectra after taking log to the base 10 of the three processes corresponding to Figure 6.1.3. The solid lines represent 95% confidence interval for the auto-spectrum of a Poisson process with the same mean rate. The dashed lines indicate the asymptotic value with λ large.

6.1.3 Modulated Point Processes

The examples considered in section (6.1.1-2) are renewal processes in which the events are independently distributed. In practice, it often happens that the occurrence of an event depends on the previous one or is a function of the events that happened earlier. The modulated point process is an example. One type of modulated point process that will be considered is generated by the system illustrated in Figure (6.1.6). The modulating effects of the sine wave generator is such that it increases the firing rate of the pulse generator when the sine wave is positive and decreases the firing rate of the pulse generator when the sine wave is negative. Two examples of modulated point processes are considered below: one with the sine wave frequency higher than the mean firing rate and the other with the sine wave frequency lower than the mean firing rate.

Figure (6.1.7) shows the interval histogram, auto-intensity and the auto-spectrum of a modulated point process with $\hat{P}_M$=0.02875 spikes/msec. and frequency of modulating sine wave equal to 52 Hz. In Figure (6.1.7a), the interval histogram shows a multi-mode structure with peaks at 23, 35 and 55 msec. The dominant peak at 35 msec. indicates the mean interval might be $1/\hat{P}_M$. However, it is difficult to relate the other two peaks to the features of the process. In Figure (6.1.7b), the auto-intensity shows strong periodicity at intervals of approximately 20 msec. which can be related to the frequency of the modulating sine wave (=52 Hz). This information shows up even more vividly in the auto-spectrum

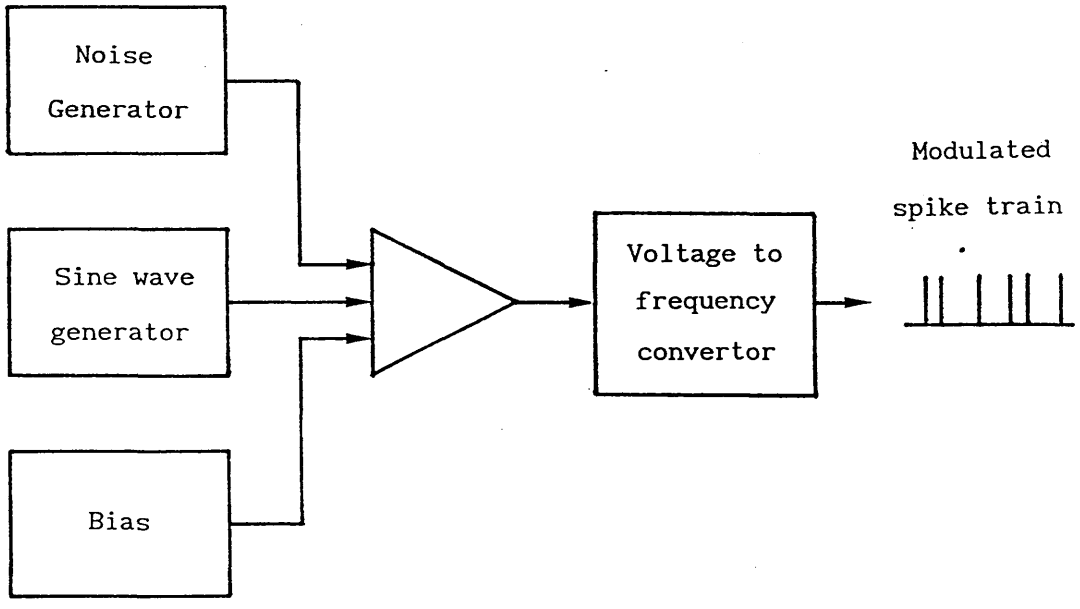

Figure 6.1.6. Schematic diagram illustrating the method used to generate a spike train which is modulated to give a sharp frequency component at the frequency of the sine wave.

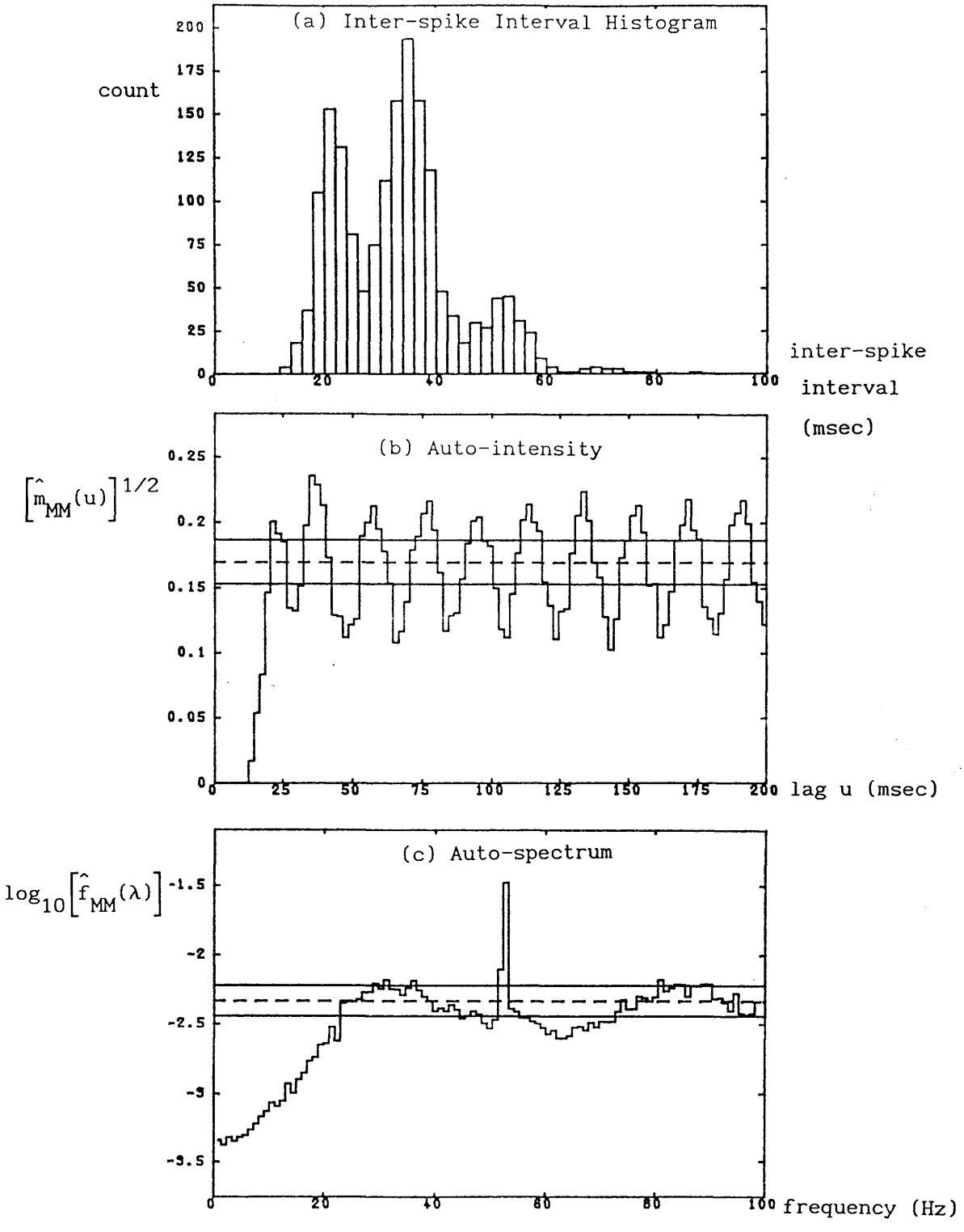

Figure 6.1.7. Estimates of (a) Inter-spike interval histogram, (b) square root of the auto-intensity and (c) logarithm to the base 10 of the auto-spectrum of a modulated point process with a mean rate of 28.75 spike/sec. and modulated at 52 Hz. The solid lines in (b) and (c) represent the bounds for the 95% confidence interval for a Poisson process with the same mean rate. The dashed line in (b) is the value of the auto-intensity for lag u large; whereas in (c) it is the value of auto-spectrum for λ large.

in Figure (6.1.7c) where a sharp peak at about 52 Hz is seen.

Figure (6.1.8) shows another example with $\hat{P}_M$=0.041 spikes/msec and frequency of modulating sine wave equal to 10 Hz. In Figure (6.1.8a), a multi-mode structure with a dominant peak at about 15 msec. is evident in the interval histogram. In this case, even the dominant peak does not correspond to the mean interval which should be $1/\hat{P}_M$=24 msec. From the auto-intensity estimate illustrated in Figure (6.1.8b), the sharp peak at about 24 msec. reflects the mean rate of the process, but the modulated frequency is not at all clear. From the auto-spectrum in Figure (6.1.8c), the frequency of the modulating sine wave again appears distinctly as a sharp peak at about 10 Hz. It is important to note that the broad peak at 60 Hz does not necessarily represent the mean rate of the process as it does in the previous examples (see Figure 6.1.5 and 6.1.7c).

From the above examples, it is clear that for a non-renewal process like the modulated point processes considered above, the interval histogram is not as useful as the auto-intensity and auto-spectrum. In fact the interval histogram does not define the point process completely if the point process is not renewal in nature. In the situation where one wants to detect a single frequency component of a point process, the most sensitive measure is probably using the auto-spectrum as illustrated by the two examples considered above. A consideration of such examples also eliminates the tendency to interpret the first broad peak in the auto-spectrum as the mean fire rate of the process. In fact, the

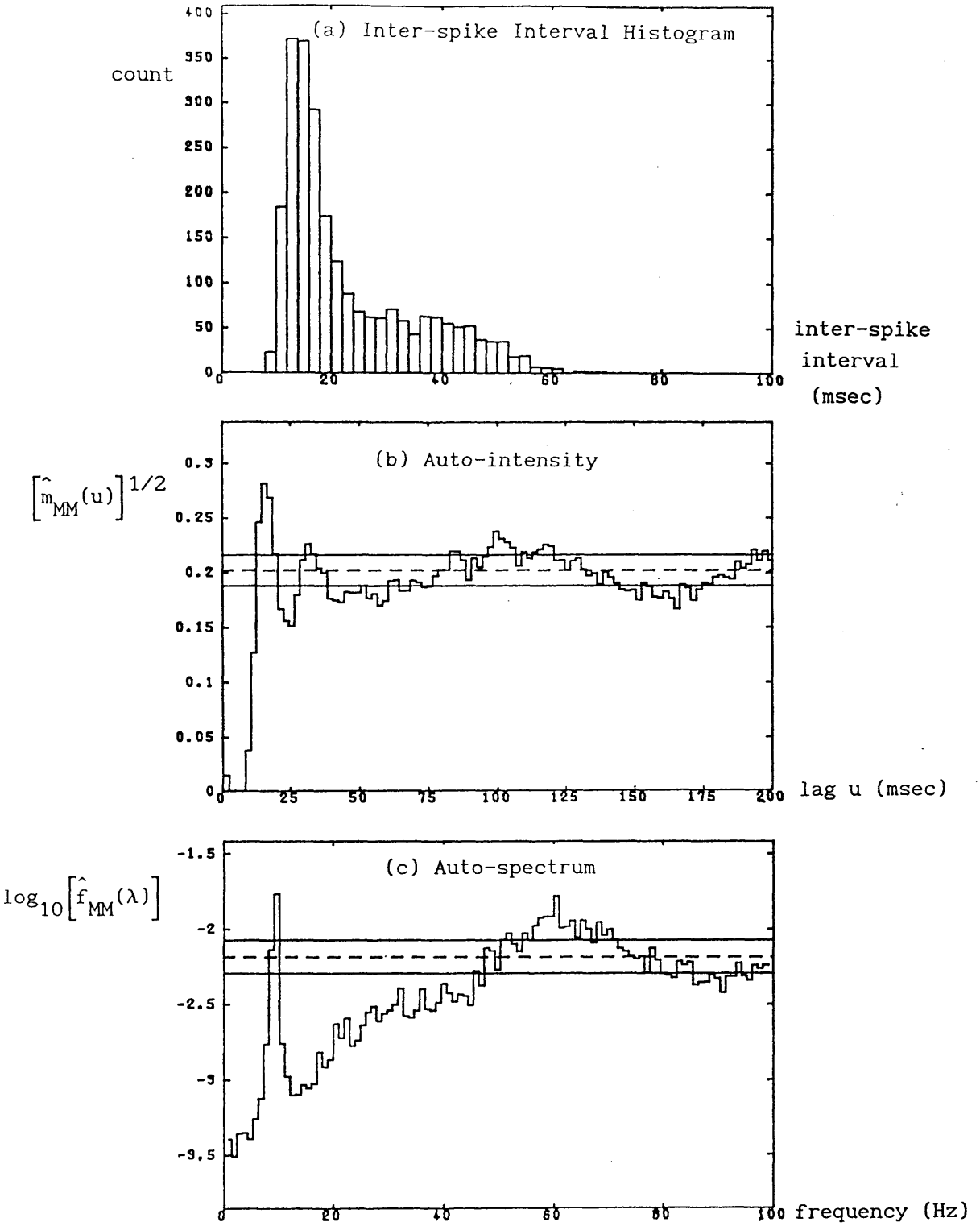

Figure 6.1.8. Estimates of (a) Inter-spike interval histogram, (b) square root of the auto-intensity and (c) logarithm to the base 10 of the auto-spectrum of a modulated point process with a mean rate of 40.67 spike/sec. and modulated at 10 Hz. The solid lines in (b) and (c) represent the bounds for the 95% confidence interval for a Poisson process with the same mean rate. The dashed line in (b) is the value of the auto-intensity for lag u large; whereas in (c) it is the value of auto-spectrum for λ large.

asymptotic value of the auto-spectrum which is equal to $\log_{10}(P_M/2\pi)$, should be used to estimate the mean rate.

6.1.4 Point Processes with Bursting Characteristics

The aim of this section is to simulate the kind of repetitive firing which is found in the ipsilateral Renshaw interneurones. The spike train is characterised by high frequency repetitive firing followed by a period where no firing occurs. The experimental system employed to simulate the process is illustrated in Figure (6.1.9). The noise bandwidth and the threshold of the encoder are adjusted to obtain bursting spike trains of different mean rates. Two examples are considered below.

Figure (6.1.10) shows a simulated bursting spike train with $\hat{P}_M$=0.00852 spikes/msec. The bursting is evident in Figure (6.1.10a). An examination of the auto-intensity in Figure (6.1.10b) shows a distinct peak at approximately 14 msec. This corresponds to a frequency of 71 Hz which might relate to the frequency of firing within a burst. The rest of the auto-intensity values lie mainly within the confidence limits. The auto-spectrum illustrated in Figure (6.1.10c) shows two peaks at about 5 Hz and 75 Hz, and a trough centered at 25 Hz. The peak at 5 Hz might relate to the frequency of firing between bursts whereas the peak at 75 Hz might relate to the frequency of firing within a burst. The trough at 25 Hz probably refers to the frequency components that is lacking since the spikes either fire

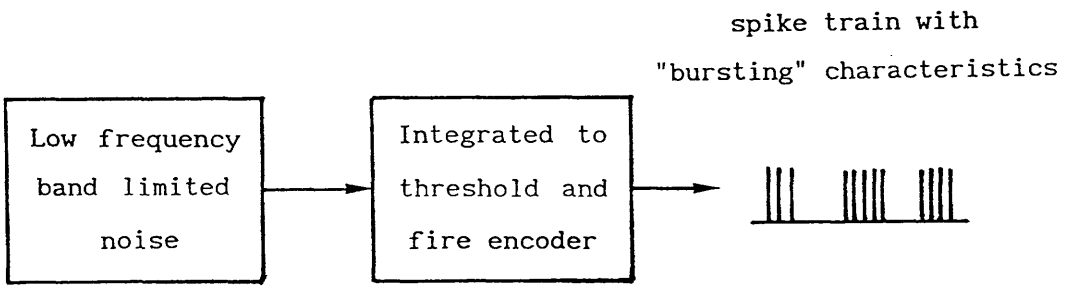

Figure 6.1.9. Schematic diagram illustrating the method used to generate a spike train that exhibits "bursting" characteristics.

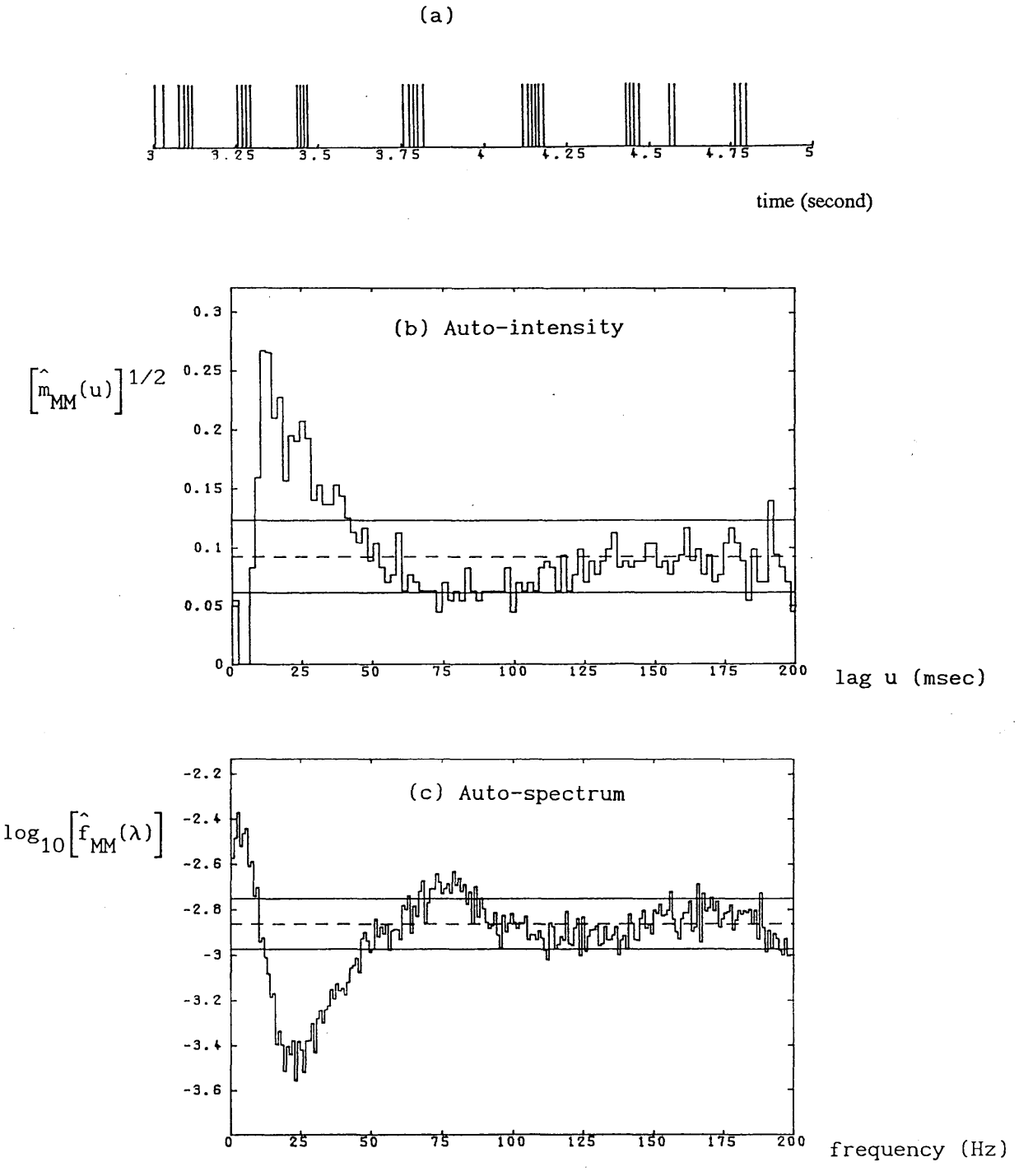

Figure 6.1.10. (a) A section of a spike train which exhibits "bursting" characteristics with mean rate 8.52 spikes/sec. along with the estimates of (b) the square root of the auto-intensity and (c) the log to the base 10 of the auto-spectrum.

at high frequencies (about 75 Hz) or at low frequencies (about 5 Hz).

Figure (6.1.11) shows another example of a simulated bursting spike train with $\hat{P}_M$=0.04382 spikes/msec. Similar interpretations as above can be made.

In the two examples above, the auto-spectrum is very useful in deducing information concerning the frequency content of the spike train: A peak above the upper confidence level indicating a significant extra frequency component, whereas a trough indicating a significant less frequency component, both relative to a Poisson process of the same mean rate.

The examples of spectra of point processes, as illustrated in Figures (6.1.1-6), are useful in emphasising features which differ from spectra associated with ordinary time series. The spectrum of a Poisson process, for example, was seen to be a constant proportional to the mean rate of the process (Figure 6.1.1-2). In general, the spectrum of point process, satisfying the assumption that events widely separated in time are independent, approach a constant value proportional to the mean rate of the process. One may conclude, therefore, that the spectrum of a point process consists of two components : one represented by a Poisson process of the same mean rate, and the other indicating departures from a Poisson process of the same mean rate (Lewis, 1972b; Rosenberg et al., 1982). The latter would appear as components of the spectrum lying outside the

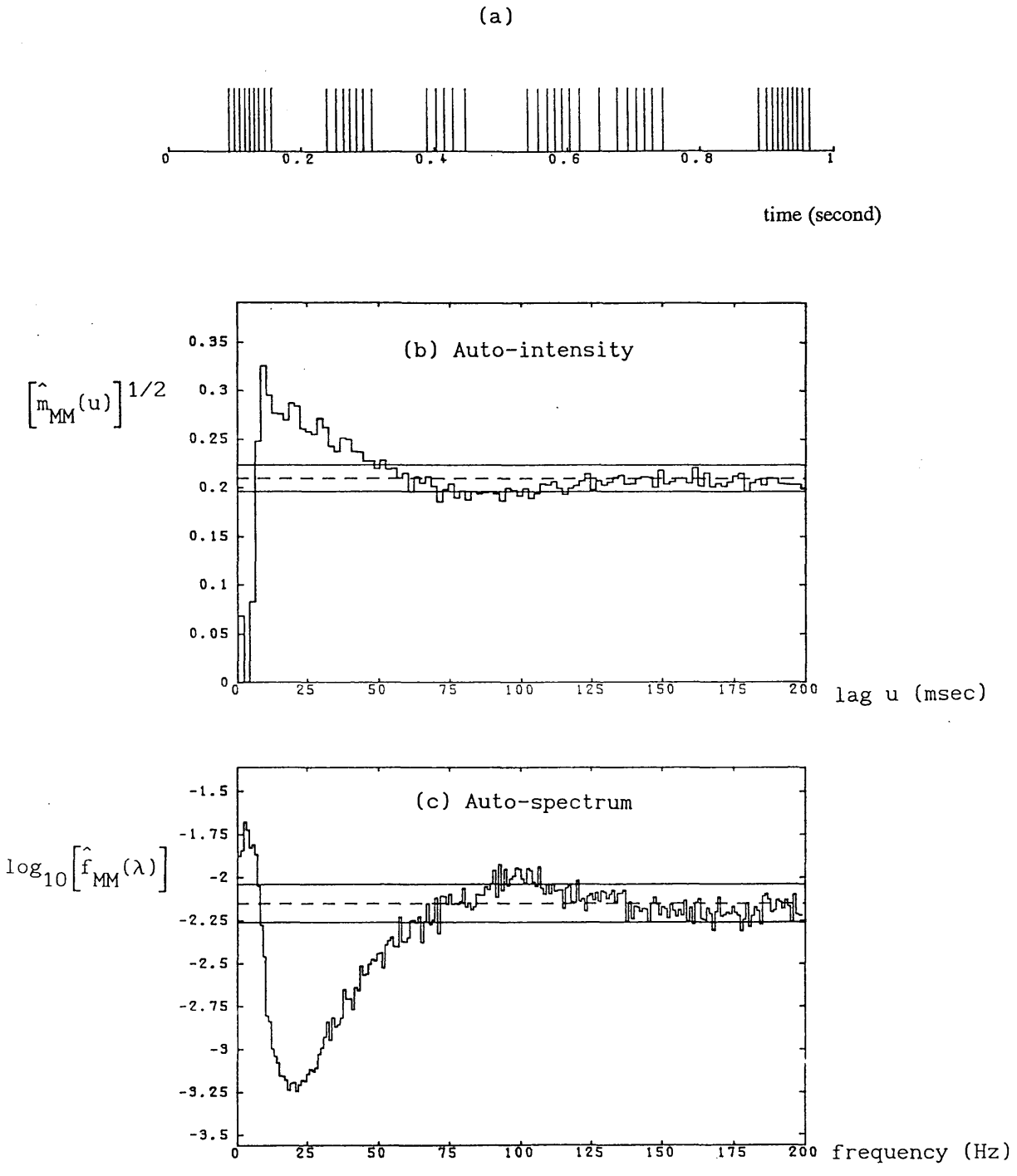

Figure 6.1.11. (a) A section of a spike train which exhibits "bursting" characteristics with mean rate 43.82 spikes/sec. along with the estimates of (b) the square root of the auto-intensity and (c) the log to the base 10 of the auto-spectrum.

confidence interval in the estimated spectrum.

6.2 Simulation of a Single-Input, Single-Output Neurone Model

The neurone model described in section (5.2) is used to generate the output spike train under the influence of a Poisson point process. Two cases are considered: (1) To simulate the effect of different excitatory post-synaptic potential (EPSP) sizes and (2) To simulate the effects of inhibitory post-synaptic potential (IPSP) on the relation of the input and output spike trains. The objective of the investigation is to identify the underlying physiological mechanisms that occur within a neurone from the recording of the input and output spike trains. This provides a non-invasive method of analysing the neurophysiological system avoiding some complicated methods like of intra-cellular recording. In fact, in the later sections, it has been demonstrated that some clear patterns of firing can be identified in the Ia and motor unit interactions based on the time and frequency domain analysis techniques (see Chapter 2 for some examples of this).

6.2.1 The Simulation of an EPSP Neurone Model

The model neurone is illustrated in Figure (6.2.1). The size and duration of the impulse response from the second-order filter is determined by the time constant and the gain of the filter. This is adjusted to simulate EPSP's of two different magnitudes but the same duration; the magnitude in the first case being half of that of the second case. The input spike train in both cases is a Poisson point process of mean rate 24.5 spike/sec.

(a)

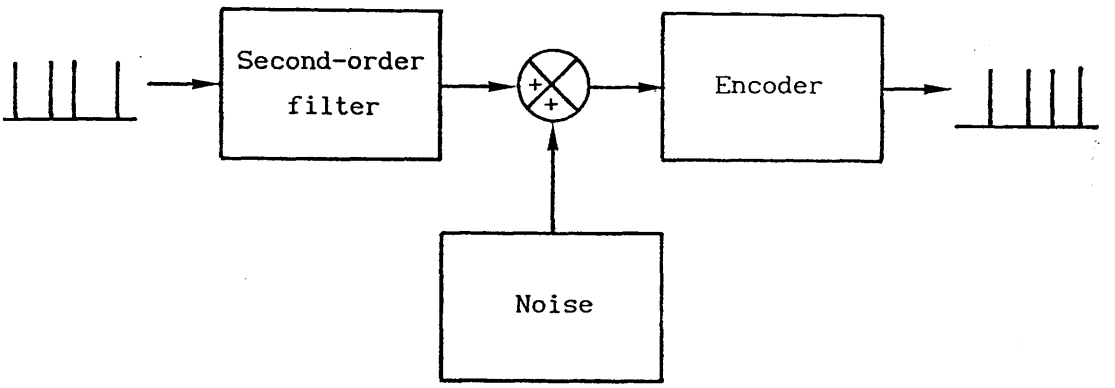

(b)

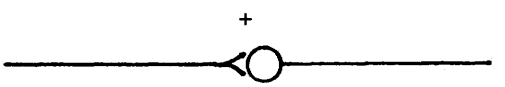

Figure 6.2.1. (a) Schematic diagram representing a single-input, single-output EPSP neurone model along with (b) the conventional physiological symbol that represents the neurone.

and the input and output spike trains were recorded for a period of 60 seconds. The common and different features of the two cases are discussed below.

Figure (6.2.2) shows the cross-intensities obtained from the two data sets. In both cases, the peaks occur at about 17 msec. These peaks indicate the probability of an output spike to occur given an input spike has occurred 17 msec. earlier is significantly higher than that by chance alone. Hence, the peak may be considered as the mean time delay or latency of the neurone model. The magnitude of the peak in the first case (Figure 6.2.2a) is approximately half of that in the second case (Figure 6.2.2b), indicating an increase in the magnitude of EPSP would increase the probability of an output spike occurring at the mean latency. This may be understood since one can think of an increase in the signal magnitude would increase the signal to noise ratio and hence increasing the degree of association. It should also be noted that the patterns of association, as indicated in the two cross-intensities, occur to the right hand side of the time origin as predicted by causality.

Information concerning the strength of association and time delay may also be deduced from the frequency domain measures. In Figure (6.2.3), the respective coherence estimates obtained from the two data sets indicate that the size of the EPSP's has a direct effect on the magnitude and range of associations in the frequency domain. In Figure (6.2.3a), the coherence estimate fluctuates about 0.2 and vanishes for frequencies greater than 60

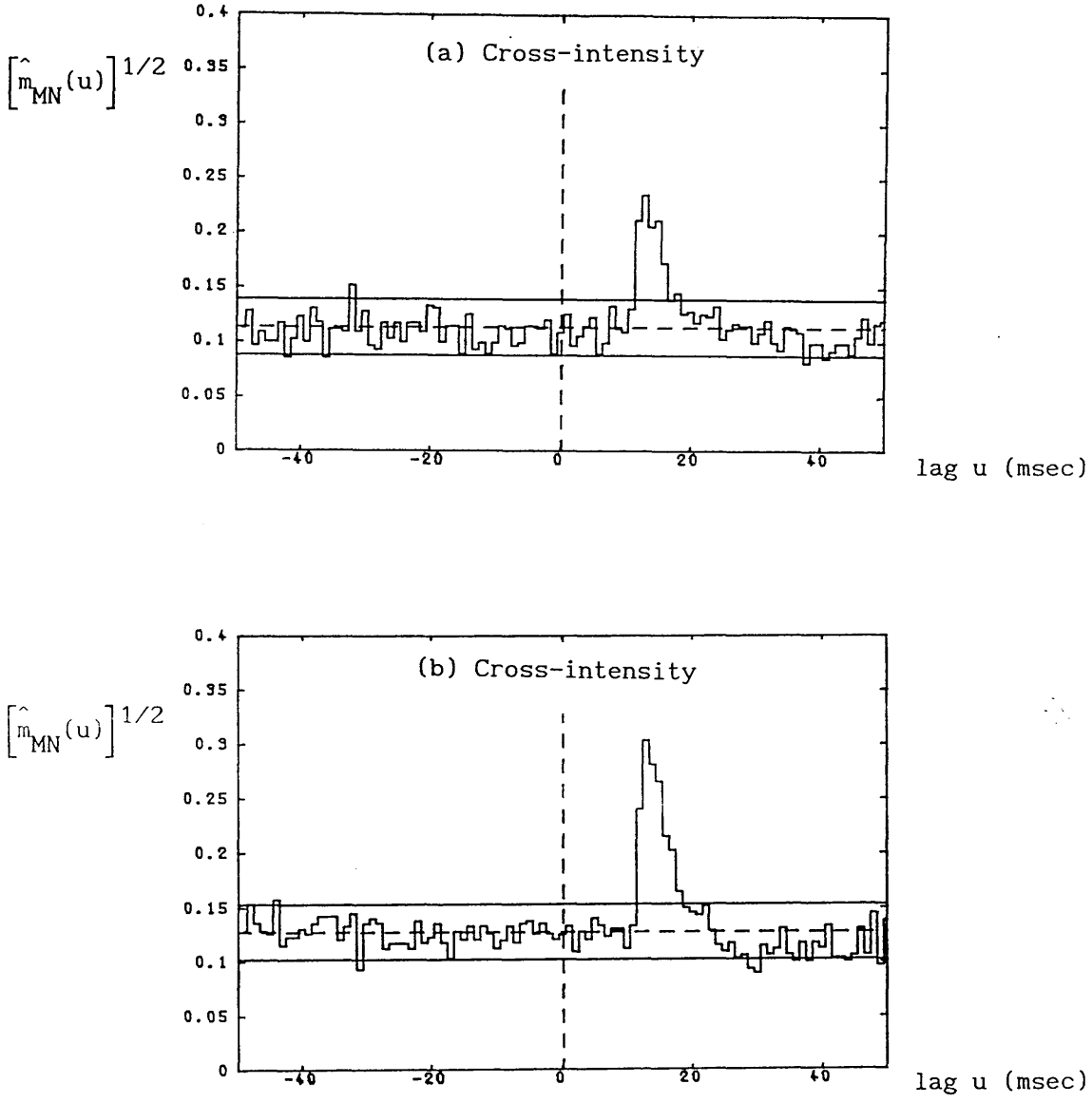

Figure 6.2.2. A comparison of two cross-intensities generated from two model neurones with different EPSP sizes. The EPSP magnitude used in the model associated with the cross-intensity in (a) is half of that of (b). In (a) the firing rates of the input and output spike trains are 25.4 and 12.73 spikes/sec. respectively, whereas in (b) are 25.4 and 16.15 spikes/sec. respectively. Poisson input is used in both (a) and (b).

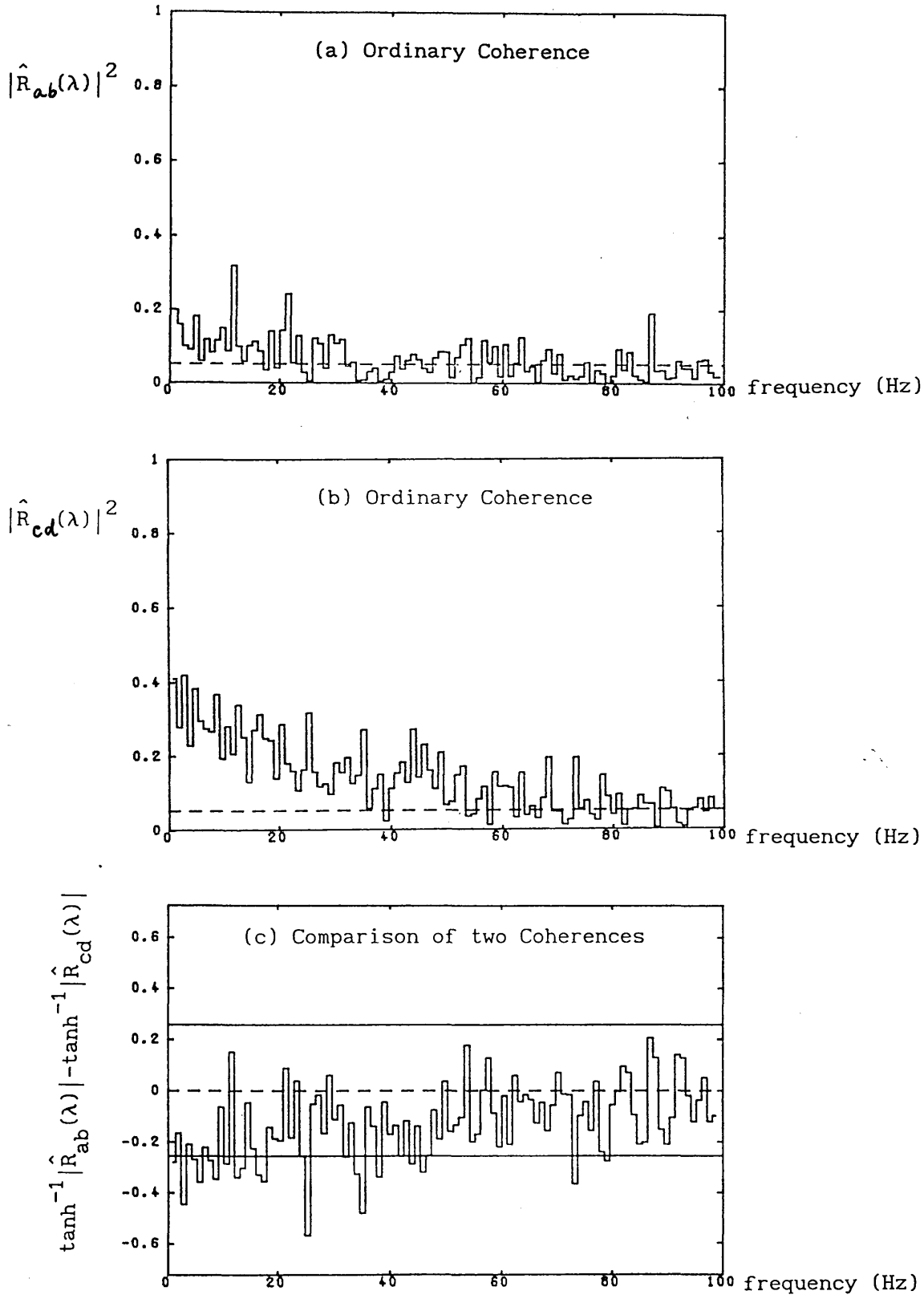

Figure 6.2.3. A comparison of the estimates of the coherences generated from two model neurones with different EPSP sizes. The EPSP magnitude used in the model associated with the coherence in (a) is half that of (b). The difference of the inverse hyperbolic-tangent transform of the moduli of these two coherences is shown in (c). The solid horizontal lines represent the critical values of an approximate 95% confidence level of a two-tailed test of the hypothesis that the two moduli are equal.

Hz. On the other hand, the coherence estimate in Figure (6.2.3b) fluctuates about 0.3 and vanish at a higher frequency. A quantitative comparison of the two coherences may be performed by the difference of coherence test described in section (4.3.2). The result is illustrated in Figure (6.2.3c). The first coherence is seen to be significantly lower than the second one at the low frequencies especially at about 25 Hz and 35 Hz.

Another point to note is that the association in the frequency domain usually occurs in the low frequency range. This phenomenon has been investigated by Halliday (1986) in the case of a muscle spindle model and was shown that the time constant in the encoder is responsible for this. Since the same encoder is used in this neurone model, the same effect is expected.

The information concerning the delay may be deduced from the phase spectra illustrated in Figure (6.2.4). The two phase spectra are essentially the same in the frequency range up to 35 Hz; the linear relationship represents a slope of approximately $-3/30=-0.1$ rad/Hz indicating a time delay of $0.1/2\pi=16$ msec. This agrees with the findings from the cross-intensity functions (see Figure 6.2.2). However, beyond 40 Hz, the two phase spectra behave quite differently and the first phase spectrum has more noise components. This is explained by the fact that the variance of the phase spectrum is given by (Amjad, 1989)

$$\lim_{T\to\infty} \mathrm{Var}\{\hat{\theta}(\lambda)\} = (1/2K)\left[|R(\lambda)|^{-2} - 1\right] \qquad (6.2.1)$$

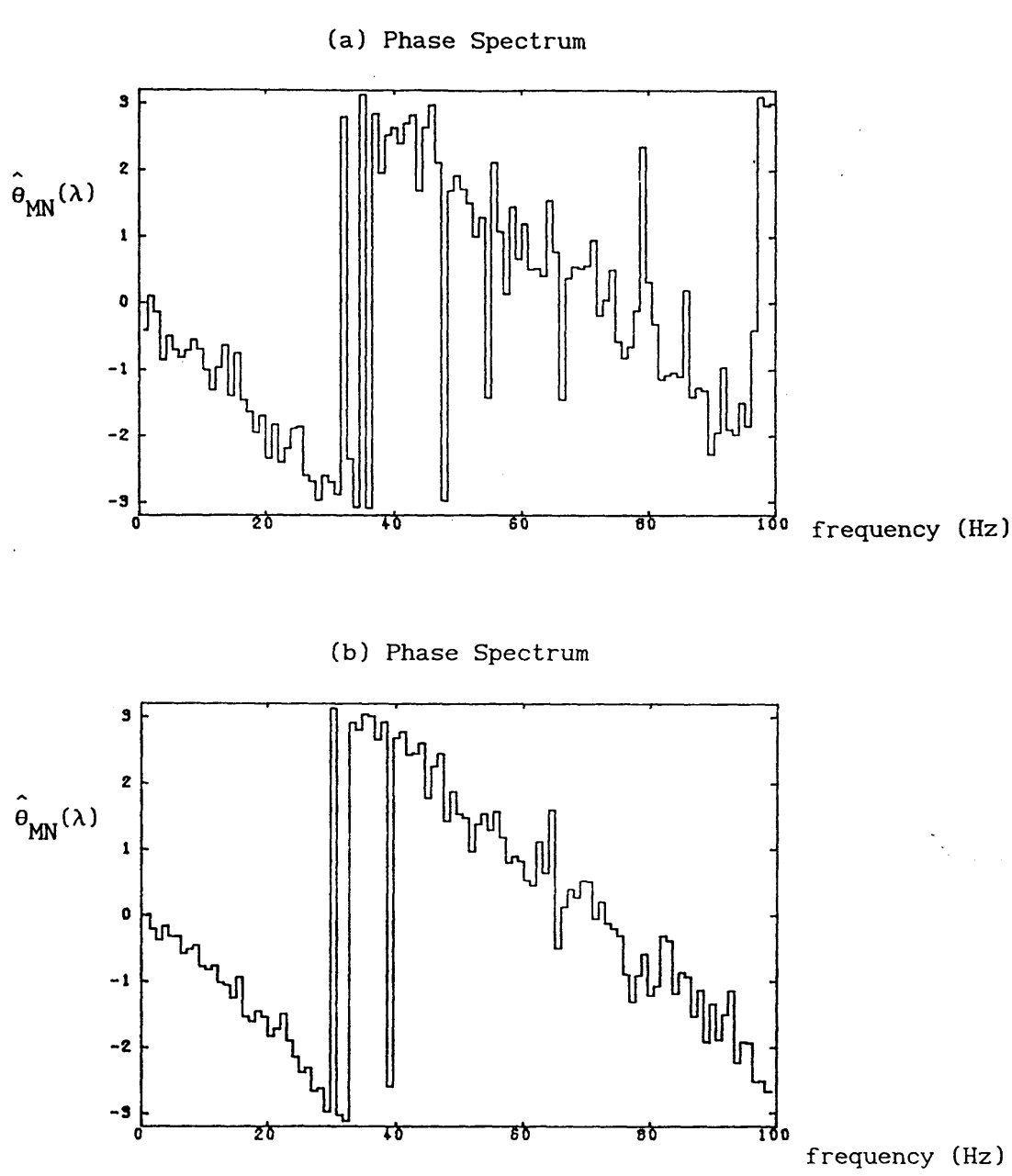

Figure 6.2.4. Estimates of the phase spectra generated from two model neurones with different EPSP sizes. The EPSP magnitude used in the model associated with the phase spectrum in (a) is half of that of (b). The linear portions of the two graphs indicate that both systems are dominated by approximately the same amount of delay.

where $\hat{\theta}(.)$ is the phase estimate, T is the record length, K is the number of disjoint sections used in the spectral estimates and $|R(\lambda)|$ is the coherency at frequency λ. The implication of expression (6.2.1) is that for small coherence values, the variance of the phase estimate would be very large and hence interpretation is difficult.

Now, we examine the impulse responses obtained from the two data sets. The impulse responses are estimated from the inverse Fourier transform of the quantity $\hat{f}_{MN}(\lambda)/\hat{f}_{MM}(\lambda)$ based on expressions (3.3.29b) and (3.3.30). They are illustrated in Figure (6.2.5). The two impulse responses are both characterised by a peak at the mean latency of about 17 msec. The magnitude of the peak in the first case (Figure 6.2.5a) is again approximately half of that of the second one (Figure 6.2.5b), as in the case of the cross-intensities of the two data sets (Figure 6.2.2). In fact, a close examination of the impulse responses would reveal that they are the scaled version of the respective cross-intensity functions. This can be proved by the arguments that follow. First recall expression (3.3.28), the relation between the impulse response $s_1(u)$ and the cumulant density functions $q_{MM}(u)$ and $q_{MN}(u)$ is given by

$$q_{MN}(u) = \int s_1(v) q_{MM}(u-v) dv \qquad (6.2.2)$$

If M is a Poisson point process, using expression (4.4.8), we have

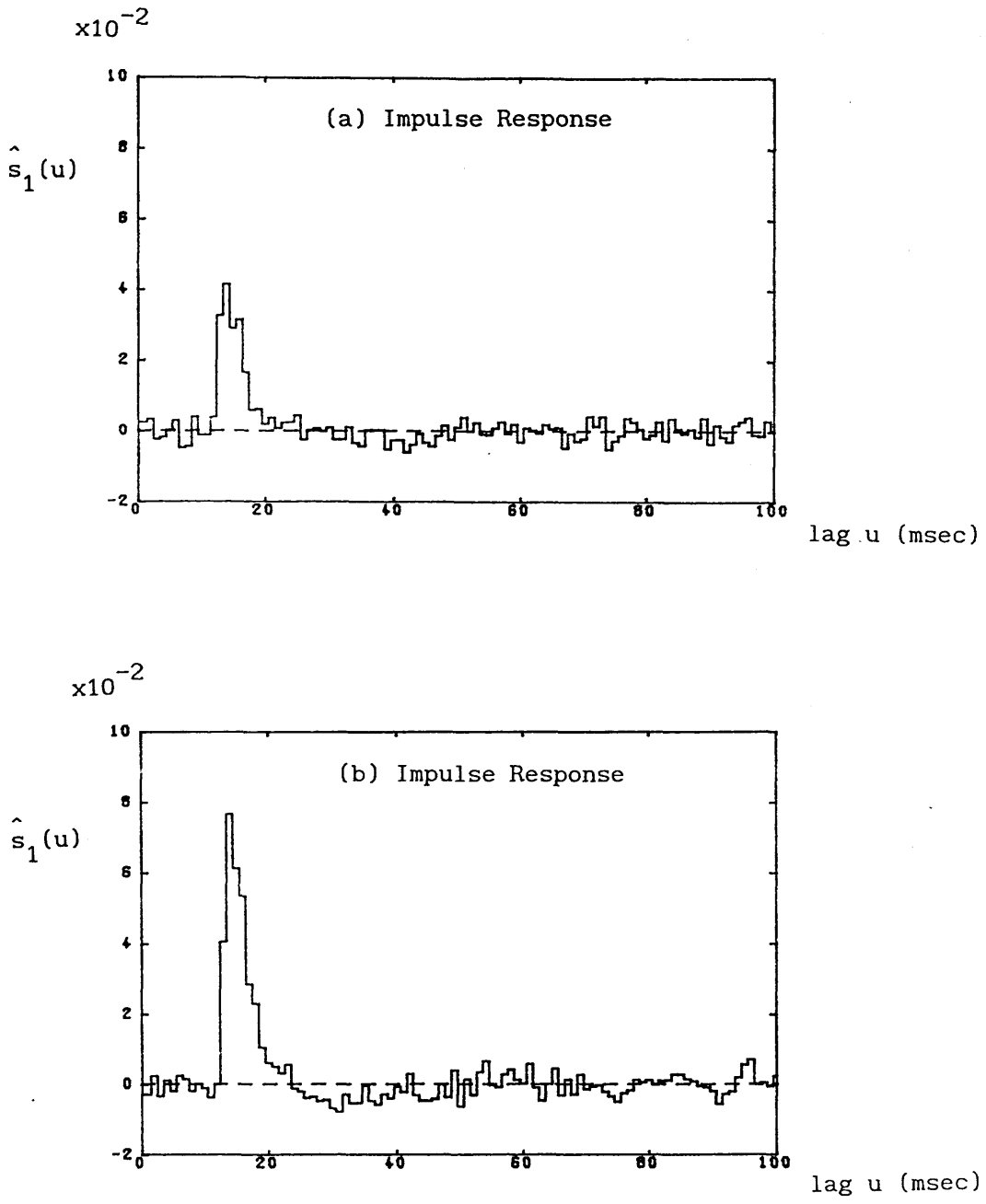

Figure 6.2.5. Estimates of the impulse response functions generated from two model neurones with different EPSP sizes. The EPSP magnitude used in the model associated with the impulse response in (a) is half of that of (b).

$$q_{MM}(u) = \begin{cases} P_M\delta(u) & u=0 \\ 0 & \text{otherwise} \end{cases} \qquad (6.2.3)$$

Substituting expression (6.2.3) into expression (6.2.2), one immediately arrives at the result

$$s_1(u) = q_{MN}(u)/P_M \qquad (6.2.4)$$

Rewriting expression (6.2.4) in terms of the cross-intensity function, one has

$$s_1(u) = m_{MN}(u) - P_N \qquad (6.2.5)$$

Expression (6.2.5) concludes the argument that for a Poisson point process input, the impulse response is essentially a shifted version of the cross-intensity function. We will discuss the significance of this as follows.

First, the fact that the linear model upon which the above argument is based on works so well indicates that the EPSP neurone model, although incorporating a non-linear encoder, is essentially dominated by linear characteristics. Another point to note is that the examples of the neurone model discussed in this section are dominated by a time delay. In fact, this is true for most point process systems that have been studied (see Amjad, 1989; Halliday, 1986; Rigas, 1983). It means that under the influence of a Poisson point process, the cross-intensity would be dominated by a single peak. Now from the arguments above, the impulse response would also be dominated by a single peak and the shape of

this peak may be considered to be close to a delta function. Since the impulse response and the transfer function form a Fourier transform pair, one would expect the transfer function to be approximately uniform.

Figure (6.2.6) shows the transfer functions estimated from the two data sets based on expression (3.3.29). The transfer function estimate in Figure (6.2.6a) reveals a certain degree of uniformity up to a frequency of 60 Hz. After that, the variance is seen to increase as the frequency increases. For the transfer function estimate in Figure (6.2.6b), it is seen to be uniform at a level of about -0.5 until reaching 60 Hz. The variance of the estimates is less than that of the first graph. The behaviour of the variance can be explained in a similar manner as in the case of phase spectra. A similar expression for the variance of the transfer function exists (Amjad, 1989), ie.

$$\lim_{T\to\infty} \mathrm{Var}\left\{\log_e|\hat{S}(\lambda)|\right\} = [1/2K]\left[|R(\lambda)|^{-2} - 1\right] \qquad (6.2.6)$$

where $\hat{S}(.)$ is the transfer function estimate, K is the number of disjoint sections used in the spectral estimates and $|R(\lambda)|$ is the coherency at frequency λ.

6.2.2 The Simulation of an IPSP Neurone Model

The objective of this section is to investigate the situation where each input spike produces an IPSP which has a inhibitory effect on the emission of the output spikes. The model

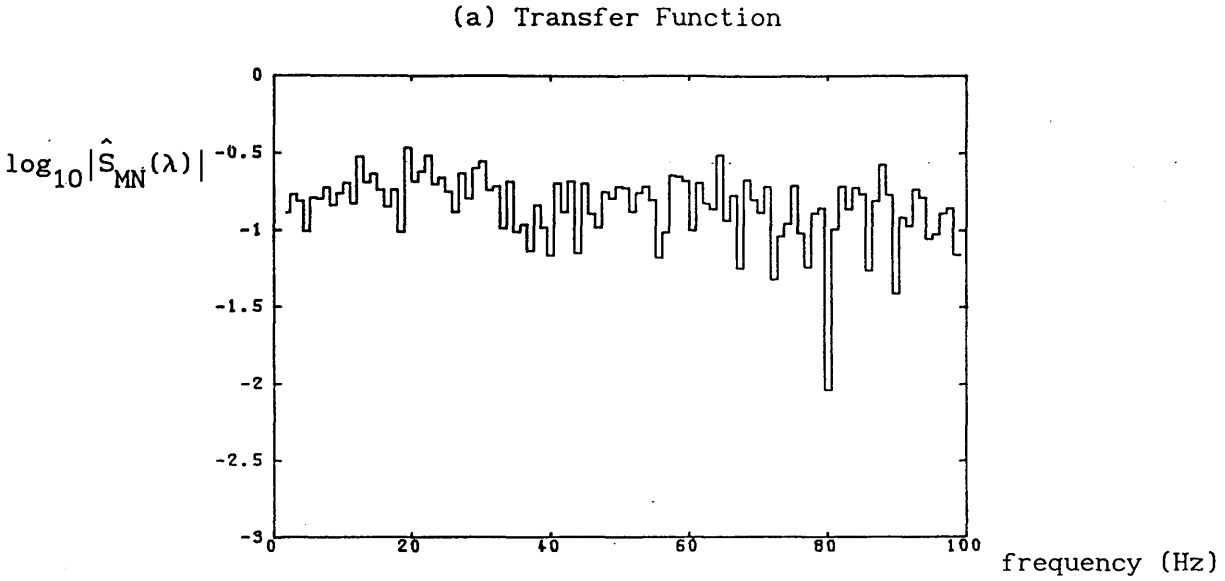

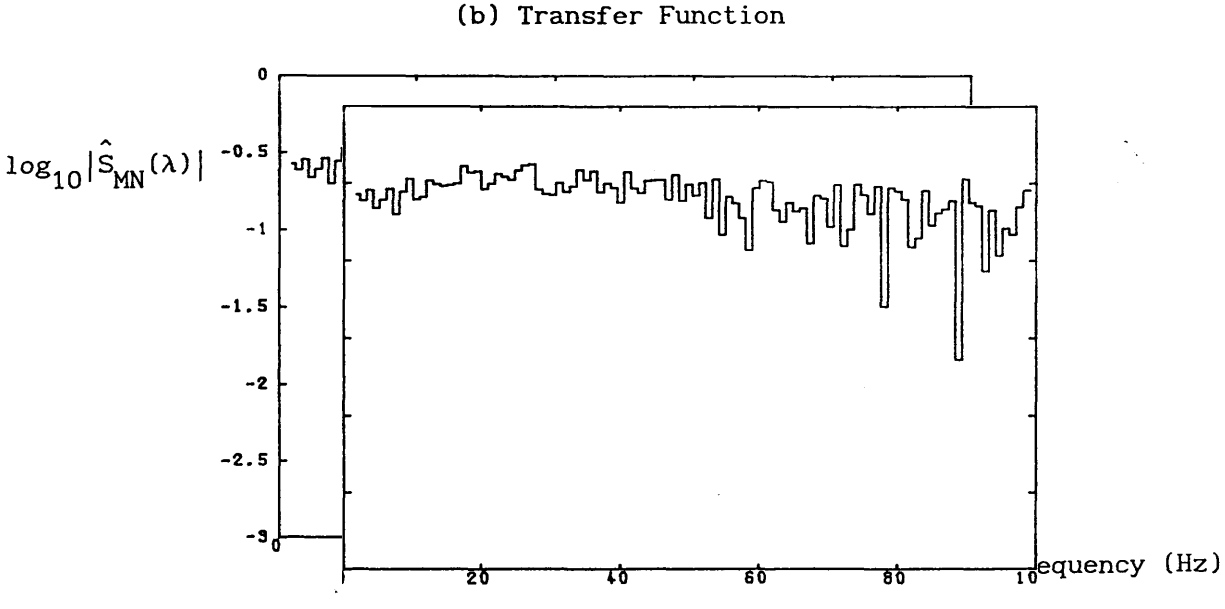

Figure 6.2.6. Transfer function estimates corresponding to the impulse response estimates illustrated Figure 6.2.5. The transfer function and the impulse response form a Fourier transform pair.

employed to simulate the neurone is illustrated in Figure (6.2.7). The only difference between the IPSP and the EPSP neurone model is the sign of the impulse response of the second-order filter that goes into the encoder. The IPSP neurone model is stimulated using Poisson point processes of two different mean rates, 30 spikes/sec. in the first case and 50 spikes/sec. in the second case. The input and output spike trains are recorded for a duration of 60 seconds.

Figure (6.2.8) shows the cross-intensities of the two data sets. Both graphs are dominated by a steep trough that touches the x-axis at approximately 16 msec. This implies that the emission of an output spike 16 msec. after an input spike is completely inhibited. The duration of the inhibition effect in the first case is seen to be about 20 msec. whereas in the second case it is about 30 msec. This is explained by the increase of the frequency of the input spike train. In addition, the mean firing rate of the output spike in the first case is seen to be higher than that of the second case, indicating the increase of inhibition effect.

The impulse response obtained from the data sets in the two cases are shown in Figure (6.2.9). The impulse response is estimated based on expressions (3.3.29b) and (3.3.30). Both impulse responses show a similar shape characterised by a trough with minima at about 17 msec. However, the magnitude of the trough in the first case is greater than that of the second. One interesting point to note is that the shape of the troughs, when

(b)

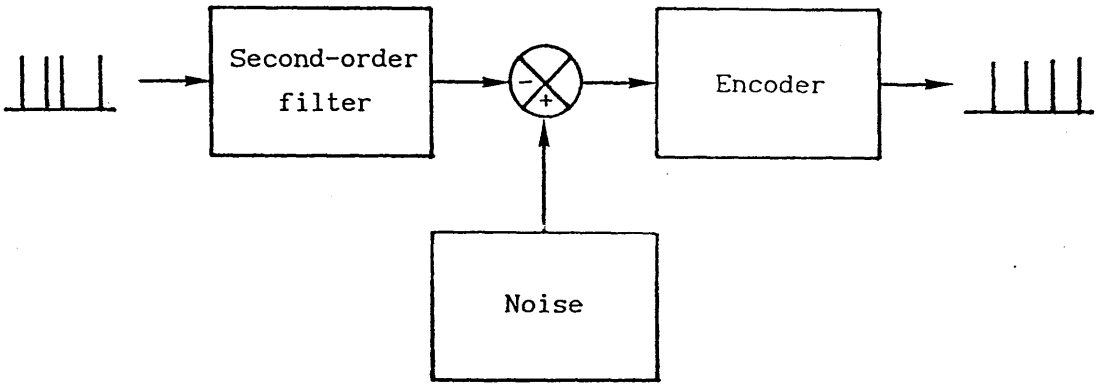

(a)

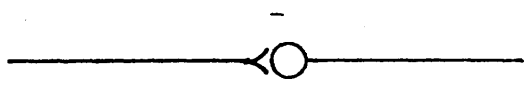

Figure 6.2.7. (a) Schematic diagram representing a single-input, single-output inhibitory post-synaptic potential (IPSP) neurone model along with (b) the conventional physiological symbol that represents the neurone.

(a) Cross-intensity

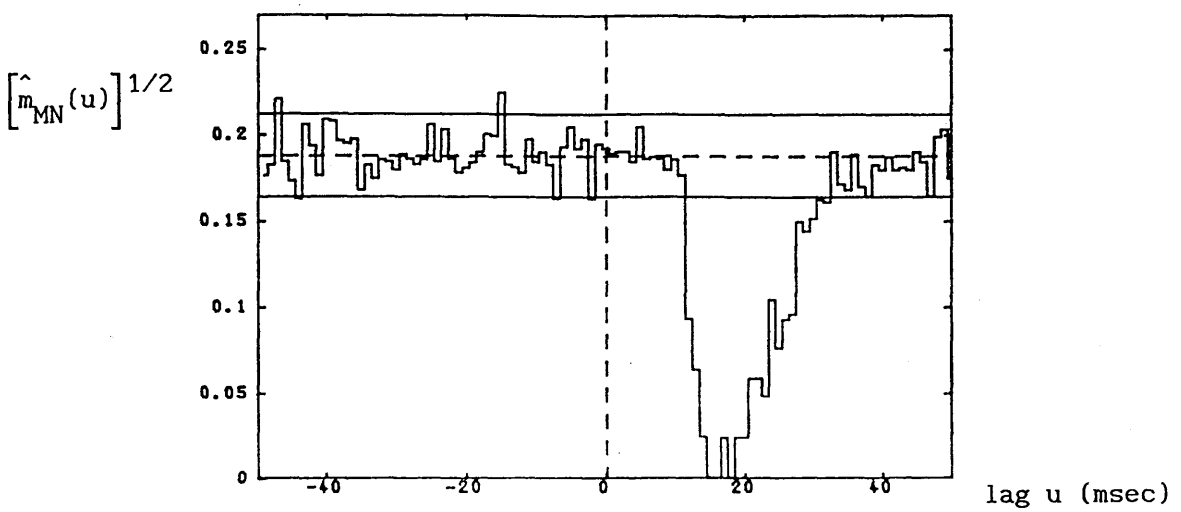

(b) Cross-intensity

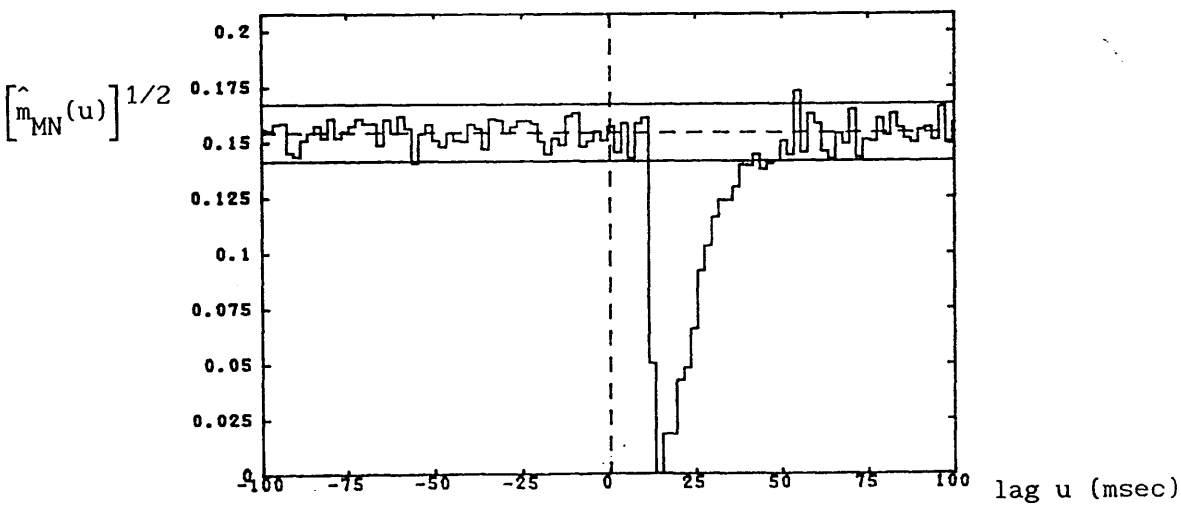

Figure 6.2.8. A comparison two cross-intensities generated from a IPSP model neurone with different input spike rates. In (a) the firing rates of the input and output spike trains are 29.4 and 35.27 spikes/sec. respectively, whereas in (b) are 50 and 23.73 spikes/sec. respectively. Poisson input is used in both (a) and (b).

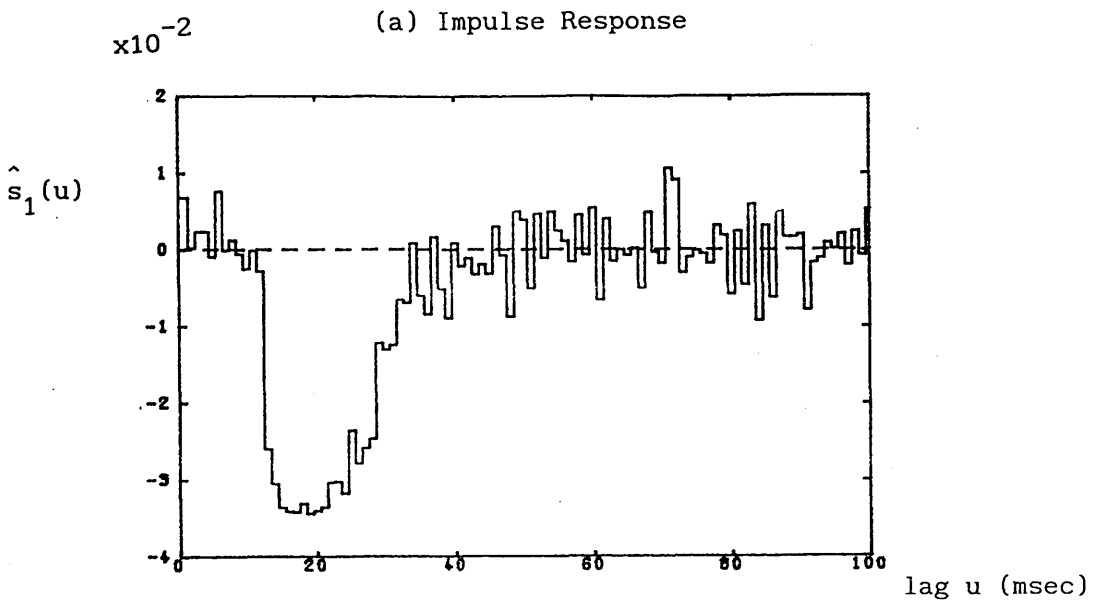

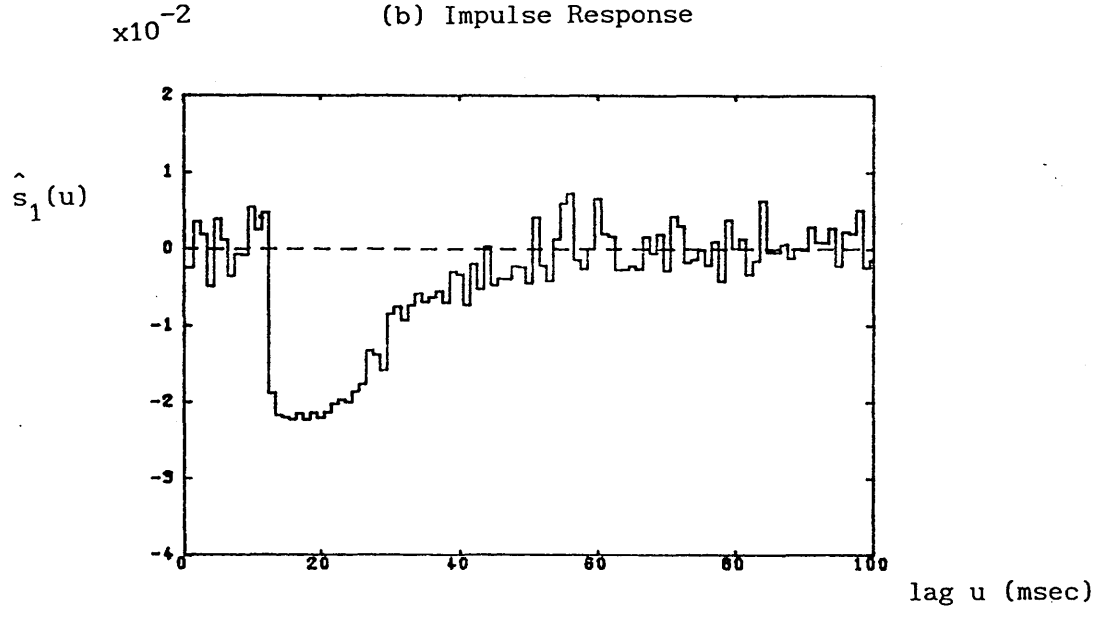

Figure 6.2.9. A comparison of two impulse responses generated from a IPSP model neurone with Poisson inputs of different firing rates. In (a) the firing rates of the input and output spike train are 29.4 and 35.27 spikes/sec. respectively, whereas in (b) are 50 and 23.73 spikes/sec. respectively. They are estimated from the inverse Fourier transform of the respective transfer function estimates based on the spectral estimates.

compared with the respective cross-intensities, shows appreciable differences: the trough in the impulse response is smoother than that of the cross-intensity.' The factor that accounts for this is probably due to the non-linear nature of the model. The proof given in expressions (6.2.2-5) are based on the assumption of a linear model. The IPSP neurone model is probably "less linear" than that of the EPSP neurone model and hence the impulse response of the system is not necessarily the scaled version of the cross-intensity even if the input in this case is Poisson.

The implication of the above example is that although one may estimate the impulse response function using the short-cut method based on the cross-intensity when the input is Poisson, limitations do exist when the system concerned possesses non-linear characteristics.

The transfer function estimates for the two data sets are given in Figure (6.2.10). The calculated estimates are based on expression (3.3.29). From the Figures, both transfer function estimates show the properties of a low pass filter. This implies that the the high frequency components of the input process are filtered out. This may be seen in the coherence estimates illustrated in Figure (6.2.11) where both coherence estimates show a high degree of association in the low frequency range up to about 30 Hz. In addition, the increase in input firing rate is seen to increase the magnitude of the coherence at a few distinct frequencies as is evident in Figure (6.2.11c).

(a) Transfer Function

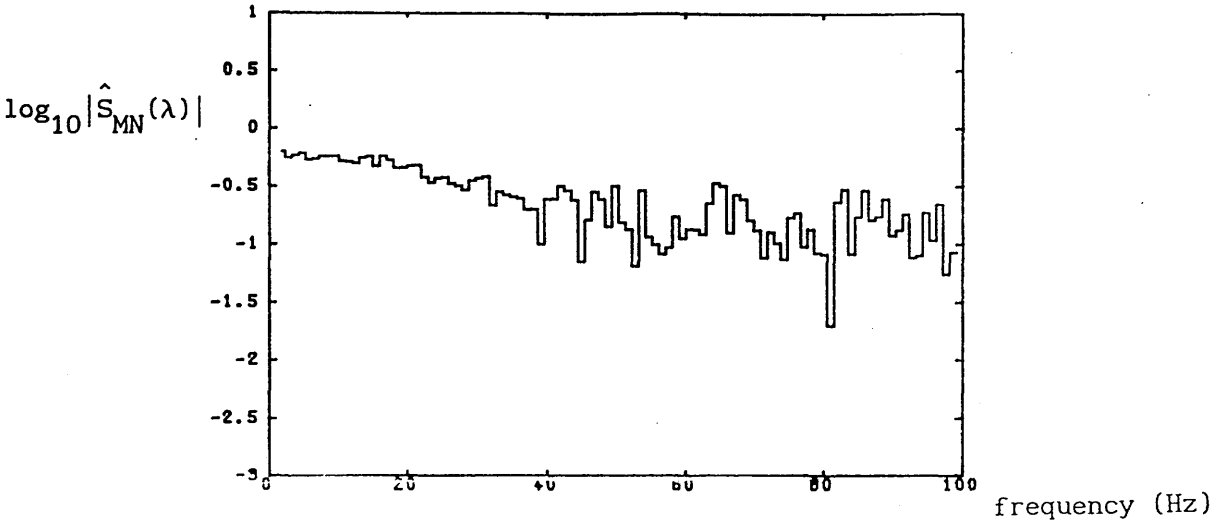

(b) Transfer Function

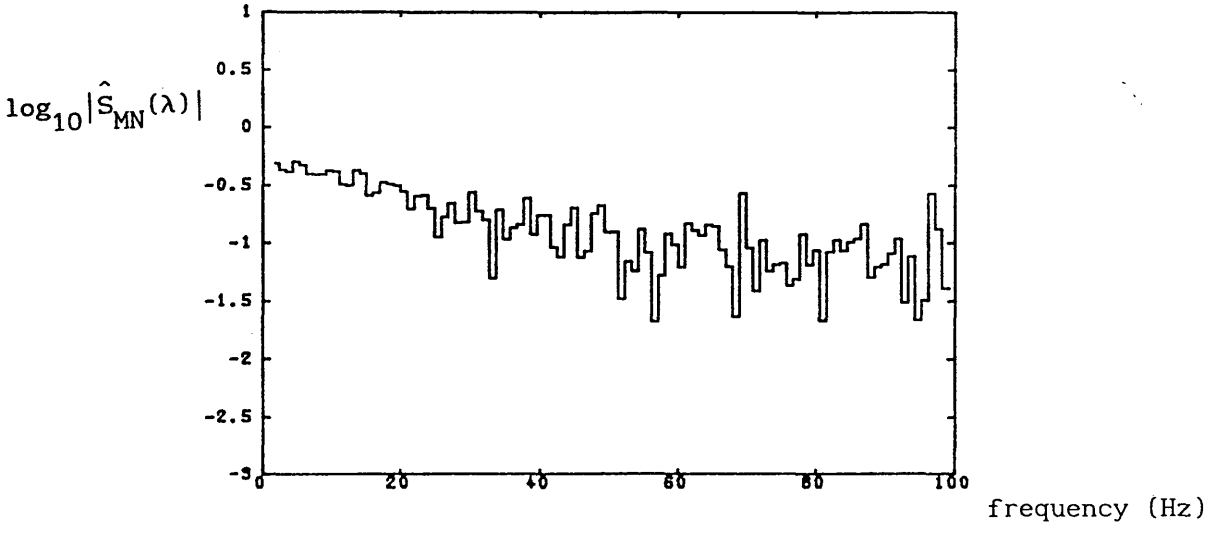

Figure 6.2.10. Transfer function estimates corresponding to the impulse response estimates illustrated Figure 6.2.9. The transfer function and the impulse response form a Fourier transform pair.

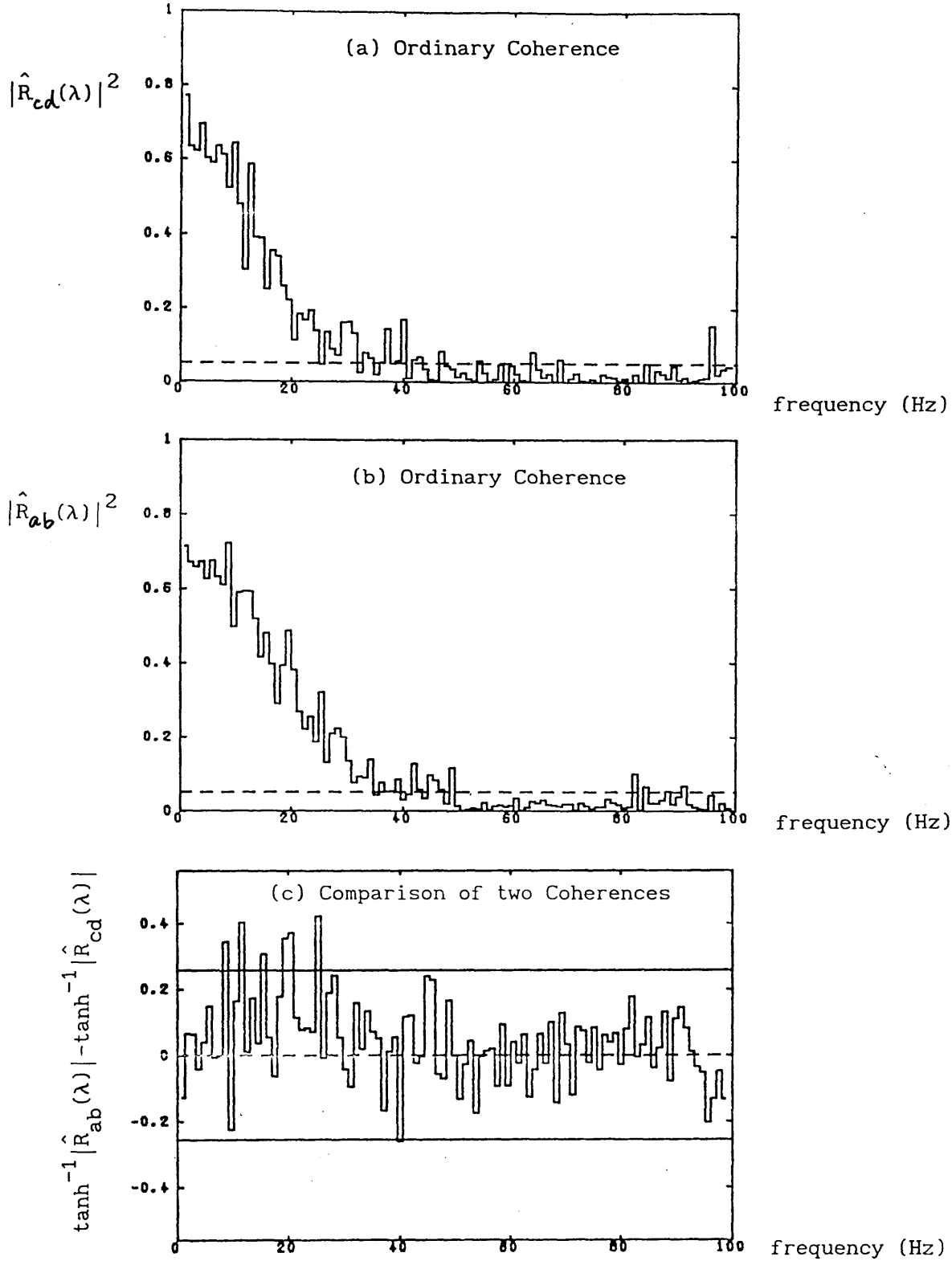

Figure 6.2.11. A frequency domain representation of the cross-intensities in Figure 6.2.8. where (a) is the coherence obtained with a Poisson input firing at 29.4 spikes/sec. and (b) is the coherence obtained with a Poisson input firing at 50 spikes/sec. The difference of the inverse hyperbolic-tangent transform of the moduli of these two coherences is shown in (c). The solid horizontal lines represent the critical values at approximate 95% confidence level of a two-tailed test of the hypothesis that the two moduli are equal.

Finally, Figure (6.2.12) shows the phase spectra obtained from the two data sets. Both phase spectra are characterised by a linear portion starting at $\theta=\pi$. The shape of the phase spectra suggests that it is analogous to the situation in ordinary time series where the input-output relationship is dominated by a delay and a negative regression coefficient (Brillinger, 1975d). Before we exploit the underlying reason in the point process case, it would be appropriate to explain the situation in the case of ordinary time series.

Suppose x(t) and y(t) are two ordinary time series given by

$$y(t) = \alpha\, x(t-\tau) \qquad (6.2.7)$$

where α is the regression coefficient and τ is the time delay between x and y, ie. y is just a delayed and scaled version of x. We see that the transfer function between x and y is given by

$$|S(\lambda)| = |\alpha| \qquad (6.2.8)$$

and the phase spectrum is given by

$$\theta(\lambda) = \begin{cases} -\lambda\tau \mod 2\pi & \text{if } \alpha>0 \\ \pi-\lambda\tau \mod 2\pi & \text{if } \alpha<0 \end{cases} \qquad (6.2.9)$$

Hence in the case when $\alpha<0$ the phase spectrum would be a straight line starting at $\theta=\pi$.

In the point process case, the inhibition effect of each

(a) Phase Spectrum

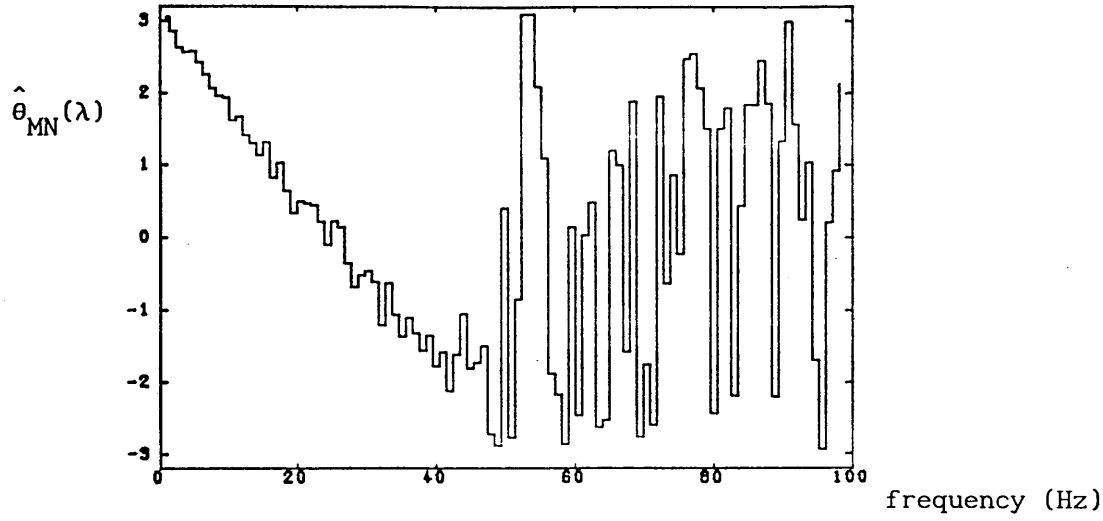

(b) Phase Spectrum

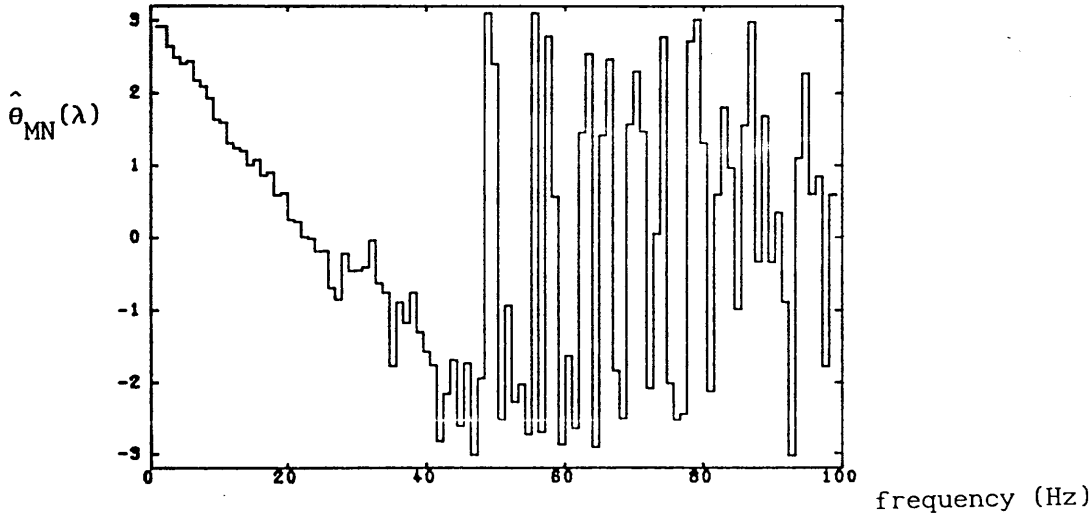

Figure 6.2.12. The phase spectra obtained from the IPSP neurone model with Poisson input of different firing rates. In (a) the input firing rate is 29.4 whereas in (b) is 50 spikes/sec. The phase spectra characteristically begin at $\theta=\pi$ radians in contrast with those obtained in a EPSP model illustrated in Figure 6.2.4.

input spike train would cause the cross-intensity to be dominated by a dip. The impulse response, which is the look-alike of the cross-intensity, would also be dominated by a dip. One can think of the dip as a peak inverted. The negative sign introduces an extra π radians phase change to the Fourier transform of the impulse response function. Hence one would expect the phase spectrum to start at π instead of 0 in an IPSP neurone model.

6.3 Analysis and Simulation of Neuronal Networks in which a Pair of Neurones Receive one or Several Common Inputs

The analysis of the neuronal networks discussed in the following section are based on the use of a linear model discussed in sections (3.3-4). In the simplest case in which the system involves an input point process M and an output point process N, the linear model implies the relationship (Brillinger, 1983)

$$d_N^{(T)}(\lambda) \approx S(\lambda)d_M^{(T)}(\lambda)+d_\varepsilon^{(T)}(\lambda) \qquad (6.3.1)$$

where S(.) is the transfer function, and $d_N^{(T)}(.)$, $d_M^{(T)}(.)$ and $d_\varepsilon^{(T)}(.)$ are the finite Fourier-Stieltjes transform of the process N, M and the zero mean stationary error process N_ε respectively. Note that the two terms $S(\lambda)d_M^{(T)}(\lambda)$ and $d_\varepsilon^{(T)}(\lambda)$ in expression (6.3.1) are independent. Expression (6.3.1) is used to provide a basis for the analysis of the behaviour of paired neurones with single or multiple inputs. In this section, a common-input, two-output neuronal network is considered. Then the analysis is extended to a two-input, two-output neuronal network.

6.3.1 Paired Neurones with a Common Point Process Input

The schematic diagram of the neuronal network is illustrated in Figure (6.3.1) where the common point process input to the two neurones is denoted by N_1 and the two outputs are denoted by N_4 and N_5. Processes N_2 and N_3 represent independent inputs to the two neurones respectively. The common input, N_1 is assumed to be

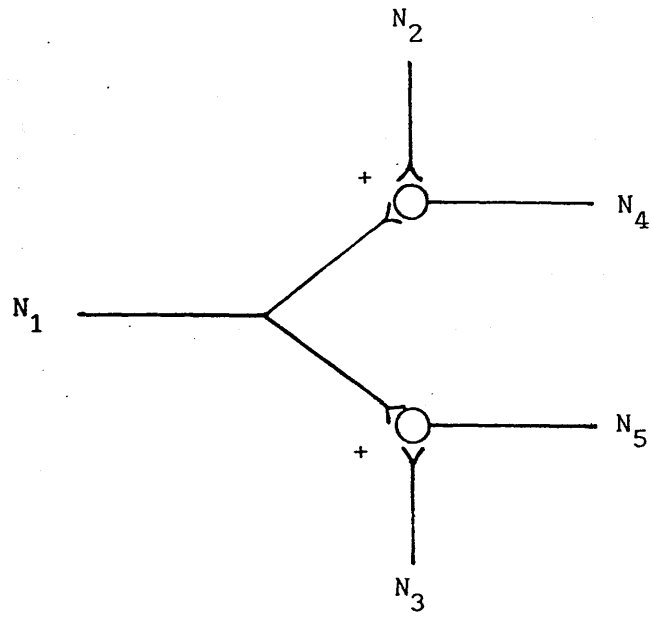

Figure 6.3.1. Diagrammatic representation of a neuronal network in which two neurones N_4 and N_5 share the common input N_1. Process N_2 is a second input to N_4, and is independent of the common input N_1, and of N_3. N_3 is a common second input to N_5 and is also independent of N_1.

independent of processes N_2 and N_3, which, in turn, are independent of each other. Applying expression (6.3.1), the finite Fourier-Stieltjes transform of N_4 may be written as

$$d_4^{(T)}(\lambda) = S_{14}(\lambda)d_1^{(T)}(\lambda)+S_{24}(\lambda)d_2^{(T)}(\lambda)+d_{\varepsilon 14}^{(T)}(\lambda)+d_{\varepsilon 24}^{(T)}(\lambda) \quad (6.3.2)$$

where the subscripts in each term indicate particular processes, $S_{24}(\lambda)$ and $d_{\varepsilon 24}^{(T)}(\lambda)$, for example, denote the transfer function relating N_2 and N_4, and the finite Fourier transform of the error process associated with this particular input/output relation. Similarly, for N_5, the finite Fourier-Stieltjes Transform may be written as

$$d_5^{(T)}(\lambda) = S_{15}(\lambda)d_1^{(T)}(\lambda)+S_{35}(\lambda)d_3^{(T)}(\lambda)+d_{\varepsilon 15}^{(T)}(\lambda)+d_{\varepsilon 35}^{(T)}(\lambda) \quad (6.3.3)$$

Using expressions (6.3.2-3), the magnitude of the cross-spectrum of the processes N_4 and N_5, based on the definition in expression (3.3.16), is given by

$$\begin{aligned} |f_{45}(\lambda)| &= \lim_{T\to\infty} (1/2\pi T)\left|E\{\overline{d_4^{(T)}(\lambda)}d_5^{(T)}(\lambda)\}\right| \\ &= f_{11}(\lambda)|S_{14}(\lambda)|\ |S_{15}(\lambda)| \end{aligned} \quad (6.3.4)$$

Note that the contribution due to the independent input vanishes in expression (6.3.4).

In section (6.2), it was shown that the (EPSP) neuron model under investigation is dominated by a delay and hence the transfer function is essentially uniform over a certain frequency range.

From this, one may rewrite expression (6.3.4) as

$$|f_{45}(\lambda)| \cong f_{11}(\lambda) * [\text{constant}] \qquad (6.3.5)$$

over a certain frequency range. Hence one would expect to see the features of the spectrum of the common input in the cross-spectrum. This idea may be extended to the coherence function, which is the normalised version of the cross-spectrum. Now, using the result in expressions (6.3.2-3) and (3.3.37), the coherence between processes N_4 and N_5 may be written as

$$|R_{45}(\lambda)|^2 = \frac{|f_{45}(\lambda)|^2}{f_{44}(\lambda)f_{55}(\lambda)} \qquad (6.3.6)$$

where

$$|f_{45}(\lambda)|^2 = f_{11}^2(\lambda)|S_{14}(\lambda)|^2|S_{15}(\lambda)|^2$$

$$f_{44}(\lambda) = f_{11}(\lambda)|S_{14}(\lambda)|^2+f_{22}(\lambda)|S_{24}(\lambda)|^2+f_{\varepsilon 24}(\lambda)+f_{\varepsilon 14}(\lambda)$$

$$f_{55}(\lambda) = f_{11}(\lambda)|S_{15}(\lambda)|^2+f_{33}(\lambda)|S_{35}(\lambda)|^2+f_{\varepsilon 35}(\lambda)+f_{\varepsilon 15}(\lambda)$$

In expression (6.3.4), if the contributions from the independent inputs and the noise process are large compared with that of the common input, and are constant over the range of frequencies of interest, then

$$|R_{45}(\lambda)|^2 \approx f_{11}^2(\lambda) * [\text{constant}] \qquad (6.3.7)$$

Hence, under the appropriate conditions, one might expect that the coherence between the discharges from a pair of neurones with a common input would represent a scaled version of the square of the

auto-spectrum of the common input.

Two examples illustrating the relation between the auto-spectrum of the common input to a pair of model neurones and the coherence between the discharge from these neurones are illustrated in Figures (6.3.2) and (6.3.4). In the first example, the common input is the same modulated spike train described in Figure (6.1.8). Figure (6.3.2a) shows the auto-spectrum of the common input in which the frequency components of the process are widely separated. Immediately below is the coherence estimated from simultaneously recorded samples of the discharge from the pair of model neurones (Figure 6.3.2b). The peaks in the coherence are seen to clearly reflect the two dominate frequency components in the spectrum of the common input, and therefore provide a reasonable representation of its frequency content.

When it is possible to record from a suspected input point process, the partial coherence between the output point processes taking into account a possible contribution from the suspected input may be estimated. The partial coherence will then provide an indication of whether the observed coupling between the pair of neurones is only a consequence of this input. In the case that the common input provides the only source of coupling between the two neurones, as is the case for this example, one would expect that the sample partial coherence (of order-1) would be close to zero, as is observed in in Figure (6.3.2c).

In contrast to the frequency domain representation of the

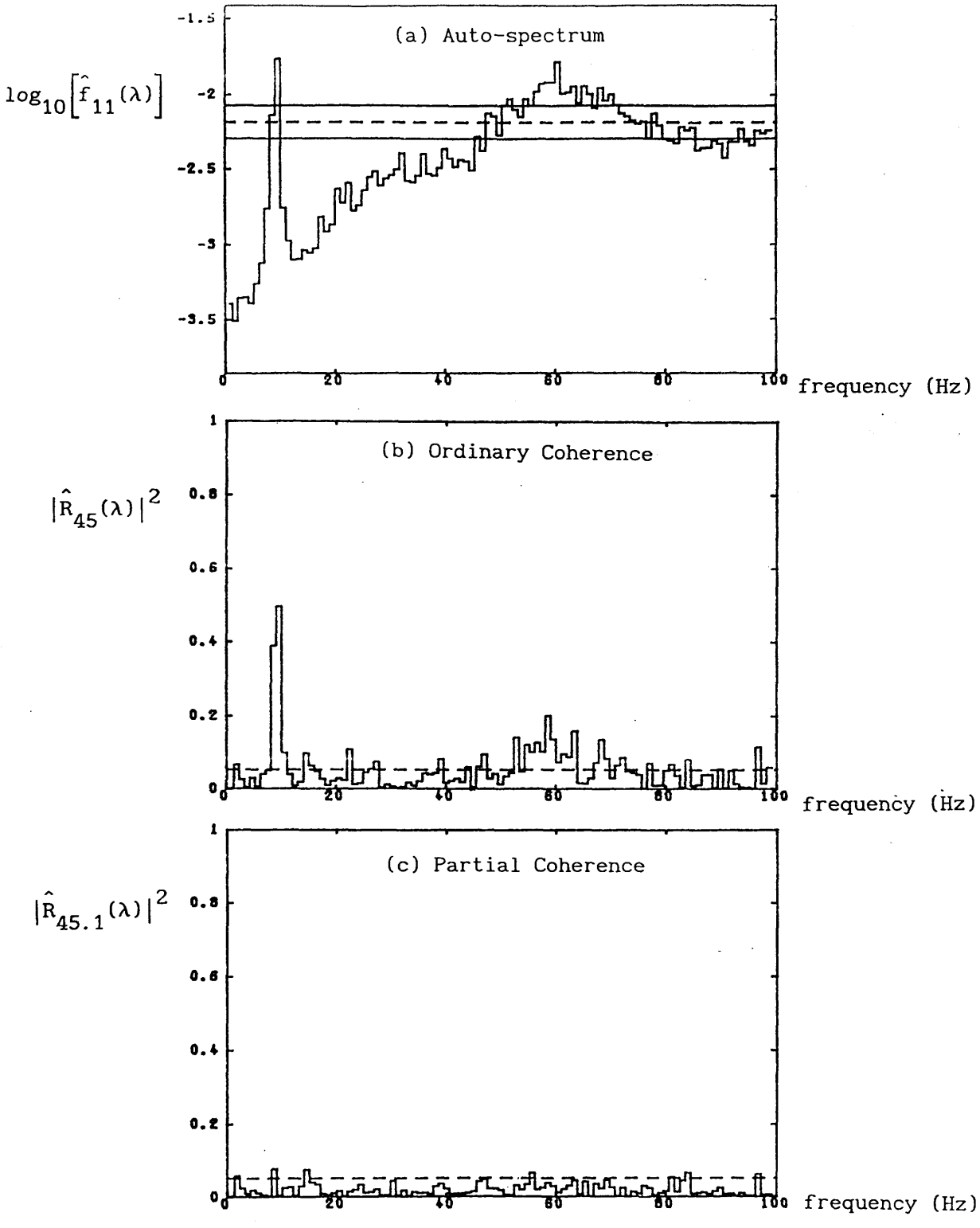

Figure 6.3.2. The estimated (a) auto-spectrum of the common input. (b) The ordinary coherence of the discharges of the two neurones and (c) the partial coherence between the discharges from the two neurones after taking into account the contribution from the common input. The firing rates of the common input and the outputs are 40.67, 33.57 and 21.85 spikes/sec. respectively. The solid horizontal lines in (a) represents an approximate 95% confidence interval for the estimated auto-spectrum, and the dashed horizontal line the asymptotic value of the estimate. The horizontal dashed lines in (b) and (c) represent the upper level of the 95% confidence intervals for the coherence under the assumption that the two processes are independent.

relation between the two output point processes, Figure (6.3.3) shows the analogous time domain representation of these relations. In Figure (6.3.3b), the cross-intensity, taken as the time domain analogue of the coherence, has a sharp peak at about u=10 msec. corresponding to the difference of delays within the two model neurones. There is, however, no indication of any secondary features in the cross-intensity that may unambiguously be related to the frequencies apparent in the auto-intensity estimates of the common input (Figure 6.3.3a). In addition, the significant peaks indicated in the coherence estimates (Figure 6.3.2b) appear as non-significant fluctuations within the confidence interval in the cross-intensity estimate (Figure 6.3.3b).

In the second example the two periodic components of the common input differ only by 20 Hz compared with a difference of 53 Hz for the first example. The coherence between the output point processes is shown in register with and below the auto-spectrum of the common input (Figure 6.3.4). One of the two frequency components of the common input appears as the broad peak in the coherence centered at about 30 Hz and the other as the sharp peak at 52 Hz. The peak at 52 Hz corresponds to the sinusoidal modulation frequency of the common input. The non-significant partial coherence (Figure 6.3.4c) indicates that the common input is the only source of coupling between the two neurones.

The time domain description for the second example is illustrated in Figure (6.3.5). The cross-intensity between N_4 and N_5 has a peak displaced to the right of the origin by an amount

(a) Auto-intensity

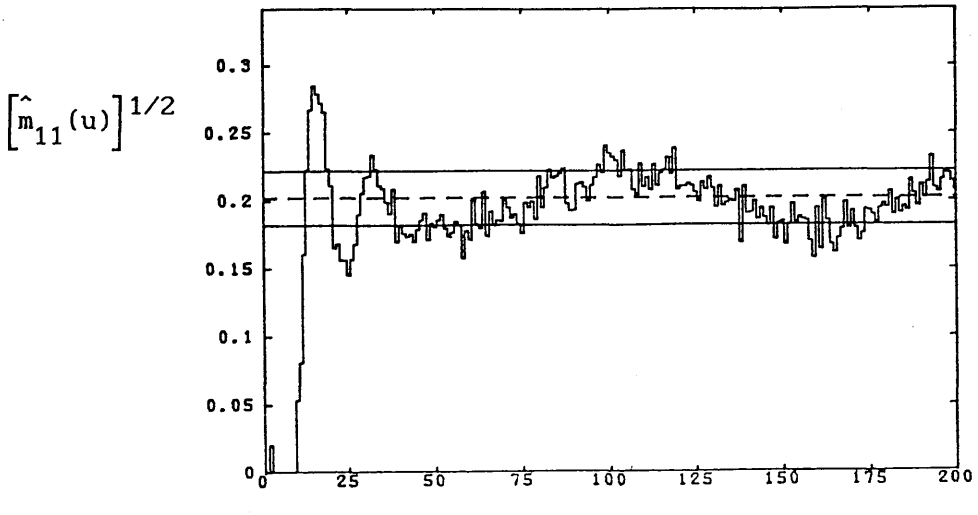

(b) Cross-intensity

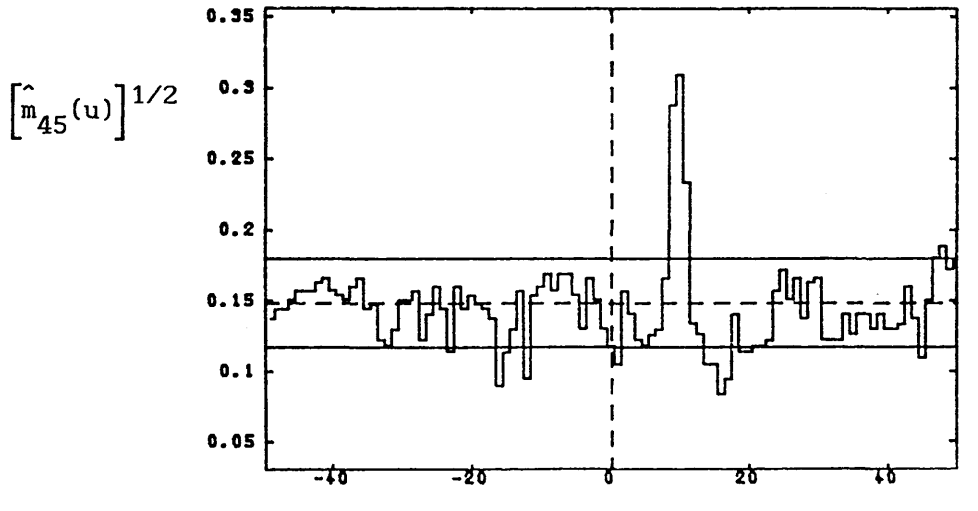

Figure 6.3.3. Estimated (a) auto-intensity of the common input and (b) cross-intensity between the two output spike trains. The solid horizontal lines represent approximate 95% confidence intervals, and the dashed horizontal lines the asymptotic value of the estimates.

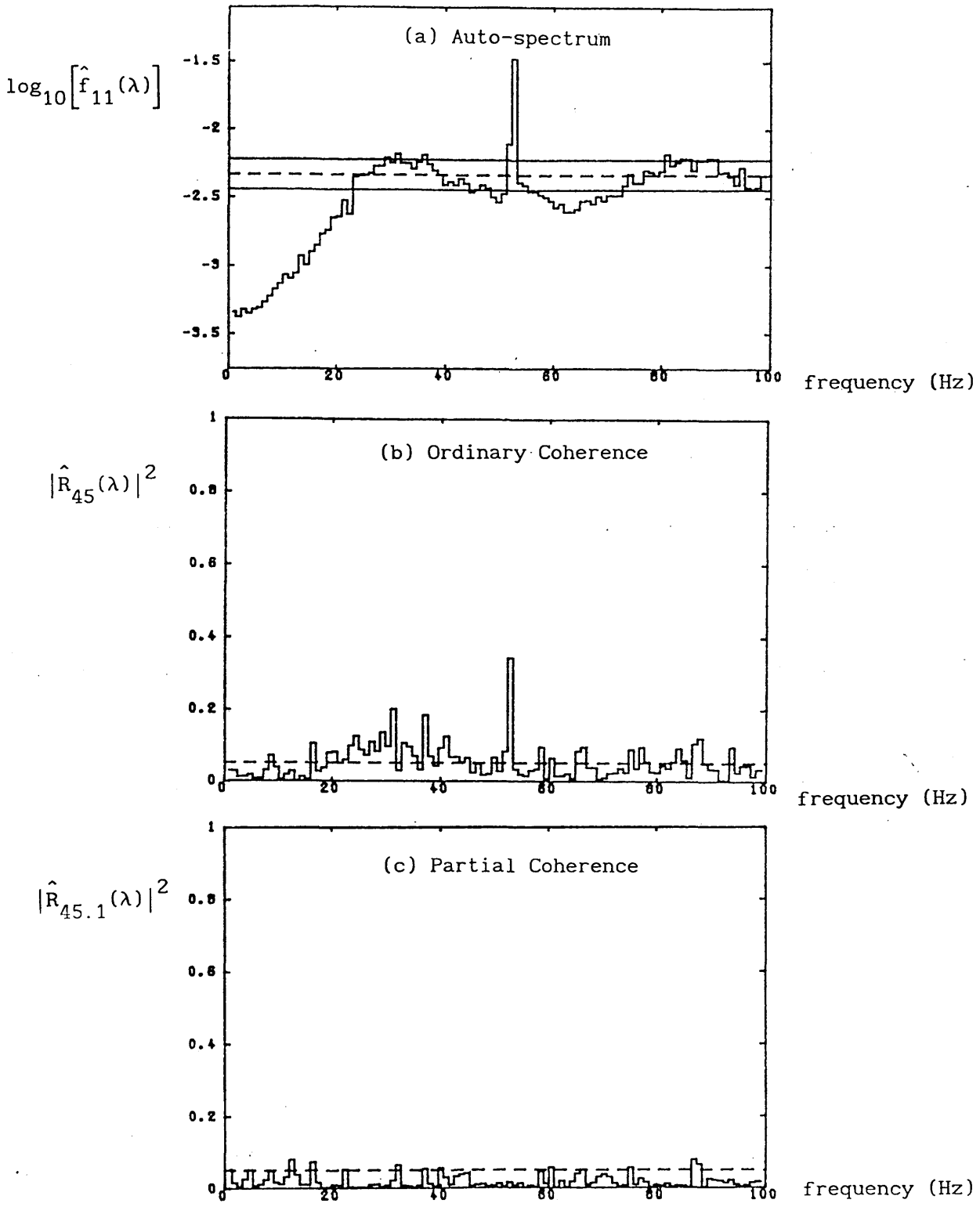

Figure 6.3.4. The estimated (a) auto-spectrum of the common input, (b) The ordinary coherence of the discharges of the two neurones, and (c) the partial coherence between the discharges from the two neurones after taking into account the contribution from the common input. The firing rates of the common input and the outputs are 28.75, 15.12 and 17.07 spikes/sec. respectively. The solid horizontal lines in (a) represents an approximate 95% confidence interval for the estimated auto-spectrum, and the dashed horizontal line the asymptotic value of the estimate. The horizontal dashed lines in (b) and (c) represent the upper level of the 95% confidence intervals for the coherence under the assumption that the two processes are independent.

(a) Auto-intensity

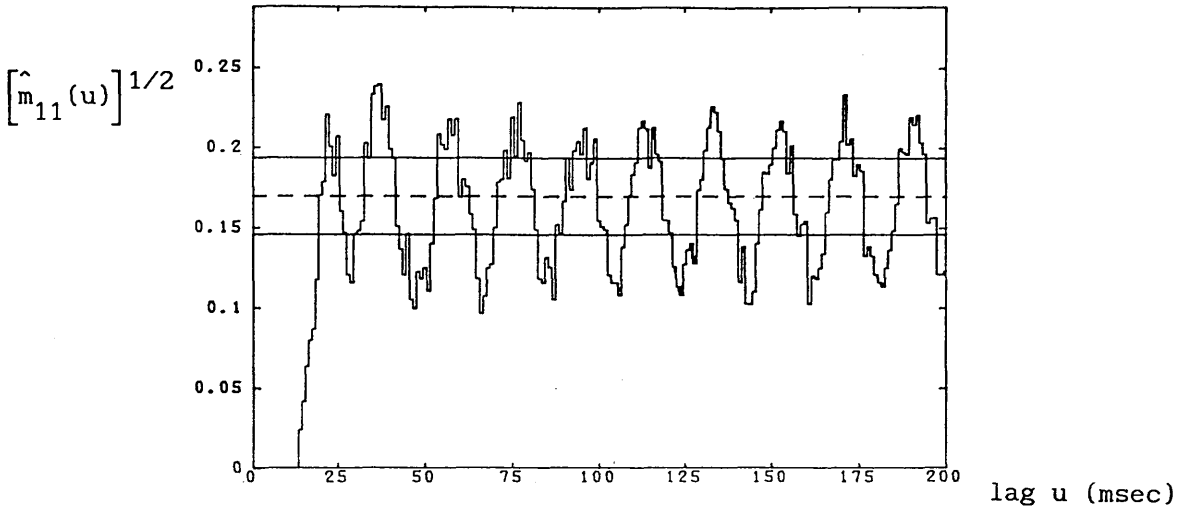

(b) Cross-intensity

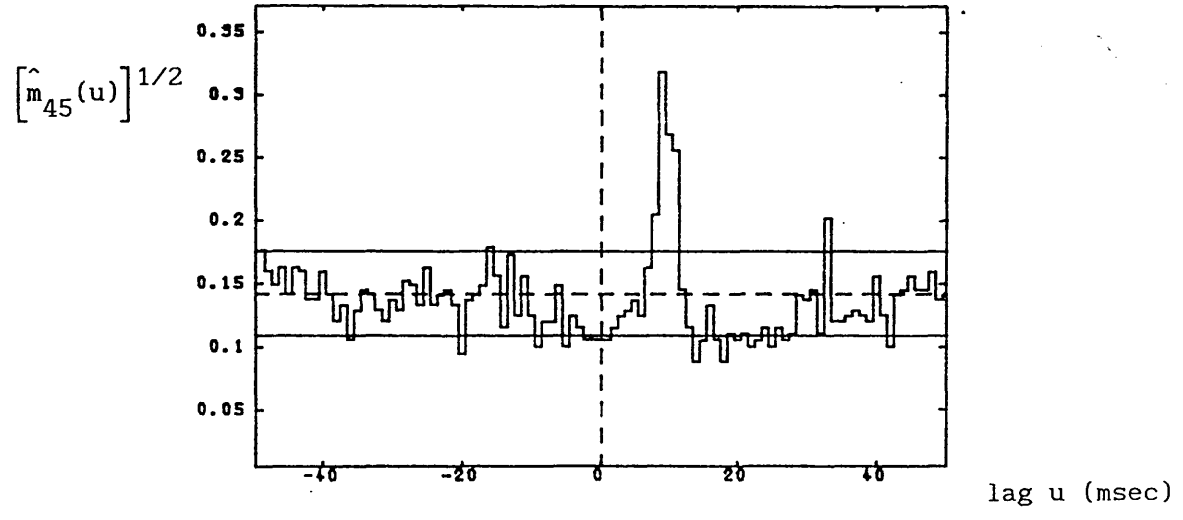

Figure 6.3.5. Estimated (a) auto-intensity of the common input and (b) cross-intensity between the two output spike trains. The solid horizontal lines represent approximate 95% confidence intervals, and the dashed horizontal lines the asymptotic value of the estimates.

equal to the difference between the delays in the two model neurones (Figure 6.3.5b). Although the cross-intensity contains a suggestion of a periodic secondary characteristic to the right of the origin, it is well within the confidence interval and the frequency of this component does not reflect any of the frequency components of the common input as shown in its auto-spectrum (Figure 6.3.4a).

6.3.2 Paired Neurones with Two Common Point Process Inputs

The following example is based on the schematic neuronal network shown in Figure (6.3.6). The independent common inputs to the paired neurones are denoted by N_1 and N_2. The output point processes from the pair of neurones are denoted by N_5 and N_6. Processes N_3 and N_4 represent independent inputs to the neurones as indicated in Figure (6.3.6). By a direct extension of the procedure set out in section (6.3.1), the coherence between processes N_5 and N_6 may be written as

$$|R_{56}(\lambda)|^2 = \frac{|f_{56}(\lambda)|^2}{f_{55}(\lambda)f_{66}(\lambda)} \qquad (6.3.8)$$

where

$$f_{56}(\lambda) = f_{11}(\lambda)\overline{S_{15}(\lambda)S_{16}(\lambda)} + f_{22}(\lambda)\overline{S_{25}(\lambda)S_{26}(\lambda)}$$

$f_{55}(\lambda)$ = Spectra of all inputs to N_5 + Error spectra

$f_{66}(\lambda)$ = Spectra of all inputs to N_6 + Error spectra

In this situation, under appropriate conditions, the coherence would have components proportional to the magnitude squared of the

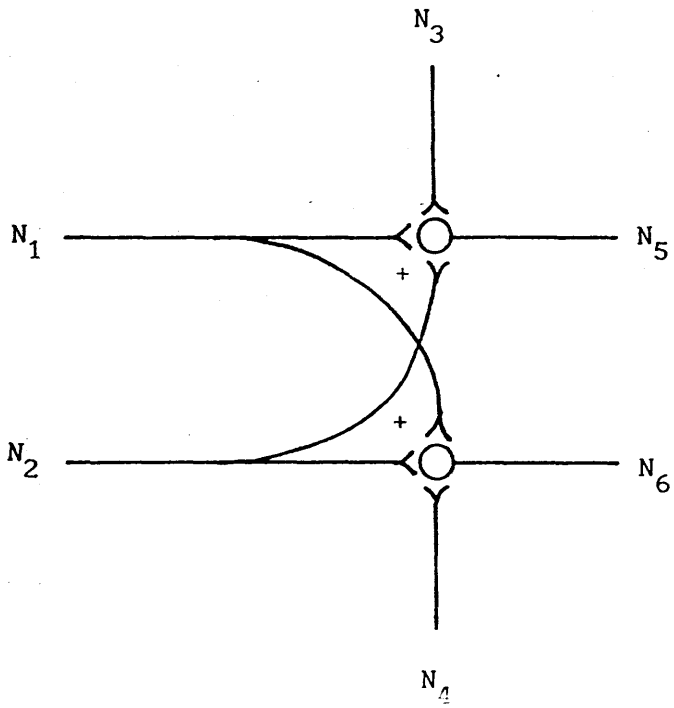

Figure 6.3.6. Diagrammatic representation of a neuronal network in which two neurones N_5 and N_6 share the common inputs N_1 and N_2. Processes N_3 is an input to N_5 that is independent of N_1, N_2 and N_4. N_4 is an input to N_6 that is independent of N_1, N_2 and N_3.

sum of scaled versions of the two input auto-spectra.

Figure (6.3.7) gives examples of the auto-spectra of two common input processes N_1 and N_2 and the coherence computed between the two output processes N_5 and N_6. The first input N_1 has a significant frequency component at about 10 Hz (Figure 6.3.7a) whereas the second input N_2 has a broad peak in the neighbourhood of 50 Hz (Figure 6.3.7b). These components are clearly reflected in the coherence computed between the two outputs N_5 and N_6 as displayed in Figure (6.3.7c).

The time domain representation of these relations is shown in Figure (6.3.8). The sharp peak at about 0 msec. in the cross-intensity between the output processes indicates that the two neurones discharge synchronously (Figure 6.3.8c). The spacing between the successive secondary peaks is about 20 msec. which corresponds to a frequency of 50 Hz, close to the frequency of firing of the second common input (see Figure 6.3.8b and 6.3.7b). There is, however, no indication of the frequency components contained in the first common input (see Figure 6.3.8a and 6.3.7a). Consequently, the auto-intensities of the output processes do not necessarily further the analysis of the properties of suspected common inputs, and in fact may be misleading with respect to inferences concerning the frequency content of these inputs.

The analysis of influences on the relation between the output point processes may be furthered when it is possible to

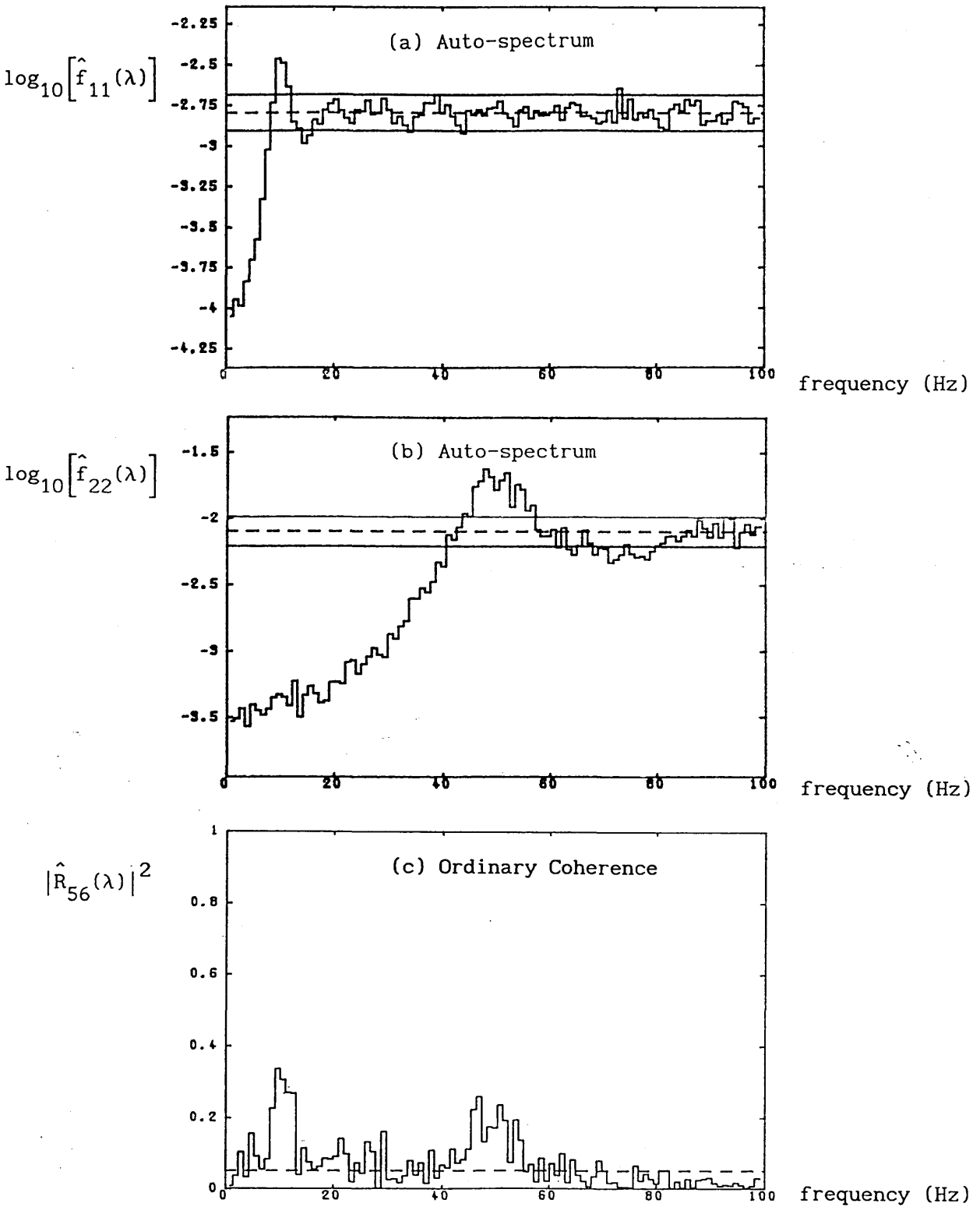

Figure 6.3.7. Estimated (a,b) auto-spectra of the two shared inputs N_1 and N_2 to the pair of neurones N_5 and N_6, and (c) the coherence between the spike trains from N_5 and N_6 generated in response to the common inputs. The firing rates of N_1, N_2, N_5 and N_6 are 10.05, 50.12, 39 and 51.68 spikes/sec. respectively. The solid horizontal lines in (a,b) represent an approximate 95% confidence intervals, and the dashed horizontal lines the asymptotic value of the estimates. The dashed horizontal lines in (c) represents the upper limit of the 95% confidence interval assuming the processes N_5 and N_6 are independent.

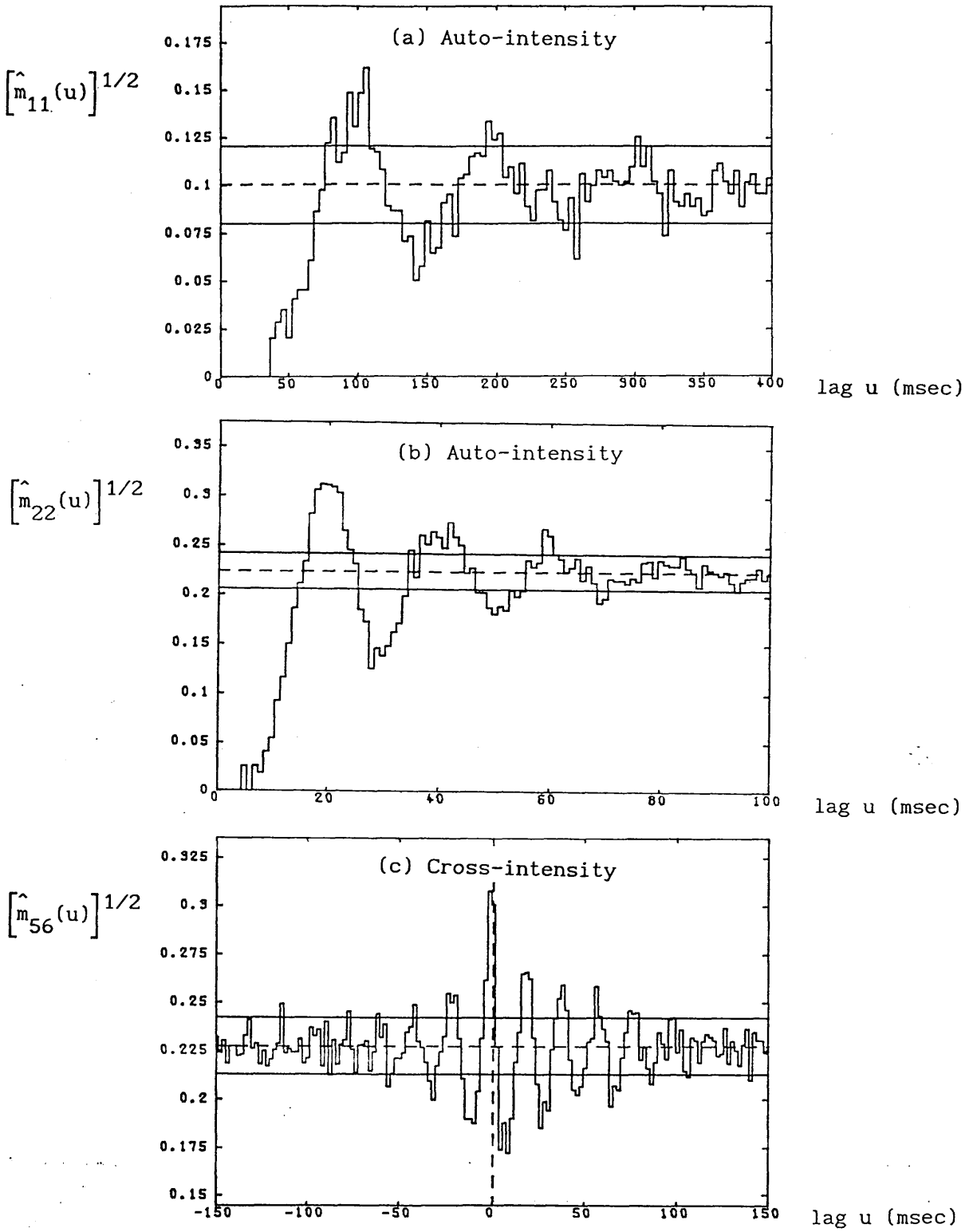

Figure 6.3.8. Estimated (a,b) auto-intensities of the two shared inputs N_1 and N_2, and (c) the cross-intensity between the spike trains from N_5 and N_6 in response to the effects of the presence of both common inputs. The solid horizontal lines in (a,b,c) represent approximate 95% confidence intervals for the estimates and the dashed horizontal lines the asymptotic values of the estimates.

record from several suspected input processes in addition to the two output processes. Several possible partial coherences may be estimated in an attempt to assess the pattern of connectivity between all the recorded processes. For the network of Figure (6.3.6), there are two possible first-order partial coherences, one taking into account the contribution to the coupling between N_5 and N_6 made by N_1 and the other taking into account the contribution from N_2 to this coupling. These first-order partial coherences are illustrated in Figure (6.3.9a-b). The partial coherence in Figure (6.3.9a) takes into account the contribution that process N_1 makes to the coherence between N_5 and N_6. It shows, by the absence of a peak at 10 Hz ie. the dominant frequency component of N_1, that the lower frequency component of the coherence between the two output processes in Figure (6.3.7c) is probably attributed entirely to process N_1. The partial coherence in Figure (6.3.9b), which takes into account the contribution to coupling between the output processes attributable to N_2, suggests that the peak at 50 Hz in the coherence of Figure (6.3.7c) may be a consequence of this process.

One may proceed further and estimate the second-order partial coherence which assesses the extent to which the coupling between the two outputs that is due to the presence of the two inputs N_1 and N_2. The sample second-order partial coherence, illustrated in Figure (6.3.9c), indicates that the coupling between N_5 and N_6 is entirely due to the two common inputs.

From the above results, one may draw the immediate

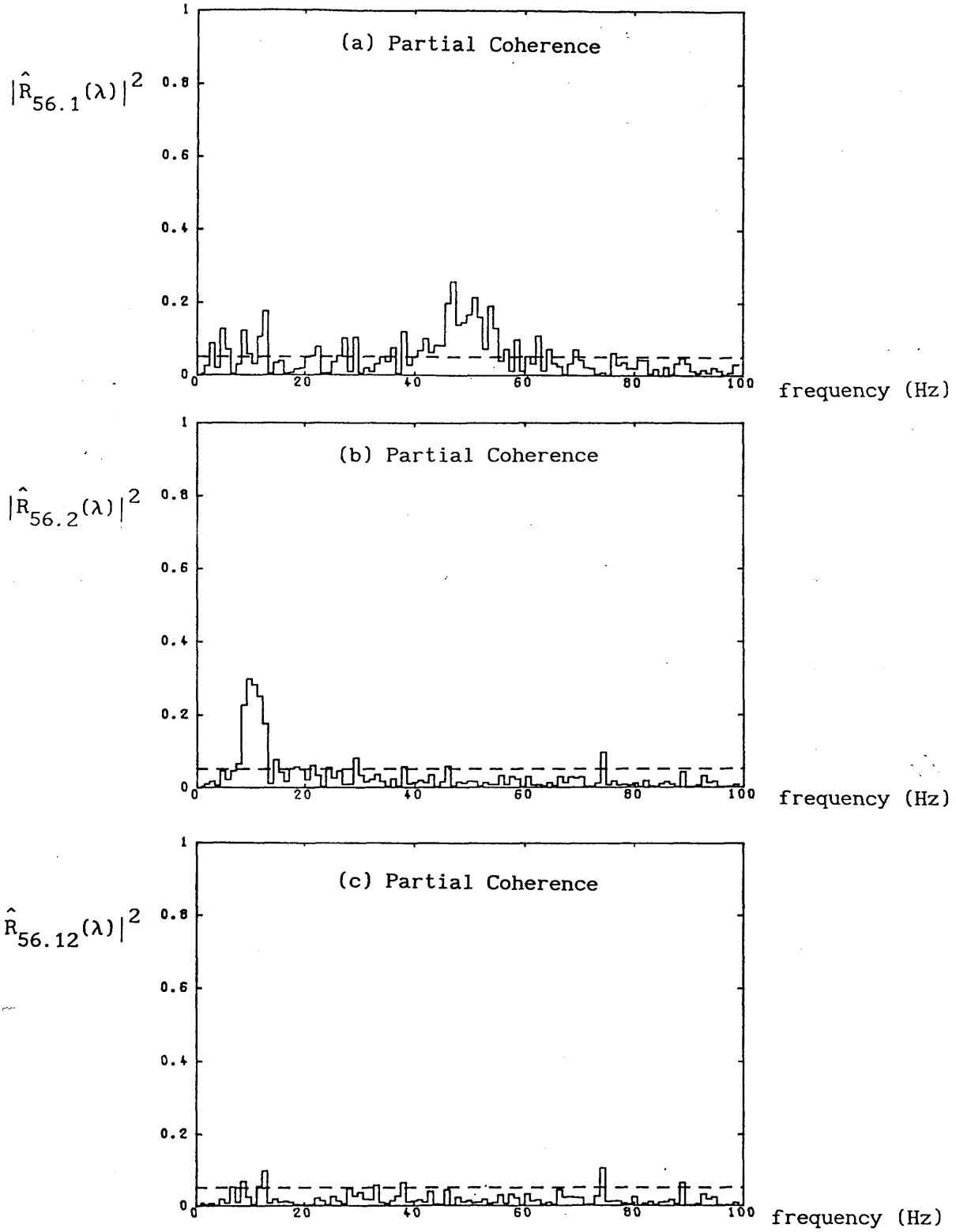

Figure 6.3.9. Estimated (a) first-order partial coherence between N_5 and N_6 taking into account the contribution to this coherence from common input N_1, and (b) first-order partial coherence between N_5 and N_6 taking into account the contribution from process N_2, and (c) second-order partial coherence between N_5 and N_6 taking into account the contribution from both processes N_1 and N_2. The dashed horizontal lines in (a,b,c) represent the upper level of the approximate 95% confidence intervals under the assumption that the two processes are independent.

(a) Cross-intensity

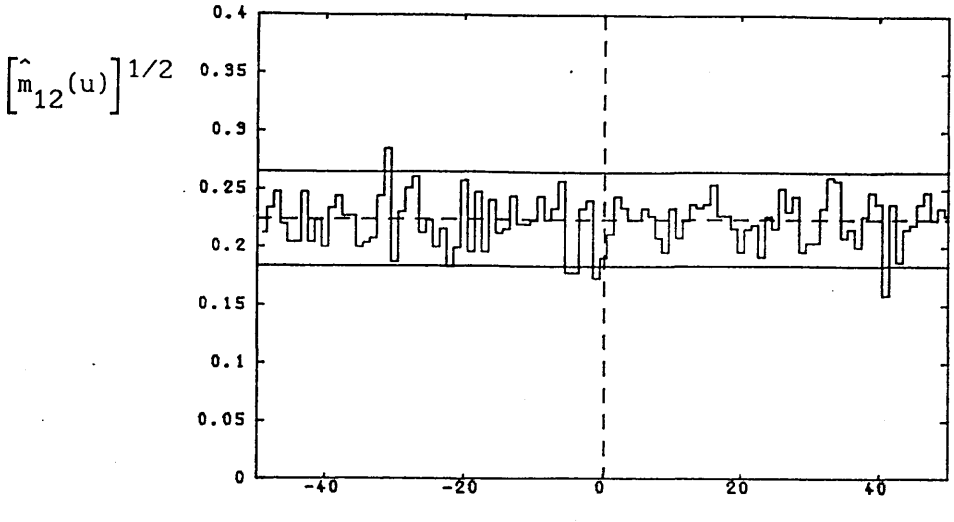

(b) Ordinary Coherence

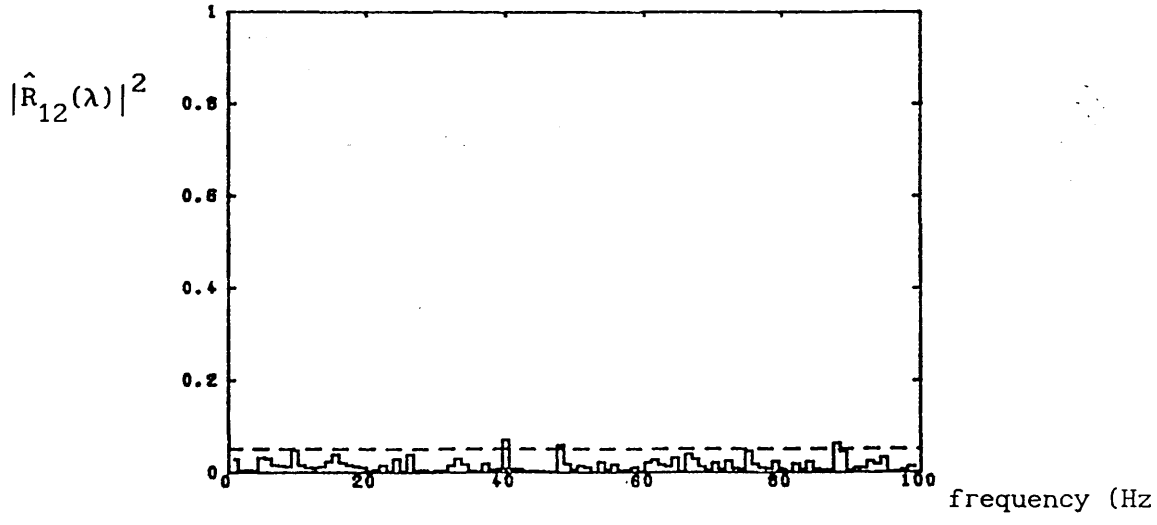

Figure 6.3.10. Estimated (a) cross-intensity and (b) ordinary coherence between processes N_1 and N_2. In (a) the solid horizontal lines represent the 95% confidence interval, the dashed horizontal line the asymptotic value of the estimate assuming the two processes are independent. In (b) the dashed horizontal line represent the 95% confidence interval if the two processes are independent.

conclusions that (1) the linear model works well for the EPSP neuronal network model and (2) the two common inputs are independent of each other. The second condition is justified by the fact that for a linear model, the operation of the 1st-order partial coherence of mathematically removing the contribution of a process is equivalent to physically removing this process only when the process is independent of other inputs (see Appendix 2 for proof). This is further supported by the cross-intensity and coherence between the two input processes N_1 and N_2 as illustrated in Figure (6.3.10). The random fluctuation of the cross-intensity within the confidence limits (Figure 6.3.10a) and the zero coherence (Figure 6.3.10b) indicate that the two inputs are independent.

6.3.3 Paired Neurones with Common Spike Train and Continuous Inputs

The usefulness of a Fourier approach for investigating patterns of connectivity is further demonstrated by the next example in which one of the two input processes to the two model neurones is a continuous signal, whereas the other is a point process (Figure 6.3.11). The continuous signal is generated by passing a pseudo-gaussian white noise through a band-pass filter consists of a high-pass filter and a low-pass Chebychev filter. The spectrum of the continuous input has a relative broad peak in the range of 20 to 60 Hz and a ripple in the upper stop band due to the Chebychev filter (Figure 6.3.12b), whereas the simulated spike train input has a strong periodic component at about 10 Hz (Figure 6.3.12a).

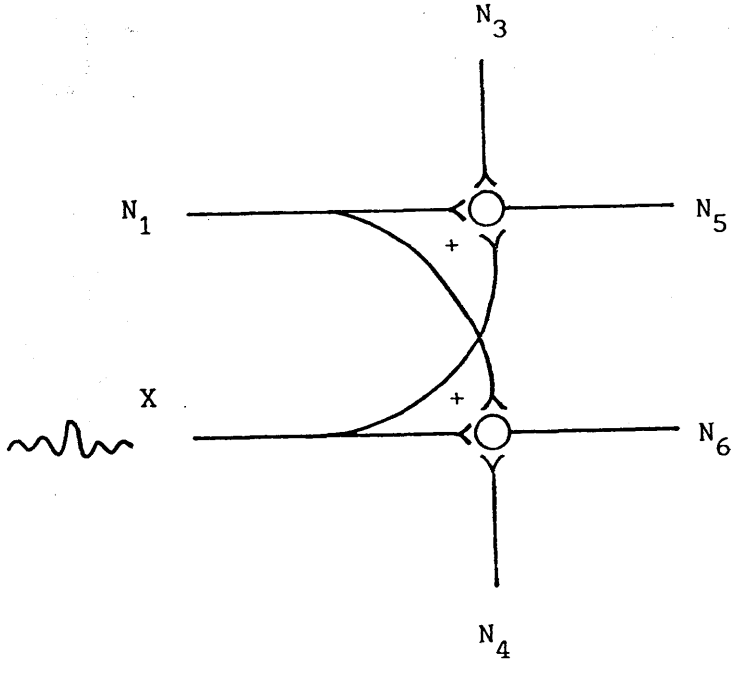

Figure 6.3.11. Diagrammatic representation of a neuronal network in which two neurones share the common inputs from a spike train N_1 and a continuous signal X. Process N_3 is an input to N_5 that is independent of N_1, X and N_4. N_4 is an input to N_6 that is independent of N_1, X and N_3.

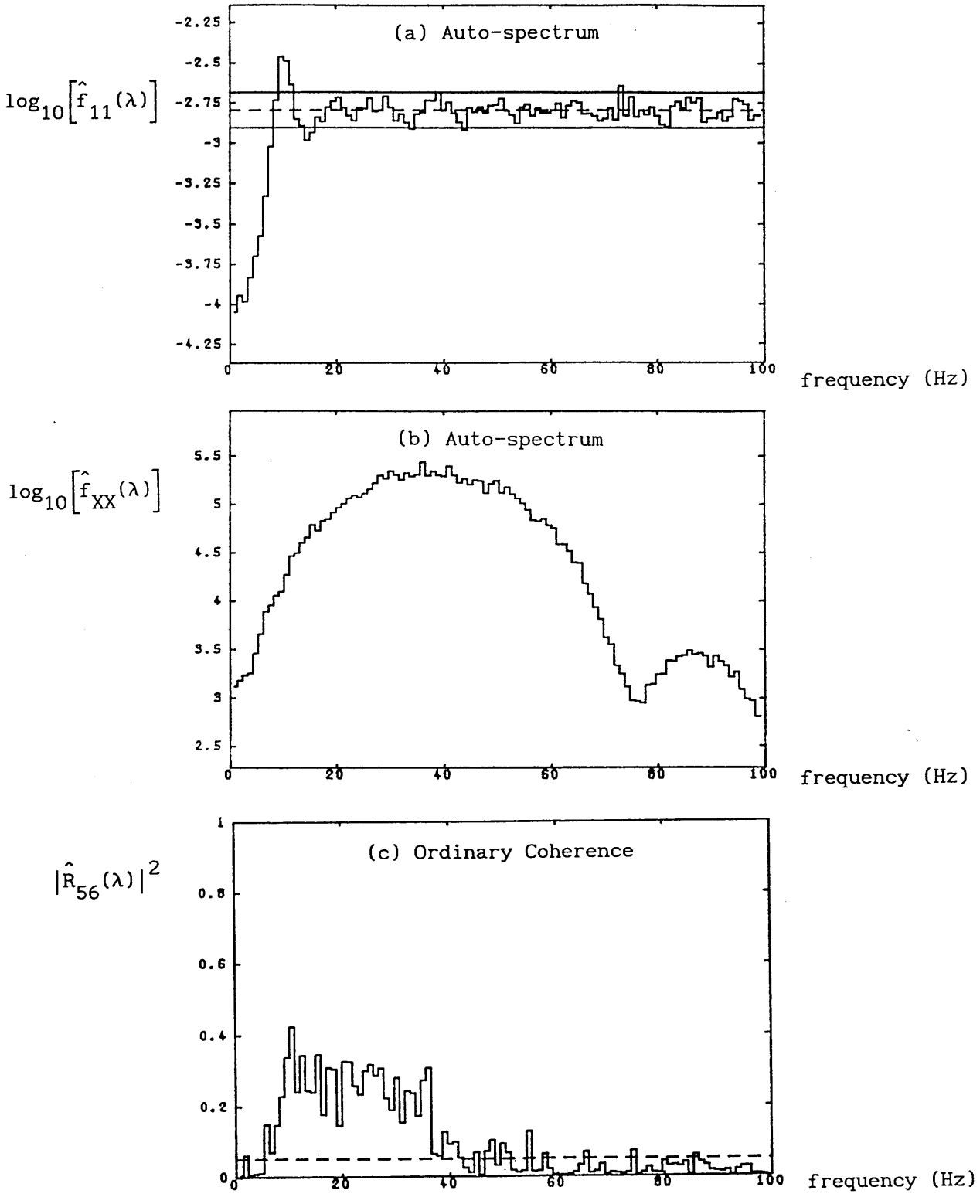

Figure 6.3.12. Estimated (a,b) auto-spectra of the two common inputs N_1 and X to the pair of neurones N_5 and N_6, and (c) the coherence between the spike trains from N_5 and N_6 generated in response to the common inputs. The firing rates of N_1, N_5 and N_6 are 10, 20 and 29 spikes/sec. respectively. The solid horizontal lines in (a) represent an approximate 95% confidence interval, and the dashed horizontal lines the asymptotic value of the estimates. The dashed horizontal lines in (c) represents the upper limit of the 95% confidence interval assuming the processes N_5 and N_6 are independent.

The coherence between the two output spike trains N_5 and N_6 shows a significant peak over the frequency range 10 to 40 Hz (Figure 6.3.12c) suggesting that the both input processes contribute to the coupling. As in the case with the two input spike trains in section (6.3.2), one may extend the analysis by recording from suspected input processes, and then investigate the pattern of connectivity between the recorded processes utilising partial coherences. The partial coherence of order-1, taking into account the contribution that the continuous process makes to the coupling between the two output processes, indicates a reduction of the peak in the range 25 to 40 Hz (Figure 6.3.13a). This partial coherence shows not only that the continuous process contributed to the coupling of the output processes over the frequency range 25 to 40 Hz, but also that another process also contributes to this coupling over a much narrower band of frequencies centered at 10 Hz. Therefore it indicates the presence of an independent source of coupling between the output processes. The partial coherence of order-1 between the output processes after taking into account the contribution of another suspected common input N_1 (Figure 6.3.13b) indicates the disappearance of the peak centered at 10 Hz, implying that this source of coupling is largely due to N_1. The partial coherence of order-2 (Figure 6.3.13c) taking into account the contribution to output coupling attributed to both the continuous and spike train inputs (Figure 6.3.13c) is not significantly different from what one would expect if the coupling between the output processes was due entirely to the two suspected input processes.

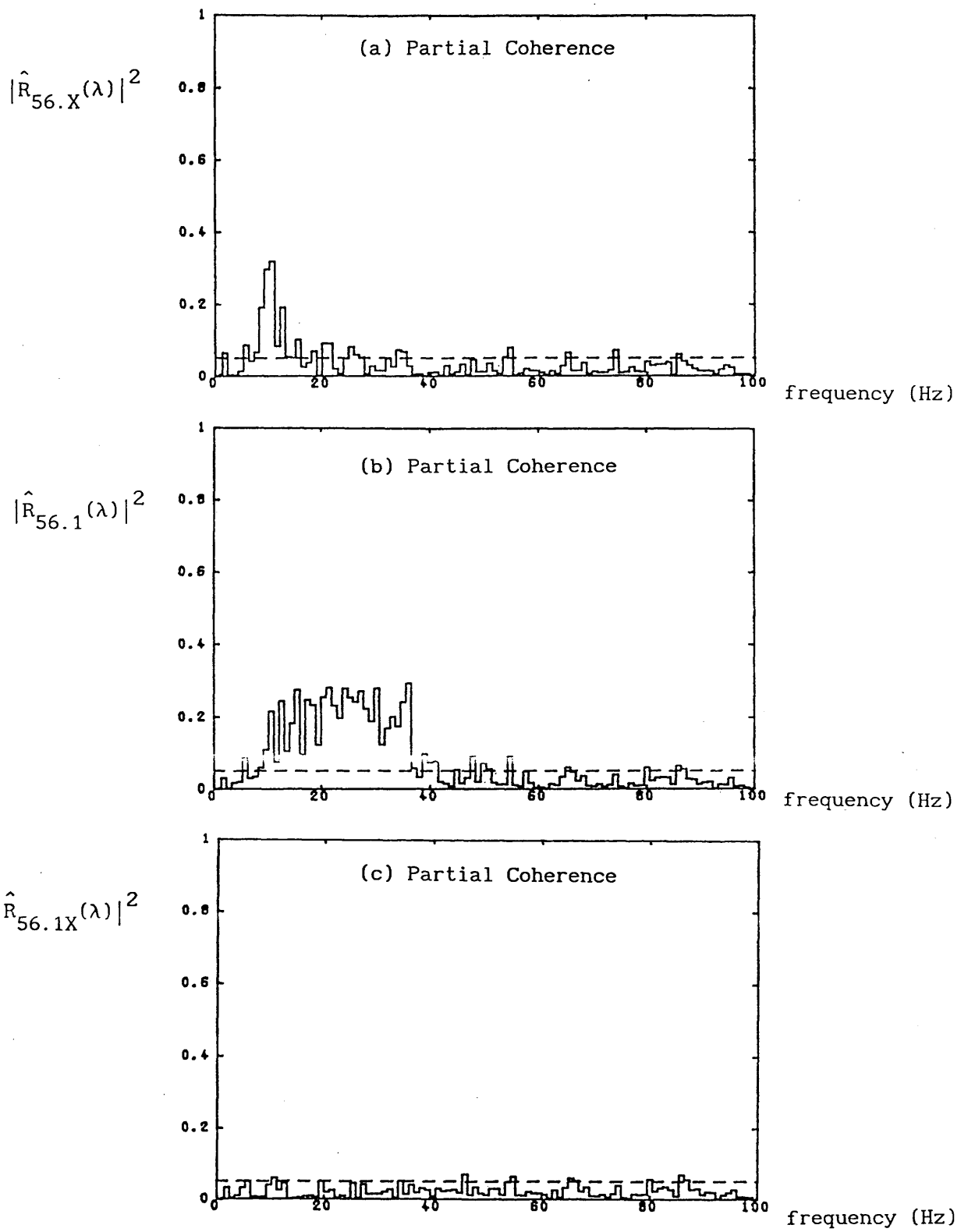

Figure 6.3.13. Estimated (a) first-order partial coherence between N_5 and N_6 taking into account the contribution to this coherence from common input X, and (b) first-order partial coherence between N_5 and N_6 taking into account the contribution from process N_1 , and (c) second-order partial coherence between N_5 and N_6 taking into account the contribution from both processes N_1 and X. The dashed horizontal lines in (a,b,c) represent the upper level of the approximate 95% confidence intervals under the assumption that the two processes are independent.

The above example illustrates how a Fourier approach to the analysis of the structure of a neuronal network naturally accommodates both spike trains and continuous signals. In addition, this particular approach can easily be extended to a consideration of the connectivity patterns between an arbitrary number of neurones. A possible generalisation is given in Appendix 3.

Although partial coherence has proved very useful in investigating the contribution that a suspected input may make to the coupling between the two neurones, it should be used with caution. The derivation of partial coherence is based on the use of a linear model in which it may be defined as the limiting correlation between the finite Fourier-Stieltjes transforms of two processes N_1 and N_2 after subtracting off from each the linear contribution that a third process M makes to these two processes. If, however, as demonstrated in Appendix 4, the common input exerts a non-linear effect on the coupling between two processes, the sample partial coherence between these processes may not be close to zero, although the single common input may be the only source of coupling between the two spike trains.

6.4 Covariance Analysis of the Firing Behaviour of a Neurone Model

It has been shown in the previous examples that the frequency domain analysis is particular powerful in investigating interactions between the frequency components of the processes, whereas the time domain analysis is useful in revealing the timing relations between them. In this section, the time domain analysis is extended to investigate aspects of the non-linear interactions that occur within a neurone model. Third-order cumulant densities are used to assess the statistical dependence between two spike trains. One feature in the cumulant describing the interactions between the discharge of a single Ia afferent and the response of a single motor unit was a period of depression following the motor unit spike. The time course of this depression followed that reported in the literature for after-hyperpolarisation (Burke and Rudomin, 1977). A simple neurone model incorporating after-hyperpolarisation is used to investigate the idea that the third-order cumulant density derived from the Ia and motor unit spike trains provides an indirect measure of the time course of post-spike depression.

6.4.1 Third-Order Cumulant Density Function

The third-order cumulant density for three spike trains N_1, N_2 and N_3 provides a measure of the joint statistical dependence between the three processes in time domain. By a direct extension of the second order case, the third-order cumulant density

function may defined as

$$q_{123}(u,v)dtdudv = E\Big\{[dN_1(t)-P_1dt][dN_2(t+u)-P_2du][dN_3(t+v)-P_3dv]\Big\} \tag{6.4.1}$$

The timing convention follows that of Figure (6.4.1).

After some manipulations of expression (6.4.1), it may also be expressed as, (Brillinger, 1975b)

$$q_{123}(u,v) = P_{123}(u,v)-P_1P_{23}(v-u)-P_2P_{13}(v)-P_3P_{12}(u)+2P_1P_2P_3 \tag{6.4.2}$$

The definitions and estimation procedures for the first and second-order densities are given in Chapter 3 and 4 respectively. The third-order product density $P_{123}(u,v)$ may be interpreted as the joint probability density of the occurrence of the three spikes at specified time intervals and is defined as

$$P_{123}(u,v)dtdudv = E\Big\{[dN_1(t)][dN_2(t+u)][dN_3(t+v)]\Big\} \tag{6.4.3}$$

An estimate for the third-order product density can be constructed as (Brillinger, 1975b)

$$\hat{P}_{123}(u,v) = J_{123}^{(T)}(u,v)/b^2T \tag{6.4.4}$$

where the third-order counting variate $J_{123}^{(T)}(u,v)$ is defined as

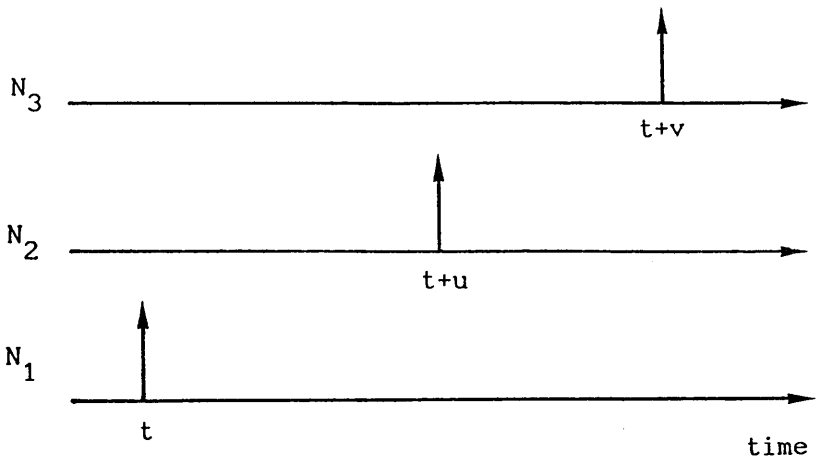

Figure 6.4.1. Diagrammatic representation of the convention used to represent the relative times of occurrence of spikes from three processes N_1, N_2 and N_3 in the third-order cumulant density function $q_{123}(u,v)$.

$$J_{123}^{(T)}(u,v) = \#\{(j,k,l): u-b/2<s_k-t_j\leq u+b/2 \text{ and } v-b/2<r_l-t_j\leq v+b/2\} \quad (6.4.5)$$

where t_j denotes the times of the N_1 events, s_k the N_2 events and r_l the N_3 events respectively. This variate counts the number of occurrences of an N_2 event inside a bin of width b which is u time units away from a N_1 event, and a N_3 event inside a bin of width b which is v time units away from the same N_1 event.

Now the third-order cumulant density function may be estimated naturally by

$$\hat{q}_{123}(u,v) = \hat{P}_{123}(u,v)-\hat{P}_1\hat{P}_{23}(v-u)-\hat{P}_2\hat{P}_{13}(v)-\hat{P}_3\hat{P}_{12}(u)+2\hat{P}_1\hat{P}_2\hat{P}_3 \quad (6.4.6)$$

This estimate has the advantage of being very computationally efficient as opposed to the alternative method based on the third-order periodogram in the frequency domain (Halliday, 1986). The theory for the estimation of the variance of this parameter is not complete and requires further investigation.

Third-order cumulant densities may be computed between two spike trains, in which case the non-linear influence that the pattern of events in one train exert on the second may be examined. The timing conventions used in the computations of the cumulants are set out in Figure (6.4.2).

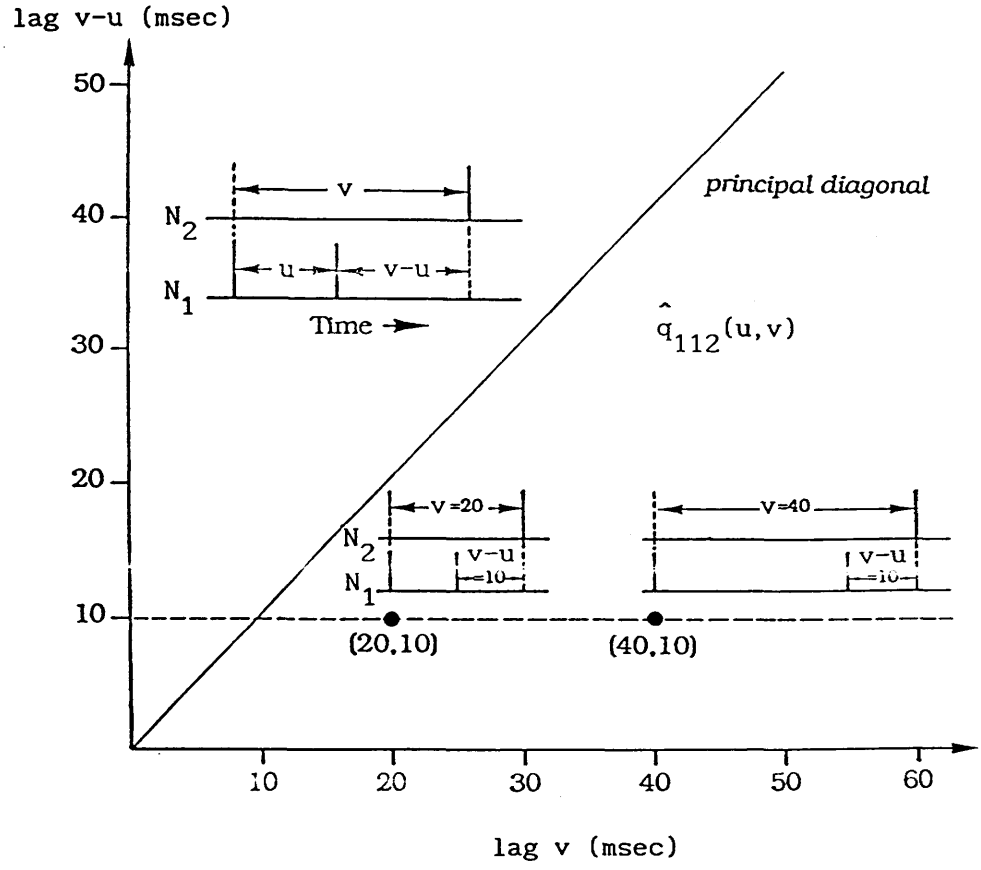

Figure 6.4.2. Diagrammatic representation of the timing convention of the third-order cumulant density function $\hat{q}_{112}(u,v)$ used to investigate the nonlinear effects of the input process N_1 on the output process N_2. The x and y axes represent the v and v-u axes of the contour plot of the cumulant and the principal diagonal represents the regions in which the value of the contour plot is singular.

6.4.2 The Model

The after-hyperpolarisation is incorporated into a traditional 'integrate to threshold and fire' model (see Chapter 5) by taking each output spike as input to a feedback element whose impulse response has the same time course as the after-hyperpolarisation. The input to the encoder component of the model is then the sequence of EPSP's (excitatory post-synaptic potentials) generated from the response of a second-order linear filter to the input spike train, the sequence of after-hyperpolarisation potentials and an added independent noise source. (See Figure 6.4.3)

6.4.3 Results

Recordings involving a single Ia afferent and a single motor unit have been performed and third-order cumulant densities were employed to assess the influence in which two spikes in the Ia afferent train have on the time of occurrence of a subsequence motor unit spike. To simulate the system, a point process with Gaussian inter-spike intervals was used as the input to the neurone model. Figures (6.4.4-5) show the comparison of the third-order cumulant density derived from real data with that derived from model generated data. It concludes that with appropriate parameters chosen, the model can be employed to simulate the general effects of the system relating the Ia and the motor unit spike trains.

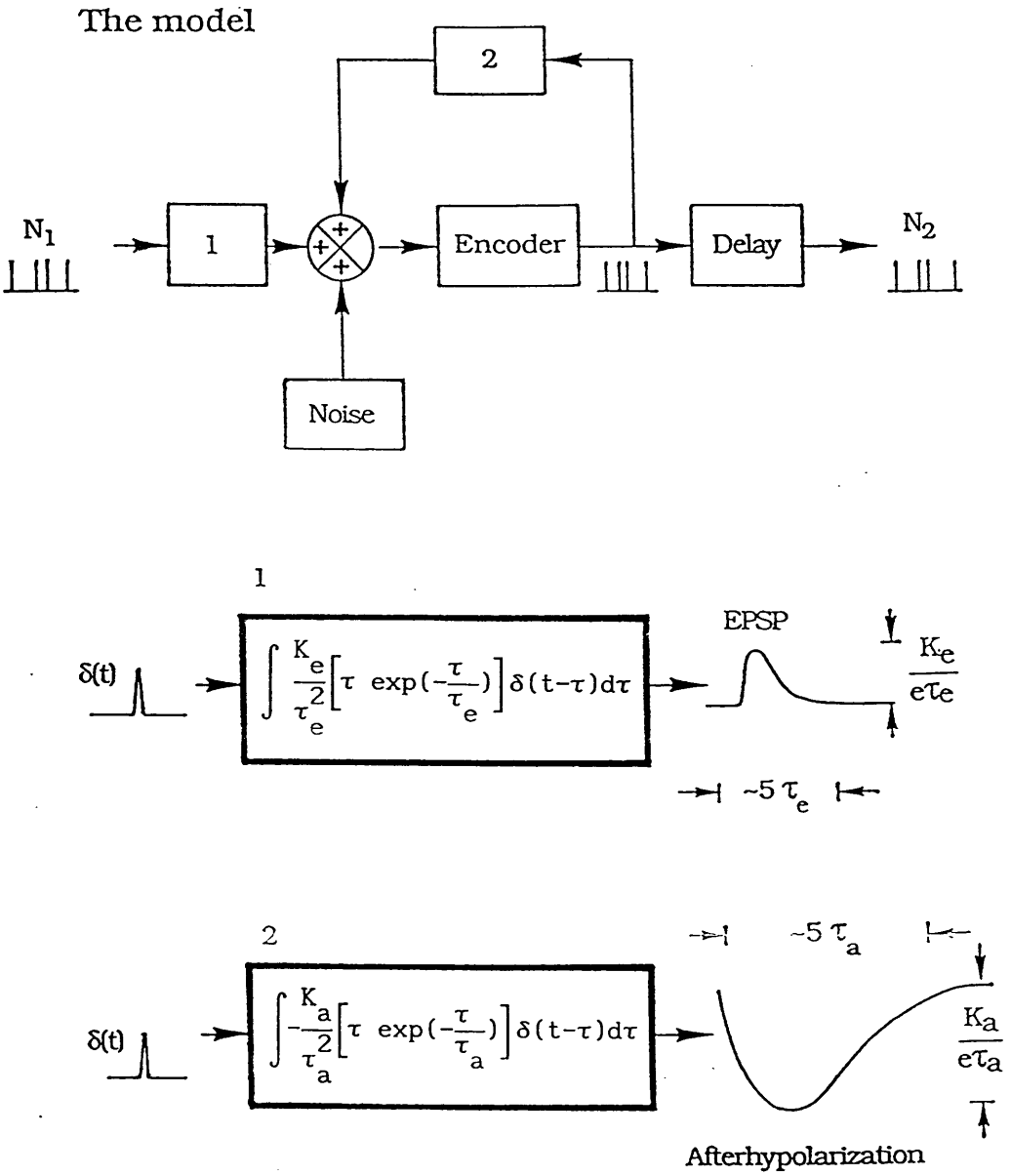

Figure 6.4.3. Schematic diagram representing (a) the neurone model incorporating the effects of after-hyperpolarisation, below which is the (b) impulse response of the second-order filter used to generate the time course of an EPSP and (c) the impulse response of the feedback used to simulate the time course of the after-hyperpolarisation effects.

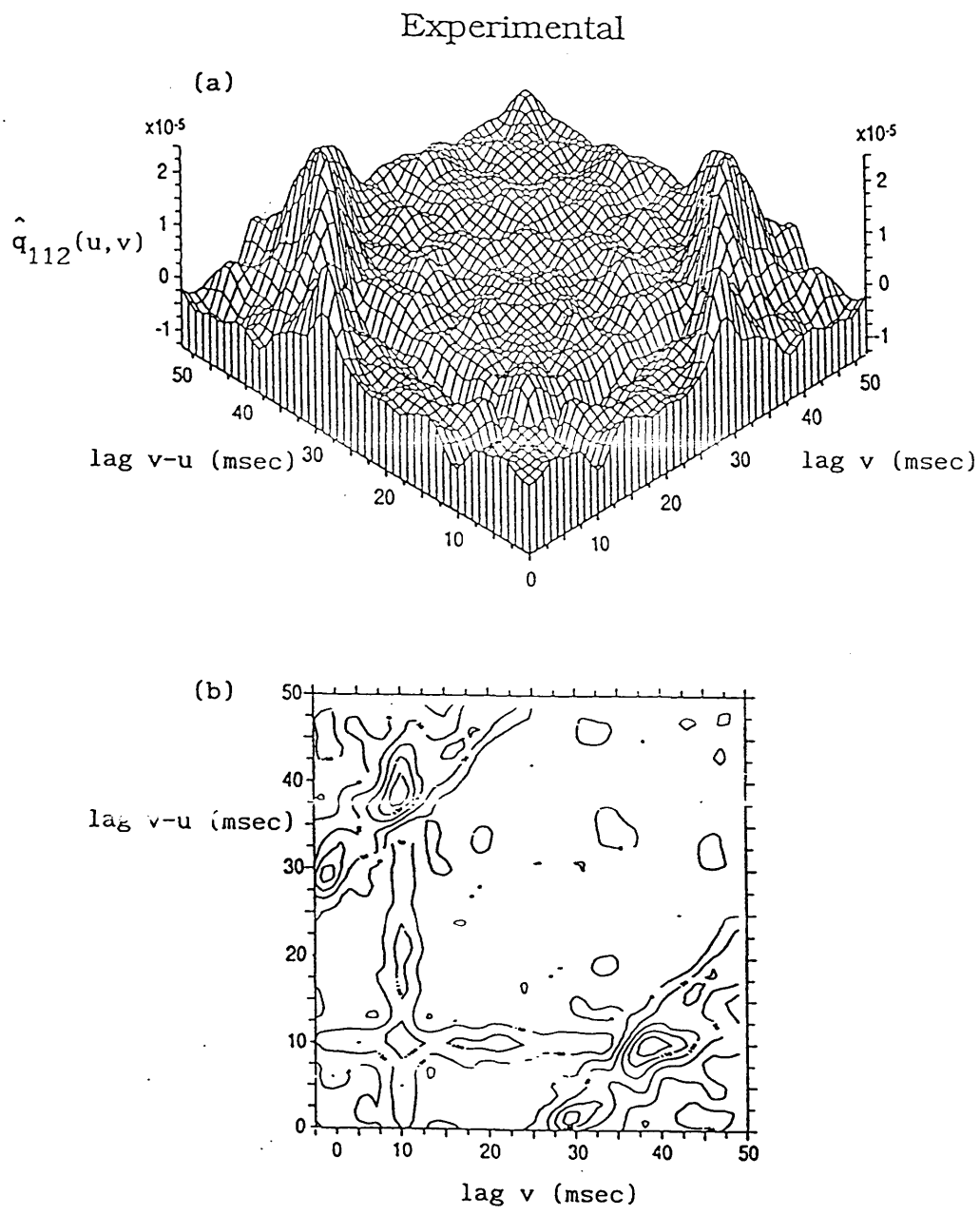

Figure 6.4.4. Estimated (a) isometric and (b) contour plots of the third-order cumulant density function $\hat{q}_{112}(u,v)$ derived from physiological data involving an Ia afferent spike train N_1 and a motor unit spike train N_2 (refer to chapter 2 for details).

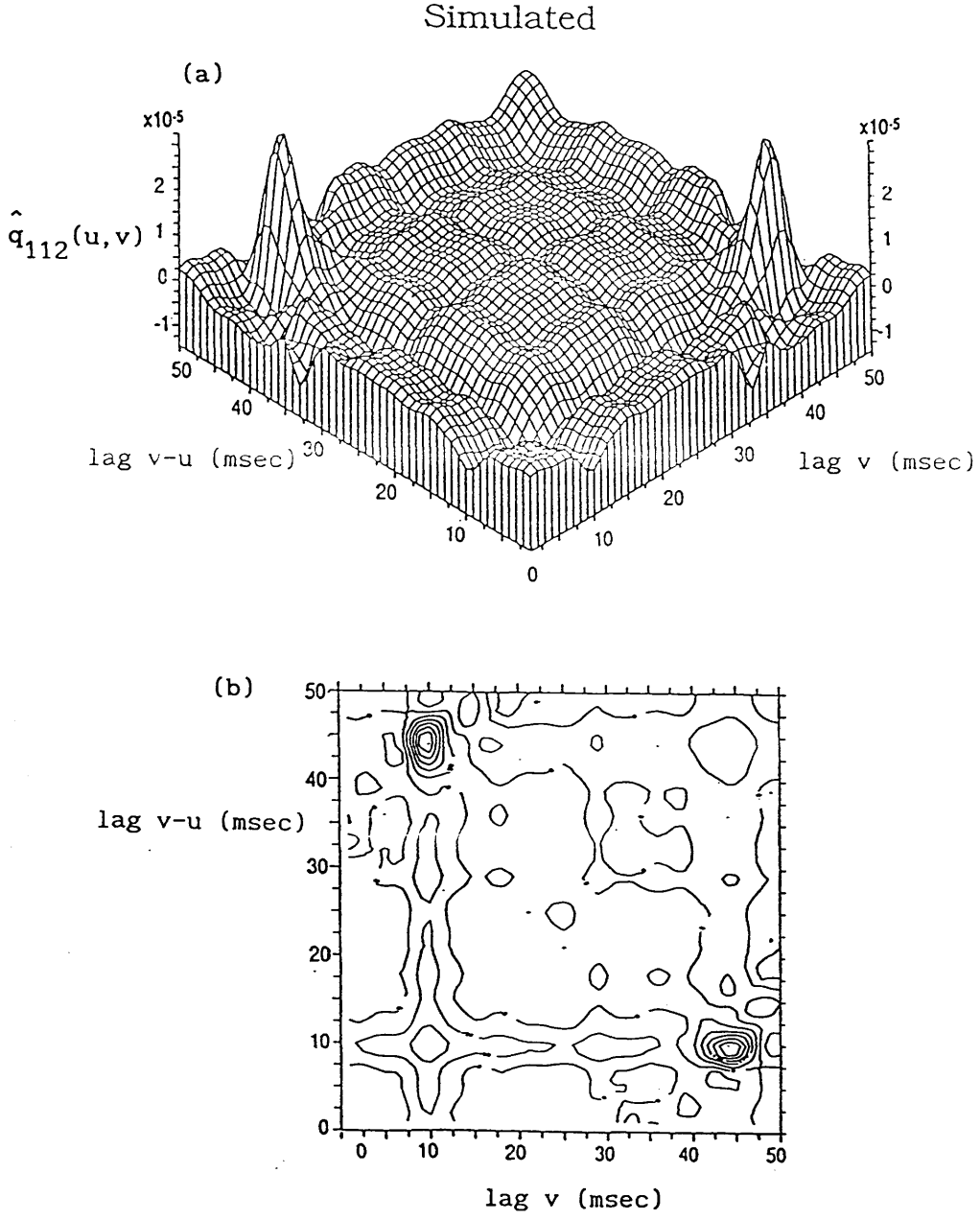

Figure 6.4.5. Estimated (a) isometric and (b) contour plots of the third-order cumulant density function $\hat{q}_{112}(u,v)$ derived from simulated data. The input spike train is one with Gaussian distributed intervals to simulate the firing of the Ia afferent in real situation.

A comparison of the cross-intensity and a slice through the third-order cumulant at v-u=10 msec. computed from the real and model generated data is shown in Figure (6.4.6). The choice of v-u=10 msec. corresponds to the mean monosynaptic latency uncorrected for conduction delays. In this example the period of post-spike depression is not evident from the cross-intensity, whereas the slice through the cumulant clearly reveals the period of post-spike depression. Hence the third-order cumulant density may be considered to be more sensitive in revealing non-linear features of the system when the input has a nonlinear influence on the output spike train.

The dependence of the trough in the third-order cumulant density upon the feedback loop was investigated using a Poisson point process as stimulus. Figures (6.4.7-8) illustrate the third-order cumulant density estimate upon the presence and absence of the feedback loop in the model responsible for the after-hyperpolarisation. Note that the values along the line v-u=v in this case corresponds to singularities and hence should be ignored. It is clear that the presence of the trough is due to the effect of the post-spike depression caused by the feedback loop.

A series of analyses using different values of after-hyperpolarisation duration was performed. The results are shown in Figures (6.4.9-12) and are summarised by the slices at v-u=10 msec. shown in Figure (6.4.13a-d). The companion graph (Figure 6.4.13e) shows that there is a direct relation between the

duration of the trough in the cumulant and the duration of the after-hyperpolarisation.

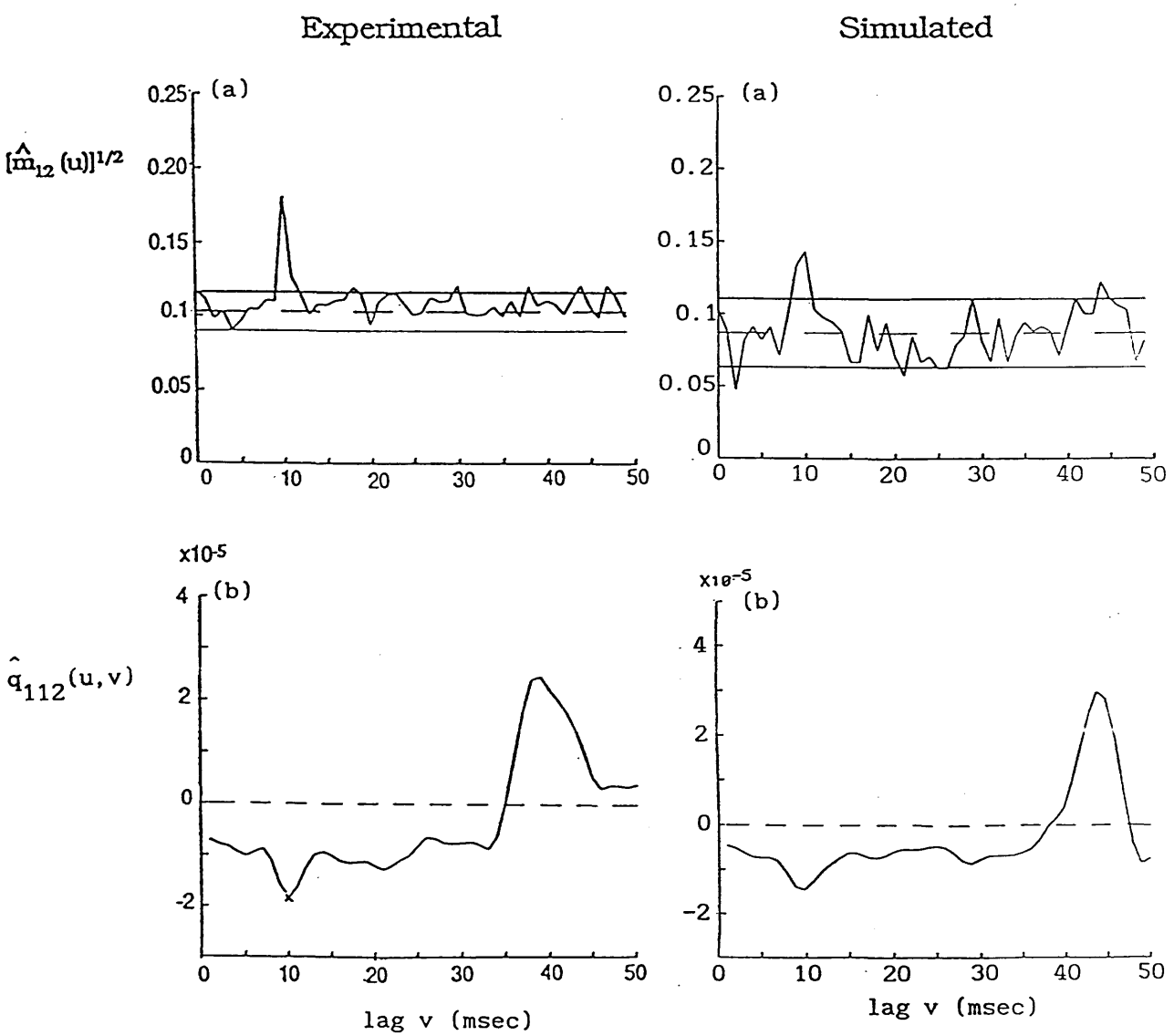

Figure 6.4.6. **A comparison of the (a) cross-intensity of the input and** output processes, and (b) a slice at v-u=10 msec. corresponding to the mean latency through the third-order cumulant density between the results obtained from the real and simulated data. In (a) the solid horizontal lines represent the 95% confidence interval assuming the input and output processes are independent, and the dashed lines represent the asymptotic value of the estimates.

Figure 6.4.7. Estimated (a) isometric and (b) contour plots of the third-order cumulant density function derived from the model generated data incorporating after-hyperpolarisation using a Poisson input.

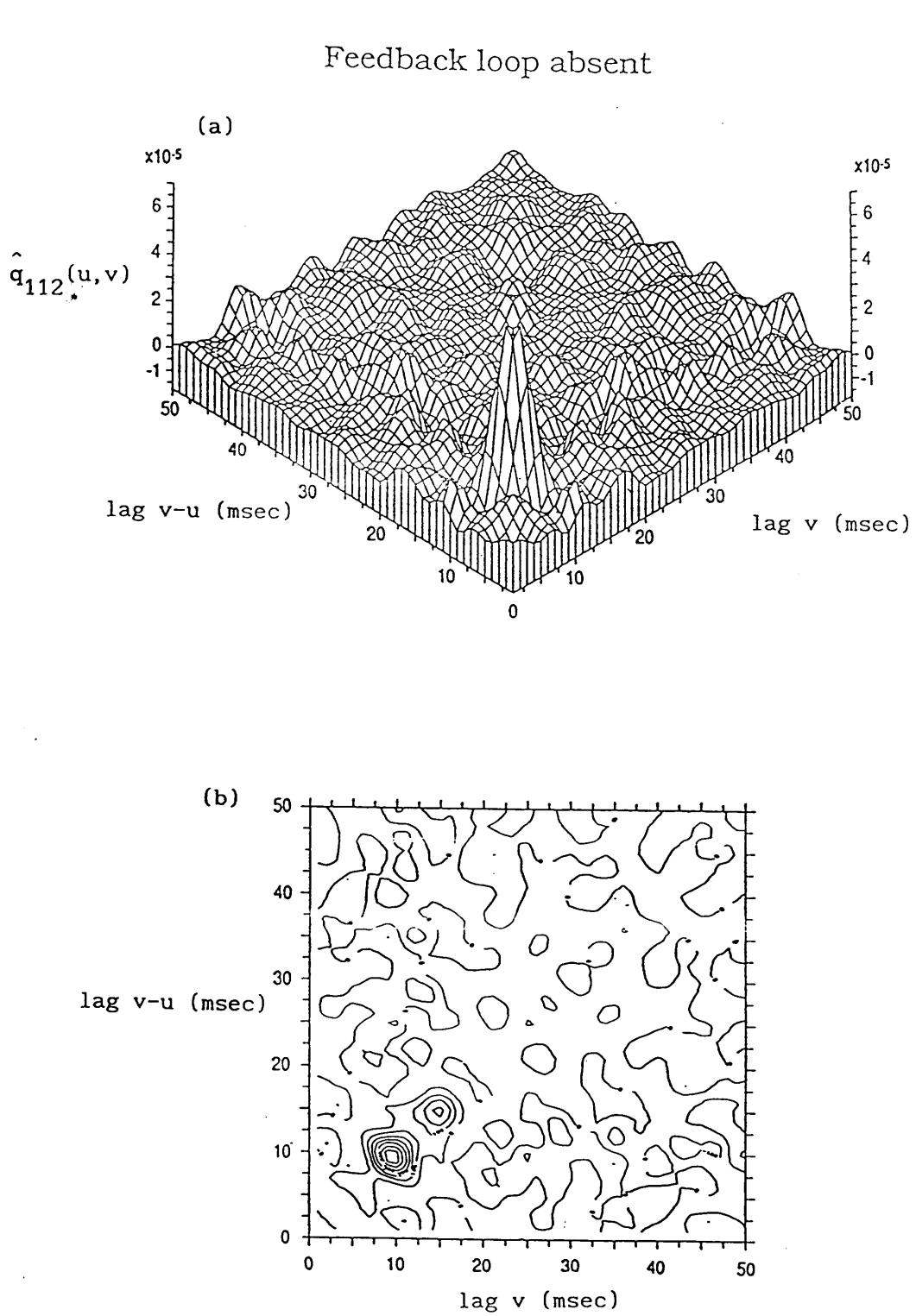

Figure 6.4.8. Estimated (a) isometric and (b) contour plots of the third-order cumulant density function derived from the model generated data after the feedback loop associated with the after-hyperpolarisation is removed.

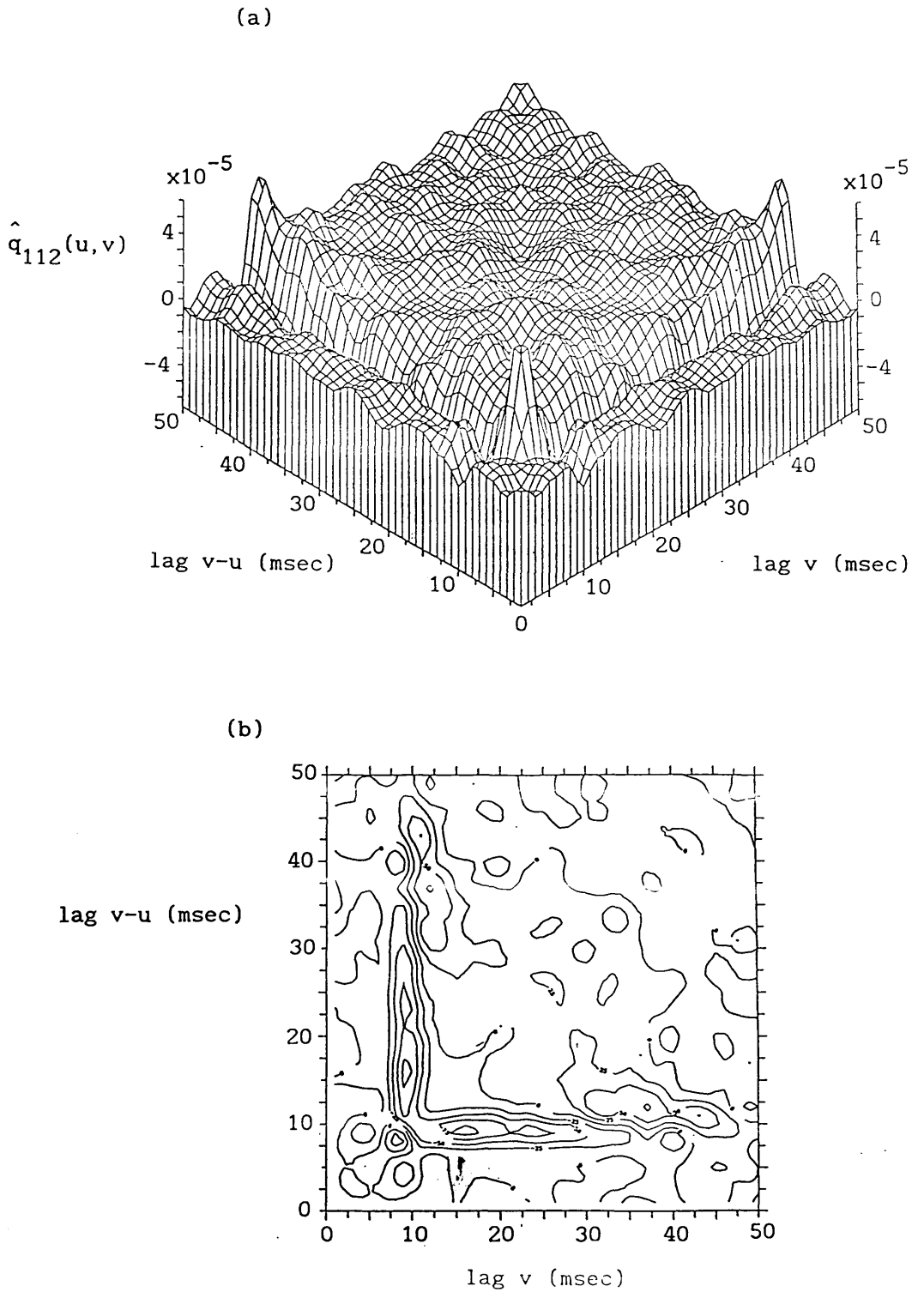

Figure 6.4.9. Estimated (a) isometric and (b) contour plots of the third-order cumulated density function derived from the model generated data incorporating after-hyperpolarisation. The duration of the time course of the after-hyperpolarisation is set to approximately 20 msec.

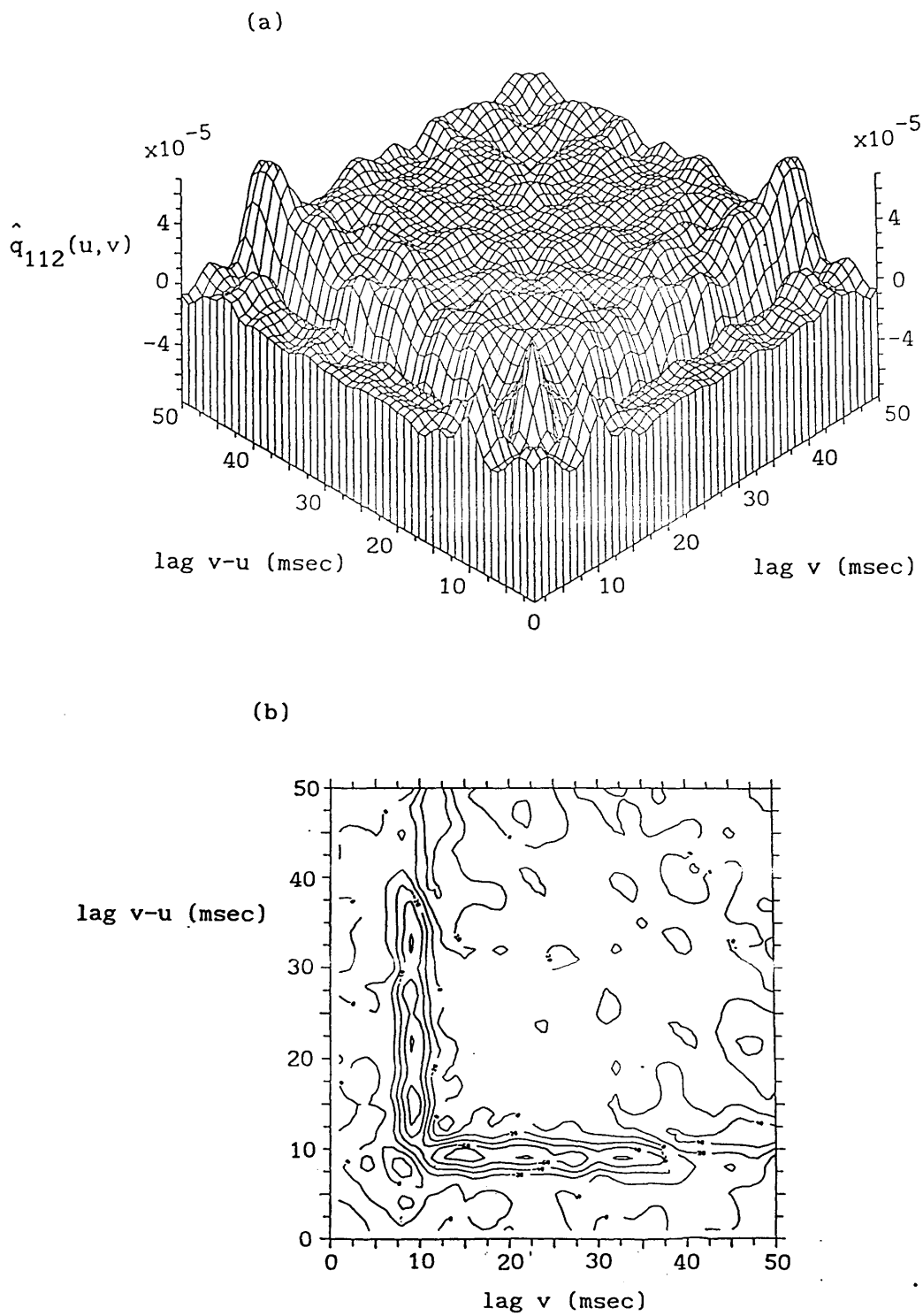

Figure 6.4.10. Estimated (a) isometric and (b) contour plots of the third-order cumulated density function derived from the model generated data incorporating after-hyperpolarisation. The duration of the time course of the after-hyperpolarisation is set to approximately 30 msec.

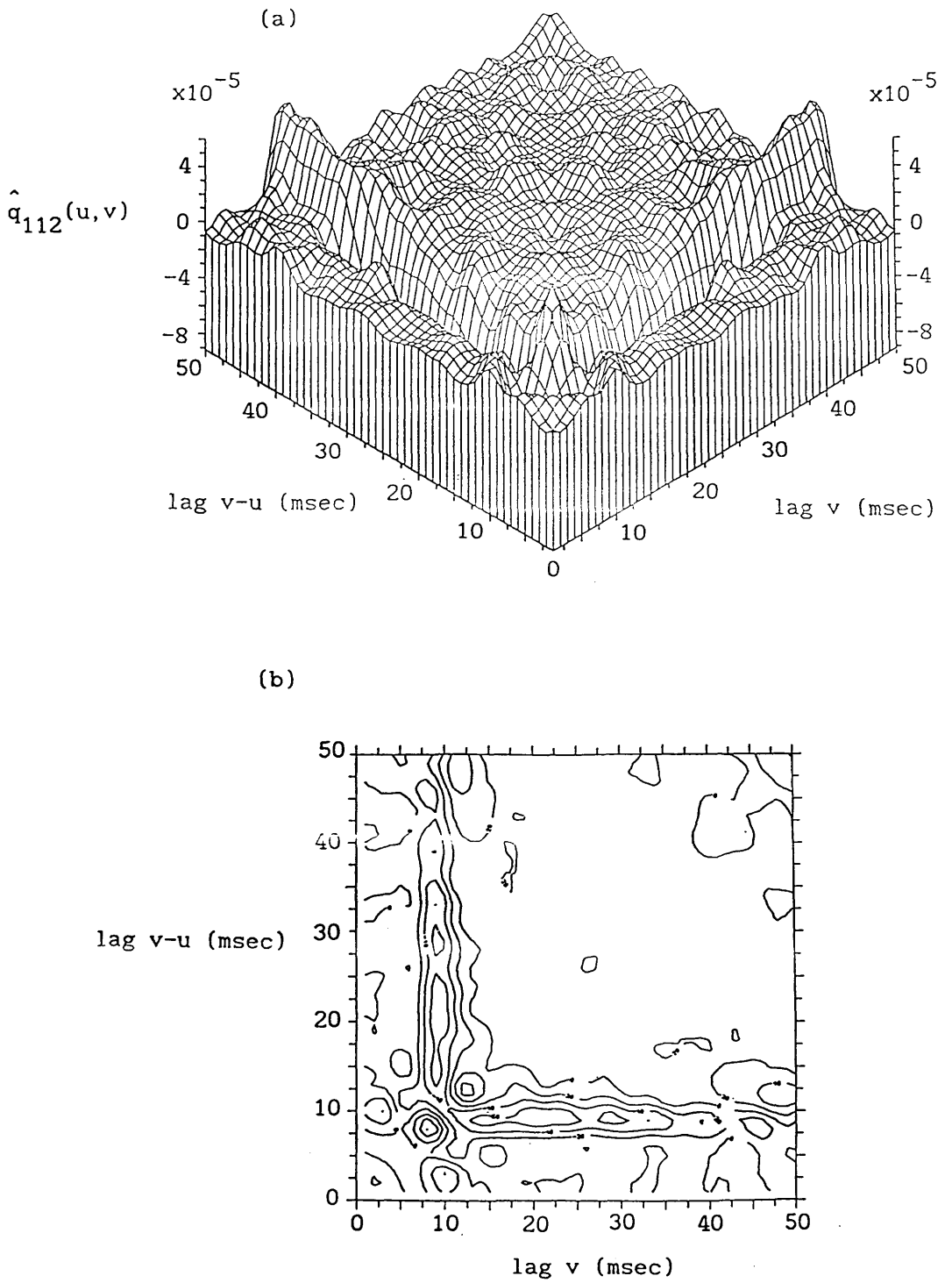

Figure 6.4.11. Estimated (a) isometric and (b) contour plots of the third-order cumulated density function derived from the model generated data incorporating after-hyperpolarisation. The duration of the time course of the after-hyperpolarisation is set to approximately 40 msec.

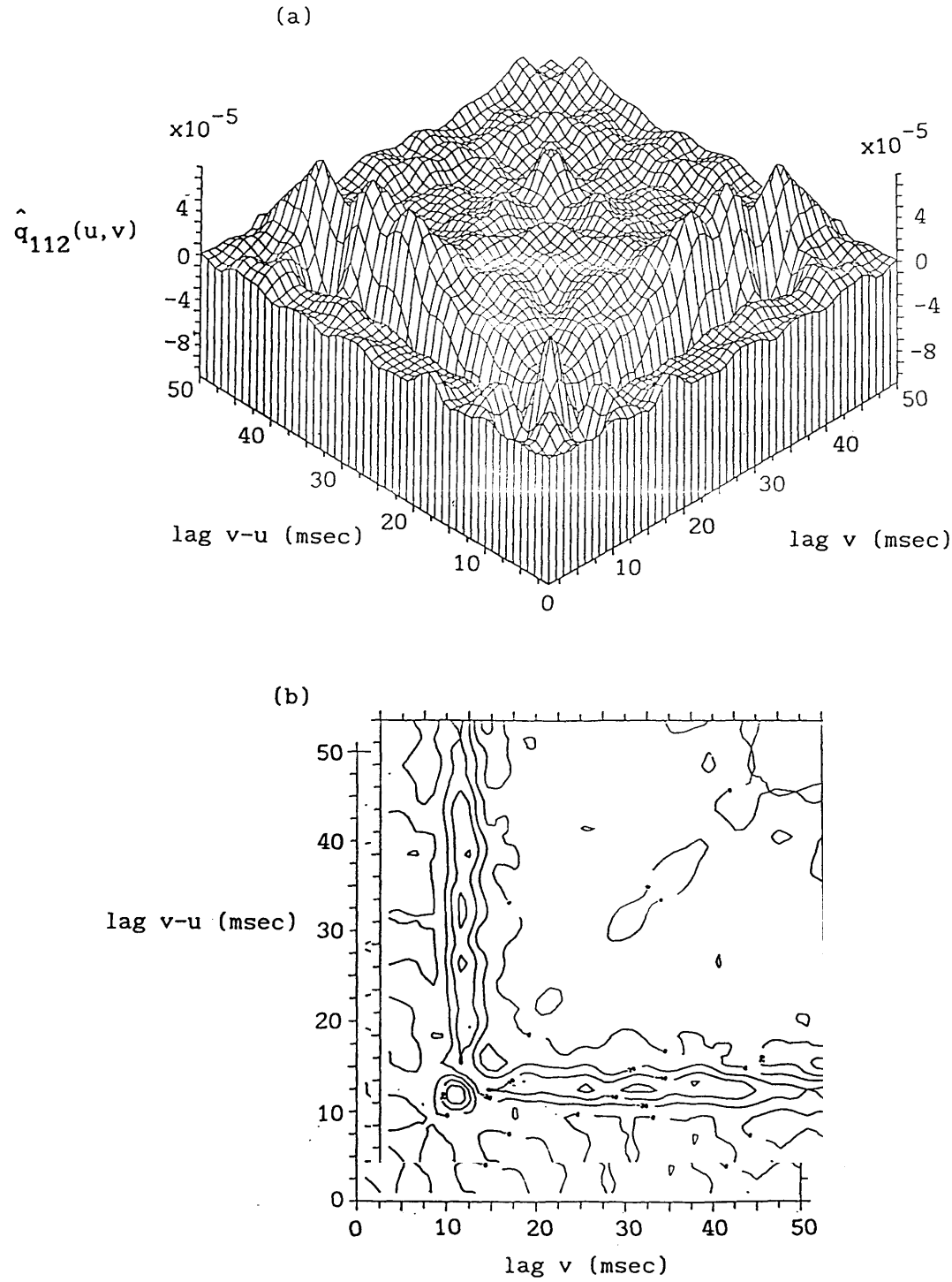

Figure 6.4.12. Estimated (a) isometric and (b) contour plots of the third-order cumulated density function derived from the model generated data incorporating after-hyperpolarisation. The duration of the time course of the after-hyperpolarisation is set to approximately 50 msec.

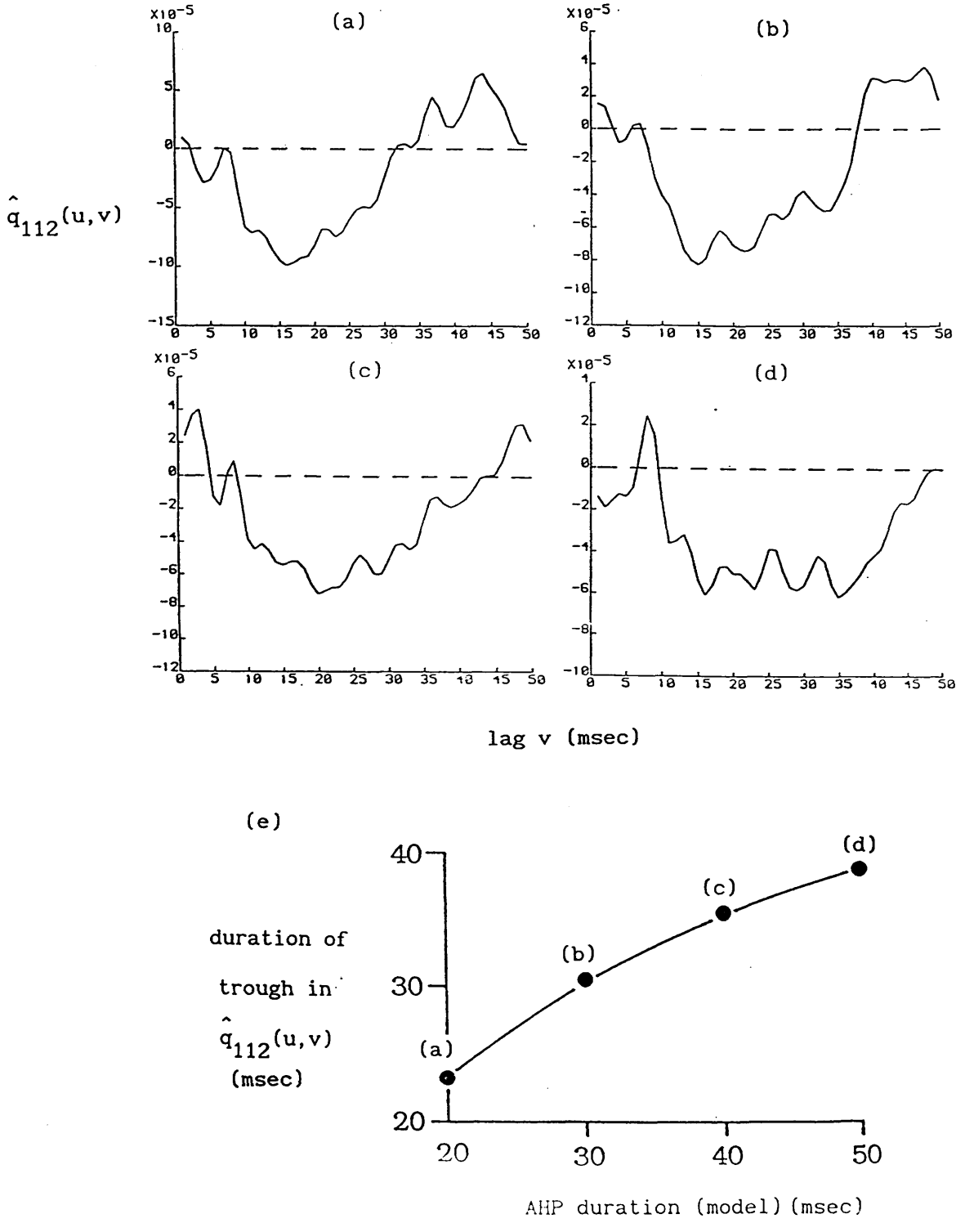

Figure 6.4.13. Slices at v-u=10 msec. through the third-order cumulant density estimates with after-hyperpolarisation durations of (a) 20, (b) 30, (c) 40 and (d) 50 msec. respectively. In (e) the graph of trough duration observed in the cumulants versus after-hyperpolarisation duration is plotted.

Chapter 7

Future Work

Chapter 7 Future Work

In Chapters 3 to 5, the mathematical, statistical and computational aspects of linear point process system analysis techniques have been discussed. The application of these techniques, illustrated by various examples in Chapter 6, has proved fruitful in analysing systems that involve both point process signals and continuous signals, and multiple inputs and multiple outputs. In particular, the coherence in its ordinary and partial forms proved to be a sensitive and powerful tool in measuring associations between processes. Also it has been attempted to characterise a system in which the input point process exerts a non-linear effect upon the output point process based on the third-order cumulant density function. It has been shown that the third-order cumulant can detect interactions that are not apparent in the cross-intensity. This represents one aspect of the usefulness of higher order parameters. However, the statistical properties of the third-order cumulant are not fully understood and the application should not be limited to a single-input, single-output system. In addition to the higher order time domain parameters, the higher order spectra are also in need of further investigation. Hence the investigation and application of higher order time and frequency domain parameters leads to an immediate area of possible future work.

Brillinger (1988a, b) has proposed and demonstrated the use of maximum likelihood approach for estimating biologically meaningful parameters. The maximum likelihood approach is a

parametric approach that provides estimates of the parameters involved in the model directly. Examples of such parameters include the threshold, time duration of the after-hyperpolarisation, etc. This method has only been applied to a few examples, and is in need of further investigation.

The third possible direction of future work is the Lanczos analysis of electric current flow in excitable cells. This is discussed in the last section in this chapter.

7.1 Higher Order Parameters

Recently higher order statistics, especially in the form of cumulant density functions, have been widely used in a large number of fields. Higher order cumulant density functions provide measures of higher order interactions (in time domain) between point processes whereas higher order spectra may be used in characterising non-linear systems. However the statistical properties and implications of these parameters are not fully understood. For example, the statistical properties of the third-order cumulant estimate based on expression (6.4.6), have not been worked out. Although an alternative estimate for the third-order cumulant density based on the inverse Fourier-Stieltjes transform of the third-order spectra is possible and the variance of this estimate has been worked out (Rigas 1983), the computational time involved is longer (Halliday 1986). In the frequency domain possible future work involves, for example, the development of a statistical test for zero quadratic

coherence (Amjad, 1989).

7.2 Maximum Likelihood Methods

Maximum likelihood is a well established statistical procedure in which one sets down an expression for the probability of occurrence of the data set of interest. This expression is referred to as the likelihood function, and is expressed in terms of the data values and the parameters of the particular probability model used to account for the data. The maximum likelihood method then selects the set of parameters that maximises the likelihood function. In the situation where one is interested in determining the influences that lead to the generation of a particular recorded spike train the procedure may be outlined as follows.

If the probability for a spike to occur at time t given the history of the process is represented by p_t, the likelihood function for a particular spike train may be written as

$$\prod_{t=0}^{T} p_t^{dN(t)} (1-p_t)^{1-dN(t)} \qquad (7.2.1)$$

where T is the record length and dN(t) is the differential increment which has a value of 1 if a spike has occurred in the interval $(t, t+\Delta t]$ and 0 otherwise. The symbol Π is the standard product operator. The object is then to propose a model for p_t. One might, for example, proceed as follows. If U_t represents the membrane potential at the trigger zone, the cell may be assumed to fire at time t if U_t exceeds a threshold ϕ. One may then set up a

function in terms of U_t and ϕ that represents the probability p_t. The expression of U_t includes terms that contribute to U_t such as other inputs to the cell, refractory period, after-hyperpolarisation, etc. Each of these terms may be associated with one or several parameters. The maximum likelihood approach then chooses the set of parameters for a particular spike train that maximise the likelihood function. Maximum likelihood methods therefore provide direct estimates of biologically relevant parameters. The implementation is, however, very computationally intensive.

7.3 Lanczos Analysis of Electric Current Flow in Excitable Cells

In solving the cable equation for a neurone of arbitrary complexity the voltage distribution at time t+1 is related to that at time t by an equation of the form:

$$V_{t+1} = \mathbf{A}\, V_t \qquad (7.3.1)$$

where in the case of an active cable **A** may be a function of V. Because of the complex geometric properties of a neurone it is difficult to acquire insights into their computational properties. Several methods have been devised which allow the complex branching structure to be reduced to an equivalent unbranched cable (Butz and Cowan, 1974; Koch and Poggio, 1985 and Rall, 1989). An alternative to these methods, which is not subject to geometric constraints is to apply the Lanczos transformation (Lanczos, 1950 and Whitehead, Watt and Morrison, 1977). In simple cases the Lanczos procedure separates the representation of the dendritic tree into two or more linear cables. This decomposition means that certain combinations of events within a dendritic tree cannot be seen by the soma. In cases where the equivalent cable does not separate or decompose exactly these same events are found to influence regions of the cable far from the soma and thus propagate only weakly to the soma. In either case the reduction of a complex dendritic tree to a single non-uniform cable greatly improves one's ability to visualise and quantify the behaviour of the system. It is intended to develop this approach and to use it to try to get an understanding of which events and combinations of

events are meaningful to a real neurone and which are not.

Appendices

Appendix 1 Conventional Symbols used in the EAI 2000 Analogue Computer

In this thesis the symbols used to represent the various components in analogue computing follow the conventions used in the the EAI 2000 Analog Reference Handbook (1978). The components may be classified into two classes: (1) analogue components which are characterised by a analogue output and (2) logical components where the output is either a 1 or 0. These are described briefly below.

A.1.1 Analog Components

(a) Coefficient Unit

Function: Continuous multiplication of an analogue variable times a constant coefficient.

Symbol:

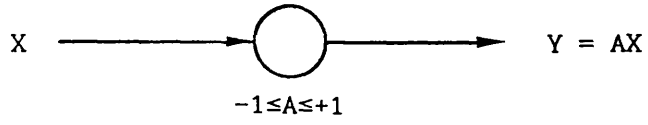

Explanation: A coefficient unit with input X and output Y; the value of the coefficient being A.

(b) Summer

Function: Continuous summation of several analogue variables.

Symbol:

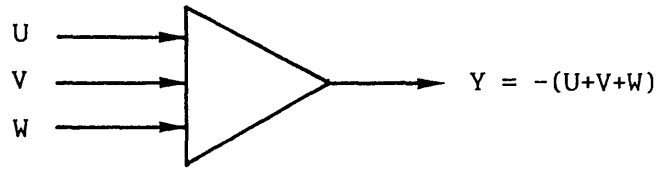

Explanation: A summer circuit with inputs U, V and W; the output being Y. Note that the output is inverted.

(c) Integrator

Function: Continuous integration, with respect to time, of an analogue variable.

Symbol:

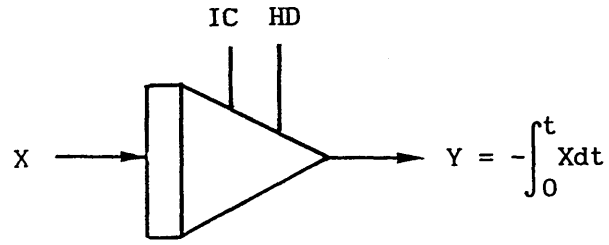

IC	HD	Effects
0	0	None
1	0	Reset Y

Explanation: The integrator circuit integrates the input X with respect to time and gives the output Y. The control logic inputs IC (Initial Condition) and HD (HolD) may be used to reset the output (see the inserted table).

(d) Selector Switch

Function: Analog signal switching.

Symbol:

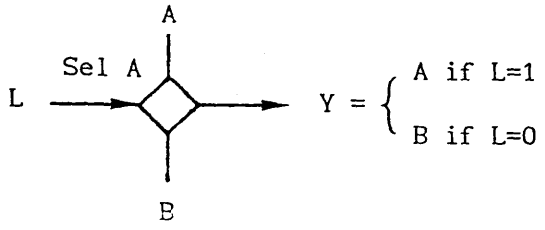

Explanation: The output Y is either equal to A or B depending on the selector L. If L=1, Y becomes A. Otherwise Y=B.

A.1.2 Logic Components

(a) Flip-Flop

Function: Store a logic value.

Symbol:

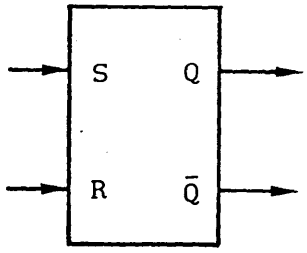

S	R	Q_{n+1}
0	0	Q_n
0	1	0
1	0	1
1	1	$\bar{Q}_n$

Explanation: The input S (Set) sets the output Q, whereas the input R (Reset) resets the output Q. Note that the output

remains unchanged when S=R=0. However in the case S=R=1, the output toggles.

(b) Comparator

Function: Compare two analogue variables.

Symbol:

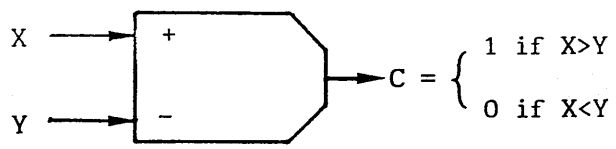

Explanation: The output C is equal to 1 if the non-inverted input X is greater than the inverted input Y, and 0 otherwise.

Appendix 2 Physical and Mathematical Removal of a Common Input

The distinction between physical and mathematical removal is best illustrated by a neurone network in which a pair of neurones is influenced by two common inputs (see Figure A.2.1). N_1 and N_2 are the two common inputs, N_3 and N_4 represent two independent inputs to the two neurones respectively, and N_5 and N_6 are the two output processes.

First consider the case in which the two common inputs N_1 and N_2 are independent. The cross-spectrum between the output processes N_5 and N_6 is given by

$$f_{56}(\lambda) = f_{11}(\lambda)\overline{S_{15}(\lambda)}\overline{S_{16}(\lambda)}+f_{22}(\lambda)\overline{S_{25}(\lambda)}\overline{S_{26}(\lambda)} \qquad (A.2.1)$$

where the overbar "———" denotes complex conjugate of a quantity. The residual cross-spectrum $f_{56.1}(\lambda)$ is then given by

$$\begin{aligned} f_{56.1}(\lambda) &= f_{56}(\lambda)-f_{51}(\lambda)\overline{f_{16}(\lambda)}/f_{11}(\lambda) \\ &= f_{22}(\lambda)\overline{S_{25}(\lambda)}\overline{S_{26}(\lambda)} \end{aligned} \qquad (A.2.2)$$

Expression (A.2.2) is in fact equivalent to the situation in which the pair of neurones is influenced by one common input N_2 as illustrated in Figure (A.2.2), hence it can be concluded that mathematical removal of the contribution from N_1 is equivalent to physically removing N_1. Removing N_2 is similar.

However, in general, if N_1 and N_2 are dependent, the

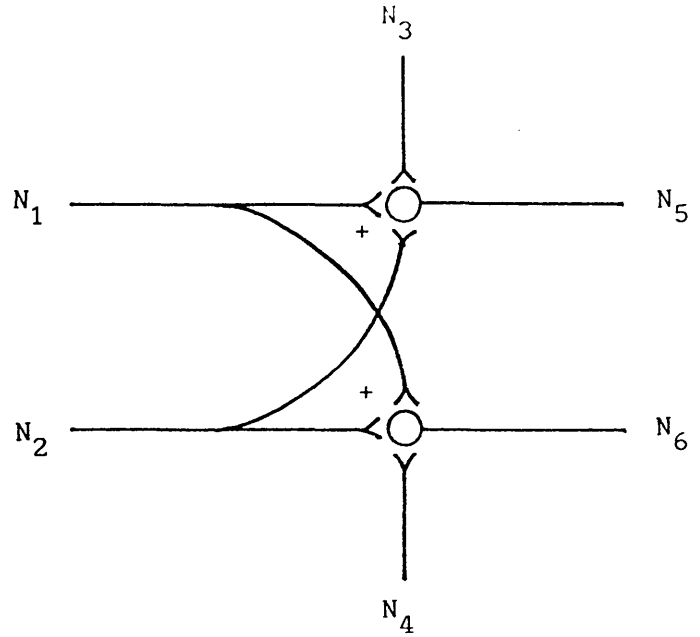

Figure A.2.1. Diagrammatic representation of a neuronal network in which two neurones N_5 and N_6 share the common inputs N_1 and N_2. Processes N_3 is an input to N_5 that is independent of N_1, N_2 and N_4. N_4 is an input to N_6 that is independent of N_1, N_2 and N_3.

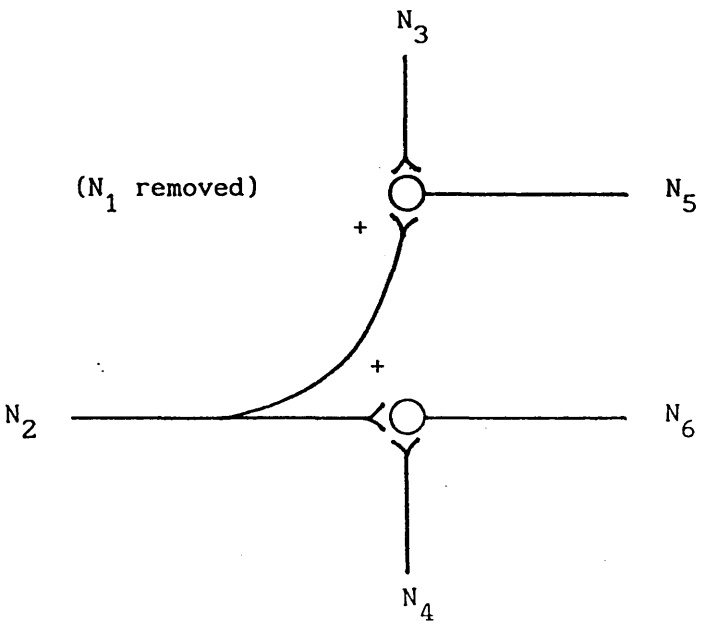

Figure A.2.2. Diagrammatic representation of the case in which N_1 is physically removed. This situation is equivalent to mathematically removing the contribution of N_1 in Figure A.2.1 when N_1 and N_2 are independent.

cross-spectrum between N_5 and N_6 in this case becomes

$$f_{56}(\lambda) = f_{11}(\lambda)\overline{S_{15}(\lambda)}S_{16}(\lambda)+f_{22}(\lambda)\overline{S_{25}(\lambda)}S_{26}(\lambda)$$
$$+f_{12}(\lambda)S_{15}(\lambda)S_{26}(\lambda)+f_{21}(\lambda)S_{25}(\lambda)S_{16}(\lambda) \qquad (A.2.3)$$

Note the addition of the cross-spectral terms. The residual cross-spectrum $f_{56.1}(\lambda)$ would be

$$f_{56.1}(\lambda) = \overline{S_{25}(\lambda)}S_{26}(\lambda)\left[f_{22}(\lambda)-f_{12}(\lambda)f_{21}(\lambda)/f_{11}(\lambda)\right]$$
$$= f_{22.1}(\lambda)S_{25}(\lambda)S_{26}(\lambda) \qquad (A.2.4)$$

where $f_{22.1}(\lambda)$ is the residue auto-spectrum of N_2 after removing the associated linear components of N_1. Hence in general, the mathematical removal of a process implies removing all the components that are associated with that process, which in general is not the equivalent to removing the process physically.

Appendix 3 The Coherence Between Two Processes with Multiple Common Inputs

Consider the situation in which a pair of neurones A and B is influenced by m independent common inputs $C_1, C_2, .., C_m$ as illustrated in Figure (6.3.1), where $\alpha_1, .. \alpha_p$ and $\beta_1, .., \beta_q$ represent independent inputs to A and B respectively. In addition, $S_{C_1A}(\lambda), .., S_{C_mA}(\lambda)$, $S_{C_1B}(\lambda), .., S_{C_mB}(\lambda)$, $S_{\alpha_1A}(\lambda), .., S_{\alpha_pA}(\lambda)$ and $S_{\beta_1B}(\lambda), .., S_{\beta_qB}(\lambda)$ represent the transfer functions relating the input processes C, α and β to output processes N_A and N_B. By a direct extension of the procedures used in Section (6.3), the cross-spectrum between processes N_A and N_B may be shown to be

$$f_{AB}(\lambda) = \sum_{k=1}^{m} f_{C_kC_k}(\lambda)\overline{S_{C_kA}(\lambda)}S_{C_kB}(\lambda) \qquad (A.3.1)$$

where the overbar "———" denotes complex conjugate of a quantity. The auto-spectra of N_A and N_B may be written in the form

$$f_{AA}(\lambda) = \sum_{k=1}^{m} \left[f_{C_kC_k}(\lambda)\overline{S_{C_kA}(\lambda)}S_{C_kA}(\lambda) \right] + \sum_{k=1}^{p} \left[f_{\alpha_k\alpha_k}(\lambda)\overline{S_{\alpha_kA}(\lambda)}S_{\alpha_kA}(\lambda) \right]$$

and

$$f_{BB}(\lambda) = \sum_{k=1}^{m} \left[f_{C_kC_k}(\lambda)\overline{S_{C_kB}(\lambda)}S_{C_kB}(\lambda) \right] + \sum_{k=1}^{q} \left[f_{\beta_k\beta_k}(\lambda)\overline{S_{\beta_kB}(\lambda)}S_{\beta_kB}(\lambda) \right] \qquad (A.3.2)$$

The coherence $|R_{AB}(\lambda)|^2$ is now given by $|f_{AB}(\lambda)|^2 / f_{AA}(\lambda) f_{BB}(\lambda)$.

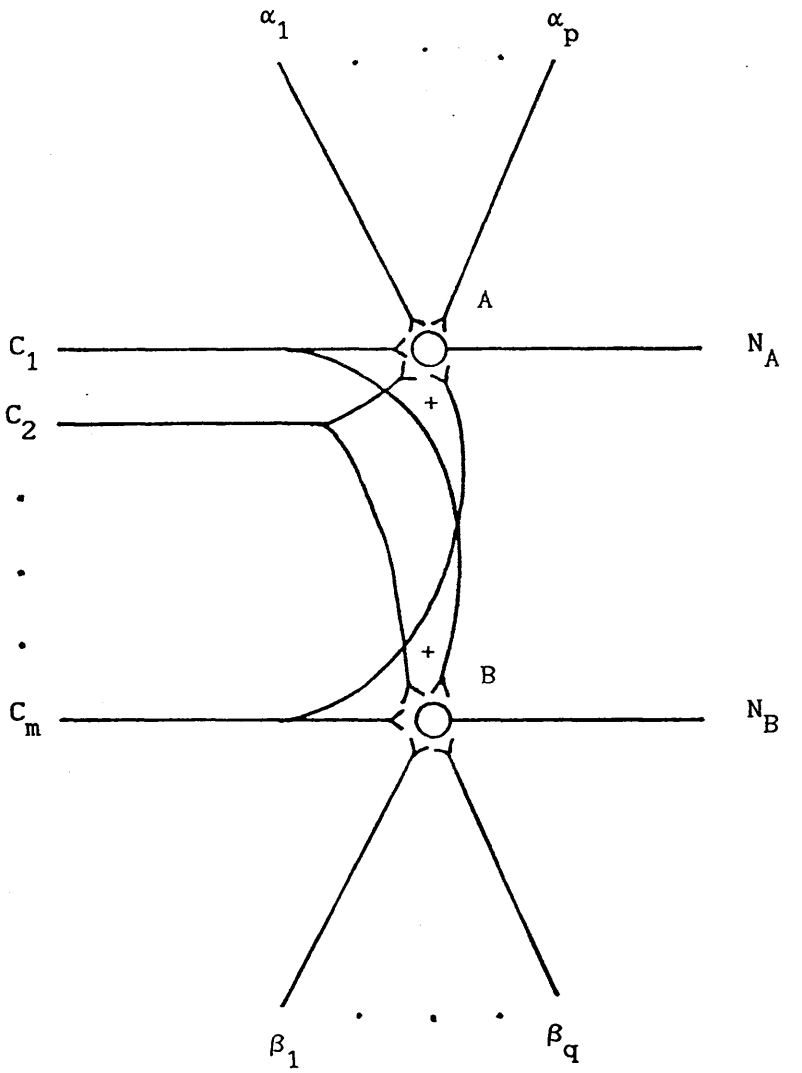

Figure A.3.1. Diagrammatic representation of a generalised neuronal network in which a pair of neurones is influenced by multiple common inputs $C_1,..,C_m$. $\alpha_1,..,\alpha_p$ are the independent inputs to A only whereas $\beta_1,..,\beta_q$ are independent inputs to B only.

Each factor in the denominator of $|R_{AB}(\lambda)|^2$ will contain contributions from the common input processes as well as from each of the independent inputs, whereas the numerator of $|R_{AB}(\lambda)|^2$ will only contain contributions from the common inputs. Adding the error terms to the linear model will introduce additional spectral terms to each of the auto-spectra in the denominator in $|R_{AB}(\lambda)|^2$.

Appendix 4 The Interpretation of Partial Coherence Related to Non-linear Characteristics in a Common Input Neuronal Network Model

When assessing the effect that a third point process may have on the coupling between two other point processes the interpretation of the partial coherence in cases where there is no difference between the ordinary and partial coherence requires considerable care. This absence of a difference may occur for several possible reasons. The third process may not influence the coupling between the other two processes or the common input exerts a non-linear effect on the coupled output processes. In the nonlinear case even if the common input is the only source of coupling between two output processes there may no difference between the ordinary coherence and the partial coherence taking into account the contribution from the third process.

Consider the case in which N_c provides the only source of coupling between processes N_1 and N_2 (see Figure A.4.1). Assume that the output processes N_k, k=1,2, can be modelled as

$$dN_k(t)-s_k=\int a_k(t-u)dN_c(u) + \iint b_k(t-u,t-v)dN_c(u)dN_c(v) +noise_k \qquad (A.4.1)$$

where s_k is the intensity of N_k when $N_c \equiv 0$, $a_k(u)$ and $b_k(u,v)$ are the first and second-order kernels. Expression (A.4.1) is a direct extension of the linear model developed in section (3.3.3) to include a quadratic non-linearity (for a discussion of this kind of model in the case of ordinary time series, see Marmarelis

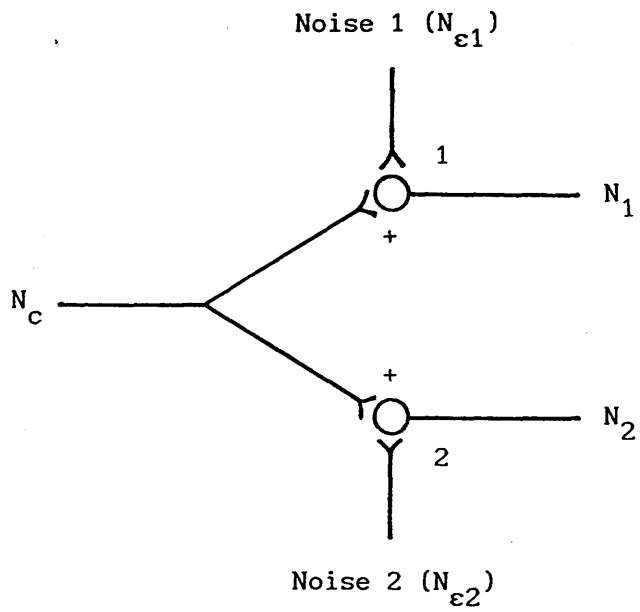

Figure A.4.1. Diagrammatic representation of a neuronal network in which two neurones share the common input N_c. Noise process $N_{\varepsilon 1}$ is a second input to N_1 that is independent of the common input N_c, and of $N_{\varepsilon 2}$. $N_{\varepsilon 2}$ is a common second input to N_2 that is also independent of N_c. The system considered in this case involved nonlinear features.

and Marmarelis, 1978; Brillinger, 1965).

Suppose the noise term present an independent contribution to the system, the cross-spectrum $f_{12}(\lambda)$ for the non-linear system may be written as

$$f_{12}(\lambda) = \overline{A_1(\lambda)}A_2(\lambda)f_{cc}(\lambda)+2\int B_1(\lambda-\mu,\mu)\overline{B_2(\lambda-\mu,\mu)}f_{cc}(\mu)f_{cc}(\lambda-\mu)d\mu \qquad (A.4.2)$$

where a_k and A_k are Fourier transform pair and similar for b_k and B_k. From expression (A.4.2), the residual cross-spectrum $f_{12.c}(\lambda)$ is given by

$$f_{12.c}(\lambda) = 2\int B_1(\lambda-\mu,\mu)\overline{B_2(\lambda-\mu,\mu)}f_{cc}(\mu)f_{cc}(\lambda-\mu)d\mu \neq 0 \qquad (A.4.3)$$

Hence, in general, the partial coherence $|R_{12.c}(\lambda)|^2 = |f_{12.c}(\lambda)|^2/f_{11.c}(\lambda)f_{22.c}(\lambda)$ is not necessarily zero when the system is non-linear, even in the case N_c is the only source of coupling between the two output processes.

The possible presence of non-linearities must be taken into account in the interpretation of partial coherences, particularly in situations when there is no difference between the ordinary and partial coherences. One cannot conclude, in general, that the absence of a difference means that process N_c has no effect on the coupling between N_1 and N_2.

References

References

Abramowitz, M. and Stegun, I.A. (1964): "Handbook of Mathematical Functions", National Bureau of Standards, Washington.

Akaike, H. (1966): "Notes on Higher Order Spectra", Ann. Inst. Statist. Mathematics, 18, 123-126. 126.

Amjad, A.M. (1989): "Identification of Point Process Systems with Application to Complex Neuronal Networks", Ph.D. Thesis, University of Glasgow.

Amjad, A.M., Breeze, P., Conway, B.A., Halliday, D.M. and Rosenberg, J.R. (1989): "A Framework for the Analysis of Neuronal Networks", Progress in Brain Research, vol 80, 243-255.

Anderson, T.W. (1971): "Statistical Analysis of Time Series", Wiley, New York.

Andersson, B.F., Lennerstrand, G. and Thoden, U. (1968): "Response Characteristics of Muscle Spindle Endings at Constant Length to Variation in Fusimotor Activation", Acta. Physiol. Scand. 74, 301-318.

Angers, D. and Delisle, G.Y. (1971): "Study of the Action of Static and Dynamic Fusimotor Fibres with a Mechanical Model of the Mammalian Muscle Spindle", IEEE Trans. Bio-Med. Engr., BME-18, 175-180.

Barlett, M.S. (1950): "Periodogram Analysis and Continuous Spectra", Biometrika , 37, 1-16.

Barlett, M.S. (1963a): "The Spectral Analysis of Point Processes", J. R. Statist. Soc. B, 25, 264-280.

Barlett, M.S. (1963b): "Statistical Estimation of Density

Functions", Sankhya A, 25, 245-254.

Barlett, M.S. (1966): "An Introduction to Stochastic Processes", 2nd edition, Cambridge University Press, Cambridge.

Bayly, E.J. (1968): "Spectral Analysis of Pulse Frequency Modulation in the Nervous Systems", IEEE Trans. on Bio-Med. Engineering, vol BME-15, 257-265.

Bendat, J.S. and Piersol, A.G. (1971): "Random Data: Analysis and Measurement Procedures", Wiley-Interscience, New York

Bendat, J.S. and Piersol, A.G. (1986): "Random Data: Analysis and Measurement Procedures", 2nd ed (Revised and Expanded), Wiley-Interscience, New York.

Bessou, P. and Pages, B. (1975): "Cinematographic Analysis of Contractile Events produced in Intrafusal Fibres by Stimulation of Static and Dynamic Fusimotor Axons", J. Physiol. 252, 397-427.

Beutler, F.J. and Leneman, O.A.Z. (1968): "The Spectral Analysis of Impulse Processes", Information and Control, 12, 236-258.

Bhat, U.N. (1969): "Sixty Years of Queueing Theory", Management Sci. 15, 280-294.

Bingham, C., Godfrey, M.D. and Turkey, J.W. (1967): "Modern Techniques in Power Spectrum Estimation", IEEE Trans. Audio Electroacoustics, AU-15, 56-66.

Blackman, R.B. and Tukey, J.W. (1959): "The Measurement of Power Spectra from the Point of View of Communication Engineering", Dover Publication Inc., New York.

Bloomfield, P. (1976): "Fourier Analysis of Time Series: An Introduction". 1st edition, Wiley, New York.

Box, G.E.P. (1954): "Some Theorems on Quadratic Forms applied to

the Study of Analysis of Variance Problems", Ann. Math. Statist. 25, 290-302.

Box, G.E.P. and Jenkins, G.M. (1970): "Time Series Analysis, Forecasting and Control", Holden-Day, San Francisco, California.

Boyd, I.A. (1962): "The Structure and Innervation of the Nuclear Bag Muscle Fibre System and the Nuclear Chain Muscle Fibre System in Mammalian Muscle Spindles", Phil. Trans. R. Soc. B. 245, 83-136.

Boyd, I.A. (1980): "The Isolated Mammalian Muscle Spindle", Trends in Neurosciences, 3, 258-265.

Boyd, I.A., Gladden, M.H., McWilliam, P.N. and Ward, J. (1977): "Control of Dynamic and Static Nuclear Bag Fibres and Nuclear Chain Fibres by Gamma and Beta Axons in Isolated Cat Muscle Spindles", J. Physiol. 265, 133-162.

Boyd, I.A. and Ward, J. (1975): "Motor Control of Nuclear Bag and Nuclear Chain Intrafusal Fibres in Isolated living Muscle Spindles from the Cat", J. Physiol. 244, 83-112. Bracewell, R.N. (1986): "The Fourier Transform and its Applications", McGraw-Hill, New York.

Brigham, E.O. (1974): "The Fast Fourier Transform", Prentice-Hall, New Jersey.

Brillinger, D.R. (1965): "An Introduction to Polyspectra", Ann. Math. Statist. 36, 1351-1374.

Brillinger, D.R. (1968): "Estimation of the Cross-Spectrum of a Stationary Bivariate Gaussian Process from its Zeros", J. R. Statist. Soc. B., 30, 145-159.

Brillinger, D.R. (1969): "Asymptotic Properties of Spectral

Estimates of Second Order", Biometrika, 56, 375-390.

Brillinger, D.R. (1970a): "The Identification of Polynomial Systems by Means of Higher Order Spectra", J. Sound. Vib. 12, 301-313.

Brillinger, D.R. (1970b): "The Frequency Analysis of Relations between Stationary Spatial Series", Proc. Twelfth Bien. Sem. Can. Math. Congr., ed. Pyke, R., 39-81.

Brillinger, D.R. (1972): "The Spectral Analysis of Stationary Interval Functions", Proc. Seventh Berkeley Symp. Prob. Statist., eds. Le Cam, L., Neyman, J. and Scott, E.L., 483-513, University of California Press, Berkeley.

Brillinger, D.R. (1974a): "Fourier Analysis of Stationary Processes", Proc. IEEE, 62, 1628-1643.

Brillinger, D.R. (1974b): " Cross-Spectral Analysis of Processes with Stationary Increments Including the G/G/∞ queue", Ann. Probab., 2, 815-827.

Brillinger, D.R. (1975a): "Statistical Inference for Stationary Point Processes", in "Stochastic Processes and Related Topics", volume 1, ed. Puri, M.I., 55-79, Academic Press, New York.

Brillinger ,D.R (1975b): "Estimation of product densities", Comp. Sci. Statist., Ann. Symp. Interface 8th, 431-438, UCLA, Los Angeles.

Brillinger, D.R. (1975c): "The Identification of Point Process Systems", Ann. Probab., 3, 909-929.

Brillinger, D.R. (1975d): "Time Series: Data Analysis and Theory", 2nd edition, Holder-Day, San Francisco, California.

Brillinger, D.R. (1976a): "Estimation of Second Order Intensities

of a Bivariate Stationary Point Process", J. R. Statist. Soc., B 38, 60-66.

Brillinger, D.R. (1976b): "Measuring the Association of Point Processes: a Case History", Am. Math. Monthly, 86, 16-22.

Brillinger, D.R. (1978a): "Comparative Aspects of the Study of Ordinary Time Series and of Point Processes", in "Developments in Statistics", volume 1, 33-134, ed. Krishnaiah, P.R. Academic Press, New York.

Brillinger, D.R. (1978b): "A Note on the Estimation of Evoked Response", Biol. Cybernetics 31, 141-144.

Brillinger, D.R. (1980): "Some Aspects of the Analysis of Evoked Response Experiments", Proceedings of the International Symposium of Statistics and Related Topics, Ottawa, Canada, May 5-7, 1980: Edited by A. K. Md. Ehsanes Saleh, M. Csörgö, D. A. Dawson and J. N. K. Rao (North-Holland, Amsterdam, 1980)

Brillinger, D.R. (1981): "The General Linear Model in the Design and Analysis of Evoked Response Experiments", J. Theoret. Neurobiol, 1, 105-119.

Brillinger, D.R. (1983): " The Finite Fourier Transform of a Stationary Process", in "Handbook of Statistics", eds. Brillinger, D.R. and Krishnaiah, P.R., Elsevier, Amsterdam.

Brillinger, D.R. (1986): "Some Statistical Methods for Random Process Data from Seismology and Neurophysiology", Technical Report no. 84, Department of Statistics, University of California, Berkeley.

Brillinger, D.R. (1988a): "The Maximum Likelihood approach to the Identification of Neuronal Firing Systems", Ann. Biomedical

Engineering, 16, 3-16.

Brillinger, D.R. (1988b): "Maximum Likelihood Analysis of Spike Trains of Interacting Nerve Cells", Biological Cybernetics.

Brillinger, D.R., Bryant, H.L.,JR., and Segundo, J.P. (1976): "Identification of Synaptic Interaction", Biol. Cyber. 22, 213-228.

Brillinger, D.R. and Rosenblatt, M. (1967a): "Asymptotic Theory of kth Order Spectra", in "Spectral Analysis of Time Series", ed. Harris, B., 153-188, Wiley, New York.

Brillinger, D.R. and Rosenblatt, M. (1967b): "Computation and Interpretation of kth Order Spectra", in "Spectral Analysis of Time Series", ed. Harris, B., 189-232, Wiley, New York.

Brillinger, D.R. and Tukey, J.W. (1984): "Spectrum Analysis in the Presence of Noise: Some Issues and Examples", in "The Collected works of J.W. Tukey, Vol. 3, ed. Brillinger, D.R., 1002-1141, Monterey, Wadsworth, California.

Brownlee, K.A. (1965): "Statistical Theory and Methodology in Science and Engineering", 2nd ed., Wiley, New York.

Bryant, H.L.,JR., Ruiz Marcos, A. and Segundo, J.P. (1973): "Correlation of Neuronal Spike Discharges Produced by Monosynaptic Connections and Common Inputs", J. Neurophys. 36, 205-225.

Burke, R.M. and Rudomin, P. (1977): "Spinal Neurones and Synapses", Handbook of physiology, Sect. a: The Nervous System, volume 1, Cellular biology of neurones, Part 2 (eds Brookhart, J.M. and Mountcastle, V.B.), American Physiological Society, Bethesda, U.S.A., 877-944.

Butz, E.G. and Cowan, J.D. (1974): "Transient Potentials in

Dentritic Systems of Arbitrary Geometry", Biophysical J., 14, 661-689.

Chatfield, C. (1980): "The Analysis of Time Series: An Introduction", 2nd edition, Chapman and Hall, London.

Chen, W.J. and Poppele, R.E. (1978): "Small signal analysis of response of mammalian muscle spindles with fusimotor stimulation and a comparison with large-signal responses", J. Neurophysiol, 41, 15-27.

Conway, B.A., Halliday, D.M. and Rosenberg, J.R. (1989): "Covariance Analysis of the Time Course of Motoneuronal Depression", Six International Symposium, Motor Control 89, Albena.

Conway, B.A., Lau, W.N., Murray-Smith, D.J. and Rosenberg, J.R. (1990): "Techniques for the Analysis of Neuronal Interactions", Physiology Society Glasgow Meeting, Glasgow.

Cope, T.C., Fetz, E.E. and Matsumura, M. (1987): "Cross-correlation Assessment of Synaptic Strength of Single Ia Fibre Connections with Triceps Surae Motoneurones in Cats", Journal of Physiology, 390, 161-188.

Cox, D.R. (1955): "Some Statistical Methods Connected with Series of Events", J. R. Statist Soc., B17, 129-164.

Cox, D.R. (1962): "Renewal Theory", Methuen, London.

Cox, D.R. (1965): "On the Estimation of the Intensity Function of a Stationary Point Process", J. R. Statist. Soc. B., 27, 322-337.

Cox, D.R. and Isham, V. (1980): "Point Processes", Monographs on Applied Probability and Statistics, Chapman and Hall, London.

Cox, D.R. and Lewis, P.A.W. (1966): "The Statistical Analysis of Series of Events", Chapman and Hall, London.

Cox, D.R. and Lewis, P.A.W. (1972): "Multivariate Point Processes", Proc. 6th Berkeley Symp. Math. Statist. Prob., 2, 401-448.

Cox, D.R. and Miller, H.D. (1965) "The Theory of Stochastic Processes", Chapman and Hall, London.

Cramer, H. and Leadbetter, M.R. (1967): "Stationary and Related Stochastic Processes", Wiley, New York.

Crowe, A. and Matthews, P.B.C. (1964): "The Effects of Stimulation of Static and Dynamic Fusimotor Fibres on the Response to Stretching of the Primary Endings of Muscle Spindles", J. Physiol. 174, 109-131.

Daley, D.J. and Vere-Jones, D. (1988): "An Introduction to the Theory of Point Processes", Springer, New York.

Datta, A.K. and Stephens, J.A. (1990), "Synchronization of Motor Unit Activity during Voluntary Contraction in Man", Journal of Physiology, 422, 397-419.

Doob, J.L. (1953): "Stochastic Processes", Wiley, New York.

Downie, I.C. and Murry-Smith, D.J. (1981): "Simulation of Systems Involving Pulse Frequency Modulation with Special Reference to Modelling of Muscle Spindles", Proc. 1981 UKSC Conf on Comp Sim Harrogate, Westbury House, Guilford, 143-152.

Draper, N. and Smith, H. (1966): "Applied Regression Analysis", Wiley, New York.

Dutia, M.B., Murray-Smith, D.J., Rosenberg, J.R. and Wilson, R. (1977): "The Dependence of Driving of Ia Axons on Muscle Length and Fusimotor Stimulation Frequency", J. Physiol.,

273, 30-31P.

EAI 2000 Analog Reference Handbook (1978), Electronic Associates Inc., West Long Branch, New Jersey 07764.

Edgley, S.A. and Jankowska, E. (1987): "An International Relay for Group I and II Muscle Afferents in the Midlumber Segments of Cat Spinal Cord", J. Physiol. 389, 647-674.

Ellaway, P.H. and Murthy, K.S.K. (1981a): "The Origins and Characterisitics of Cross-Correlated Activity between γ-motoneurones in the Cat", Quarterly Journal of Experimental Physiology, 70, 219-232. 232.

Ellaway, P.H. and Murthy, K.S.K. (1981b): "The Source and Distribution of Short-term Synchrony between γ-motoneurones in the Cat", Quarterly Journal of Experimental Physiology, 70, 233-249.

Emonent-Denand, F., Laporte, V., Matthews, P.B.C. and Petit, J. (1977): "On the Subdivision of Static and Dynamic Fusimotor Axons on the Primary Endings of the Cat Muscle Spindle", J. Physiol. 268, 827-860.

Feinberg, S.E. (1974): "Stochastic Models for Single Neurones Firing Trains: A Survey", Biometrics, 30, 399-427.

Feller, W. (1971): "Introduction to Probability Theory and its Application", vol. 1, 3rd edn. vol. 2. 2nd edn., New York, Wiley.

Ferrell, W.R., Rosenberg, J.R., Baxendale, R.H., Halliday, D.M. and Wood, L. (1990): "Fourier Analysis of the Relation between the discharges of Quadriceps Motor Units and Periodic Mechanical Stimulation of Cat Knee Joint Receptors", Experimental Physiology, 75, 737-750.

Gentleman, W.M. and Sande, G. (1966): "Fast Fourier Transforms - for Fun and Profit", AFIPS, 1966 Fall Joint Computer Conference, 28, 563-578, Spartan, Washington.

Godfrey, M.D. (1965): "An Exploratory Study of the Bi-Spectrum of Economic Time Series", Applied Statistics, 14, 48-69.

Goodman, N.R. (1963): "Statistical Analysis based upon a Certain Multivariate Complex Gaussian Distribution (An Introduction)", Ann. Math. Statist. 34, 152-177.

Grenander, U. and Rosenblatt, M. (1957): "Statistical Analysis of Stationary Time Series", Wiley, New York.

Haight, F.A. (1967): "Handbook of the Poisson Distribution", Wiley, New York.

Halliday, D.M. (1986): "Application of Point Process System Identification Techniques to Complex Physiological Systems", Ph.D. Thesis, University of Glasgow.

Hannan, E.J. (1960): "Time Series Analysis", Methuen, London.

Hannan, E.J. (1970): "Multiple Time Series", Wiley, New York.

Hannan, E.J. and Thomson, P.J. (1971): "The Estimation of Coherence and Group Delay", Biometrika, 58, 469-482.

Harris, T.E. (1980): "On the use of Windows for Harmonic Analysis with Discrete Fourier Transforms", Proc. IEEE, 66, 51-83.

Hasan, Z. and Houk, J.C. (1972): "Nonlinear Behaviour of Primary Spindle Receptors in Response to Small Slow Ramp Stretches", Brain Res, 44, 680-683.

Hasselmann, K., Munk, W. and MacDonald, G. (1963): "Bispectra of Ocean Waves", in "Time Series Analysis, ed. Rosenblatt, M., Wiley, New York.

Hawkes, A.G. (1971): "Spectra of some Self-Exciting and Mutually

Excited Point Processes", J. R. Statist. Soc. 58, 1, 83-90.

Hoopen, M. ten (1974): "Examples of Power Spectra of Univariate Point Processes", Kybernetik 16, 145-154.

Houk, J.C., Rymer, W.Z. and Crago, P.E. (1981): "Nature of the Dynamic Response and its relation to the High Sensitivity of Muscle Spindles to Small Changes in Length", in Muscle receptors and movement (eds Taylor, A. and Prochazka, A.), Macmillan, London, 33-43.

Hullinger, M., Matthews, P.B.C. and North, J. (1977a): "Static and Dynamic Fusimotor Action on the Response of Ia Fibres to low frequency sinusoidal stretching of widely ranging amplitude", J. Physiol, 267, 811-838.

Hullinger, M., Matthews, P.B.C. and North, J. (1977b): "Effect of combining Static and Dynamic Fusimotor Stimulation on the Response of the Muscle Spindle Primary Ending to Sinusoidal Stretching", J. Physiol, 267, 839-856.

Hung, G., Brillinger, D.R. and Stark, L. (1979): "Interpretation of Kernels. II. Some Signed 1st and 2nd Degree (Main Diagonal) Kernels of the Human Pupillary System", Math. Biosci. 46, 159-187.

Hung, G. and Stark, L. (1977): "The Kernel Identification Method (1910-1977) - Review of Theory, Calculation, Application and Interpretation", Mathematical Biosciences, 37, 135-190.

Jenkins, G.M. (1961): "General Considerations in the Analysis of Spectra", Technometrics, 3, 133-166.

Jenkins, G.M. (1963a): "Contribution to a Discussion of paper by M.S. Bartlett", J. R. Statist. Soc., B, 25, 290-291.

Jenkins, G.M. (1963b): "Cross-Spectral Analysis and the Estimation

of Linear Open Loop Transfer Functions", in "Time Series Analysis", ed. Rosenblatt, M., Wiley, New York, 267-278.

Jenkins, G.M. and Watts, D.G. (1968): "Spectral Analysis and its applications", Holden-Day, San Francisco, California.

Jenson, A. (1948): "An elucidation of Erlang's works through the theory of Stochastic Process", The Life and Works of A.K. Erlang, pp. 23-100, Copenhagen Tel Co.

Johansson, H. (1981): "Reflex Control of γ-motoneurones", Umea University Medical Dissertation, Department of Physiology, University of Umea, Umea, Sweden.

Jones, R.H. (1965): "A reappraisal of periodogram in spectral analysis", Technometrics 7:531-542.

Katzenelson, J. and Gould, L.A. (1962): "The design of non-linear filters and control systems", I, Inform. Control, 5,108-143.

Katznelson, Y. (1968): "Introduction to Harmonic Analysis", Wiley, New York.

Kendall, M.G. and Stuart, A. (1961): "The Advanced Theory of Statistics", volume 2, Griffin, London.

Kendall, M.G. and Stuart, A. (1966): "The Advanced Theory of Statistics", 2nd edition, volume 1, Griffin, London.

Kendall, D.G. (1975): "The Genealogy of Genealogy Branching Processes before (and after) 1873", Bull. London Math. Soc. 7, 225-253. 253.

Khintchine, A.Y. (1960): "Mathematical Methods in the Theory of Queueing", Griffin, London.

Kirkwood, P.A. (1979): "On the Use and Interpretation of Cross-Correlation Measurements in the Mammalian Central Nervous Systems", J. Neurosci. 1, 107-132.

Kirkood, P.A., Sears, T.A., Tuck, D.L. and Westgaard, R.H. (1982): "Variations in the Time Course of the Synchronization of Intercostal Motoneurones", Journal of Physiology 327, 105-136.

Knuth, Donald, E. (1981): "Seminumerical Algorithms", 2nd ed., vol. 2 of "The Art of Computer Programming", (Reading, Mass. Addision-Wesley) 3.2-3.3

Koch, C. and Poggio, T. (1985): "A simple algorithm for solving the Cable Equation in Dendritic Trees of Arbitrary Geometry", J. Neuroscience Methods 12, 303-315.

Koopmans, L.H. (1974): "The Spectral Analysis of Time Series", Academic Press, New York.

Koopmans, L.H. (1983): "A Spectral Analysis Primer", in "Handbook of Statistics", volume 3, eds Brillinger, D.R. and Krishnaiah, P.R., Elsevier, Amsterdam, 169-184.

Krausz, H.I. (1975): "Identification of Non-Linear Systems using Random Impulse Train Inputs", Biol. Cybernetics, 19, 217-230.

Kuznetsov, P.I. and Stratonovich, R.L. (1965): "A Note on the Mathematical Theory of Correlated Random Points", in "Non-Linear Transformations of Stochastic Processes", eds. Kuznetsov, P.I., Stratonovich, R.L. and Tikhonov, V.I., Pergamon, Oxford, 101-115.

Lanczos, C. (1950): "An Iteration Method for the solution of the problem of Linear Differential and Integral Operators", Journal of Research of the National Bureau of Standards, 45, 255-282.

Lau, W.N. (1988a): "Programs for Storage and Generation of Point

Process Stimuli", Progress Report PS 88001.

Lau, W.N. (1988b): "Program for Generation of Poisson Point Process", Progress Report PS 88002.

Lau, W.N. (1988c): "First Year Report on Point Process Identification Techniques Applied to Physiological Systems", University of Glasgow.

Lau, W.N. (1988d): "DIGAD - Program for Generation of Poisson Point Process Stimuli and Collection of Point Process and Analog Data", Progress Report PS 88003.

Lau, .N., Halliday, D.M., Murray-Smith D.J., Rosenberg, J.R. and Conway, B.A. (1989a) "Covariance Analysis of the Firing Behaviour of a Neurone Model", Sixth International Symposium, Motor Control 89, Albena.

Lau, W.N. (1989b): "Second Year Report on Application of Point Process Identification Techniques to Physiological Systems", University of Glasgow.

Lee, Y.W. and Schetzen, M. (1965): "Measurement of the Wiener Kernels of a Non-Linear System by Cross-Correlation", Int. J. Control, 2, 237-254.

Leonov, V.P. and Shiryaev, A.N. (1959): "On a Method for the Calculation of Semi-invariants", Theor. Prob. Appl. 4, 319-329.

Lewis, P.A.W. (1970): "Remarks on the Theory, Computation and Application of the Spectral Analysis of Series of Events", J. Sound Vib. 12, 353-375.

Lewis, P.A.W. (1972a): "Stochastic Point Processes". Wiley, New York.

Lewis, P.A.W. (1972b): "Remarks on the theory, computation, and

application of the spectral analysis of series of events", Journal Sound and Vibration, 12, 353-375.

Lotka, A.J. (1957): "Elements of Mathematical Biology", Dover, New York.

Maclain, C.G., McWilliam, P.N., Murray-Smith, D.J. and Rosenberg, J.R. (1977): "A Possible Mode of Action of Static Fusimotor Axons as revealed by System Identification Techniques", Brain Res. 135, 351-357.

Mann, H.B. and Wald, A. (1943): "On Stochastic Limit and Order Relationships", Ann. Math. Statist. 14, 217-226.

Mardia, K.V., Kent, J.T. and Bibby, J.M. (1982): "Multivariate Analysis", Academic Press, London.

Marmarelis, P.Z. and Naka, K-I. (1974): "Identification of Multiple-Input Biological Systems", IEEE Trans. Biomedical Engineering, volume 21, 2, 88-101.

Marmarelis, P.Z. (1975): "Contribution to a discussion of paper by D.R. Brillinger", Ann. Probab. 3, 924-927.

Marmarelis, P.Z. and Marmarelis, V.Z. (1978): "Analysis of Physiological Systems", Plenum Press, New York.

Matthews, P.B.C. (1962): "The Differentiation of Two Types of Fusimotor Fibre by their Effects on the Dynamic Response of Muscle Spindle Primary Endings", Q. J. Exp. Physiol., 47, 324-333.

Matthews, P.B.C. (1981): "Review Lecture: Evolving Views on the Internal Operation and Functional Role of the Muscle Spindle", J. Physiol. 320, 1-30.

Matthews, P.B.C. and Stein, R.B. (1969): "The Regularity of Primary and Secondary Muscle Spindle Afferent Discharges",

J. Physiol. 202, 59-82.

Meyer, A.U. (1961): "Pulse Frequency Modulation and its Effect in Feedback Systems", Ph.D. dissertation, Northwestern University, Evanston.

Meyer, P.L. (1980): "Introduction Probability and Statistical Applications", 2nd edition, Addison-Wesley.

Michalski, A., Gerstein, G.L., Czarkowska, J. and Tarnecki, R. (1983): "Interactions between Cat Striate Cortex Neurons", Experiment Brain Research, 51, 90-107.

Mood, A.M., Graybill, F.A., Boes, D.C. (1963): "Introduction to the Theory of Statistics", McGraw-Hill, London.

Moore, G.P., Perkel, D.H. and Segundo, J.P. (1966): "Statistical Analysis and Functional Interpretation of Neural Spike Data", A. Rev. Physiol 28, 493-552.

Moore, G.P., Segundo, J.P., Perkel, D.H. and Levitan, H. (1970): "Statistical Signs of Synaptic Interactions in Neurones", Biophysical Journal 10, 876-900.

Neave, H.R. (1971): "The Exact Error in Spectrum Estimators", Ann. Math. Statist. 42, 961-975.

Neave, H.R. (1972): "A Comparison of Lag Window Generators", J. Amer. Statist. Ass. 67,152-158.

Nyquist, H (1928): "Certain Topics in Telegraph Transmission Theory", Trans. AIEE, 617-649.

Otnes, R.K. and Enochson, L. (1978): "Applied Time Series Analysis", vol 1, John Wiley and Sons, New York.

Papoulis, A. (1962): "The Fourier Integral and its Applications", McGraw-Hill, New York.

Parzen, E. (1957): "On Consistent Estimate of the Spectrum of a

Stationary Time Series", Ann. Math. Statist. 28, 329-348.

Parzen, E. (1958): "On Asymptotically Efficient Consistent Estimates of the Spectral Density Function of a Stationary Time Series", J. R. Statist. Soc. B. 20, 303-322.

Parzen, E. (1961): "Mathematical Considerations in the Estimation of Spectra", Technometrics, 3, 167-190.

Parzen, E. (1967): "On Empirical Multiple Time Series Analysis", in Proc. Fifth Berkeley Symp. Math. Statist. Prob. 1, eds. Le Cam, L. and Neyman, J. Berkeley: University of California Press, 305-340.

Pavlidis, T. and Jury, E,I. (1965): "Analysis of a New Class of Pulse Frequency Modulated Feedback Systems2, IEEE Trans Auto Control, 10, 35-43.

Perkel, D.H., Gerstein, G.L. and Moore, G.P. (1967a): "Neuronal Spike Trains and Stochastic Point Processes. I. The Single Spike Train", Biophys. J. volume 7, 391-418.

Perkel, D.H., Gerstein, G.L. and Moore, G.P. (1967b): "Neuronal Spike Trains and Stochastic Point Processes. II. Simultaneous Spike Trains", Biophys. J. volume 7, 419-440.

Press, W.H., Flannery, B.P., Teukolsky, S.A. and Vetterling, W.T. (1986): "Numerical Recipes", Cambridge University Press.

Priestley, M.B. (1962): "Basic Considerations in the Estimation of Spectra", Technometrics, 4, 551-564.

Priestley, M.B. (1987): "Spectral Analysis and Time Series", Academic Press, London.

Rall, W. (1989): "Cable Theory for Dendritic Neurones", in "Methods in Neuronal Modelling", eds. Koch, C. and Segler, I, pp 9-62, MIT Press, Cambridge, Mass.

Ramakrishnan, A. (1950): "Stochastic Processes Relating Particles Distributed in a Continuous Infinity of States", Proc. Cambridge Phil. Soc. 46, 596-602.

Ramirez, R.W. (1974): "The Fourier Transform's Errors are Predictable, therefore Manageable", Electronics 47, 96-103.

Rao, C.R. (1984): "Linear Statistical Inference and its Applications", Wiley, New York.

Rice, J.A. (1973): "Statistical Analysis of Self-Exciting Point Processes and Related Linear Models", Ph.D. Thesis, University of Berkeley.

Rigas, A.G. (1983): "Point Processes and Time Series Analysis: Theory and Applications to Complex Physiological Problems", Ph.D. Thesis, University of Glasgow.

Robinson, E.A. (1967): "Multichannel Time Series Analysis with Digital Computer Programs", Holden-Day, San Francisco.

Rosenberg, J.R., Murray-Smith, D.J. and Rigas, A. (1982): "An Introduction to the Application of System Identification Techniques to Elements of the Neuromuscular System", Trans. Inst. Meas. and Control, 4, 187-202.

Rosenberg, J.R., Amjad, A.M., Breeze, P., Brillinger, D.R. and Halliday, D.M. (1989): "The Fourier Approach to the Identification of Functional Coupling between Neuronal Spike Trains", Prog. Biophys. Molec. Biolo., volume 53, 1-31.

Rosenblatt, M. (1956a): "A Central Limit Theorem and a Strong Mixing Condition", Proc. Nat. Acad. Sci. (USA), 42, 43-47.

Rosenblatt, M. (1956b): "Remarks of some Non-Parametric Estimates of a Density Function", Ann. Math. Statist., 12, 832-837.

Rosenblatt, M. (1959): "Statistical Analysis of Stochastic

Processes with Stationary Residuals", in "Probability and Statistics", ed. Grenander, U., Wiley, New York, 246-275.

Sampath, G. and Srinivasan, S.K. (1977): "Stochastic Spike Trains of Single Neurones", in "Lecture Notes in Biomathematics", volume 16, ed. Levin, S., Springer-Verlag, Berlin.

Schuster, A. (1989): "On the Investigation of Hidden Periodicities with Application to a Supposed 26 day period of Meteorological Phenomena", Terr. Magn. 3, 13-41.

Schwalm, D. (1971): "Identification of Multiple-Input Multiple-Output Linear Systems by Correlation Methods", Int. J. Control, 13, 6, 1131-1135.

Shepherd, G.M. (1974): "The Synaptic Organisation of the Brain", 1st edition, 79-110, Oxford University Press, London.

Shiryaev, A.N. (1960): "Some Problems in the Spectral Theory of Higher-Order Moments", I, Theory Probab. Applic, 5, p.265.

Shumway, R.H. (1988): "Applied Statistical Time Series Analysis", Prentice-Hall International.

Smith, W.L. (1958): "Renewal theory and it ramifications (with discussion)", J.R. Statist. Soc. B20, 284-302.

Snyder, D.L. (1975): "Random Point Processes", Wiley, New York.

Srinivasan, S.K. (1974): "Stochastic Point Processes and their Applications", Griffin, London.

Tick, L.J. (1961): "The Estimation of Transfer Functions of Quadratic Systems", Technometrics, 3, 563-567.

Tick, L.J. (1963): "Condition Spectra, Linear Systems, and Coherency", in "Time Series Analysis", ed. Rosenblatt, M., Wiley, New York, 197-203.

Tukey, J.W. (1959a): "An Introduction to the Measurement of

Spectra", in "Probability and Statistics", ed. Grenander, U., Wiley, New York, 300-330.

Tukey, J.W. (1959b): "The Estimation of Power Spectra and Related Quantities", in "On Numerical Approximation", University of Wisconsin Press, Madison, 389-411.

Tukey, J.W. (1967): "An Introduction to the Calculations of Numerical Spectrum Analysis", in "Advanced Seminar on Spectral Analysis of Time Series", ed. Harris, B., Wiley, New York, 25-46.

Tukey, J.W. (1977): "Exploratory Data Analysis", Addison-Wesley, USA.

Tukey, J.W. (1980): "Can We Predict where 'Time Series' should go next?", in "Directions in Time Series", eds. Brillinger, D.R. and Tiao, G.C., Inst. Math. Statist., Hayward.

Volterra, V. (1959): "Theory of Functionals and of Integrals and Integro - Differential Equations", Dover, New York.

Weisberg, S. (1985): "Applied Linear Regression", 2nd edition, Wiley, New York.

Welch, P.D. (1972): "The use of Fast Fourier Transform for the Estimation of Power Spectra: a Method based on Time Averaging Processing", eds. Rabiner, L.R. and Rader, C.M., IEEE Press, New York.

Westergaard, H. (1968): "Contribution to the History of Statistics", Agathon, New York.

Whitehead, R.R., Watt, A., Cole, B.J. and Morrison, I. (1977): "Computational Methods for Shell-Model Calculations", Advances in Nuclear Physics 9, 123-176.

Wiener, N. (1958): "Non-Linear Problems in Random Theory", MIT

Press, Cambridge.

Windhorst, U. and Schwestka, R. (1982): "Interaction between Motor Units in Modulating Discharge Patterns of Primary Muscle Spindle Endings", Experimental Brain Res. 45, 417-427.

Wold, H.O.A. (1965): "Bibliography on Time Series and Stochastic Processes", Oliver and Boyd, London.

Yaglom, A.M. (1962): "An Introduction to the Theory of Stationary Random Functions", Prentice-Hall, Englewood Cliffs.